Investigating the role of Histone Deacetylase HDAC4 in long-term memory formation

A thesis presented in partial fulfilment of the requirements for the degree of

Doctor of Philosophy

in

Genetics

at Massey University, Manawatu

New Zealand.

MASSEY
UNIVERSITY

Silvia Schwartz

2016

ABSTRACT

Epigenetic mechanisms are emerging as master regulators of cognitive abilities such as learning and memory. It has been previously shown that the histone deacetylase HDAC4 plays a critical role in memory formation in both mammals and insects although the specific mechanisms through which it acts have not yet been elucidated. HDAC4 undergoes nucleocytoplasmic shuttling and, in neurons, it is largely cytoplasmic implying it may play both nuclear and non-nuclear functions. To identify upstream regulators and downstream targets of *HDAC4*, a genetic interaction screen was performed in the fruit fly *Drosophila melanogaster*, a powerful model system to study the genetic mechanisms of neurological disease. Twenty-nine genes were found to interact with *HDAC4* suggesting they are part of the same molecular pathway. Functional network analysis revealed that many of the genes could be grouped into three biological categories comprising transcriptional factors, SUMOylation machinery enzymes and cytoskeletal regulators/interactors. Within the latter, *Ankyrin2* was selected for further analysis as it is implicated in synaptic stability and in human intellectual disability. In addition HDAC4 harbours a conserved ankyrin binding domain. Immunohistochemical analyses showed widespread distribution of Ankyrin2 throughout the adult brain and coincident distribution with HDAC4 was observed in the axons of the mushroom body, a key structure for memory formation in flies. Both *HDAC4* and *Ankyrin2* were also found to regulate mushroom body development. RNAi-mediated depletion of *Ankyrin2* in the adult brain impaired long-term memory in the courtship suppression assay, a model of associative memory and preliminary evidence of a physical association between HDAC4 and Ankyrin2 was also demonstrated. The genes identified in the screen provide new avenues for investigation of the mechanisms through which *HDAC4* regulates memory formation and preliminary analyses suggest that interaction with the cytoskeletal adaptor Ankyrin2 may involve remodelling of the actin/spectrin cytoskeleton, phenomenon that underlies memory related processes like synaptic plasticity and neuronal excitability.

ACKNOWLEDGEMENTS

This was the year of the Summer Olympic Games and I could not help the feeling of participating to a sort of Olympic Games myself… as a PhD student. In particular, this sport event corresponded exactly with my thesis writing and made me realise that academic life and sport training share similarities. As in sport training, the good days are rare. Most of the time, it is hard, it takes a long time, things go wrong, better and then wrong again and in order to be successful at either, your commitment must be to the process, not to the final prize. However, with dedication, passion, patience and a good dose of optimism the final goal would gradually approach.

Firstly, I would like to express my gratitude to my supervisor Dr Helen Fitzsimons for the endless support, encouragement and the inestimable enthusiasm for my project. Being trained and mentored by someone who really understands the "sport" is an amazing experience and I am in awe of your depth of knowledge and optimism that helped me during the most difficult days. You taught me that every day is a good day because there is something new to learn. An immense appreciation goes to my co-supervisors, Professor Kathryn Stowell and Dr Tracy Hale for their massive knowledge, precious advice and suggestions, and for their priceless availability and dedication. Yes… I have been a very lucky student.

To Dr Matthew Savoian, Mr Doug Hopcroft, Ms Niki Murray and Ms Jordan Taylor (MMIC), thank you not only for your fundamental technical expertise but also for being such nice persons. In particular to Matthew, for the support and for sharing your life experiences and wise advice. To Dr Dave Wheeler for his assistance with bioinformatics analysis, for the greatest eggs I have ever had and for the amusing fights with Tracy about New Zealanders versus Australians. I learnt a lot!

Special thanks go to Olaf and Steve for helping me setting up the behavioural equipment that allowed me to work efficiently during the last months. You are geniuses!

To my lab mates, Sarah, Patrick F., Patrick M., Lance and Raoul for the nicest work environment I have ever encountered. You made this long and difficult path smoother and enjoyable. I will miss you a lot. To Ann, Cynthia, Colleen and Paul for being so perfectly organised and for your endless availability. You really are the backbone of the institute.

Thank you to Dr Patrick Biggs and Amanda for the lovely way you welcomed me here in New Zealand and for the delicious dinners. Thanks to the friends I met here, who were boosting my moral especially during the writing period: Simren, Max, Mariela, Flavia, Ermanno, Arvina, Patry, Luca, Yimi, Angi, Gabor, Zsuzsa, Szabolcs, Alex, Ben, and to all the people who simply asked me 'how are you?' That really made a difference. Thanks to my best friends back home for the virtual support and for keeping me up to date on their important life events: Giulia, Valeria, Andrea, Virginia, Fabiola, Beatrice, Sara, Alessia.

To my family, for the endless support and for always being proud of me, even for the very small things. I know being far away was a hard thing for you to handle, as it was for me, but you always kept a smile on your faces and showed me how interested and happy you were about my experience at 20,000 Km of distance.

Last but not the least, to Mauro and his family. Without you and your love, the New Zealand experience would have never happened and I will never stop thanking you, also because you convinced me that a cat would have been of great help and you were right, our sweet Tori helped us in the difficult moments.

I always believe that after a wonderful and rich experience 'the best is yet to come'… Well, it will be very hard to exceed what I experienced here in New Zealand but I will do my best to, at least, get close to that.

This project was funded by the Health Research Council of New Zealand.

TABLE OF CONTENTS

LIST OF FIGURES

LIST OF TABLES

ABBREVIATIONS

°C	Degree Celsius
AIS	Axon initial segment
Ank1	Ankyrin1
Ank2	Ankyrin2
Ank3	Ankyrin3
ANK-B	Ankyrin B
ANK-G	Ankyrin G
ANK-R	Ankyrin R
Arc1	Activity-regulated cytoskeleton associated protein 1
Att	Arginine tolerance test
Aβ	Amyloid-beta
BDSC	Bloomington Drosophila Stock Centre
bp	Base pair
Ca^{++}	Calcium
CaMK	Calcium/calmodulin-dependent kinase
cAMP	Cyclic adenosine monophosphate
cDNA	Complementary DNA
CI	Courtship index
CIP	Calf intestinal alkaline phosphatase
Cm	Centimeters
CRE	cAMP response element
CrebB	cAMP response element binding protein B
CS	Canton special
Cy	Curly
DNA	Deoxyribonucleic acid
DroID	Drosophila interactions database
dsRNA	Double stranded RNA
EDTA	Ethylenediaminetetraacetic acid
EGFP	Enhanced green fluorescent protein
EGTA	Ethylene glycol tetraacetic acid
Elav	Embryonic lethal abnormal visual system

FasII	Fasciclin II
FLIM	Flurescence lifetime imaging microscope
FPKM	Fragments per kilobase of transcript per million mapped
FRET	Fluorescence resonance energy transfer
GFP	Green fluorescent protein
GMR	Glass multimer reporter
GST	Glutathione S-transferase
H^+	Hydrogen
HAT	Histone acetyltransferase
HCl	Hydrochloric acid
HDAC	Histone deacetylase
HDAC4	Histone deacetylase 4
HEK293	Human embryonic kidney 293 cells
HEPES	4-(2-hydroxyethyl)-1-piperazineethanesulfonic acid
INTACT	Isolation of nuclei tagged in specific cell types
IPTG	Isopropyl-β-D-thiogalactoside
K^+	Potassium
KCl	Potassium chloride
kDa	Kilodalton
L	Litre
LI	Learning index
LoxP	Locus of X-over P1
LTM	Long-term memory
M	Molar
mA	Milliampere
MAPK	Mitogen-activated protein kinase
Mef2	Myocyte enhancer factor 2
mg	Milligram
MgCl2	Magnesium chloride
MI	Memory index
ml	Millilitre
mm	Millimeters
mM	Millimolar
mRNA	Messenger RNA

Na^+	Sodium
NES	Nuclar export signal
ng	Nanogram
NLS	Nuclear localisation signal
nm	Nanometers
NMDARs	N-Methyl-D-Aspartic acid receptors
Nrg	Neuroglian
OE	Overexpression
PCR	Polymerase chain reaction
PKA	Protein kinase A
qPCR	Quantitative Real Time PCR
Repo	Reversed polarity
RFP	Red fluorescent protein
RNA	Ribonucleic acid
RNAi	RNA interference
RNAseq	RNA sequencing
Rpm	Revolution per minute
Sb	Stubble
SDS-PAGE	Sodium dodecyl sulphate – polyacrylamide gel electrophoresis
STM	Short-term memory
STRING	Search tool for the retrieval of interacting genes/proteins
SUMO	Small ubiquitin-like modifier
SV40	Simian virus 40
TARGET	Temporal and regional gene expression targeting
Ts	Temperature sensitive
UAS	Upstream activating sequence
Ubc9	Ubiquitin Carrier Protein 9
V	Volt
VDRC	Vienna Drosophila Resource Centre
Wt	Wild-type
µg	Microgram
µl	Microlitre
µm	Micrometer

1 Introduction

1.1 Neurological disorders: a burden of our times

The development and normal function of the human brain is one of nature's most elaborate processes, which involves organisation of neuronal cells into trillions of synapses within a network. This requires a highly orchestrated regulation of gene expression in a spatially and temporally coordinated fashion. Post development, the brain maintains its structural and functional plasticity, coordinating complex processes such as learning and memory (Van der Voet et al., 2014). Dysregulation of these processes via genetic or environmental mechanisms can severely compromise brain development and functionality resulting in disorders such as dementia and intellectual disability. Dementia is a progressive disorder that results in impairments in cognitive tasks including memory, learning, problem solving and language production with Alzheimer's' disease the most common form of dementia affecting approximately two-thirds of dementia suffers (World Alzheimer report, 2015). Currently, over 46 million people live with dementia worldwide and this number is estimated to increase to 131.5 million by 2050 (Prince et al., 2015). Dementia not only is a critical health issue, but also has a huge economic impact with the total estimated worldwide cost being US $818 billion, and is calculated to become a trillion dollar disease by 2018 (Prince et al., 2015). In New Zealand, dementia is a growing healthcare challenge. In 2012, it was estimated that 53,000 people live with dementia in New Zealand and this is forecast to triple to around 150,000 by 2050. The total financial cost of dementia on the health system in 2011 was estimated as $954.8 million (Ministry of Health, 2013. New Zealand Framework for Dementia Care, www.health.govt.nz).

The causes of dementia cannot be attributed to a single factor. It is likely that a combination of factors including age, genetic inheritance and environmental factors are responsible for the origin of such condition (Ministry of Health, 2013. New Zealand Framework for Dementia Care, www.health.govt.nz). The term neurodevelopmental disorders refers to a "group of conditions with onset in the developmental period characterized by developmental deficits that produce impairments of personal, social, academic, or occupational functioning" (American Psychiatric Association, 2013) and includes intellectual disability, autism spectrum disorders, attention-deficit hyperactivity disorder, learning disorders and others like epilepsy. Their impact on cognition, social interaction, motor skills and mood, place a significant burden on families and health

system. In some cases the genetic cause is known, however it is believed that these disorders result from a combination of genetic, biological, psychosocial and environmental risk factors.

Investigating the interplay between genes, the brain and behaviour is a rapidly expanding area of the neuroscience field and understanding the molecular mechanisms underpinning normal learning and memory is paramount in order to understand the abnormal process that results in neurodegenerative and neurodevelopmental disorders. The identification of new and more specific targets would contribute to the development of more accurate pharmaceutical treatments and would provide the necessary tools and knowledge to possibly prevent the onset of such diseases in predisposed subjects.

1.2 Learning and Memory: a historical journey

The primary functions of the nervous system involve receiving, transmitting and processing internal and external stimuli allowing animal species to modify their behaviour and adapt to the changing environment surrounding them. This process of experience-dependent reshaping is known as plasticity and was initially observed by Santiago Ramon y Cajal (1894) whose studies on the microanatomy, function, degeneration and regeneration of the nervous system described the connection between neuronal circuits and brain functions (DeFelipe, 2006; Ho et al., 2011; Mayford et al., 2012) and paved the way to modern neuroscience. Cajal concluded that the histological architecture of the brain was dynamic and related to mental processes (*"Such plasticity of the cellular processes probably varies at different ages: greater in the young man, diminished in the adult and almost completely disappeared in the aged […]. Thus, it is necessary to wait for certain connections to wither and for the creation of others that would serve as tracks for the new combinations of ideas […]. The cerebral cortex has maintained its growth plasticity, its capacity for internal differentiation to adapt to the ever increasing and ever more complicated necessities in the struggle for life").* It is now known that those histological alterations Cajal referred to correspond to the changes in synaptic strength, or connectivity, which is a mechanism critical to higher brain function of learning and memory (Bailey and Kandel, 1993).

Synapses, from the Greek *synàptein* meaning "connect/join" are the computational units of the brain that allow neurons to communicate through either an electrical or

chemical signal (Figure 1.1) and the modulation of synaptic connectivity is the basic process through which learning and memory are regulated (Mayford et al., 2012).

Memory can be defined as a behavioural change elicited by an experience and learning as the process of memory acquisition (Okano et al., 2000; Kandel, 2001). More specifically learning is the process through which new information from the environment is acquired while memory can be considered as a combination of neuronal connections that recall past experiences by firing of the neurons that were involved in that experience. Molecular and chemical mechanisms cooperate to guarantee the functionality of these complex processes.

Cajal's studies opened a myriad of questions on how these mechanisms functioned at the molecular level. How do these changes in synaptic strength occur? How do organisms acquire and retain the information? Pioneering and fruitful studies to address those questions were performed in the late 1960s, by neuroscientist and recipient of the Nobel Prize in Physiology and Medicine in 2000, Eric Kandel, who carried out seminal studies on the molecular basis of learning and memory storage in neurons. Kandel's presumption was that since the fundamental structures of neurons are conserved across the animal kingdom, then the molecular mechanisms of learning and memory would also be conserved (Kandel and Spencer, 1968; Kandel, 2001).

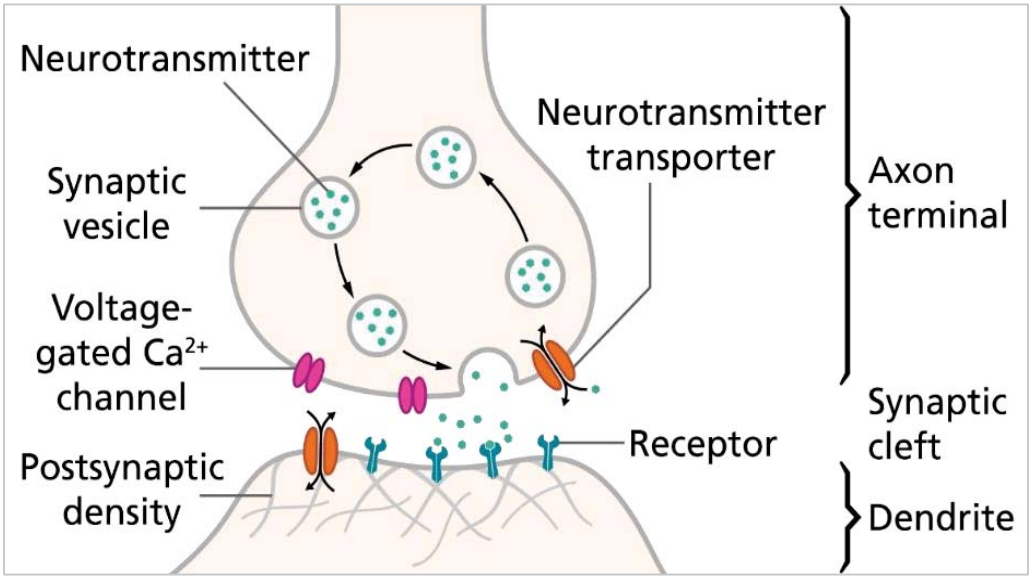

Figure 1.1 Synaptic connectivity. Cartoon showing a schematic representation of a chemical synapse. Synapses are junctions occurring between the axon of a presynaptic neuron, and the dendrite of a postsynaptic neuron. At a chemical synapse, one neuron releases chemical messengers, small molecules known as neurotransmitters, into the synaptic cleft, a space adjacent

to another neuron. Neurotransmitters are stored inside vesicles within the axon terminal of a presynaptic neuron and are released into the synaptic cleft by exocytosis. These molecules then bind to receptors localised on the dendrite of the postsynaptic neuron and ultimately are cleared through enzymatic degradation or by reabsorption by the presynaptic cell. This process is originated by a wave of electrochemical excitation, an action potential, traveling along the axon until it reaches the synapse. This causes an electrical depolarization of the membrane at the synapse resulting in the opening of calcium channels, leading to an increase in calcium concentration in the presynaptic membrane. The high calcium concentration induces conformational changes of a set of calcium-sensitive proteins attached to vesicles allowing them to fuse with the membrane of the presynaptic cell and release neurotransmitters into the synaptic cleft with consequent binding to their specific receptors in the postsynaptic cell.

The compelling characteristic of Kandel's studies resides in the strategy he adopted to address these questions. He used a reductionist approach through the use of a simple animal model, the marine snail *Aplysia californica* and a basic defence behaviour adopted by the snail, the gill reflex withdrawal. By applying pressure on the siphon, the snail reacts by withdrawing the gill. When simultaneous application of stimuli, even innocuous ones, were applied to the tail, the withdrawal response was enhanced. This process is called sensitisation and it is a type of learned fear in which a subject learns to respond strongly to an otherwise neutral stimulus. A single shock determines memory lasting minutes while spaced and repeated shock to the tail originate memories lasting days (Hawkins et al., 2006).

Kandel discovered that learning experience in *Aplysia* involved two distinct types of memory storage mechanisms, a short-term component as well as a long-term component. Short-term memory (STM) is described as a transient memory phase lasting minutes to hours that involves the covalent modification of pre-existing proteins by a variety of kinases (Hawkins at al., 2006), whereas long-term memory (LTM) is defined as an enduring memory phase lasting days, weeks or longer, which requires protein synthesis and results in the growth of new synapses (Flexner et al., 1963; Drain et al., 1991; Alberini et al., 1994; Hawkins et al., 2006; Alberini et al., 2009). Through electrophysiological and biochemical experiments on the snail tail it was discovered that a single noxious (sensitising) stimulus to the tail of *Aplysia* evoked release of the neurotransmitter

serotonin (5-HT) from modulatory neurons (Castellucci et al., 1970; Marinesco and Carew, 2002). Serotonin binds to its receptor on the sensory neurons and elicits an increase in the level of the second messenger cyclic adenosine monophosphate (cAMP) which activates the cAMP-dependent protein kinase A (PKA) which in turn phosphorylates a variety of targets including potassium (K^+) channels (Abel and Lattal, 2001). Closure of the K^+ channels by PKA blocks the ions from exiting the neurons, preventing repolarisation of the membrane. The action potential generated by depolarisation of the neurons reaches the synapses and triggers calcium (Ca^{++}) influx through voltage-dependent calcium channels (Benfenati, 2007) leading to an increased amount of neurotransmitter release at the synaptic connection between the sensory and motor neuron (Abel and Lattal, 2001). This is thought to be the molecular process underpinning STM.

The persistent activation of the sensitisation pathway by stronger stimuli or repeated stimulation, leads to a persistent increase in the level of cAMP and PKA. The catalytic subunit of PKA recruits a mitogen-activated protein kinase (MAPK), p42, forming a complex that translocates into the nucleus and phosphorylates transcription factors such as cAMP response element binding protein (CREB). Phosphorylated CREB binds the cAMP response element (CRE) on specific promoters and induces transcription.

Therefore, LTM requires changes in gene expression and protein synthesis, which results in growth of new synaptic connections, which facilitate maintenance of LTM. On contrast, STM does not require protein synthesis and it is the result of transient changes in activity and/or localisation of proteins within a neuron, which results in increased neurotransmitter release, i.e. a transient increase in synaptic strength.

As per Kandel's assumption, subsequent studies have shown that most of the upstream signalling cascade leading to CREB activation appears to be conserved through evolution and many aspects of the role of CREB in synaptic plasticity described in invertebrates have been observed in mammalian brains (Kandel, 2001, 2004, 2012). A schematic of the molecular pathway that underpins STM and LTM in both invertebrates and vertebrates is shown in Figure 1.2

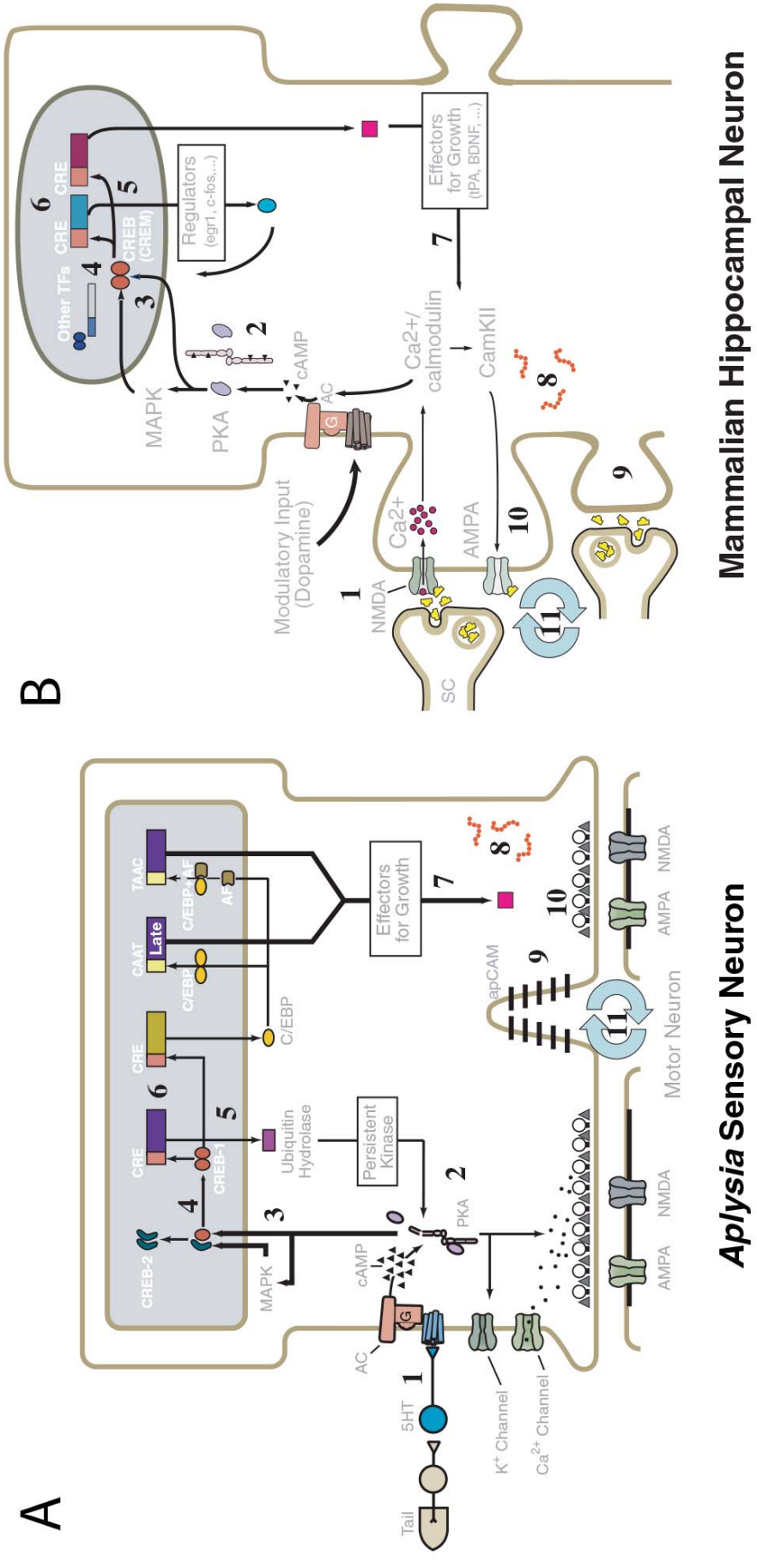
A
Aplysia Sensory Neuron
Tail
5HT
1
AC
G
cAMP
MAPK
3
4
CREB-2
CRE
CREB-1
5
6
CRE
CAAT
Late
C/EBP
TAAC
C/EBP
AP1
C/EBP
Ubiquitin Hydrolase
Persistent Kinase
PKA
2
Effectors for Growth
7
8
apCAM
9
10
11
Motor Neuron
AMPA
NMDA
K+ Channel
Ca2+ Channel
B
Mammalian Hippocampal Neuron
Modulatory Input (Dopamine)
1
NMDA
Ca2+
AMPA
10
11
SC
9
Ca2+/ calmodulin
CamKII
8
cAMP
AC
G
MAPK
PKA
2
Other TFs
4
3
6
CRE
CRE
5
CREB (CREM)
Regulators (egr1, c-fos,...)
Effectors for Growth (tPA, BDNF, ...)
7

Figure 1.2 Conserved molecular mechanisms of memory storage in *Aplysia* sensory neuron (A) and in mouse CA1 hippocampal neuron (B). 1. Synaptic stimulation induces transient release of serotonin (5-HT) which binds to cell surface receptors on the sensory neuron and fosters activation of adenyl cyclase (AC) which stimulates production of cAMP. The second messenger cAMP binds to the regulatory subunit of PKA, resulting in activation of its catalytic subunit. PKA phosphorylates proteins involved in neurotransmitter release and K^+ channels leading to reduction of K^+ outward current, broadening of the action potential and increased Ca^{++} influx. This results in an increase in the synaptic strength and enhanced neurotransmitter release leading to a transient increase in activation of the following neuron. These steps lead to short-term facilitation resulting in memories that last few minutes or hours, i.e. short-term memory. In hippocampal pyramidal neurons (B), synaptic release of glutamate triggers Ca^{++} influx through N-Methyl-D-aspartic acid receptors (NMDARs) and induction of Ca^{++}/calmodulin and CaMKII (other than AC and cAMP). These second messengers mediate the transient reinforcement of synaptic connections by covalent modifications of channel activation and the enhancement of neurotransmitter release at presynaptic terminals. 2. When synaptic stimulation reaches a certain threshold or is repeated a number of times, it results in a persistent increase in the level of cAMP leading to long-term facilitation requiring synthesis of proteins. At the molecular level, this more robust pattern of stimulation causes the catalytic subunit of PKA to recruit p42 MAPK and both translocate into the nucleus where they phosphorylate nuclear targets including other kinases that, in turn, phosphorylate transcription factors and activate gene expression. 3-6. Activation of nuclear transcription factors including CREB, leads to the expression of immediate response genes such as ubiquitin hydrolase. These transcription factors activate other downstream genes resulting in growth of new synaptic connections. 7. Synaptic capture of newly synthesized gene products. 8. Local protein synthesis at active synapses. 9. Synaptic growth and formation of new synapses. 10. Activation of pre-existing synapses. 11. Perpetuation mechanisms that lead to memory persistence.

Image source: Barco et al., 2006, Journal of Neurochemistry, protected by copyright (Wiley Materials). Permission obtained by licenced content publisher John Wiley and Sons, through the Copyright Clearance Centre Inc. permission included in this thesis.

1.3 The use of animal models to study neurodegenerative processes: *Drosophila melanogaster* the model system

Similar to the study of other biological processes, the application of animal models has been proved to be a powerful approach to investigate the molecular mechanisms that underpin cognitive functions such as learning memory. Kandel's reductionist approach through the use of a simple animal model paved the way to the now common use of invertebrates for the dissection of genetic and molecular pathways of cognitive processes, which are conserved across the animal kingdom (Kandel, 2001). Noteworthy is the fact that the use of animals deriving from a vast variety of species (snails, flies, bees, fishes, mice, rats, cats, dogs, birds) connotes a complementary strategy that has successfully led to a great advance and progress on the knowledge about the nervous system and the genetic and molecular pathway underpinning its functions, allowing researchers to scrutinise and beginning to rebuild the evolving path of the human brain.

The fruit fly *Drosophila melanogaster* has become a leading model system for neuroscientific research due the reproducibility of associative learning and memory paradigms that have been developed in combination with the ability to precisely manipulate gene expression in a temporal and spatial manner (Dukas, 2008; Sarkar, 2013).

Approximately 75% of the genes implicated in human genetic disorders are conserved in *Drosophila* (Bellen et al., 2010; Pandey and Nichols, 2011) and most genes involved in learning and memory are conserved across the animal kingdom (Kandel, 2001, 2012). In addition, the genome of *Drosophila* has been completely sequenced (Berkeley *Drosophila* Genome Project, BDGP, 2000) making it possible to generate transgenic lines in order to knockdown or overexpress any genes of interest. The most valuable feature of the fruit fly is the capacity to provide a platform for unbiased genetic screens to detect components of learning and memory pathways as well as components of neuro-pathological pathways (Sang and Jackson, 2005; Jackson, 2008). Indeed, genome-wide screen can be easily performed in the fly, whereas such an approach would be very difficult in rodents or humans. Furthermore, well established and characterised behavioural paradigms to measure learning and memory, have been developed that are reproducible and the combination of cognitive tests and genetic manipulation allow the identification and elucidation of the role of specific genes in such complex traits, making

the fly a bridge between basic research and clinical research with the prospect to provide new tools for diagnosis and medical treatments of cognitive conditions (Bier, 2005).

1.3.1. The mushroom body of *Drosophila melanogaster*: a brain structure involved in memory

Despite its small size, *Drosophila* presents a highly organised and complex brain containing approximately 200,000 neurons. Within this articulated network of neurons, the mushroom body (*corpora peduncolata*) is a structure that is fundamental for learning and memory. The mushroom body is a paired neuropile structure firstly identified by F. Dujardin in 1850, who described these brain regions in ants and bees comparing them to the vertebrate cerebral cortex and considered the site of insect intelligence (Dujardin, 1850; Heisenberg, 1998). Mushroom bodies comprise two classes of neurons: extrinsic (input and output) and intrinsic. The intrinsic neurons of the mushroom body are the Kenyon cells which provide the fundamental computational properties of the mushroom body (Yang et al., 1995). In *Drosophila* the mushroom body contains approximately 2500 Kenyon cells per hemisphere. The number of these cells differ greatly according to the species, ranging from 170,000 in bees to 230,000 in cockroaches (Heisemberg, 2003; Fahrbach, 2006). Cell lineage studies and clonal analysis have demonstrated that the Kenyon cells are produced by four equipotent neuroblasts each occupying a distinct position in the developing mushroom body cortex which generate three different populations of Kenyon cells in a sequential order (Ito et al., 1997; Lee et al., 1999) (Figure 1.3A). The γ neurons are the earliest born, from larval stage to mid-third instar larvae. Axons of those neurons form horizontal lobes (Crittenden et al., 1998). The α'/β' neurons originate between mid-third instar larval stage and puparium formation and the α/β neurons are born after puparium formation (Yang et al., 1995; Lee et al, 1999; Kunz et al., 2012). Axons of α/β and α'/β' neurons bifurcate into vertical α and α' lobes and horizontal β and β' lobes (Crittenden et al., 1998) (Figure 1.3). Studies using the P[GAL4] enhancer trap technique or the use of memory mutants, have revealed the neuronal complexity and organisation of the Kenyon cell subtypes, which exhibit a diverse and unique genetic identity with a combination of transcription factors by which they are individually identifiable in the brain (Yang et al., 1995; Aso et al., 2009; Kunz et al.,

2012). In addition, they play functionally distinct roles in learning and memory (Guven-Ozkan and Davis, 2014).

The cell bodies of these neurons reside in the dorsal-posterior area of the brain as well as their dendrites that conglomerate into a globular region beneath the cell bodies known as the calyx (Zhu et al., 2003; Kunz et al., 2012) (Figure 1.3). The axons of the Kenyon cells project towards the anterior portion of the brain via a dense structure called peduncle, forming five distinct lobes of the mushroom body, the vertical α and α′ lobes and the medial β, β′ and γ lobes (Crittenden et al., 1998; Lee et al., 1999; Aso et al., 2009; Kunz et al., 2012) (Figure 1.3A).

Single gene mutations causing defective mushroom body anatomy have been shown to interfere significantly with olfactory associative learning (Heisenberg et al., 1985) and expression of known learning genes such as *dunce* and *rutabaga* occurs predominantly in the mushroom body (Nighorn et al., 1991; Han et al., 1992; Davis, 1993). In addition, chemical ablation of the mushroom body neuroblasts through hydroxyurea treatment at early stages of development results in profound olfactory learning deficits in the adult fly (De Belle and Heisenberg, 1994) and in consolidation of short and long-term associative memory (McBride et al., 1999) implicating the mushroom body as a critical region for memory formation. However, the role of the mushroom body is not completely clear yet and many studies focus not only on the identification of genes important for a given behaviour but also in the detection of the brain regions in which these genes operate in order to expand the knowledge so far acquired on the roles and functions of these brain structures (Zars, 2000).

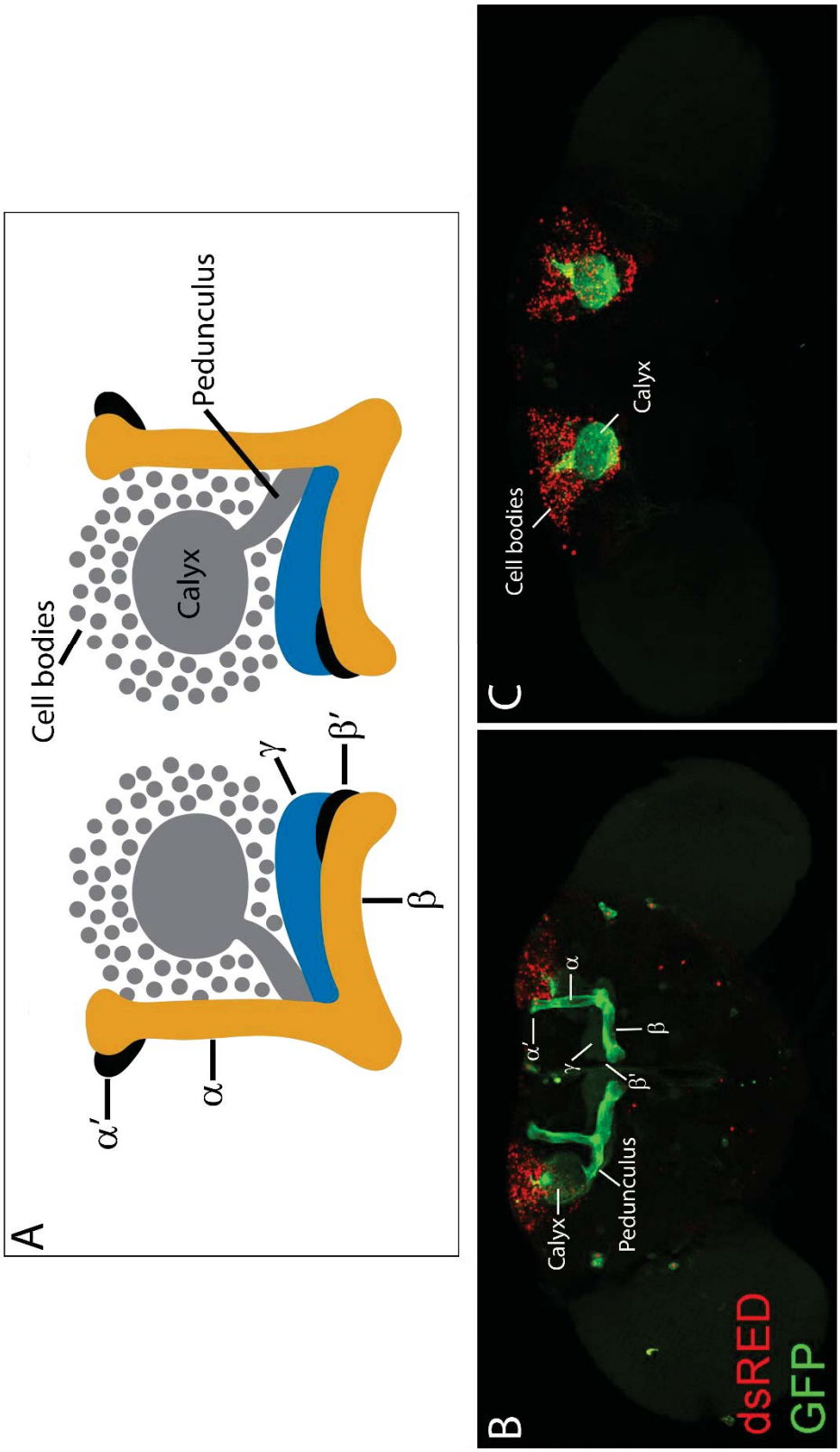
A
Cell bodies
Calyx
Pedunculus
α′
α
γ
β′
β
B
dsRED
GFP
Calyx
Pedunculus
α′
α
γ
β′
β
C
Cell bodies
Calyx

Figure 1.3 The mushroom body of *Drosophila melanogaster*. (A) Cartoon showing the mushroom body intrinsic neurons organisation. Anteriorly, the Kenyon cells project their axons via the pedunculus and form three distinct lobes named γ, α'/β', α/β. The cell bodies of the Kenyon cells are concentrated in the posterior side of the brain and extend their dendrites into a region known as the calyx. (B-C) Confocal micrograph of *elav-GAL4; UAS-CD8::GFP; dsRed* brains. GFP is linked to CD8, a membrane protein which allows visualisation of the entire brain architecture while dsRed is a nuclear marker of neuronal cells. (B) The anterior portion of the brain is shown. (C) The posterior side of the brain is presented. Confocal images generated by Dr Fitzsimons (Fitzsimons et al., 2013).

As previously mentioned, the mushroom body comprises different classes of neurons and the intrinsic mushroom body cells, the Kenyon cells, are not the sole neurons involved in learning and memory. Indeed, several studies have concentrated on studying the role of extrinsic neurons in the regulation of learning and memory, especially in the context of the olfactory memory circuitry.

Mushroom body extrinsic neurons are neurons that innervate the mushroom body or, as per Ito and colleagues definition, "the term extrinsic neuron is conferred on neurons that have processes in the mushroom body and projections extending to or from other brain regions" (Ito et al., 1998). Thus, the mushroom body receives information from input neurons and transmits information to output neurons. The dopaminergic neurons are the most prevalent input modulatory neurons in the mushroom body and project their axon terminals to specific compartments of the mushroom body lobes (Aso et al., 2014a). Dopamine receptors in the Kenyon cells are necessary to form olfactory memories (Kim et al., 2007) and dopaminergic neuron activity is required during learning to transmit information about odour aversive conditioning (Schwaerzel et al., 2003) and for long-term odour-reward memories (Ichinose et al., 2015). Moreover, a specific class of dopaminergic neuron, aSP13, was found to be critical for courtship learning (Keleman et al., 2012). These neurons convey a learning signal to the mushroom body γ neurons through the DopR1 dopamine receptor and this induces lasting changes in the male internal processing that leads to discrimination between mated females and virgins (Keleman et al., 2012).

Different classes of dopaminergic neurons have been identified and found to be involved in STM and LTM in *Drosophila* (Yamagata et al., 2015; Ichinose et al., 2015)

as well as in mammals (Kim et al., 2014) indicating a conservation in the memory processing across the animal kingdom.

Dorsal anterior lateral neurons are another class of input neurons required for LTM storage since de novo protein synthesis in these neurons was shown to be critical for normal LTM formation. Indeed, proteins that are necessary for LTM including CaMKII, Tequila and Period, have been detected to localise in these neurons and transcriptional activity of *CamKII* and *Period* was elevated after training in the aversive olfactory associative paradigm, suggesting these neurons are a site of protein synthesis (Chen et al., 2012).

While the input circuitry has been well characterised, there is a dearth of information regarding the output neurons, which have been described in detail only recently by Rubin and colleagues in two landmark papers (Aso et al., 2014a, b). They adopted a genetic approach and anatomical techniques to thousands of different transgenic flies to map the neurons of the mushroom body. They found that approximately 2000 Kenyon cells converge the information on only 34 output neurons. These neurons extend their dendrites to the axons of the Kenyon cells and project axons to neuropils outside the mushroom body providing loci for the convergence of all information necessary for learned associative responses. Moreover, through the use of molecular genetics to block neuronal activity and the use of light to activate neurons, i.e. optogenetics, the roles of the output neurons in the mushroom body were examined revealing that distinct groups of output cells must be activated for flies to avoid odours that have been associated with punishment. This suggests that the output cells are required to signal whether a stimulus should be approached or avoided (Aso et al., 2014b).

Although these findings were mainly collected from dissection of the olfactory conditioning circuitry, overall a very complex and intricate picture emerges on the function of such neural circuitries in the formation of memory, a process that does not rely on a single brain structure but rather on the collaboration and coordinated activity of different neuropils within the fly brain.

1.3.2 *Drosophila* and its genetic tractability

The ability to generate transgenic flies that can be used to manipulate gene expression or neuronal circuitry makes *Drosophila* a powerful model for genetic analysis of neuronal

pathways. Genetic manipulation in *Drosophila* is now routine and transgenic fly lines for overexpression or knockdown of a gene of interest can be generated in the laboratory or purchased from stock centres. One of the most powerful genetic tools is the enhancer trapping approach in which endogenous promoters are harnessed to provide tissue-specific expression allowing for a precise manipulation of gene function in specific cells of *Drosophila* (Meinertzhagen et al., 1998). This approach led to the development of the yeast-based GAL4/Upstream Activating Sequence (UAS) binary system which allows for targeted gene expression in specific cell populations (Brand and Perrimon, 1993; McGuire et al., 2004) and is the gold standard for genetic manipulation of gene expression in a temporal and spatial fashion. GAL4 encodes for a transcription factor of 881 amino acids which binds to UAS cis-regulatory sites and activates transcription of downstream genes (Fischer et al., 1988). In 1993, Brand and Perrimon designed the bipartite GAL4/UAS system for targeted gene expression as it allows the selective activation of any cloned gene in a tissue- and cell-specific manner (Brand and Perrimon, 1993). In the bipartite system, two individual fly lines each harbour one of the components. One line carries a transgene construct containing the UAS element and the downstream gene of interest. The other line contains GAL4 under the control of a minimal promoter and an enhancer that drives expression in the tissue of interest. This line is also known as a GAL4 driver. In order to activate expression of the gene of interest, the two lines are mated (Figure 1.4) and the F1 progeny expresses the gene of interest in a tissue-specific manner reflecting the pattern of GAL4 expression (Phelps and Brand, 1998; Duffy, 2002).

The utility of maintaining the GAL4 and UAS elements in separate lines is that many hundreds of GAL4 driver lines have been developed and characterised, allowing UAS transgene expression in almost all tissues via crossing to the appropriate GAL4 driver. A number of drivers is available for specific subregions of the brain, allowing investigation of those areas in a more detailed manner (Aso et al., 2009).

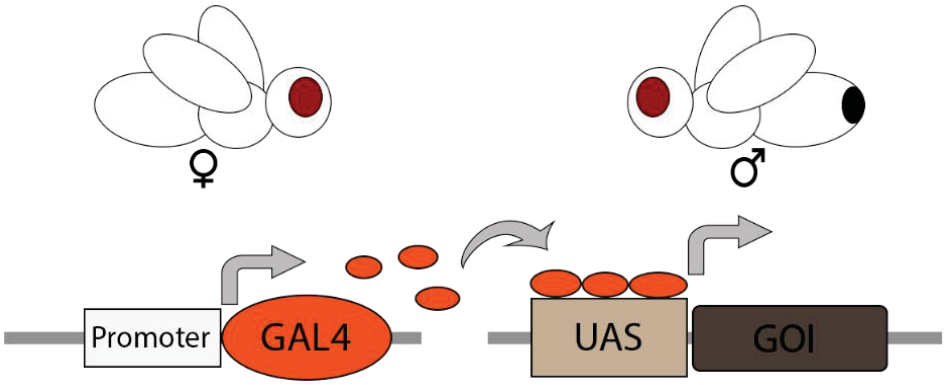

Figure 1.4 The GAL4/UAS binary system in *Drosophila*. This system allows for directed tissue-specific expression of a gene of interest by linking a specific tissue-promoter to the transcription factor GAL4. The gene of interest is cloned downstream the UAS element and GAL4-mediated activation of UAS-gene is activated by means of a genetic cross between the two lines.

This tool has been further adopted in order to allow control of transgene expression both in specific cells during distinct phases of development. The temporal and regional gene expression targeting (TARGET) system is based on the GAL4/UAS system with the inclusion of $GAL80^{ts}$, a temperature-sensitive mutant which binds to GAL4 and represses its transcriptional activity at 18°C (Suster et al., 2004; McGuire et al., 2004; del Valle Rodríguez et al., 2012). At higher temperatures, i.e. 29-30°C, the repressive activity of $GAL80^{ts}$ is relieved and GAL4-dependent expression is induced (Figure 1.5). This system allows for spatiotemporal gene expression by selecting the appropriate GAL4 driver and manipulating the temperature at which the flies are raised, transgene expression can be limited to the desired stage of development. This is of particular benefit in the study of memory formation as it distinguishes between developmental and adult-specific processes.

The GAL4/UAS bipartite system can be used to target expression of RNAi or a wild-type or mutant form of a gene or for ectopic expression of non-*Drosophila* genes, e.g. human Amyloid-beta (Aβ) disease models. The GAL4/UAS system can also be used to induce effectors such as inhibitors of neurotransmission, e.g. coupling it with the *Shibire* temperature sensitive mutant that blocks neurotransmission (Kitamoto, 2001), or the channel rhodopsin that is activated by light, for optogenetic studies and manipulation of neuronal transmission (Riemensperger et al., 2016). These effectors can then be combined

with a particular GAL4 driver to investigate whether output from particular neuronal circuit is required for behaviour.

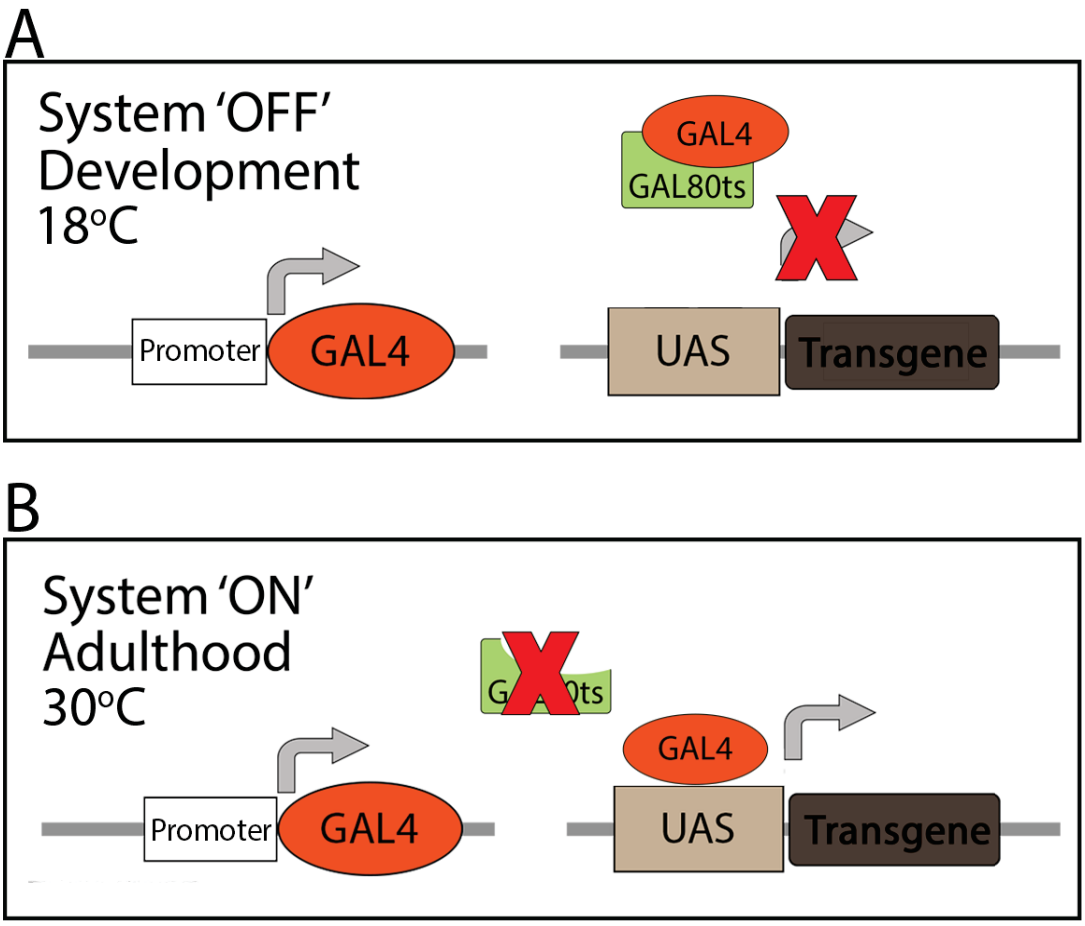

Figure 1.5 TARGET system. (A) At the temperature of 18°C, the temperature-sensitive mutant GAL80^{ts} prevents binding of GAL4 to the UAS element, thus preventing GAL4-dependent transcription. (B) At 30°C the GAL80^{ts} mutant in unable to bind GAL4 due to conformational changes thus GAL4 binds the UAS and induces transcription of the transgene. Abbreviations: UAS = upstream activating sequence.

The GAL4/UAS system is particularly useful for RNAi-mediated knockdown of gene expression. Libraries of fly strains bearing transgenes for expression of hairpin RNAs have been established and are commercially available in stock centres such as the Vienna Drosophila Resource Centre, which has generated and possesses a major

collection of *Drosophila* UAS-RNAi inducible strains, covering 88.2% of the *Drosophila* genome.

1.3.3 The use of behavioural paradigms to test learning and memory

As for every other organism, fruit flies respond behaviourally to a variety of stimuli surrounding them including temperature (Dillon et al., 2009), humidity (Perttunen and Erkilä, 1952; Enjin et al., 2016), light (Hardeland, 1971; Rieger et al., 2007; Vinayak et al., 2013), and chemicals e.g. pheromones (Touhara and Vosshall, 2009), through vision, olfaction, taste, thermosensors and humidity sensors. Flies are able to learn and memorise these cues, thus adapting their behavioural response according to the nature of the stimuli, i.e. rewarding or punitive (Waddell and Quinn, 2001; Vang et al., 2012). As cellular mechanisms underlying simple forms of learning and memory are evolutionary conserved between invertebrate and vertebrate systems (Kandel, 2001), fruit flies have been adopted to dissect behavioural and genetic pathways of learning and memory. Their behavioural repertoire and neural system renders them amenable to the study of genes involved in these processes and are an advantageous organism to perform memory assays since numerous flies of "identical genotype can be tested so that behavioural measurements can be made on populations rather than individuals, yielding instant statistics" (Quinn et al., 1974). Classical conditioning assays of associative memory have been developed and include olfactory conditioning (Quinn, 1974; Tully and Quinn, 1985) and the conditioned courtship suppression paradigm (Siegel and Hall, 1979) which are the most frequently employed assays.

The classical olfactory conditioning for *Drosophila* was developed by Quinn (1974). This paradigm is a type of Pavlovian conditioning which requires flies to associate an odour (conditional stimulus) with either a negative (electric shock in case of aversive conditioning) or positive (sucrose, in case of rewarding conditioning) stimulus (unconditioned stimulus). Groups of flies are alternatively exposed to two different odours, one of which is associated with the unconditioned stimulus and flies learn to associate the odour with the unconditioned stimulus. Memory of the conditioning is tested in a T-maze where the trained flies choose between the two odours (Figure 1.6). A performance index is calculated based on the percentage of flies avoiding (aversive conditioning) or preferring (rewarding conditioning) the odour associated with the unconditioned stimulus, to provide a quantitative measurement of memory (Pitman et al.,

2009). By increasing the time between the acquisition and testing, short or long lasting forms of memory can be evaluated (Pitman et al., 2009).

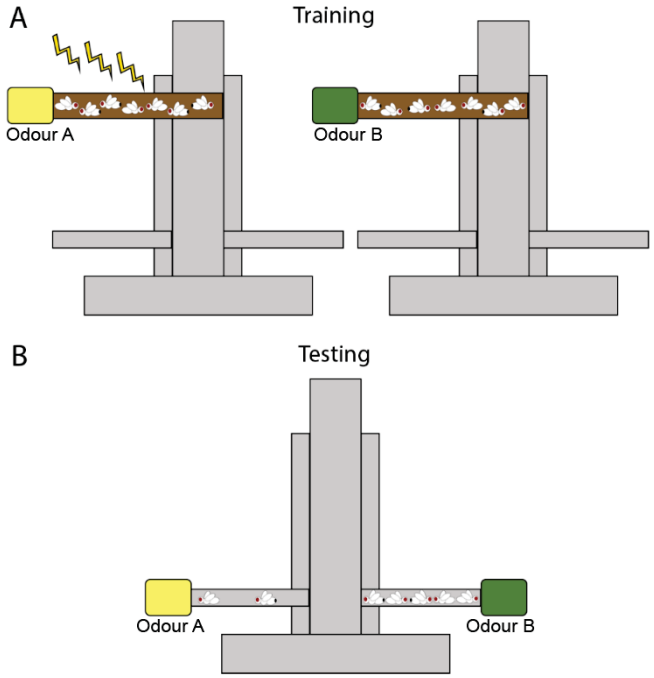

Figure 1.6 Aversive odour conditioning assay. Schematic representation of the aversive odour conditioning paradigm. (A) Training session. A group of flies is trained by associating an odour (odour A) to an aversive stimulus (electroshock) whereas odour B is not associated with the noxious stimulus. (B). Testing session. After training, flies are placed in a T-maze connected to the two different odours and flies are tested for memory retention according to the choice they apply in the maze. The percentage of flies avoiding the aversive odour (odour A in this example) is a measure of the memory performance.

The conditioned courtship suppression paradigm developed by Siegel and Hall in 1979, is an ideal test as it does not require complex equipment and it is reproducible. It is based on natural sexual behaviour and it involves only natural stimuli, relying on olfaction, visualisation and gustation. Courtship is a complex process in which a male and a female reciprocate visual, chemosensory (olfactory and gustatory), and auditory stimuli (Hall, 1994). Courtship-stimulating pheromones, the predominant cuticular hydrocarbons on the female cuticle, act at a very short distance, i.e. a few millimetres, and are perceived by contact (gustation) and olfaction (Siwicki et al., 2005). Courtship suppression is a type of associative memory in which male courtship behaviour is modified by experience

with an unreceptive female. Freshly mated females are unreceptive to courtship activity of another male, which comprises a sequence of stereotyped behaviours: following the female, tapping her with the forelegs, vibrating one wing and attempting copulation (Figure 1.7).

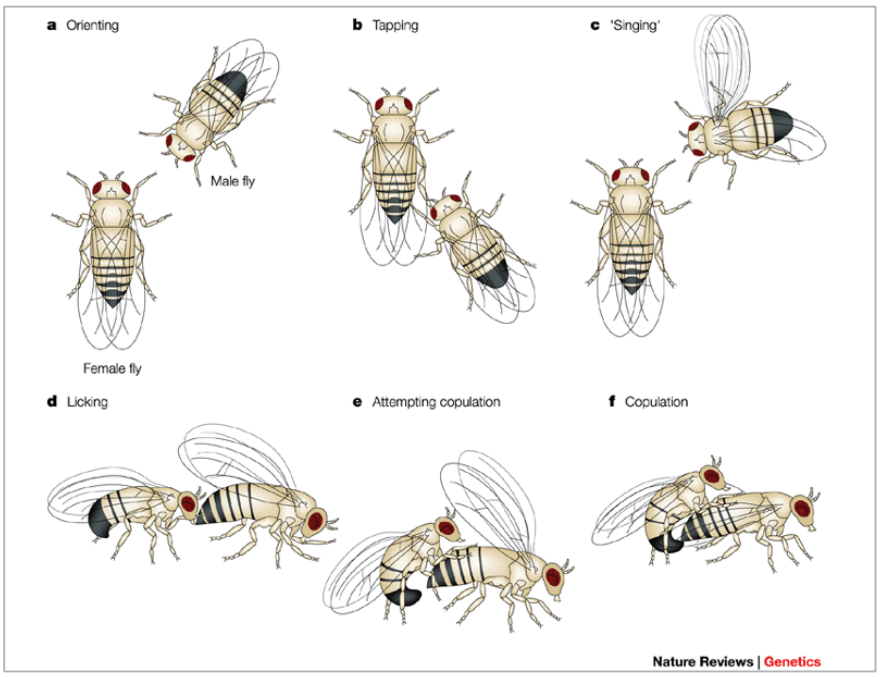

Figure 1.7 Sequence of courtship behaviour steps undertaken by male fruit flies. a) The male fruit fly orientates towards the female, b) then follows and taps her, c) sings a species-specific courtship song by vibrating one wing and d) eventually, he licks the genitalia of the female, and e) bends his abdomen in an attempt at copulation with the female. Image source from Sokolowski, 2001, Nature Reviews, protected by copyright (Nature Reviews Genetics). Permission obtained by licenced content publisher Nature Reviews Genetics, through the Copyright Clearance Centre Inc. Permission included in this thesis.

Whereas a virgin female generally responds to this behaviour by mating, males with intact memory learn that they have been rejected by a female and reduce their courtship activity compared to sham (non-trained) males (Siegel and Hall, 1975; McBride et al., 1999; Keleman et al., 2009; Ejima and Griffith 2010; Fitzsimons et al., 2011). This assay allows measurement of short and long-term memory depending on the hours a male spends with the mated female during the training session. For short-term memory, pairing

the male with a mated female for one hour results in a short-term suppression of courtship lasting for about three hours (Siegel et al., 1979; Pitman et al., 2009). Long-term memories last for at least a few days and are formed by coupling the male with a mated female for at least five to seven hours continuously (McBride et al., 1999; Keleman et al., 2007; Pitman et al., 2009). After 24 hours, all males, trained and sham, are coupled with new mated females and courtship activity is measured as the percentage of time spent courting (courtship index, CI). A memory index (MI) is calculated as the ratio between the CI of every trained male by the mean value of the CI of the sham males of the same genotype. A range of values between zero and one is obtained, with zero indicating the highest memory score possible and one indicating memory not different from a sham control (Ejima and Griffith, 2007; Fitzsimons et al., 2011) (Figure 1.8). For every experimental procedure, sham males of each genotype are housed alone during the training session and serve as controls to verify that courtship activity of a specific genotype is intact.

Conditioned courtship suppression shares many of the molecular and physiologic mechanisms involved in classical olfactory conditioning. As previously described, in the classical olfactory conditioning flies are trained to associate a conditioned stimulus, e.g. an odour, with a an unconditioned stimulus, e.g. an electric shock or a sucrose reward, such as the flies modify their behaviour accordingly when the conditioned stimulus is presented alone (Quinn et al. 1974; Davis 2005; Busto et al. 2010). In courtship conditioning, pheromones associated with mature virgin female flies serve as the conditioned stimulus, whereas an aversive pheromone cue associated with mated females serves as the unconditioned stimulus (Siegel and Hall 1979; Tompkins et al. 1985; Mehren et al., 2004; Ejima et al., 2005; Winbush et al., 2012). The failure to successfully copulate may also act as an unconditioned stimulus for associative courtship memory formation (Mehren et al. 2004; Winbush et al., 2012).

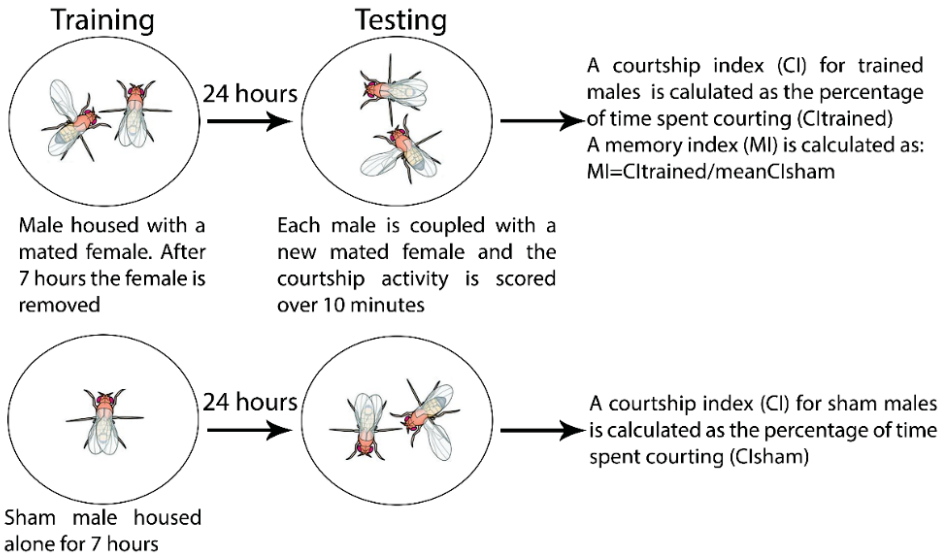

Figure 1.8 Conditioned courtship suppression assay. In order to measure LTM, a training session is conducted by coupling individual males with a freshly mated female in a specific training chamber for a period of seven hours, while sham males are housed alone and serve as controls to verify that courtship activity of a specific genotype is intact. After 24 hours, all males, trained and sham, are coupled with new mated females in the testing chambers and courtship activity is measured over a period of ten minutes, as the percentage of time spent courting (courtship index, CI). A memory index (MI) is then calculated as the ratio between the CI of every trained male and the mean value of the CI of the sham males of the same genotype. A range of values between zero and one is obtained, with zero indicating good memory and one indicating memory similar to a sham control, e.g. no memory.

When a formerly conditioned male encounters the conditioned stimulus in a subsequent trial, the male reduces courtship in expectation of the unconditioned stimulus. Long-term courtship suppression is distinct from aversive and appetitive olfactory conditioning in that flies are trained to modify an ethologically important behaviour in response to repeated and prolonged exposure to a complex stimulus. However, many of the molecular mechanisms underlying long-term memory are conserved between the learning paradigms, such as the activation of cAMP-PKA-CREB pathway that leads to increased gene transcription and protein synthesis necessary for LTM formation in the first few hours after training (Roth et al. 2010; Winbush et al., 2012).

1.4 The role of epigenetics in learning and memory formation

In eukaryotes, genetic information is organised into a higher order structure known as chromatin, whose role is to facilitate packaging of the DNA inside the nucleus and to control DNA replication, recombination, repair and transcription. The core structure is the nucleosome composed of 146 base pairs of DNA wrapped around an octamer of histone proteins (histones 2A, 2B, 3, and 4 with two copies of each molecule). The interaction between histones and DNA is partially mediated by the N-terminus of histone proteins which are subjected to biochemical changes on their lysine residues, e.g. acetylation, ubiquitination, SUMOylation, phosphorylation (Roth and Sweatt, 2009; Kleefstra et al., 2014). These changes are catalysed by chromatin modifiers which covalently modify histone proteins altering the strength of the DNA-histone association (Morrison et al., 2007), which regulates accessibility of co-activators to their DNA targets and thus activation of gene expression. Such post-translational modifications of the chromatin fall under the definition of epigenetics and are able to influence activity-dependent changes in gene expression (Roth and Sweatt, 2009) resulting in long-lasting changes in phenotypes that are not encoded in the DNA sequence of a cell (Peixoto and Abel, 2013). Epigenetic modifications also include DNA alterations, e.g. methylation, which is not known to occur in *Drosophila* (Dunwell and Pfeifer, 2014).

1.4.1 Histone Acetyltransferases (HATs)

Acetylation is a reversible modification involving two type of chromatin modifying enzymes: histone acetyltransferases (HATs) and histone deacetylases (HDACs).

HATs add an acetyl moiety to the ε amino group of conserved N-terminal lysine residues (Morrison et al., 2007; Haggarty et al., 2011) neutralising the positive charge of the histone residues. This leads to a reduced attraction between histones and the negatively charged DNA resulting in a relaxation of chromatin which is thus accessible to transcription factors and correlates with transcriptional activation. In contrast, HDACs remove acetyl groups, thereby enhancing the attraction between DNA and histones that renders the chromatin inaccessible to transcription factors (Figure 1.9).

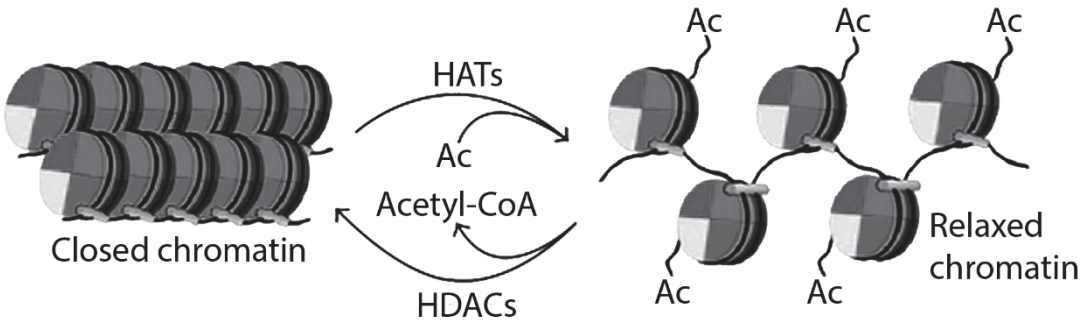

Figure 1.9 Acetylation-deacetylation mechanism. Schematic representation of acetylation/deacetylation of histone proteins. Histone acetyltransferases (HATs) add acetyl-CoA groups to the lysine residues within the N-tails of histones leading to relaxed state of chromatin (euchromatin). On the contrary, histone deacetylases (HDACs) remove the acetyl groups provoking a tighter association between histones and DNA that results in a closed chromatin structure (heterochromatin).

In recent years, genome-sequencing studies in human neurodevelopmental disorders have uncovered mutations in many genes encoding chromatin modifiers (Ronan et al., 2013). Epigenetic mechanisms, especially through acetylation and deacetylation of the histone tails, are emerging as master regulators of cognitive abilities such as learning and memory (Levenson and Sweatt, 2005). The interest in their functions has increased since evidence reveals that these mechanisms are employed in post-mitotic neurons to consolidate and stabilise cognitive-behavioural memories (Day and Sweatt, 2011).

A correlation between histone acetylation and memory formation was initially observed in a pioneering study by Schmitt and Matthies (1979), who used radioactive acetate incorporation to demonstrate an increase in histone acetylation in the mouse hippocampus after training when compared to untrained subjects. Subsequent studies have established that the increase in histone acetylation correlated with enhanced memory formation. Mice heterozygous for the histone acetyltransferase CREB binding protein ($CBP^{+/-}$) displayed impairments in histone acetylation, LTM formation and late long-term potentiation, which is a persistent increase in synaptic strength. The memory impairment could be reversed by administration of HDAC inhibitors and by enhancing expression of CBP-dependent genes (Alarcon et al., 2004). CBP is a co-factor of many transcription factors and possesses acetyltransferase activity involved in LTM consolidation. Furthermore, transgenic mice with a mutated form of CBP in which acetyltransferase activity was hindered, displayed impaired consolidation of STM to LTM, whereas

acquisition of new information and STM was normal, suggesting that histone acetylation is involved in consolidation of memory formation process (Korzus et al., 2004). A further study showed that in rats, increased histone acetylation though the use of HDAC inhibitors, enhanced long-term potentiation at the synapse in the hippocampus in a contextual fear conditioning paradigm (Levenson et al., 2004).

By contrast, histone deacetylation correlates with cognitive impairments and suppression of memory formation (Abel et al., 1998; Morris and Monteggia, 2013) and a number of studies show that pharmacological inhibition of HDAC activity enhances learning and memory (described in more detail in section 1.4.2.2).

1.4.2 Histone Deacetylases (HDACs)

Unlike HATs, HDAC family members display a structural diversity which confers heterogeneity of function therefore rendering HDACs challenging but promising targets for drug discovery and therapeutic intervention for a variety of disease including neurodegenerative conditions and cancer (Abel and Zukin, 2009). A striking feature of these enzymes, and a reason why their characterisation is a current focus, is that they deacetylate a variety of non-histone proteins, which means the role of HDACs is not limited to histone modifications but rather they have been shown to regulate different cellular processes in both the nucleus and the cytoplasm (Glozak et al., 2005; Brandl et al., 2009; Delcuve et al., 2012). Indeed, phylogenetic analysis of bacterial HDAC relatives suggests that they precede the evolution of histone proteins and raises the possibility that the primary activity of some "histone deacetylase" enzymes is directed against non-histone substrates (Gregoretti et al., 2004). Accumulating evidence shows the involvement of HDACs in the regulation of fundamental neurological functions such as neuronal growth, synaptic plasticity, learning and memory formation (Grégoire and Yang, 2005; Penney and Tsai, 2014; Fitzsimons, 2015; Volmar and Wahlestedt, 2015).

In mammals, eighteen different HDACs have been identified and categorised into four different classes (I, II, III and IV) according to their sequence similarity to the yeast *Saccaromyces cerevisiae* HDAC counterparts (Figure 1.6).

Class I HDACs are closely related to the yeast class I HDAC transcriptional regulator RPD3 (Reduced potassium dependency 3). This class includes: HDAC1, 2, 3, 8, which are all ubiquitously expressed and are also highly expressed in the brain. HDAC1 and

HDAC2 are found in neuronal progenitors and in glia, whereas HDAC3 localises in both the cytoplasm and nucleus of neurons throughout the brain. HDAC8 is highly expressed in the liver (Buggy et al., 2000; De Ruijter et al., 2003; Lucio-Eterovic et al., 2008). Class I HDACs all possess high deacetylase activity which contribute to the majority of histone deacetylation in the cell (Morrison et al., 2007; Morris and Monteggia, 2013).

Class II HDACs share homology of the catalytic domains with yeast HDA1. Class II HDACs are tissue-specifically regulated able to shuttle between the nucleus and the cytoplasm via intrinsic nuclear import/export signals (Miska et al., 1999; McKinsey et al., 2000a, 2000b; Grozinger and Schreiber, 2000; Wang et al, 2000; McKinsey et al., 2001; Wang and Yang, 2001; Miska et al., 2001; Kao et al., 2001). These enzymes possess a weak enzymatic activity by themselves. Indeed several studies showed that class II HDACs require recruitment of class I enzymes to carry out deacetylase activity and to form repressive complexes in the nucleus (Kao et al., 2000; Fischle et al., 2001, Fischle et al., 2002). Class II HDACs can be divided into two subgroups: class IIa including HDAC4, 5, 7, 9, and class IIb comprising HDAC6 and 10.

Class IIa HDACs are characterised by a large N-terminal domain possessing conserved motifs which mediate protein-protein interaction. These include a MEF2 binding domain that mediates binding of transcription factor MEF2 resulting in HDACs nuclear retention (Miska et al., 1999; Bertos et al., 2001; Kao et al., 2001; Cohen et al., 2009), conserved serine residues which are subjected to calcium/calmodulin-dependent kinase (CaMK) phosphorylation and when phosphorylated create a docking site for chaperone 14-3-3 that mediates nuclear export of HDACs (McKinsey et al., 2000a, 2000b; Grozinger and Schreiber, 2000; Kao et al., 2001; Bertos et al., 2001; Zhao et al., 2001; Chawla et al., 2003; Li et al., 2004). The C-terminal of these proteins contains a highly conserved catalytic domain. Class IIa HDACs are highly expressed in heart, skeletal muscle and brain (Verdin et al., 2003; Majdzadeh et al., 2008a; Darcy et al., 2010).

Class IIb members are characterised by two separate catalytic domains and are mostly expressed in testis (HDAC6) and in liver, spleen and kidney (HDAC10). Both exhibit nucleocytoplasmic shuttling although they are predominantly localised in the cytoplasm (Yang and Grégoire, 2005).

Class IV contains a sole member, HDAC11, whose functions are not completely understood yet. It is expressed in a tissue-specific manner and is highly expressed in brain and testes (Gao et al., 2002).

Class III consists of seven sirtuins, sharing sequence homology to yeast SIR2 (silent information regulator 2). These are NAD-dependent enzymes which show different subcellular localisation and biological function (Nakagawa and Guarente, 2011), whereas class I, III and IV are zinc (Zn^{++})-dependent (Figure 1.10).

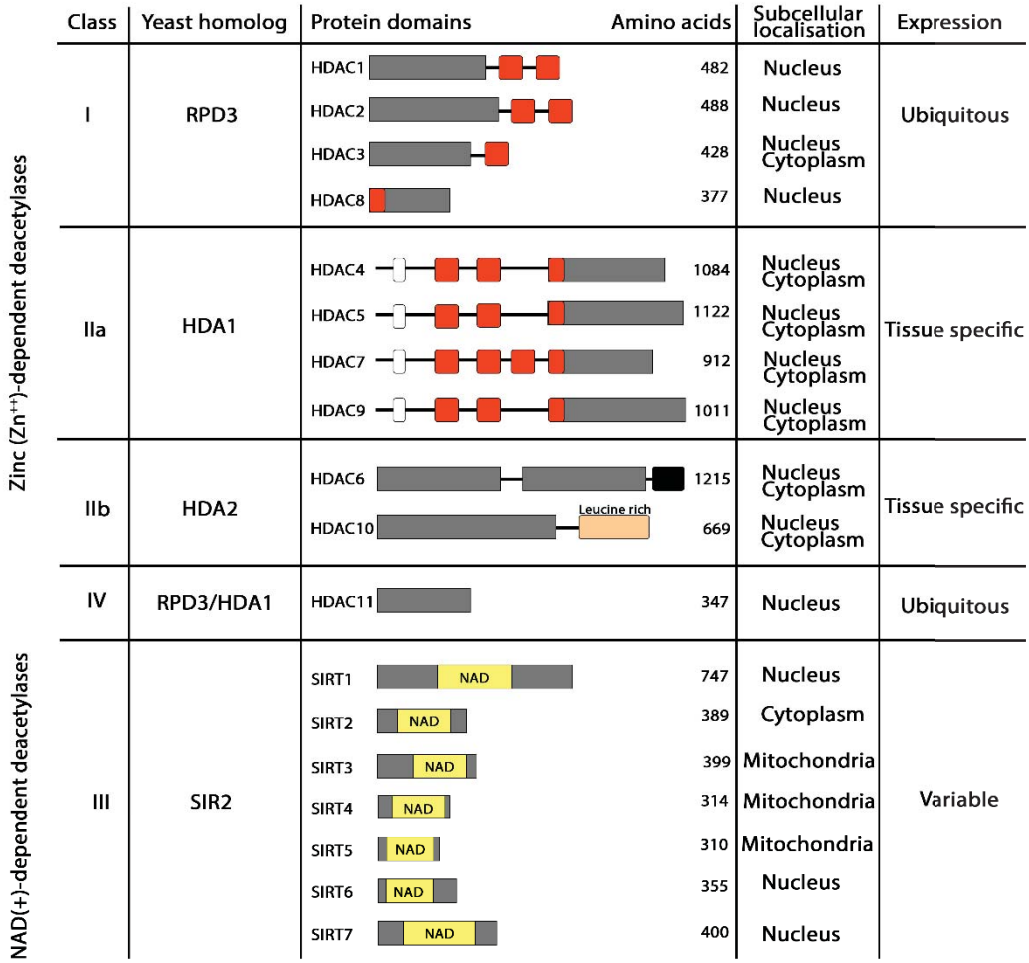

Figure 1.10 Human HDAC family members. Schematic representation of HDAC family member proteins. The catalytic domain is indicated by grey rectangles. Orange squares represent serine phosphorylation sites. Class IIa HDACs are characterised by an N-terminal extension containing a MEF2 binding site (white rectangles). HDAC6 contains an identical duplication of two catalytic domains and a zinc finger domain (black rectangle).

1.4.2.1 HDACs in *Drosophila melanogaster*

The *Drosophila* genome contains five zinc-dependent HDACs. Rpd3 and HDAC3, which are the homologues of human class I HDACs, HDAC1, HDAC2 and HDAC3

respectively, HDAC4 and HDAC6 are homologues of class IIa and IIb respectively, and HDAC11 is homologue of vertebrate HDAC11 (Cho et al., 2005; Foglietti et al., 2006; Fitzsimons et al., 2011). Each HDAC modulates the expression of different genes and their temporal expression pattern through development has been determined (Cho et al., 2005). In *Drosophila*, class I enzymes, Rpd3 and HDAC3 were found to be highly expressed in the embryo while HDAC4 and HDAC6 were found to be highly expressed in the adult suggesting that these class II HDACs might perform important biological functions in adult flies (Cho et al., 2005).

1.4.2.2 Inhibition of HDAC activity improves memory

Both genetic-based approaches, such as manipulation of the expression levels of the genes encoding HDACs, and chemical inhibition through pharmacological inhibitors have been used to gain insight into the roles of HDACs in neurons, and the majority of this research has until recently been focused on class I HDACs to which most of the HDAC inhibitors were targeted.

HDAC inhibitors are classified into four chemical families, the short-chain fatty acids, including sodium butyrate, phenylbutyrate and valproic acid, the hydroxamic acids e.g. trichostatin A (TSA), suberoylanilide hydroxamic acid (SAHA) and Scriptaid, the epoxyketones e.g. trapoxin, and the benzamides (Abel and Zukin., 2009). They all chelate the zinc ion at the deacetylase active site of Zn^{++}-dependent enzymes (Ziemka-Nalecz and Zalewska, 2014). Pharmacological inhibition of HDACs has been consistently found to improve cognitive functions in learning and memory paradigms (Lattal et al., 2007; Bredy and Barad, 2008; Guan et al., 2009; McQuown et al., 2011; Giralt et al., 2012; Gräff and Tsai, 2013). For example, Ma and colleagues trained mice to a subthreshold level which would not usually result in retention of LTM, but were able to form a robust memory when administered sodium butyrate (Stefanko et al., 2009). Moreover, pharmacological inhibition of HDAC3 with the specific HDAC3 inhibitor RGFP1356 via steroetaxic injection into the mouse hippocampus resulted in increased acetylation of lysine residue K8 of histone H4 and enhanced long-term memory in the novel object recognition test (McQuown et al., 2011).

However, treatment with HDAC inhibitors does not always correlate with memory enhancement. Administration of Scriptaid to *Drosophila* prior to training prevented LTM

formation, although it had no effect on STM (Fitzsimons et al., 2011). Selective pharmacological inhibition of HDAC1 with MS-275 in the mouse hippocampus was reported to cause impairments in extinction of fear memory, an hippocampus-dependent task that involves forming a new memory to override a fear memory (Bahari-Javan et al., 2012).

It has to be highlighted that most of the HDAC inhibitors that have been used to study memory lack specificity for individual HDACs, a feature which may account for the sometimes conflicting results. It is likely that enhanced gene expression due to an increased histone acetylation leads to up-regulation of pro and/or anti memory genes that may mediate distinct responses in different cell types (Dietz and Casaccia, 2010).

However, different considerations need to be stressed. HDACs may not present a unique and individual function, but according to their genetic interaction they may modulate different and, often, opposite roles according to the neuron cell type they are expressed in. It is also very likely that different HDACs are critical for specific types of memory or they may act during different phases of memory. For instance, a subset of HDACs might mediate memory consolidation through regulation of gene expression within few hours after learning, whereas a different subset of HDACs may be required for memory maintenance over prolonged periods of time (Zovkic et al., 2013).

It is therefore paramount to determine the specific role and function of individual HDACs through the identification of their genetic partners and pathways in order to develop molecules that can selectively inhibit specific HDACs with the goal to decipher their individual functions.

1.5 Histone Deacetylase HDAC4 and its role in memory formation

Interest in the role of class II HDACs in memory formation has raised in recent years, especially with increased evidence that they can target non-histone proteins and mediate several cellular processes including neuronal function. An increasing body of evidence indicates that the histone deacetylase HDAC4 plays critical roles in the regulation of neurological functions including neuronal survival (Bolger and Yao, 2005; Bolger et al., 2007; Chen et al., 2009), synaptic plasticity and memory formation (Sando et al., 2012; Kim et al., 2012; Fitzsimons et al., 2013) and several studies link HDAC4 to neurological disorders such as Alzheimer's disease (Neuner et al., 2016; Shen et al., 2016), Huntington's disease (Mielkarek et al., 2013a, 2015), Parkinson's disease (Takahashi-

Fujigasaki and Fujigasaki, 2006), schizophrenia (Kim et al., 2010) and autism (Nardone et al., 2014).

HDAC4 is highly expressed in the nervous system and in early studies, HDAC4 mRNA was found to be enriched in rodent brains (Grozinger et al., 1999; Wang et al., 1999) exhibiting a heterogeneous distribution throughout most of the brain regions (Broide et al., 2007). In the mouse brain, HDAC4 was found to be predominantly cytoplasmic in most neurons, displaying however variable nuclear localisation in some areas such as the cerebral cortex and the cerebellum, while the majority of dentate granule cells displayed non-nuclear localisation of HDAC4. In the substantia nigra intense nuclear immunoreactivity was detected and within the hippocampus, HDAC4 immunoreactivity was punctate in the cytoplasm. Some of these puncta were present in dendritic spines where the strongest immunoreactivity was associated with the postsynaptic density (Darcy et al., 2010). A similar pattern of expression was observed in the invertebrate brain. In *Drosophila,* HDAC4 was found to localise to the Kenyon cells of the mushroom body, a region of the brain essential for memory formation, and was strongly detected in the axon bundles that form the lobes of the mushroom body as well as in the calyx, the dendritic region of the mushroom body. HDAC4 was also found in a subset of Kenyon cells where it localised to punctate nuclear bodies (Fitzsimons et al., 2013), a similar pattern to that observed in rodent neurons (Darcy et al., 2010).

HDAC4 undergoes tightly controlled nucleocytoplasmic shuttling in response to spontaneous electrical activity in neurons (Chawla et al., 2003) and this is rendered possible by the presence of nuclear localisation and export signals within the amino and carboxy-terminus of HDAC4 (Figure 1.11). As for the other class IIa members, HDAC4 possesses a carboxy-terminus that harbours the deacetylase domain, highly conserved across vertebrates and invertebrates and a hydrophobic motif that serves as a functional nuclear export signal (NES) (Wang et al., 2001). The amino-terminus harbours highly conserved motifs mediating protein-protein interaction, subcellular localisation and serves as a nuclear localisation signal (NLS) (Wang et al., 2001).

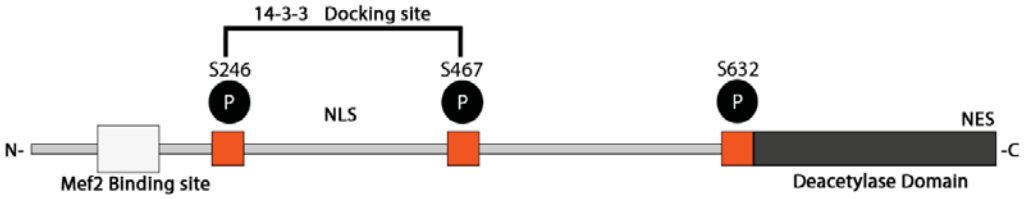

Figure 1.11 HDAC4 translocation regulatory domains. Within the N-terminus, conserved serine residues (orange squares) represent the critical determinant of HDAC4 localization. The serine residues are a target for phosphorylation mediated by CaMK protein and, once phosphorylated, they create a docking site for 14-3-3 chaperone proteins which escort HDACs into the cytoplasm. Moreover, the Mef2 binding domain mediates binding of transcription factor Mef2, resulting in HDAC4 nuclear retention. Abbreviations: NLS = nuclear localisation signal; NES = nuclear export signal.

1.5.1 *Drosophila* HDAC4

In *Drosophila*, HDAC4 is the sole class IIa HDAC, it is highly conserved with the vertebrate form with 57% amino acid identity and 84% similarity across the deacetylase domain and 35% identity and 59% similarity across the whole protein (Fitzsimons et al., 2013).

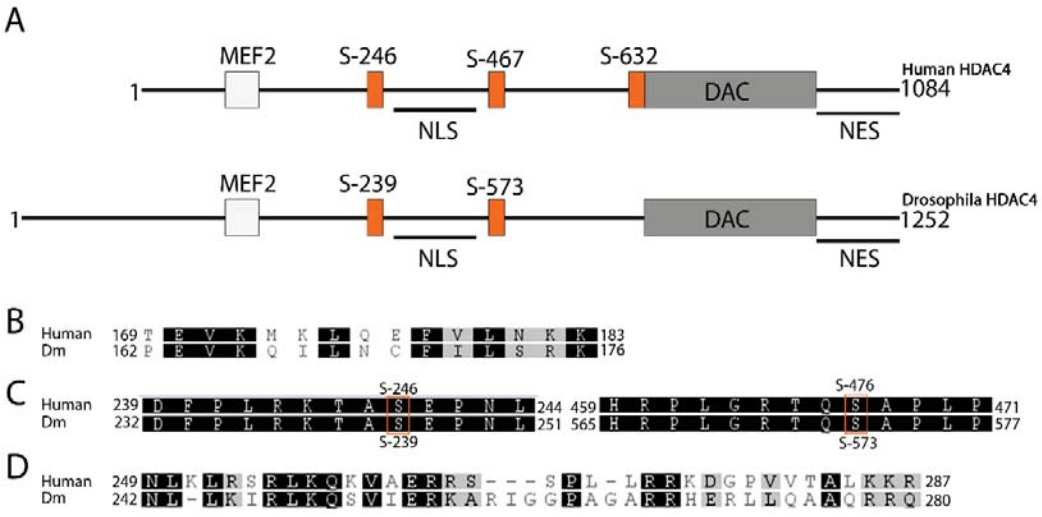

Figure 1.12 Domain organisation and alignment of *Drosophila* and human HDAC4 proteins. (A) Human HDAC4 GenBank accession NP_006028, 1084 amino acids, Uniprot ID P56524; *Drosophila* HDAC4, isoform D, GenBank accession AFI26265.1, 1252 amino acids, Uniprot ID I1V504. Regions of human HDAC4 essential for function and corresponding regions of

Drosophila HDAC4 are shown. The deacetylase domain is shown in gray, Mef2 binding domain in white and serine residues are indicated in orange. (B-D) Sequence alignment of *Drosophila* HDAC4 with regions of human HDAC4 essential for function. Alignment performed using Geneious Software version 7.1.9 which measures similarity by using a substitution matrix Blosum62 that scores for all possible exchanges of one amino acid with another. The Blosum62 matrix measures alignments between sequences with no more than 62% global similarity and it is the default matrix in alignment applications such as BLAST, since it is able to detect similarities in divergent proteins (Henikoff and Henikoff, 1992). (B) Mef2 binding region showing an identity of 42% increasing to 64% when a Blosum62 matrix is applied. (C) Serine residues are highly conserved between *Drosophila* and humans with 100% identity. (D) Residues responsible for nuclear localization of vertebrate HDAC4 are also highly conserved with 35% identity increasing to 55% when a Blosum62 matrix is applied. Image modified from Fitzsimons et al., 2013.

1.5.2 HDAC4: a master regulator of memory

In recent years, data from studies in humans and several animal models suggest that HDAC4 plays a critical role in memory formation. In humans, deletion or mutation of HDAC4 is associated with Brachydactyly mental retardation syndrome (BDMR), the neurological symptoms of which include intellectual disability, behavioural abnormalities, cognitive deficits and autism spectrum disorder (Williams et al., 2010). Similarly, in *Drosophila* RNAi knockdown of *HDAC4* in the brain abolished LTM formation when tested in the courtship suppression assay (Fitzsimons et al., 2013) and in the mouse, selective loss of *HDAC4* in the brain through brain-specific conditional knockout resulted in deficits of hippocampal-dependent learning and memory (Kim et al., 2012)

However, increased nuclear HDAC4 is associated with memory impairment. In one individual with Brachydactyly mental retardation syndrome, a heterozygous mutation of a single cysteine insertion (+ C) was detected (Williams et al., 2010). This generates a premature stop codon resulting in a truncated product with loss of the deacetylase domain and nuclear export signal. Sando and colleagues (2012) expressed this human + C allele in mouse cortical primary neurons and showed that this truncated form of HDAC4 is a gain-of-function nuclear repressor associated with neuronal loss, synaptic transmission deficits and impairment of spatial learning and memory performances, despite the loss of the deacetylase domain (Sando et al., 2012). This result suggests a potent role for HDAC4 in neuronal functions not dependent on deacetylase activity, in line with previous studies

showing that vertebrate HDAC4 possesses minimal if any deacetylase activity (Lahm et al., 2007; Bottomley et al., 2008; Mielcareck et al., 2013b).

In *Drosophila*, overexpression of *HDAC4* also impairs LTM (Fitzsimons et al., 2013) and it is unclear if this is due to increased nuclear or cytoplasmic HDAC4, however similarly to the abovementioned study, the catalytic activity of HDAC4 was dispensable. Flies were generated to overexpress a catalytically inactive HDAC4 in which the histidine at position 968 was replaced with an alanine. This histidine residue, corresponding to human H803, is conserved across vertebrates and invertebrates and is critical for the active site as mutation of this residue acutely attenuates catalytic activity (Cohen et al., 2009; Wang et al., 1999). These flies displayed similar memory impairment as flies overexpressing wild-type *HDAC4* (Fitzsimons et al., 2013).

Together, these data from vertebrate and invertebrate models strongly suggest that HDAC4 is essential for memory formation, however it can also act as a memory repressor, and this is likely due to its nuclear activity. This would suggest that the effect that HDAC4 has on memory is dependent on precise regulation of nucleocytoplasmic shuttling. The lack of requirement for an active deacetylase domain is also consistent with the ability of HDAC4 to bind to and repress the activity of transcription factors which allows HDAC4 to modulate gene expression independent of deacetylase activity. When in the nucleus, HDAC4 acts as a transcription repressor by inhibiting the activity of transcription factors such as MEF2. In mice homozygous null for the *Atm* gene, mutations of which cause a neurodegenerative disorder known as ataxia telangiectasia, HDAC4 accumulates in the nuclei of Purkinje cells, which are neurons in the cerebellum that regulate movement. Both MEF2 and CREB were found to immunoprecipitate with HDAC4 and this is correlated with altered neuronal gene expression (Li et al., 2012). Genome-wide profiling analysis was performed on cultured neurons transduced with the constitutively nuclear HDAC4 mutant 3SA, which showed that a group of genes that were known to be essential for synaptic function were repressed (Sando et al., 2012). However, HDAC4 is predominantly non-nuclear in neurons (Bolger and Yao, 2005; Darcy et al., 2010) and it is unclear whether HDAC4 plays a role in regulation of transcription during memory formation. The role of HDAC4 in the cytoplasm is unknown, but its presence in this subcellular domain, particularly its localisation to synapses, strongly suggests a role beyond transcriptional regulation and there is some evidence that HDAC4 may play a pro-memory and/or neuroprotective role in this compartment.

In cultured primary rodent neurons, expression of a cytoplasmic restricted mutant of HDAC4 lacking its N-terminal domain (ΔN), in a HDAC4 knockdown context, correlated with increased expression of plasticity-related genes and increased size of post-synaptic density in comparison to wild-type controls (Sando et al., 2012). The cytoplasmic role of HDAC4 was also examined in *Atm*$^{-/-}$ mice that display locomotor deficits associated with ataxia telangiectasia. Lentiviral vectors expressing a cytoplasmic-restricted mutant of HDAC4 were injected into the cerebellum and these mice showed improved locomotor activity in comparison to sham-injected *Atm*$^{-/-}$ controls. In *C. elegans*, depletion of *hda4*, a homolog of mammalian class II HDACs with a conserved NLS, enhanced learning and LTM in a thermotaxis model. Expression of wild-type or nuclear restricted 3SA mutant of human HDAC4, repressed the enhanced memory phenotype and restored it to a wild-type level, whereas expression of a cytoplasmic restricted mutant, ΔN118, had no impact on memory. This mutant however was shown to enhance memory when expressed in wild-type worms, indicating pro-memory effects of cytoplasmic HDAC4 (Wang et al, 2011). However, in this study the endogenous localisation of Hda-4 was not examined. The conserved NLS suggests it may preferentially localise in the nuclei of neuronal cells acting as a repressor of transcription. Depletion of its expression levels may thus relieve the transcriptional repression resulting in expression of genes possibly involved in long-term memory processes (Fitzsimons, 2015).

Taken together these data reveal a fundamental role for *HDAC4* in memory formation, with both overexpression and knockdown or knockout resulting in memory impairment. HDAC4 subcellular compartmentalisation emerges as a critical mediator of HDAC4 function, with increased nuclear HDAC4 resulting in impairments of memory whereas the cytoplasmic role is yet to be determined. Overall, a complex and puzzling picture emerges which warrants further investigation in order to elucidate the functions of HDAC4 in the different cellular compartments, and the molecular pathways in which it acts.

1.6 Ankyrin proteins

Mammalian HDAC4 possesses an ankyrin repeat binding domain within the N-terminus, which is conserved among class IIa HDACs (Wang et al., 2005; McKinsey et al., 2006), and this domain is also conserved in *Drosophila* (Figure 1.13).

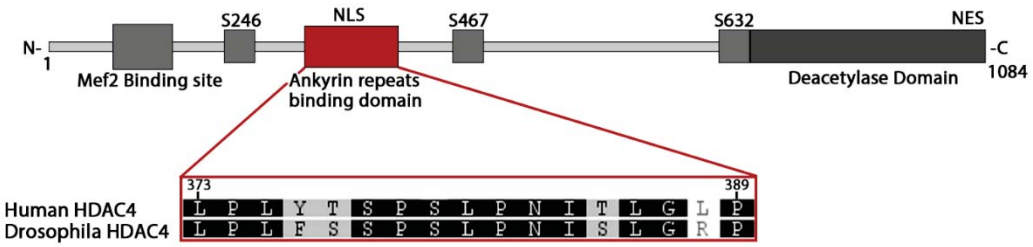

Figure 1.13 Domain structure of HDAC4 highlighting the ankyrin repeats binding domain. The ankyrin binding domain is highlighted in red and alignment between human and *Drosophila* is shown. Alignment colour legend: black = identical, gray = similar, white = not similar.

The ankyrin repeat is a common protein sequence motif that mediates protein-protein interactions and proteins harbouring this domain are implicated in a broad range of biological processes, raising the possibility that HDAC4 may interact with several proteins through this domain and participate in distinct biological processes.

Ankyrins are a family of ubiquitously expressed and closely related proteins, whose major function in the cell is to link integral membrane proteins to the underlying spectrin-actin cytoskeleton (Bennett, 1978, Bennett and Baines, 2001). These membrane proteins include ion channels e.g. Na^+/K^+ ATPase, H^+/K^+ ATPase, Na^+ channels, Na^+/Ca^{++} exchanger, anion exchangers, calcium release channels such as the ryanodine receptor and the inositol (1,4,5)-trisphosphate receptor, cell adhesion molecules like CD44, NgCAM, neurofascin, L1CAM, neuroglian, NrCAM, LAD-1, as well as cytoplasmic proteins such as clathrin and tubulin (Mohler et al., 2002).

The structural domain organisation of canonical ankyrins is represented in Figure 1.14. They comprise an N-terminal domain or membrane binding domain which mediates ankyrin binding to integral membrane proteins. This domain contains 24 ANK repeat motifs, each consisting of 33 amino acids organised as two anti-parallel α-helices. Contiguous ANK repeats are connected by a β-hairpin loop and these motifs are key mediators of protein-protein interactions (Sedgwick and Smerdon 1999; Cunha and Mohler, 2009). A central spectrin-binding domain anchors the ankyrin-associated proteins to the spectrin/actin cytoskeleton. This domain contains a ZU5 domain of 160 amino acids and functions as both a critical spectrin-binding region and more versatile protein interaction module (Cunha and Mohler, 2009; Yasunaga et al., 2012). Interactions are mediated by the electrostatic charges of the β-spectrin's repeat (negative) and the

positive charges of the ZU5 domain. The C-terminal domain is comprised of a death domain that mediates apoptotic events and more general protein-protein interaction functions (Liu et al., 2014) and a regulatory domain which is the least conserved. This domain not only regulates ankyrin inter- and intra-molecular interactions and recruitment of ankyrins to different subcellular domains (Cunha and Mohler, 2009) but also defines specificity among ankyrins which although structurally similar, do not present overlapping functions (Mohler et al., 2004).

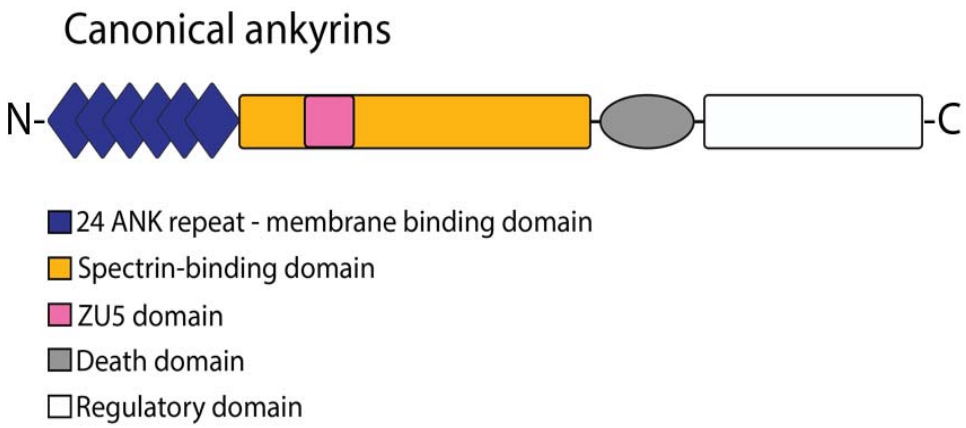

Figure 1.14 Schematic representation of the domains organisation of canonical ankyrins. Canonical ankyrins possess a membrane binding domain composed of 24 ANK repeats followed by a central spectrin domain including a ZU5 domain which mediates association to the spectrin-based cytoskeleton. The C-terminus contains a death domain and a variable regulatory domain.

Ankyrins play a pivotal role in providing structural stability to the cell and are involved in the asymmetric distribution of integral membrane proteins into specialised regions of the plasma membrane, functioning as key regulators of cell polarity. Neurons are highly polarised cells in morphology and function, with dendrites that receive signals from other neuronal cells and axons that initiate and propagate those signals as action potentials. The separation between the somato-dendritic and axonal regions is maintained through a precise molecular organisation of these subdomains allowing control of the directional flow of the information throughout the neuron. This is accomplished by the presence of scaffolding proteins such as ankyrins and spectrins that regulate the arrangement of different sets of proteins into specialised membrane domains of the

neuronal cell (Bouley et al, 2000). Mammalian axons show a high density clustering of voltage-gated ion channels in a specific region named the axon initial segment where the initiation of action potentials occurs (Bender and Trussel, 2012) (Figure 1.15). This region operates as a filter between the axonal and dendritic domains controlling protein trafficking and maintaining neuronal cell polarity. Enrichment of ankyrins in this region is critical for its assembly and stability, and it has been shown that decreased levels of expression of a specific form of ankyrin, ANKYRIN-G, in the mouse brain results in loss of axon initial segment stability leading to flaws in protein trafficking and axonal transport (Sun et al., 2014b). A similar region has also been identified in *Drosophila* neurons (Wright and Zinn, 2009; Katsuki et al., 2009; Trunova et al., 2011).

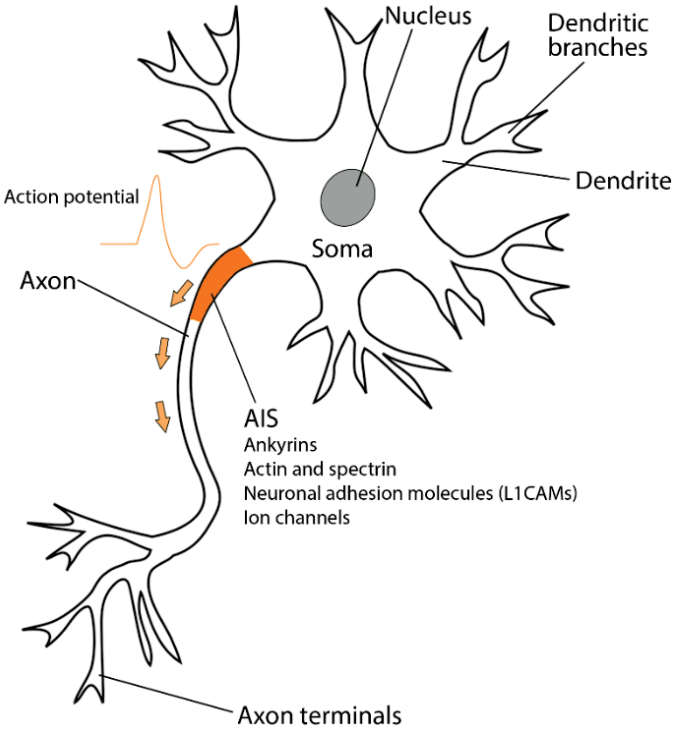

Figure 1.15 The axon initial segment. Axon initial segment of mammalian neurons. Synaptic inputs are integrated at the somato-dendritic domain which includes the soma, dendrites and dendritic branches, with consequent generation of the action potential at the axon initial segment (highlighted in orange - AIS). This region includes voltage gated Na^+ and K^+ channels and cell adhesion molecules clustered through interactions with the scaffolding protein ankyrins, which link the axon initial segment membrane proteins to a submembrane actin and ßIV-spectrin complex (Leterrier and Dargent, 2014). Ankyrin distribution at the axon initial segment is required to maintain axonal and dendritic polarity. Abbreviation: AIS = axon initial segment.

The human genome contains three distinct genes encoding for three different classes of ankyrins, each able to generate multiple alternative spliced isoforms that can associate with different proteins in diverse subcellular localisations.

The *ANKYRIN1* gene encodes for ANKYRIN-R (ANK-R), first characterised in erythrocytes and later detected in granule and Purkinje cells of the cerebellum, in neurons of the spinal cord and hippocampus, in striated muscles, endothelial cells and macrophages (Rubtsov and Lopina, 2000; Mohler et al., 2002). The *ANKYRIN2* gene encodes for a polypeptide known as ANKYRIN-B (ANK-B), first discovered in neurons and glial cells (Otto et al., 1991).

The *ANKYRIN3 (ANK3)* gene encodes for ANKYRIN-G (ANK-G) which is found in unmyelinated neurons (Rubtsov et al., 2000) and associates with the voltage-dependent sodium and potassium channels at the nodes of Ranvier and at the proximal domain of axons, where it is required for the assembly of the axon initial segment. Multiple transcript variants encoding different isoforms have been found for this gene. A 190 kDa isoform is abundant in unmyelinated neurons (Rubtsov et al., 2000), whereas giant isoforms of 270-480 kDa associate with the voltage-dependent sodium channels at the nodes of Ranvier of myelinated neurons and at the axon initial segment (Kordeli et al., 1995). These giant isoforms (Figure 1.16) contain a 40 kDa serine/threonine-rich domain glycosylated with N-acetyl-D-glucosamine monosaccharide residues which may be responsible for the targeting of ANK-G specifically to the aforementioned regions of the neuronal cell (Cunha and Mohler, 2009).

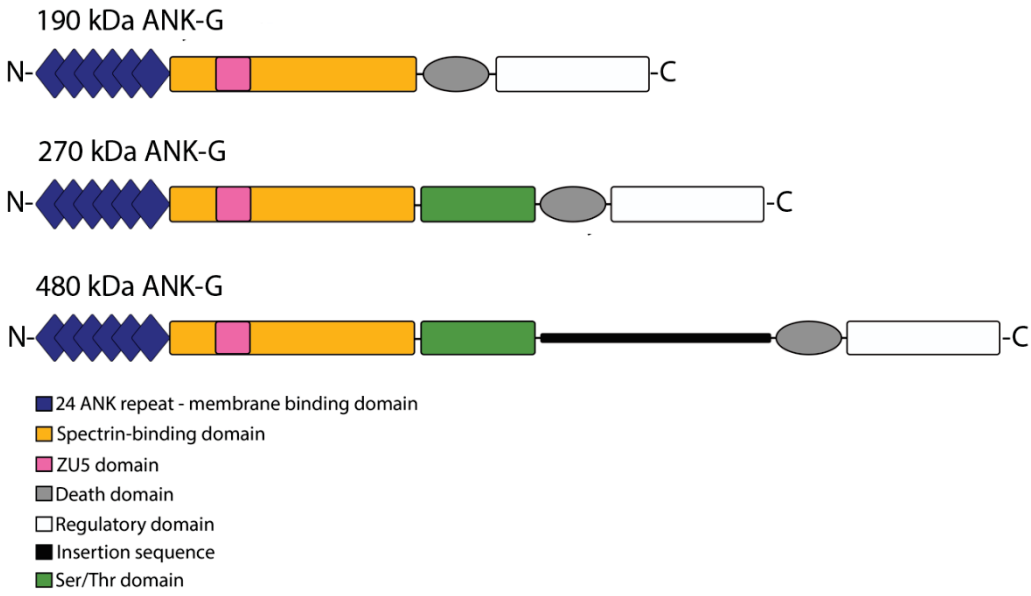

Figure 1.16 Schematic representation of ANK-G variants within the vertebrate nervous system. Three isoforms of ANK-G are differentially expressed in the vertebrate nervous system. A 190 kDa form is localised in unmyelinated neurons and two giant isoforms of 270 and 480 kDa are specifically localised at the axon initial segment and the nodes of Ranvier of myelinated neurons. Abbreviations: Ser = serine; Thr = threonine.

ANK-G-null axons acquire dendritic features both in cultured neurons as well as in the mouse brain, indicating it is an essential regulator of neuronal polarity (Hedstrom et al., 2008; Sobotzik et al., 2009). Mice with cerebellar reduction of ANK-G show loss of voltage gated sodium channels and L1-type CAM neurofascin at the axon initial segment and the nodes of Ranvier, leading to a decreased ability of neurons to fire action potentials and defects in the filtering machinery at the proximal axon, with malfunctions in the targeted localisation of axonal and dendritic proteins (Sun et al., 2014b). In recent years, genome-wide analyses have linked mutation of *ANK3* to neurodevelopmental disorders such as autism, bipolar disorder and schizophrenia (Ruberto et al., 2011; Leussis et al., 2012; Iqbal et al., 2013; Zhang et al., 2014).

The *Drosophila* genome contains two distinct genes encoding for two different ankyrin proteins, the *Dank1* gene encodes Ankyrin1 (*Ank1*) which is ubiquitously expressed, while *Dank2* encodes for Ankyrin2 (*Ank2*) which is selectively expressed in the nervous system. These two proteins display 66.2% amino acid identity over the ankyrin repeat domain, and 36% and 51.7% identity over the acidic and basic regions of the spectrin-binding domain, respectively (Bouley et al., 2000). Although Ank1 and Ank2

are not direct orthologs of mammalian forms, the expression pattern of *Drosophila* Ank1 is similar to mammalian ANK-R, and Ank2 is the closest homolog of human ANK-G (Iqbal et al., 2013). In particular *Drosophila* Ank2 and human ANK-G share 57% overall amino acid identity and 71.2% identity over the ankyrin repeat region (Figure 1.17). Similarly to mammalian ANK-G, several splice variants of Ank2 exist. Koch and collaborators (2008) developed a standard nomenclature system for *Ank2* splice variants. The short category (Ank2-S) includes an Ank2 isoform of 1159 aa, the medium category (Ank2-M) includes isoforms 2386 to 2465 aa, the long category (Ank2-L) incorporates isoforms whose lengths range from 4083 to 4264 aa and the extra-long category (Ank2-XL) contains an isoform of 11640 aa. It was previously shown that shorter isoforms of Ank2 (Ank2-S), are highly expressed in the cell body of neuronal cells and are not essential for fly viability whereas longer isoforms are localised at the axonal regions and are essential for *Drosophila* synaptic plasticity (Hortsch et al., 2002). Studies in larvae showed that Ank2-L is highly localised in the axon and minimally detected in the cell bodies whereas the XL forms are preferentially localised in the cell body in a punctate pattern but also accumulate in the axon (Koch et al., 2008). These forms have been found to be fundamental for fly viability and for synaptic stability and maintenance. Mutation and genetic knockdown studies affecting longer isoforms of Ank2 (L and XL) showed defects in stability of the neuromuscular junction, reduction of the terminal button size, disassembly of presynaptic active zone and destruction of the synaptic microtubule cytoskeleton (Koch et al., 2008; Pielage et al., 2008).

Figure 1.17 Ankyrin repeat region alignment between human ANK-G and *Drosophila* Ank2. (A-B) Conserved domain region of *Drosophila* Ank2 and human ANK-G, from NCBI http://www.ncbi.nlm.nih.gov. (C) The ankyrin repeat region of *Drosophila* Ank2 was aligned to the ankyrin repeat region of human ANK-G using the Geneious software (version 7.1.9) showing an identity percentage of 66.3% increasing to 82.1% when a Blosum 62 (BLSM62) substitution matrix is applied to produce a more accurate alignment. Isoforms used for alignment derived from Uniprot, *Drosophila* Ank2 isoform Z code X2JC49, human ANK-G Q12955. Amino acids from 149 to 935. Alignment colour legend: black = identical, gray = similar, white = not similar.

1.7 Aims and objectives

Despite differences in brain size and complexity, vertebrate and invertebrate studies have similarly shown that normal levels of HDAC4 in brain cells are essential for memory. The main regulatory mechanism underlying HDAC4 function may reside in its intrinsic ability to commute between the nucleus and the cytoplasm, where it may regulate distinct memory processes through the interaction with specific factors.

However, there are still several gaps in knowledge regarding the role of HDAC4 in memory, which raise the following questions: is the memory impairment resulting from overexpression of *HDAC4* a result of repression of genes required for memory formation? Are non-transcriptional and/or non-nuclear functions of *HDAC4* required for memory formation? What is the role of HDAC4 in the cytoplasm? What are the upstream regulators and downstream targets of *HDAC4*?

The focus of this project is attempt to answer some of these questions via the following objectives:

1. **Identification of genes transcriptionally regulated by *HDAC4* in the brain.** Overexpression of *HDAC4* in the brain abolishes memory formation in *Drosophila*. In order to determine whether this is a result of transcriptional repression, transcriptome analysis will be performed via RNA sequencing.

2. **Identification of genes that interact in the same molecular pathway as *HDAC4*.**

   In order to detect genes that interact with *HDAC4* through both transcriptional and non-transcriptional mechanisms, a genetic screen for modifiers of the rough eye phenotype will be adopted. RNAi lines of genes involved in neurological functions such as development, synaptic plasticity and memory, will be crossed to flies in which overexpression of *HDAC4* is induced in the eye photoreceptors and the eye phenotype of the F1 progeny will be analysed for enhancement, or suppression of the *HDAC4*-induced rough eye phenotype in eyes co-expressing the RNAi gene and *HDAC4* overexpression.

3. **Characterisation of candidate *HDAC4* gene targets and/or genetic interactors.**

   Candidate genes detected to interact with *HDAC4* in the transcriptome analysis and/or in the eye screen will be selected for further analysis in order to characterise whether they are expressed in the brain and if they are involved in memory formation. To this end, RNAi-mediated depletion of the genes of interest will be induced in the fly brain and courtship suppression memory assays will be performed.

4. **Investigation of a physical interaction between HDAC4 and the selected candidates**.

   This will be achieved first via immunohistochemistry of adult brains to determine whether HDAC4 and the candidate genes distribute to the same regions of the fly brain and secondly via GST pull-down assays to test for physical interactions, using HDAC4 as bait

2 MATERIALS AND METHODS

2.1 *Drosophila melanogaster* strains

Drosophila strains used in this study are listed in Tables 7.1 and 7.2, Appendix 7.1. For the sake of clarity and brevity, in the following sections, all fly strains will be described by their name rather than their complete genotypes.

With regards to gene and protein nomenclature in *Drosophila*, Flybase-approved gene symbols and names are used throughout this thesis, which are described as per Flybase guidelines: "The name begins with a lowercase letter when the gene is named for a mutant phenotype recessive to the wild-type in a normal diploid. The name begins with an uppercase letter when the gene is named for a mutant phenotype that is dominant to the wild-type in a normal diploid. Genes named after a protein product or other molecular feature begin with an uppercase letter. The gene symbol is typically an abbreviation of the full gene name." (http://flybase.org/wiki/FlyBase:Nomenclature). Protein products are the same as the gene symbol but are not italicised

For human genes, gene symbols are italicised and uppercase while proteins designations are the same as the gene symbol, but are not italicised. In mouse and rat, genes are usually in italics with only the first letter uppercase, and proteins are all uppercase and not italicised.

2.2 Maintenance of fly strains

Flies were raised on standard medium (per litre: 10 g agar, 40 g yeast, 110 g cornflour, 130 g sugar, 20 ml molasses and 3.3 g of methyl 4-hydroxybenzoate dissolved in 37 ml of 96% ethanol), on a twelve hour light-dark cycle at 25˚C, unless otherwise indicated.

2.2.1 Genetic crosses

Five males and five virgin female flies were placed together in a 30 ml vial (Labserv), on standard medium at 25°C. For experiments requiring a larger number of progeny, approximately twelve male and twelve virgin females were placed together in a 100 ml bottle. After four to seven days, the adult flies were removed and progeny emerged after ten days.

In order to produce virgin females for setting crosses, adults were cleared from vials

or bottles and flies collected within an eight hour window were virgin since adults do not mate for about ten hours after eclosion. Females were kept on standard medium at 22°C and used within four to ten days.

2.3 Rough eye phenotype screen

GMR-GAL4; UAS-HDAC4OE flies were crossed to each RNAi line and the eye phenotypes of the F1 progeny were assessed at seven days of age. *GMR-GAL4* flies were also crossed to each RNAi line to verify whether the knockdown of each target gene had an effect on the eye phenotype in absence of *HDAC4* overexpression (*HDAC4OE*).

F1 progeny were frozen at -20˚C for at least one hour, thawed for fifteen minutes and eye phenotypes analysed under the stereomicroscope (Olympus SZX12, DP controller imaging software, manual exposure, ISO 200, zoom 108 mm, exposure time range 1/20-1/30 seconds). A semi-quantitative scoring system was used to evaluate the rough eye phenotype by observing bristle and ommatidia organisation, and shape. Lines with more than a very mild rough eye in absence of *HDAC4OE* were excluded. Control crosses were performed using strains from appropriate genetic background Canton special (CS), w^{CS10} or w^{1118}.

2.3.1 Scanning electron microscopy

One day prior to scanning electron microscopy (SEM), six to eight flies were placed into cotton-plugged vials containing paper discs soaked with water in the absence of food to allow the flies to clean their eyes in order to remove any food residue. Flies were anesthetised with CO_2 and were placed in primary modified Karnovsky's fixative (3% gluteraldehyde 2% formaldehyde in 0.1 M phosphate buffer, pH 7.2) with Triton X-100 and vacuum infiltrated until wet. The fixative was replaced and the samples were allowed to fix for at least eight hours at room temperature. Three washes of ten to fifteen minutes each, in phosphate buffer (0.1 M, pH 7.2) followed by dehydration in graded ethanol series (25%, 50%, 75%, 95%, 100%) for ten to fifteen minutes each and a final 100% ethanol wash for one hour were performed. Samples were critical point dried using liquid CO_2 as the critical point fluid and 100% ethanol as the intermediary (Polaron E3000 series II critical point drying apparatus). Samples were mounted onto aluminium stubs and sputter coated with gold (Baltec SCD 050 sputter coater) and viewed in the FEI Quanta 200 Environmental Scanning Electron Microscope at an accelerating voltage of 20 kV.

Following fixation, the abovementioned processing and SEM were conducted by Mr Doug Hopkroft and Ms Niki Murray at the Massey Microscopy and Imaging Centre (MMIC), Institute of Fundamental Sciences, Palmerston North.

2.4 Isolation of *Drosophila* heads

In order to isolate ribonucleic acid (RNA) or protein from *Drosophila* heads, a procedure was followed to isolate heads from bodies. Adult flies were anesthetised with CO_2, placed into a 15 ml tube and snap-frozen in a dry ice-96% ethanol bath for 30 minutes. Tubes were then vortexed for 30 seconds (three times, ten seconds each) to detach the heads from the bodies. Flies were tipped onto a piece of transparency positioned on a plastic petri dish lid filled with dry ice. Heads were quickly separated from the bodies using a brush and transferred to a 1.5 ml tube on dry ice. Heads were either processed directly or stored at -80°C.

2.5 Transcriptome analysis

In order to express *HDAC4* in the adult brain, homozygous *UAS-HDAC4OE* flies were crossed to *elav-GAL4; tub-GAL80^{ts}* flies and raised at the permissive temperature of 18°C. The genotype of F1 progeny was the following: *elav/+; tub-GAL80ts/+; UAS-HDAC4OE/+*, expressing *HDAC4* pan-neuronally under control of the *elav* driver and GAL80^{ts}. GAL80 is a temperature sensitive mutant which allows for targeted gene expression regulation under the control of temperature shifts (Suster et al., 2004; McGuire et al., 2004). At 18°C, GAL80 is active and prevented GAL4-mediated expression of *HDAC4*, while at 30°C GAL80 loses its repressive activity and thus GAL4 was able to induce *HDAC4* expression.

Flies of the w^{CS10} wild-type line were crossed to *elav-GAL4; tub-GAL80^{ts}* and were used as the control. Three biological replicates derived from three different crosses, were used for each genotype. Three days after eclosion, flies were transferred to 30°C and *HDAC4* overexpression was induced. Forty hours after induction, flies from each biological replicate were snap-frozen in a dry ice/ethanol bath and vortexed to remove the heads (section 2.4). Heads were collected over dry ice and RNA was extracted with Trizol (section 2.16.1) and purified with an RNeasy microarray tissue mini kit (Qiagen). Whole heads were used in order to reduce variation from individual dissection of brains and this method has been successfully employed to analyse brain-specific changes in gene

expression in *Drosophila* (Winbush et al. 2012). The aforementioned procedures were carried out by Dr Helen L. Fitzsimons.

The high quality of the RNA was confirmed on a Bioanalyzer (Agilent). Illumina libraries were prepared with an Illumina RNA TruSeq kit and run on an Illumina HiSeq with three samples per lane (NCSU Genomic Sciences Laboratory). Over 60 million 100 bp reads were obtained per sample, which were mapped to the *Drosophila* reference genome (release 5.41, FB2011_09; 15438 predicted genes). The reads were mapped using Tophat (http://tophat.cbcb.umd.edu/) and analysed for reads alignment percentage and gene coverage (Trapnell et al. 2012). Data analysis was restricted to genes with FPKM (fragment per kilobase of exon per million fragments mapped) value of at least 1.0 as employed by the ModENCODE Consortium and in other studies (Roy et al. 2010; Winbush et al. 2012) and to genes expressed in the brain (>10 on Flyatlas) (Chintapalli et al. 2007).

The Cufflinks pipeline, version 2.2.1 (http://cufflinks.cbcb.umd.edu/) was used to assemble mapped reads into transcripts, estimate their abundances and test for differential expression between samples (Trapnell et al. 2012). Assemblies resulting from Cufflinks analysis were merged together using the Cuffmerge utility, which is included in the Cufflinks package. The merged assemblies were provided to Cuffdiff, a program included in the Cufflinks package that tests the statistical significance of each observed change in expression between the samples. The statistical model used to evaluate changes assumes that the number of reads produced by each transcript is proportional to its abundance. The expression level of transcripts across the runs was normalised by the total number of mapping reads using the FPKM normalisation method (Mortazavi et al. 2008; Trapnell et al. 2012). Cuffdiff implements a linear statistical model to estimate an assignment of abundance to each transcript. Fold changes, expressed in log2 scale, raw P-values and adjusted Q-values were calculated by standard methods. Plots were generated using the cummeRbund tool (http://compbio.mit.edu/cummeRbund/) which analyses the Cuffdiff data into the R statistical computing environment, helping visualising the data (R version 3.2.0).

2.6 Immunohistochemistry on whole mount *Drosophila* brains

Antibodies used for this experimental procedure are listed in Table 2.1 (primary antibodies) and Table 2.2 (secondary antibodies):

Protein name	Clone	Class	Host	Brand	Dilution
Disc Large	4F3	Monoclonal	Mouse	DSHB	1:500
Elav	9F8A9	Monoclonal	Mouse	DSHB	1:1000
Fasciclin II	1D4	Monoclonal	Mouse	DSHB	1:200
Flag	M2	Monoclonal	Mouse	Sigma/Aldrich	1:1000
Futsch	22C10	Monoclonal	Mouse	DSHB	1:20
αNeuroglian	BP104	Monoclonal	Mouse	DSHB	1:100
Repo	8D12	Monoclonal	Mouse	DSHB	1:20
Ankyrin2-L	aa 1655-1912 of SP2523 (*Ankyrin2)*	Polyclonal	Rabbit	Dr Aberle	1:1000
Flag	F7425.2MG	Polyclonal	Rabbit	Sigma Aldrich	1:5000
GFP	Ab290	Polyclonal	Rabbit	Abcam	1:10,000

Table 2.1 List of primary antibodies and respective dilutions used for immunohistochemistry. Abbreviations: DSHB, Developmental Studies Hybridoma Bank. The Ankyrin2-L antibody is a kind gift from Dr Aberle and it has been designed to recognise a sequence corresponding to the 257 C-terminal from amino acid 1655 to amino acid 1912 of *Drosophila* SP2523 corresponding to *Ankyrin2* Fly base ID FBgn0261788 (Koch et al., 2008).

Product name	Dye	Dilution
Goat anti-mouse IgG	AlexaFluor® 488	1:500
Goat anti-rabbit IgG	AlexaFluor® 488	1:500
Goat anti-rabbit IgG	AlexaFluor® 555	1:500
Goat anti-rabbit IgG	AlexaFluor® 555	1:500
Goat anti-mouse IgG	AlexaFluor® 647	1:500
Goat anti-rabbit IgG	AlexaFluor® 647	1:500

Table 2.2 List of secondary antibodies and dilutions used for immunohistochemistry. All secondary antibodies used in this study are produced by Molecular Probes Inc. (Thermo Fisher Scientific).

In order to detect protein expression in the fly brain, whole mount brain dissection was performed as follow. Whole flies were fixed in PFAT/DMSO (4% paraformaldehyde in 1xPBS, 0.1% Triton X-100 and 5% DMSO) for 1.5 hour and then washed three times in 1X PBST (1X PBS, 0.5% Triton X-100). Flies were placed in a 60 mm glass Petri dish in presence of 1X PBST and brains were dissected under stereomicroscope using a pair of

Dumont #5 forceps with sharp tips. Dissected brains were moved into a 1.5 ml tube through a glass Pasteur pipette, then post fixed for 20 minutes in PFAT/DMSO and stored in methanol at -20°C or immediately blocked in 5% normal goat serum in PBST (blocking solution/immunobuffer). Brains were incubated in fresh blocking solution at room temperature overnight with primary antibodies (Table 2.1) then incubated in blocking solution with secondary antibodies (Table 2.2) at 4°C overnight in the dark. The following day brains were washed three times (each wash 20 minutes) with PBST and were mounted on a glass slide (1 mm-1.2 mm thick, Sail Brand) in presence of anti-fade solution (10X PBS, 9 ml glycerol, 20% n-propyl gallate). Brains were then covered with a cover glass (22x22 mm, 0.13-0.17 mm of thickness, Interlab) and mounted under the Leica SP5 DM6000B scanning confocal microscope objectives (dry 10X, dry 20X, 40X in oil, 63X in oil). Brains were imaged with excitation laser lines at 488 and/or 561 nm.

2.7 Polymerase Chain Reaction (PCR)

2.7.1 Standard PCR amplification

Primers used for PCR are listed in Table 2.3.

Oligo Name	Direction	Primer sequence
Ef1α48d	Forward	ACTTTGTTCGAATCCGTCGC
Ef1α48d	Reverse	TACGCTTGTCGATACCACCG
Ankyrin1	Forward	TCTTCACGTTGCTGCTCACT
Ankyrin1	Reverse	ATCCGCCTGATTAGCACGAG
Ankyrin2	Forward	GGCCGATATGGCACAAAACC
Ankyrin2	Reverse	TTCTTTCGACGGTGGTACGG
Lesswright (Ubc9)	Forward	ATTTCCGCTAGCAGTCCCAC
Lesswright (Ubc9)	Reverse	TGCTTGGAACCACTGGAGAC

Table 2.3 Primers used for PCR and quantitative Real Time PCR experimental procedures

.

Primers for PCR were designed using the Primer-Blast web tool, and were designed to amplify a product of 70-400 bp, with a melting temperature between 60˚-70˚C. Wherever possible, the primers were also designed over an intron to avoid amplification of genomic DNA, and the region targeted by the RNAi inverted repeats was also avoided so the RNAi itself was not amplified (RNAi is expressed as a 200-300 bp inverted repeat). In addition,

the primers were designed to amplify as many transcript isoforms as possible. All primers were tested by standard PCR before usage in Real Time PCR (qPCR) experiments.

The procedure was performed following manufacturer's instructions (BioRad). A 20 µl reaction was prepared that contained: 10 µl of SsoFast-EvaGreen supermix (BioRad) at a final concentration of 1X, 1 µl of the downstream primer, 1 µl of the upstream primer (Sigma-Aldrich, stock 10 mM), at a final concentration of 500nM, 1 µl of cDNA and 7 µl of RNase/DNase-free water. Runs were conducted in an Eppendorf Mastercycler Gradient machine (Eppendorf).

Standard cycling conditions consisted of initial enzyme activation at 95˚C for 30 seconds, followed by 45 cycles consisting of a denaturation step at 95˚C for ten seconds, annealing at 60˚C for five seconds and elongation step at 72˚C for 20 seconds then a final cooling step at 4˚C.

A total of 5 µl of the amplified products was run on a 2% agarose gel (BioRad) containing 3% ethidium bromide, at 100 V in a Mini Sub ® Cell GT cassette (BioRad) in presence of 1X TAE buffer (Tris-base, acetic acid, EDTA 0.5 M) and ethidium bromide (3 µl) to confirm a single product of the correct size was amplified.

2.7.2 High Fidelity PCR

For amplification of DNA that was to be used for cloning and subsequent expression, proofreading activity of the DNA polymerase was required and the Expand High Fidelity PCR system, 2.6 U/µl (Roche) was used.

The reaction mixture was prepared following manufacturer's instructions. Two mixes of 25 µl each were prepared separately. Mix number one contained dNTP (10mM) 200 µm, upstream primer 300 nM, downstream primer 300 nM (Sigma-Aldrich), template DNA 15 ng.

Mix number two contained the Expand buffer 10X 15 nM-MgCl2 1.5 mM, Expand enzyme 2.6 U/ reaction, H2O to a final volume of 25 µl. The mixes were combined into a 0.2 ml PCR tube on ice, gently resuspended and briefly centrifuged to collect samples at the bottom, and inserted into an Eppendorf PCR machine.

A two-step thermal cycle was set as follows: initial denaturation at 94°C for two minutes, three cycles of each of those steps: denaturation at 94°C for fifteen seconds, annealing at 42°C for 30 seconds, elongation at 72°C for one minute. Second step amplification included 25 cycles of each of the following steps: denaturation at 94°C for

fifteen seconds, annealing at 60°C for 30 seconds, elongation 72°C for one minute. Final elongation consisted in one cycle at 72°C for seven minutes, cooling at 4°C.

2.8 Sequencing

Sanger sequencing was performed to confirm correct DNA cloning. Primers used for this experimental procedure are listed in Tables 2.4, 2.5, and 2.6. Sequencing was performed in an ABI3730 capillary instrument, by the Massey Genome Service (Massey University, Palmerston North, New Zealand).

Oligo name	Direction	Primer Sequence
Ank2	Forward	GGCACAAGCTCCCCGAA
Ank2	Reverse	CCTAGATGAGCTGATTGCCCAT
GFP	Forward	CGGCATGGACGAGCTGTAC
GFP	Reverse	ACCACCCCGGTGAACAGCT

Table 2.4 Primers used to confirm the identity of the Ank2-EGFP line. Abbreviations: Ank2 = Ankyrin2; GFP = green fluorescent protein.

Oligo name	Direction	Primer Sequence
Ank1-MYC rev1	Reverse	TGAGCTGCTATGTGCAAAGG
Ank1-MYC rev2	Reverse	ATTAGCACGAGCTGCCAAGT
Ank1-MYC rev3	Reverse	TACAAGAACATGGCCCTCCT
Ank1-MYC rev4	Reverse	CGTGCATCTACCAAGAACGA
Ank1-MYC rev5	Reverse	TGCCATAACATGCATTAACCA
Ank1-MYC rev6	Reverse	TGTGGTTTAATTTTCCATGCG

Table 2.5 Primers used for sequencing of the Ankyrin1-MYC construct. Abbreviations: Ank1 = Ankyrin1; rev = reverse.

.

Oligo name	Direction	Primer Sequence
pGEX-2TK	Forward	GGGCTGGCAAGCCACGTTTGGTG
pGEX-2TK	Reverse	GAGGTTTTCACCGTCATCACC

Table 2.6 Primers used for sequencing of pGEX-2TK-HDAC4-GST

.

Genomic DNA was prepared by combining 50 µl of squishing buffer (10 mM Tris-HCl pH 8, 1 mM EDTA, 25 mM NaCl, 200 µg/ml proteinase K) with three flies in a 1.5 ml tube, then homogenising with a motorised pestle for five to ten seconds and incubating

at 37°C for 30 minutes. The proteinase K was inactivated by heating at 95°C for three minutes and then samples were centrifuged at maximum speed for one minute at room temperature. The supernatant was transferred to a new tube and 1 µl of the genomic DNA was used for sequencing.

2.9 DNA purification

2.9.1 PCR purification

In order to remove primers and nucleotides from PCR-amplified products, PCR purification was conducted using the PureLink™ Quick PCR purification Kit (Life Technologies Invitrogen) according to manufacturer's instructions.

2.9.2 Agarose gel purification

In order to isolate DNA fragments for subsequent ligation into recipient vectors, restriction digested products were extracted and purified from agarose – ethidium bromide gels. Agarose gels (1%) were stained with ethidium bromide which allowed visualisation of DNA bands under a UV light source. Bands of interest were excised with a sterile steel surgical blade (Swann-Morton) and immediately inserted into a 1.5 ml tube for subsequent DNA purification using the PureLink™ Quick Gel extraction kit (Life Technologies) according to manufacturer's instructions.

2.10 DNA manipulation

2.10.1 Restriction digest

Plasmid DNA was digested with appropriate restriction endonucleases at 37°C for three hours in a water bath. Reactions contained approximately 90-100 ng of DNA in a 40-50 µl total volume, with 15 U/µg of specific restriction endonuclease and 10% of the appropriate buffer. Buffer H was used for all reactions unless indicated otherwise and 10% bovine serum albumin (BSA) was used in presence of XhoI only. Enzymes were inactivated at 75°C for 20 minutes. Following restriction digestion, the recipient vector was incubated with 1 µl of calf intestinal alkaline phosphatase (CIP, New England BioLabs) for one hour at 37°C in order to dephosphorylate 5' ends to prevent religation.

The CIP-treated vector was ligated with the appropriate gel purified DNA fragment (section 2.9.2).

2.10.2 Ligation

Inserts were ligated into CIP-treated recipient vectors. Approximately 100 ng of vector was combined with the appropriate insert in a 5:1 molar ratio of insert to vector, in a total volume reaction of 10 µl containing 1 µl T4 DNA ligase reaction buffer 10X and 1 µl T4 DNA ligase (New England BioLabs). The ligation reaction was conducted at 16°C overnight.

2.10.3 Plasmid transformation

Ligated products were transformed into *Escherichia coli* (*E. coli*) competent cells. Strains transformed were DH5α (Invitrogen) or BL21 (New England BioLabs) for plasmid purification and recombinant protein expression, respectively. Competent cells (50-100 µl) were thawed for 30 minutes on ice and 5 µl of ligated product were added to the cells and incubated for further 30 minutes on ice. Cells were heat shocked in a water bath at 42°C for 45 seconds then immediately transferred back on ice for two minutes. 500-1000 µl of either SOC or LB media were added to the bacteria-plasmid mixture and the cells incubated for one hour on a shaking platform at 220 revolution per minute (rpm). The bacteria were then spread on LB agar plates containing ampicillin (100 mg/ml) and incubated at 37°C overnight. The subsequent day single colonies were picked for plasmid purification.

2.10.4 Plasmid DNA purification

2.10.4.1 Mini preparation of plasmid DNA

For small scale plasmid DNA extraction, single bacterial colonies from LB agar antibiotic plates were picked and inserted into 3 ml LB/100 µg/ml ampicillin (stock solution 100 mg/ml) media for overnight growth at 37°C on a shaking platform at 220-225 rpm. Approximately 20 µg of plasmid DNA was isolated using DNA-Spin™ Plasmid DNA Purification Miniprep kit (Intron) following the manufacturer's instructions.

2.10.4.2 Midi-scale preparation of plasmid DNA

In order to produce the high quality plasmid DNA required for generation of transgenic *Drosophila* (section 2.11), midi-scale preparations of plasmid DNA were necessary. Bacteria were grown at 37°C in a 1 L flask containing 250 ml of LB and 100 µg/ml ampicillin (from a 100 mg/ml stock solution), placed on a shaking platform at 220-225 rpm. The PureLink® HiPure Plasmid Midiprep Kit (Thermo Fisher Scientific) was used to isolate high quality plasmid DNA following manufacturer's instructions.

2.10.5 Addition of MYC epitope tag to the C-terminus of Ankyrin1

Enzymes and primers used for this experimental procedure are listed in Tables 2.7 and 2.8 respectively.

Restriction enzyme	**Unit/amount µl**	**Sequence recognised**	**Brand**
EcoRI	15U/1.5 µl	5'-G/AATTC-3' 3'-CTTAA/G-5'	Roche
XhoI	15U/1.5 µl	5'-C/TCGAG-3' 3'-GAGCT/C-5'	NEB
StuI	1U/0.5 µl	5'-AGG/CCT-3' 3'-TCC/GGA-5'	NEB

Table 2.7 Restriction endonucleases used for Ankyrin1-MYC subcloning. Abbreviations: NEB = New England labs.

Oligo name	**Direction**	**Primer Sequence**	**Restriction site/Tag**
Ank1-for	Forward	CTCCTCCAACAACCCGAGCAACATGGGA	N/A
Ank1-MYC-XhoI-rev	Reverse	AATAATCTCGAGTTACAGATCCTCCTCGGAGATCAGCTTCTGCTCCTGTTCATACGCCATCTTTTTC	XhoI/MYC

Table 2.8 Primers used for Ankyrin1-MYC subcloning. XhoI restriction site underlined, MYC sequence highlighted in yellow. Primers are shown in 5′ 3′ orientation. Abbreviations: Ank1 = Ankyrin1.

A full length Ankyrin1 (Ank1) cDNA (clone LD10053, GenBank code BT031123, covering transcript variants A, B, C, D, BDGP Drosophila Research Centre, Gold collection) was used in order to add a MYC epitope tag to its C-terminus. The LD library clones cDNAs (Hong L.) were made using Stratagene ZAP-cDNA synthesis kit. The cDNA was directionally cloned into EcoRI/XhoI-digested Stratagene Uni-Zap XR vector, which allows *in vivo* excision and recircularization of pBluescript SK(+/-) plasmid (Hong L., BDGP).

In order to add the MYC tag to the 3′ end of the Ank1 coding region, a 1,100 bp product corresponding to nucleotides 3942-5067 of Ank1, (up to but excluding the stop codon) was amplified from LD10053 with Expand High Fidelity polymerase (section 2.7.2, Figure 7.2A, Appendix 7.2) using the primers Ank1-for and Ank1-MYC-Xho-rev (Table 2.8). The amplified product was PCR purified (section 2.9.1) and digested with EcoRI and XhoI (section 2.10.1). EcoRI cuts internally within the PCR product, resulting in an approximately 679 bp digested product (Figure 7.2A, Appendix 7.2). This was ligated into a pUASTattB vector (~8,489 bp, Figure 7.1 and Figure 7.2A, Appendix 7.2) and transformed into *E. coli* (section 2.10.3). The resulting intermediate vector, pUASTattB-Ank1 3′-MYC (Figure 7.2B, Appendix 7.2) contains the MYC-tagged 3′ end of Ank1. In order to add the N-terminal of Ank1 coding sequence, LD10053 clone was digested with EcoRI and XhoI to release a ~4,000 bp fragment containing the N-terminal portion of Ank1 (Figure 7.2C, Appendix 7.2), which was subsequently cloned into EcoRI digested pUASTattB-Ank1 3′-MYC (Figure 7.2C, Appendix 7.2). The resulting plasmid contains the full-length ~4,679 bp Ank1-MYC construct, resulting in a plasmid of 13,168 bp (Figure 7.2D, Appendix 7.2). Following ligation (section 2.10.2), transformation (section 2.10.3) and DNA purification, (section 2.10.4.1), XhoI/StuI digests were performed to identify positive clones. A physical map of the vector was generate using SnapGene version 3.2.4 (Figure 7.3, Appendix 7.2).

2.10.6 Cloning of HDAC4 ankyrin binding region into pGEX-2TK

Enzymes and primers are listed in Tables 2.9 and 2.10.

Restriction enzyme	**Unit/amount µl**	**Sequence recognised**	**brand**
EcoRI	15U/1.5 µl	5'-G/AATTC-3' 3'-CTTAA/G-5'	Roche
BamHI	15U/1.5 µl	5'-G/GATCC-3' 3'-CCTAG/G-5'	NEB

Table 2.9 Restriction endonucleases used for pGEX-2TK-HDAC4-GST subcloning

.

Oligo name	**Direction**	**Primer Sequence**	**Restriction site**
HDAC4-GST BamHI	Forward	ATATGGATCCGCACGCGGCAGGGATGGCAT	BamHI
HDAC4-GST EcoRI	Reverse	TCTAGAATTCTCACGCCGAGTTGGGTAAATGCGG	EcoRI
pGEX-2TK **pGEX-2TK**	Forward Reverse	GGGCTGGCAAGCCACGTTTGGTG GAGGTTTTCACCGTCATCACC	N/A

Table 2.10 Primers used for amplification of HDAC4-GST.

Synthetic oligonucleotides from a modified *Drosophila* HDAC4 clone (Fitzsimons et al., 2013), BDGP GH08881, GenBank number BT030815 were designed to amplify a ~660 bp region of HDAC4 containing the putative ankyrin repeat and Mef2 binding regions (aa 144-365, sequence ARGRDGMKLKQNCSANASPEVKQILNCFILSRKSQAAASNGTTTTSPYRNRGVVKSSSGESLPAGTVTSAHPYKIPQPPPSLLKYESDFPLRKTASEPNLLKIRLKQSVIERKARIGGPAGARRHERLLQAAQRRQQKNSVLTNCNSTPDSGPNSPPSAAALAVGVVGSRGSPTSAPIQEENEEGSQYQPGQRSSINDLPLFSSPSLPNISLGRPHLPNSA.

The ~660 bp region was amplified from GH08881 with Expand High Fidelity polymerase (section 2.7.2) using the primers HDAC4-GST BamHI and HDAC4-GST EcoRI (Table 2.10), with annealing temperature set at 55°C in the first step and 72°C during the second step. A concentration of 5% dimethyl sulfoxide was added to the reaction mixture to overcome amplification issues likely caused by the high GC content (71%) of the sequence. The amplified product was digested with EcoRI and BamHI and ligated into EcoRI and BamHI sites of pGEX-2TK vector (GE Healthcare Life Sciences)

(Figure 7.4, Appendix 7.2). Transformation was carried out in DH5α competent cells following standard procedures (sections 2.10.1 and 2.10.2). A physical map of the vector was generated using SnapGene®, version 3.2.4 (Figure 7.5, Appendix 7.2).

2.11 Generation of transgenic flies

High quality plasmid DNA was prepared as previously described (section 2.10.4.2). A total of 20 μg of pUASTattB-Ank1-MYC plasmid was precipitated and re-suspended in 50 μl of injection buffer (50 mM KCl, 0.1 mM sodium phosphate buffer, pH 6.8, Sambrook et al., 1989), filtered through 0.2 μm Suppor® membrane, Acrodisc (Pall Corporation) and stored at -20°C. On each day of use the solution was centrifuged for ten minutes to reduce clogging of the needle by particulate material. About three days prior to injection, additional yeast was added to cultures of the attP stock used for microinjection. The line used had the following genotype: *(y w, P {hs-flp}; P {3xP3-RFP=attP-86F}; P {3xP3-RFP=φC31[3xP3-GFP=vas-φC31]} 102F)*. This fly strain harbours several components including: i) the attP recipient site for the attB site from the pUAST plasmid which contains the transgene of interest (Ank1-MYC in this case); ii) the *Streptomyces* phage φC31 encoding a serine integrase that mediates sequence-directed recombination between a bacterial attachment site (attB) and a phage attachment site (attP) creating the two hybrid sites attL and attR which are refractory to the integrase and prevent further integrase-catalysed movement of the integrated transgene; iii) a landing site referred to as {3xP3-RFPattP} containing an attP site located at cytological position 86F on the third chromosome, which serves as the docking site for any incoming attB-containing plasmid (the pUASTattB-Ank1-MYC in this case), the red fluorescent protein (RFP) as a marker driven by the artificial 3xP3 promoter, leading to strong RFP expression in the eyes. RFP was chosen so as to not preclude the later use of the widespread markers yellow (y) and white (w); iv) a 3xP3 GFP marker cassette which would indicate presence of the φ31 integrase whose expression is driven by the vasa regulatory element, which causes germ-cell specific expression by specifically directing zygotic transcription in these cells (Bischof et al., 2007) (Figure 2.1).

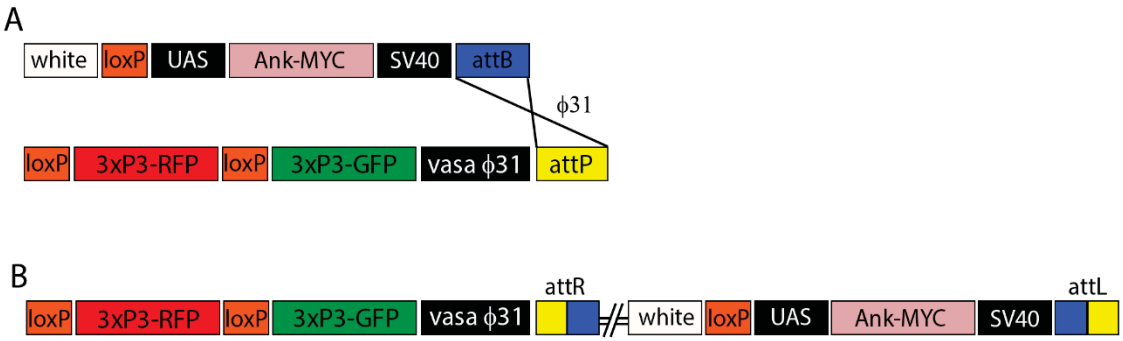

Figure 2.1 Transgenic insertion mechanism. (A) Integration mechanism of the pUASTattB vector in the attP landing site. (B) Resulting construct from attB and attP recombination. Combination sites attR-L are formed to prevent integrase to move. The GFP cassette is used as selectable marker to detect the integrase. Flies expressing GFP are noticed by green fluorescence under fluorescence microscope. Abbreviations: loxP = locus of X-over P1; UAS = upstream activating sequence; Ank-MYC = Ankyrin1-MYC; SV40 = Simian virus 40; att = arginine tolerance test; RFP = red fluorescent protein; GFP = green fluorescent protein.

On the injection day, 100 to 200 pairs of flies were tapped into polystyrene beakers (45 mm diameter, 90 mm deep) taped to a 60 mm x 15 mm polystyrene petri dish (Fisher Scientific) filled with fresh standard media streaked with a light yeast paste to promote laying of eggs, and incubated at 25°C.

Unlaid eggs were purged for one hour and discarded prior to collection of eggs for microinjection. The food plate was replaced and flies were allowed to lay for 20 minutes prior to egg collection. Eggs were collected for the plate with a fine paintbrush and dechorionated by rolling with fine forceps on double-sided tape, then aligned with the posterior area facing right on a strip of double sided tape attached to a microscope slide. About five to ten embryos were aligned over a five minute period. The slide was placed on top of silica beads in a closed glass plate and dehydrated for three to ten minutes. This varied from day to day depending on the humidity. Eggs were then immediately covered with Halocarbon oil 700 (Sigma H8898) to prevent further dehydration and to reduce cytoplasm leakage after injection, and were injected as soon as possible. Approximately 5 µl of plasmid preparation was loaded with a 20 µl Eppendorf Microloader^{TM} tip into a needle that was then attached to a micro-manipulator (Leica). The needles used were made from 1.0 mm x 0.75 mm, 10 cm long thin-walled borosilicate capillary glasses with

microfilament (A-M Systems) pulled from a laser-based micropipette puller (P-2000, Sutter Instrument®).

DNA injection into the embryos was performed with a Femtojet express transjector (Eppendorf) under pressurised nitrogen gas. A small but undetermined amount of injection preparation was injected to the posterior end of the embryos. The moicroinjection procedure was visualised with a CK2 inverted compound microscope (Olympus). Embryos that were not successfully injected were destroyed with forceps under the dissecting microscope.

The slides were incubated overnight at 18°C in a humidity chamber (QNA international MIC -101) under pressurised oxygen (approximately 2 atmospheres). On the following day, the chamber was placed at 21°C, allowing larval collection on moist tissue paper (Kimberley-Clark Kimwipe) which were immediately placed into vials of standard media and raised at 25°C.

2.11.1 Genetic crosses to establish lines

Following microinjection, surviving G_0 flies were outcrossed individually to w^{CS10} line (white eyes). The progeny were screened for presence of the selectable marker *w+*. This restores the white gene and as the local chromatin environment influences the level of expression of *w+*, transgenic flies display eye colours ranging from light orange to wild-type red eyes. Since the Ank1-MYC construct is inserted on the third chromosome (the attP site locates at cytological position 86F on the third chromosome), single *w+* transformant flies (G_1) were crossed to w^{CS10}; *TM3, Sb*, a third chromosome balancer line. Both male and female progeny that were both *Sb* and *w+* were selected (stubble bristles and orange eyes). They contained one copy of the transgenic construct on the third chromosome, which was balanced over *Sb*. In a self-cross of these flies, the Ank1-MYC insertion on the third chromosome segregated from the *Sb* balancer thus homozygous stocks could be established from the non-stubble, *w+* progeny. *Sb* flies (G_2) were therefore collected and self-crossed to obtain an Ank1-MYC homozygous line (G_3). For all insertions, red fluorescent eyes were observed as a confirmation of the attP landing site (3xP3-RFP) and green fluorescent eyes were not selected in order to remove the integrase (GFP=vas-φ31). The resulting transgenic line contained the Ank1-MYC construct with genotype w^{CS10}*; P (3xP3-RFP = attP-86F) Ank1-MYC*. Figure 2.2 shows

a representative summary of the transgenesis procedure from injection to transgenic flies growth.

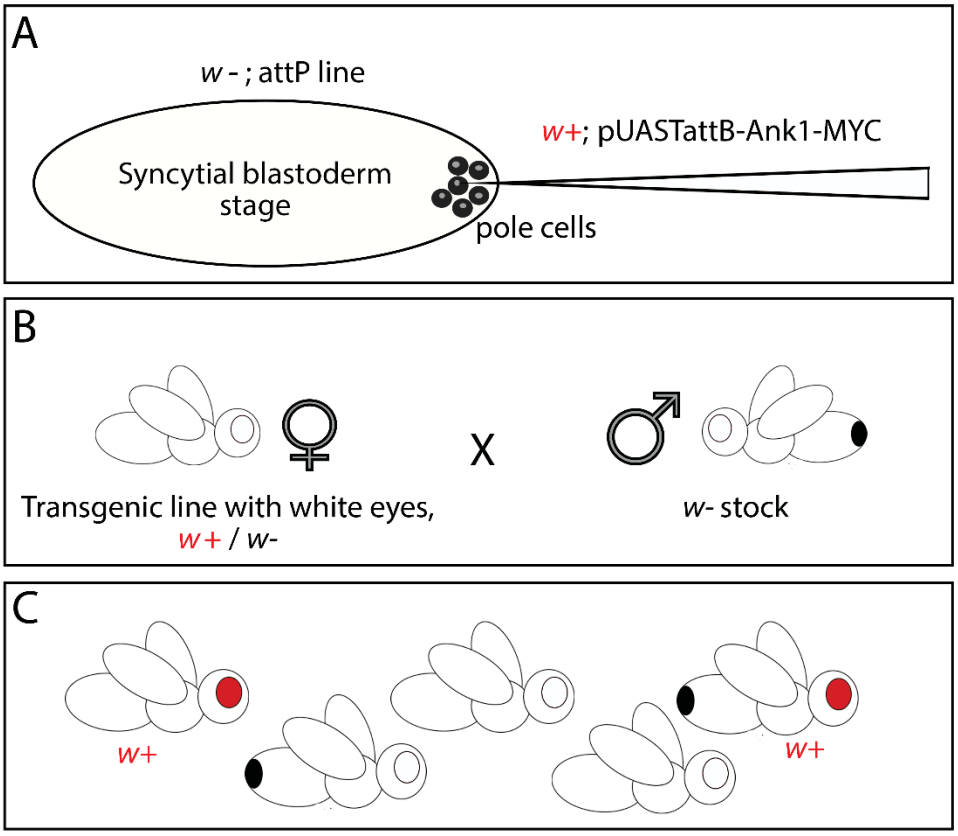

Figure 2.2 Injection procedure to generate transgenic flies. (A) *white*+ (*w*+) transgene DNA (pUASTattB-Ank1-MYC) is injected into a G_0 *w*- *Drosophila* embryos of less than one hour old. The early developmental stages of *Drosophila* embryos are characterized by rapid nuclear divisions that creates a syncytium. Prior to cellularisation, pole cells (represented in dark gray) grow in the posterior end. For germ line transmission to occur, the transgenic DNA must be injected into the pole cells designed to become germ cells. (B) Resulting flies are grown and transgenic flies harbour the *w*+ marker. Each fly is crossed to mutant *w*- strain. (C). Transgenic flies present wild-type red eyes due to the presence of *w*+.

2.12 Preparation of cell lysates

For the purpose of Sodium dodecyl sulphate - polyacrylamide gel electrophoresis (SDS-PAGE) and western blot analysis, cytoplasmic fraction lysates were prepared as follow.

Approximately 20 flies were collected into a 1.5 ml eppendorf tube with 100 µl of Buffer I (1mM dithiothreitol, 1.1 mM EDTA, 15 mM HEPES pH 7.6, 10 mM KCl, 5 mM

MgCl2, 0.5 mM EGTA, 0.35 M sucrose, H2O, 1X protease inhibitor added prior the use from a 25X stock solution). Samples were homogenised five times for three seconds pulses with a motorised pestle until the suspension appeared very milky. The suspension was transferred into a new tube in order to separate the body debris from the lysate. The lysate was homogenised again for five three second pulses to ensure all cells were lysed. Samples were quickly spun up to 2,000 rpm at 4°C for four times followed by a five times homogenisation for three seconds pulses. This process was repeated for four times. Samples were then centrifuged at 7,700 x g for fifteen minutes at 4°C to pellet the nuclei. The supernatant containing the cytoplasmic fraction was collected into a fresh 1.5 ml eppendorf tube and resuspended into 100 µl of Buffer I and stored at – 80°C.

The colorimetric BCA protein quantitation assay (Pierce BCA Protein Assay Kit, Thermo Scientific) was used to measure total protein concentration compared to a protein standard. Samples and the standard were processed according the the manufacturers' instructions and placed in a transparent 96 well plate (Greiner Bio-One CELLSTAR® 96 well transparent polystyrene plates) and read in a BioTek PowerWave HT Microplate Spectrophotometer) at 562 nm. Data were visualised through BioTek's Gen5™ analysis software.

2.13 SDS-PAGE and western blotting

Primary and secondary antibodies used for this procedure are listed in Tables 2.11 and 2.12.

Protein name	**Clone**	**Class**	**Host/ Isotype**	**Brand**	**Dilution**
α-Tubulin	N12G10	Monoclonal	Mouse	DSHB	1:500
Ankyrin2-L	aa 1655-1912 of SP2523 C-Terminal	Polyclonal	Rabbit	Dr Aberle	1:5,000-1:10,000
GFP	Ab290	Polyclonal	Rabbit	Abcam	1:5,000-1:10,000

Table 2.11 Primary antibodies and corresponding dilutions used for western blot analyses. Abbreviations: DSHB = Developmental Studies of Hybridoma Bank.

.

Product name	**Brand**	**Dilution**
ECL™ peroxidase anti-mouse NA931VS	GE Healthcare Life Sciences	1:20,000
ECL™ peroxidase anti-rabbit NA934VS	GE Healthcare Life Sciences	1:40,000
Precision Plus protein™ WesternC™ StrepTactin-HRP conjugate	Bio Rad	1:50,000

Table 2.12 Secondary antibodies and corresponding dilutions used for western blot analyses.

The cytoplasmic fractions were boiled at 95°C for five minutes in presence of 5X Laemmli buffer, pH 6.8 (2% sodium dodecyl sulphate, 5% 2-mercaptoethanol, 10% glycerol, 0.01% bromophenol blue, 60 mM Tris HCl pH 6.8) and resolved on 10% mini SDS-PAGE gels (running gel: 30% Acrylamide, 1.5 M Tris pH 8.8, 10% sodium dodecyl sulphate, 10% ammonium persulphate, tetramethylethylenediamine, stacking gel: 30% acrylamide, 1.5 M Tris pH 6.8, 10% sodium dodecyl sulphate, 10% ammonium persulphate, tetramethylethylenediamine).

A total of 40 μg of protein was loaded on the gel in presence of 1X Running buffer (final concentration 25 mM Tris, 190 mM glycine, 0.1% SDS) in a Mini-PROTEAN Tetra Cell (Bio Rad) and run at 120 V for approximately two hours. Proteins were transferred from the SDS gel onto a nitrocellulose membrane (Amersham™ Protran™ premium 0.45 μm NC, GE Healthcare Life Science) for 90 minutes at 100 mA in a Mini Trans-Blot cell blotting module (BioRad) in pre-chilled 1X Transfer buffer (final concentration 25 mM Tris, 190 mM glycine, 0.1% SDS, 20% methanol). Then, the membrane was quickly rinsed with distilled H_2O and the presence of protein bands verified by incubation in Ponceau-S stain (0.1% Ponceau Stain-S in 5% acetic acid). After washing twice with H_2O, the membrane was incubated with gentle agitation throughout all steps. After bathing in blocking buffer (5% skim milk powder in TBST) for one hour at room temperature to reduce non-specific binding, the membrane was incubated with primary antibodies (Table 2.11) diluted in 1% blocking buffer overnight at 4°C. Next day, the membranes were washed with TBS-Tween (1X TBS, 0.1% Tween-20) three times five minutes each, and incubated with appropriate secondary antibodies (Table 2.12) diluted in TBST for one hour at room temperature. The membranes were washed as previously described and proteins were detected using a chemiluminescent substrate from either Amersham™ ECL select™ Western blotting Detection Reagent (GE Healthcare) or a Pierce® ECL Plus Western Blotting Substrate (Thermo Scientific). Chemiluminescence was visualised with an intelligent dark box (FUJIFILM LAS100, lens type URF20L) and Image reader LAS1000 Pro Software, version 2.12.

2.14 Coomassie Brilliant Blue staining

For GST pull-down experiments coomassie brilliant blue staining was used to detect recombinant protein expression following standard procedures. The gel was incubated in fixing solution (50% methanol, 10% glacial acetic acid) for one hour with gentle agitation and then transferred to staining solution (0.1% Coomassie Brilliant Blue R-250, 50% methanol and 10% acetic acid) for 30 minutes with gentle agitation. The gel was destained with destaining solution (40% methanol, 10% acetic acid) until the background of the gel was fully destained. Proteins were detected in a GelDocXR machine (BioRad) on a white platform for protein detection.

2.15 GST pull-down assay

In order to detect whether a physical interaction between HDAC4 and Ankyrin2 (Ank2) occurred in *Drosophila*, a GST pull-down assay was performed. GST pull-down experiments involve the presence of a probe protein as a GST fusion construct whose coding sequence is cloned into an isopropyl-β-D-thiogalactoside (IPTG)-inducible expression vector. This fusion protein is then expressed in bacteria and induced with IPTG. Target proteins are usually lysates of cells or purified products, either labelled with [35S] methionine or unlabelled, depending on the method used to assay the interaction between the target and the probe. For unlabelled target method, the cell lysate and the GST fusion protein are incubated together with glutathione-agarose beads, and complexes recovered from the beads are resolved by SDS-PAGE and analysed by western blotting and staining (Sambrook and Russell, 2006).

For the purpose of this project, HDAC4 was fused to GST, inserted into an IPTG inducible vector, pGEX-2TK (section 2.10.6) and expressed in BL21 *E.coli* cells. A cytoplasmic lysate from Ankyrin2-Enhanced GFP (EGFP) flies (Ank2-EGFP) was used as source of Ank2 prey to conduct the pull-down reaction.

2.15.1 HDAC4-GST Fusion construct expression and induction

pGEX-2TK-HDAC4-GST midi preparation was transformed in BL21 *E.coli* cells (New England BioLabs) with standard heat shock procedure (section 2.10.3). Positive

colonies were picked individually and grown at 37°C in 3 ml LB agar/100 µg/ml ampicillin (stock solution 100 mg/ml) overnight on a shaking platform at 220-225 rpm. The subsequent day 1 ml of the overnight cultures was transferred to a starter culture of 100 ml containing carbenicillin (50 mg/ml stock solution) as a replacement of ampicillin, being carbenicillin more suitable over ampicillin for large liquid bacterial cultures because of its resistance to heat and to low pH-induced degradation over time.

Flasks were incubated at 30°C on a shaker at 225 rpm for approximately 2.5 hours, until the OD at A600 reached the value of 0.4-0.5. Fifty µl of uninduced bacterial culture were taken from each flask and was denaturated in the presence of 10 µl 6X Laemmli buffer (375 mM Tris-HCl pH 6.8, 6% Sodium Dodecyl Sulphate, 48% glycerol, 9% 2-Mercaptoethanol, and 0.03% bromophenol blue) for subsequent SDS-PAGE and coomassie brilliant blue procedure (sections 2.13 and 2.14).

Protein expression was induced with IPTG, (Sigma-Aldrich) at different concentrations: 0.01 mM, 0.05 mM, 0.075 mM, 0.1 mM (Figure 7.6, Appendix 7.2) and further incubated at 30°C shaking at 225 rpm for 1.5 hours. Fifty µl were extracted from the induced cultures, denaturated in presence of 10 µl of 6X Laemmli buffer for SDS-PAGE and coomassie brilliant blue staining (sections 2.13 and 2.14).

Induced cultures were transferred to 250 ml centrifuge tubes, immediately placed on ice and centrifuged in a Sorvall rotor at 4°C at 4,000 rpm. The supernatant was discarded and pellets stored at -20°C. Before continuing with the cell lysis and fusion protein release, both the non-induced and induced samples were used to check whether the fusion protein was expressed. Thirty µl of those samples were loaded on a 10% mini-gel, run at 100 V for 1.5 hours and the gel analysed via coomassie brilliant blue staining (section 2.14).

Pellets were then resuspended with 1 ml of CSB buffer (1X PBS, 100 mM EDTA pH 8.0, mini-complete EDTA-free tablet dissolved after filtration). Cells were lysed with three freeze thaw cycles in liquid nitrogen and a water bath at 37°C. A total of 150 µl of 10% Triton X-100 was added to the samples which were then rotated for 30 minutes at 4°C. Sample were centrifuged at 10,000 rpm for ten minutes at 4°C and the supernatant (soluble fraction) and pellets (insoluble fraction) were stored at -80°C. Ten to twenty µl of the soluble fraction were run on a mini gel and protein detected through coomassie blue staining.

2.15.2 GST pull-down

For pull-down binding assays, around 500 μg of Ank2-EGFP cytoplasmic lysate was incubated with the purified HDAC4-GST fusion protein bait. GST alone was used as negative control, and wild type cytoplasmic lysate served as control as well. The following reactions were set up including negative controls with the aim to eliminate the absorbency by GST or glutathione-sephorose-agarose beads 4% (4B) alone:

a. GST-bound glutathione-sepharose-4B beads + NEB 1X buffer (25 mM Tris-HCl pH 8.0, 1 mM EDTA pH 8.0, 10% glycerol, 150 mM NaCl and 0.225% NP40, complete EDTA-free tablet added after filtration);
b. GST-bound glutathione-sephorose-4B beads + wild type lysate;
c. GST-bound glutathione-sephorose-4B beads + Ank2-EGFP lysate;
d. HDAC4-GST fusion protein bound to glutathione-sephorose-4B beads + NEB 1X buffer;
e. HDAC4-GST fusion protein bound to glutathione-sephorose-4B beads + wild type lysate;
f. HDAC4-GST fusion protein bound to glutathione-sephorose-4B beads + Ank2-EGFP lysate.

Initially, a 50% slurry of glutathione beads was prepared according to manufacturer's instructions (75% Sepharose 4B beads, GE Healthcare). GST lysate and HDAC4-GST fusion construct lysate were bound to this 50% beads slurry as follows: in two separate 1.5 ml tube, 25μl of GST and 25 μl of HDAC4-GST lysates was added to 100 μl of 50% slurry and CSB 1X was added to the tube at a final volume of 500 μl. Tubes were incubated at 4°C for three hours on a rotating platform. Samples were then washed three times with 1 ml NEB 1X buffer.

Washes were performed by placing the tubes in a 4°C centrifuge at 500 x g for five minutes. Supernatants were discarded and one pellet volume of NEB 1X buffer (50 μl) was added to obtain a 50% slurry for a total volume of 100 μl to be used for the prey-bait binding reaction.

The following steps were rearranged from Wang and Zeng, 2000. Thirty μl of the 50% GST and 30 μl of the 50% HDAC4-GST slurry was added to a 1.5 ml tube together with 300-500 μg (300 μl) of Ank2-EGFP lysate.

This mixture was vortexed to ensure blending of all components and incubated for four hours at 4°C on a rotating platform. Samples were then centrifuged at 500 x g for five

minutes at 4°C. The supernatant was collected and added to a fresh tube and kept for next step. Pellets were washed four times with 1 ml NEB 1X buffer. The pre-cleared supernatant was added back to the pellets which absorbed non-specifically binding proteins. The tube was vortexed to mix and incubated at 4°C on a rotating platform overnight.

The subsequent day, samples were centrifuged for five minutes at 500 x g at 4°C, and pellets were washed four time with 1 ml NEB 1X buffer, discarding the supernatant each time. Fifteen µl of washed pellets was denaturated in presence of Laemmli buffer 2X, boiled for five minutes at 100°C, centrifuged at maximum speed for one minute at room temperature and both western blot and coomassie blue staining were performed. Western blot procedure was continued using anti-GFP and detected under Intelligent Dark Box, whereas coomassie blue served as a control for the presence of GST and detected in a GelDocXR, on a white board for protein detection.

2.16 RNA manipulation

2.16.1 RNA extraction

RNA extraction was performed on *Drosophila* heads following a protocol by Bogart and Andrews (2006) with slight modifications. All surfaces and pipettes were cleaned and decontaminated with RNase free solution (RNaseZap, Ambion). Buffers, tubes and tips were carefully stored in the RNase free area of the laboratory. All RNase sensitive steps were performed under a fume hood. Heads were removed from -80°C and placed immediately on ice for RNA extraction procedures. RNA was isolated from frozen tissues adding 250 µl of Trizol reagent (Ambion, Life Technologies) in a 1.7 ml tube and homogenised immediately with an electric pestle following a five minutes incubation at room temperature and centrifugation at 12,000 rpm at 4°C for ten minutes. The supernatant was transferred into a fresh tube and 50 µl of chloroform was added. Tubes were vigorously shaken and incubated for three minutes at room temperature and subjected to centrifugation at 10,000 rpm at 4°C for fifteen minutes. The aqueous phase was carefully transferred into a new tube and 150 µl of isopropanol was added following a ten minute incubation at room temperature and centrifugation at 12,000 rpm at 4°C. The supernatant was removed and pellet washed with 1 ml 75% ethanol followed by a further centrifugation at 7,500 rpm 4°C for five minutes. The supernatant was removed and quick

centrifugation was performed to remove the remaining supernatant. Tubes were air dried for ten minutes outside the fume hood and 30 µl of RNase-free water was added. The concentration was measured with a Nanodrop 3300 spectrophotometer (Thermo Fisher). One µg of RNA was used for cDNA synthesis.

2.16.2 cDNA synthesis

Reactions were set up that included 1 µg extracted RNA, 0.5 µl random N6 oligo (Roche) and DEPC-treated water for a final volume of 14.5 µl. The tubes were placed into an Eppendorf PCR machine for ten minutes at 65°C. Next, the reverse transcriptase mixture was prepared as follow: 4 µl of Transcriptor RT buffer, 2 µl of dNTPs, 0.5 µl RNase inhibitor and 1 µl of trancritptor RT enzyme (Roche), another tube containing the same components but not the transciptor RT enzyme was also prepared as the quantitative Real Time PCR control. The PCR machine programme was set to ten minutes at 25°C and 30 minutes at 55°C. When the run was over the tubes were immediately placed on ice and stored at - 20°C for subsequent usage.

2.16.3 Quantitative PCR

Quantitative Real-Time PCR (qPCR) was performed to confirm gene knockdown a subset of RNAi lines. Each UAS-RNAi line (*Ank1*, *Ank2* and *Ubc9*) was crossed to virgin *elav-GAL4* females, resulting in progeny with pan-neuronal knockdown of each RNAi. Virgin *elav-GAL4* females crossed to w^{1118} males (the background strain for the RNAi lines) served as the control. Primers used are listed in Table 2.3 section 2.7.

PCR was conducted using SsoFast-EvaGreen (BioRad) reaction master in a Lightcycler II 480 instrument (Roche), following manufacturer's instructions. Total RNA was extracted from *Drosophila* heads (section 2.16.1) and cDNA was synthesised (section 2.16.2). A 5-fold dilution of cDNA derived from wild-type flies was used as template to prepare a standard curve. A white 96 multi-well plate was used (Roche Life Technologies), and the reaction mix prepared following manufacturer's instructions (BioRad, SsoFAST-EvaGreen Supermix) using a volume of 10 µl for each well. Three independent RNA samples for each genotype were tested.

The thermal cycle consisted of one cycle of pre-incubation at 95˚C for five minutes followed by 45 cycles of amplification comprising denaturation at 95˚C for ten seconds, annealing at 60˚C for five seconds and elongation at 72˚C for 20 seconds. Melting curve,

one cycle at 97˚C, one cycle of final cooling step at 4˚C for ten seconds. The efficacy of the primers was determined to be between 95-105% (Figure 7.7, Appendix 7.2).

2.17 Courtship suppression assay

The repeat training courtship assay was used to assess memory and learning. Courtship conditioning is a form of associative learning through which male flies learn they have been rejected by a mated unreceptive female and when tested with a new mated female they will not court as much as a virgin sham male. Male flies are subjected to training and testing sessions to measure their courtship activity which will reflect their behavioural plasticity, i.e. the ability to learn and form memories (Reza et al., 2013).

Prior to the test, adult males from the testing genotypes were collected and housed alone for up to six days, in cotton-plugged vials containing 5 ml food (Winbush et al., 2012). Approximately 30 virgin CS females, four to six days old, were mated overnight with 35-40 virgin CS males, four to six days old, to obtain unreceptive females for the training session. More males were used for this coupling procedure to guarantee mating of all females. The following day virgin males from each genotype were moved through an aspirating mouth pipette into transparent acrylic round chambers containing food. Chambers had a size of 15 mm in both diameter and depth. The food was poured up to a level of 2-3 mm from the top and covered with an acrylic sliding lid to cover it (Fitzsimons at al., 2011).

Males were randomly assigned to either the trained group, accompanied with a mated female or to the sham group comprising males housed alone.

For long-term memory assessment, flies were trained in the chambers for seven hours, the female was then aspirated leaving the males alone for 24 hours. The same day, approximately 40 females were coupled to 45-50 males to generate freshly mated female for the testing session. The day after, trained and sham males were aspirated into the testing chambers with new mated female and scored for courtship activity over a ten minutes window.

Since the testing chambers were different from the training chambers having a depth of 3 mm and no food present, flies were allowed one minute to adapt to the new environment.

For learning and immediate memory tests, flies were trained for one hour and learning activity was monitored during the first and last ten minutes (Ejima and Griffith, 2010). The same flies were instantly tested for immediate memory over a period of ten minutes. For learning and immediate memory both training and testing sessions were conducted in the testing chambers. For all tests, between each session chambers were cleaned with 95% ethanol to remove any pheromone residue.

The recorder was blind to the flies' genotype to avoid biased results. Flies were either observed and analysed at the same time under a stereomicroscope or recorded using an action camera (Toshiba Camileo X-Sport with a proper lens attached to the objective for focus improvement) and tested later. All experiments were performed under ambient light conditions. The courtship activity was scored using a stopwatch that was paused every time the male stopped courting the female. Males engaged in courtship were clearly visible through well characterised stereotypical behaviours including orientation through which the male orientates toward the female, generally at 45°, then follows and tap her (tapping), sings a species-specific song while vibrating one wing (singing) and eventually licks the female's genitalia (licking), bend his abdomen and attempt copulation (McBride et al., 1999, Figure 1.7). Where copulation occurred, those flies were eliminated from the analysis.

A courtship index (CI) was calculated as the percentage of the ten minutes spent courting. In order to compare memory among genotypes, a memory index (MI) was calculated as the ratio between the courtship indexes of each trained male over the average of the courtship index of sham flies. Memory performance was measured on a scale of zero to one, with zero being the highest memory performance and one indicating no memory (Ejima and Griffith., 2007; Keleman 2007; Fitzsimons et al., 2011; Winbush et al., 2012; Fitzsimons et al., 2013, Schwartz et al., 2016).

A learning index (LI) was calculated as the ratio between the courtship activity of the last ten minutes over the activity of the first ten minutes. As per memory, values closer to zero indicated good learning whereas scores closer to one indicated no learning (Ejima and Griffith, 2010).

For experiment involving the TARGET system, crosses were maintained at 19°C. After eclosion flies were transferred at the permissive temperature of 30°C for three days prior the test, to guarantee induction of transgene expression. Approximately 30 minutes before the test all males were placed at 25°C to allow adaptation to the testing conditions.

All experimental procedures were conducted using ten to 24 males for each group (trained and sham).

2.18 Statistical analysis

For bioinformatic analysis, the statistical significance of each observed change in expression between the samples was measured by Cuffdiff package, included in the Cufflinks pipeline, version 2.2.1 used in this study. The statistical model used to evaluate changes assumes that the number of reads produced by each transcript is proportional to its abundance. The expression level of transcripts across the runs was normalised by the total number of mapping reads using the FPKM normalisation method (Mortazavi et al. 2008; Trapnell et al. 2012). Cuffdiff implements a linear statistical model to estimate an assignment of abundance to each transcript. Fold changes, expressed in log2 scale, raw P-values and adjusted Q-values were calculated by standard methods. Significance was set at $P < 0.05$.

For qPCR experiments, quantitation of the results was conducted using the comparative Ct method also known as the $2^{-\Delta\Delta Ct}$ method normalising the transcripts levels of the samples to those of housekeeping gene *Ef1α48D*. Ct values were automatically generated by the Lightcycler II 480 software. With the $2^{-\Delta\Delta Ct}$ method the data are presented as the fold change in gene expression normalised to an endogenous reference gene, the housekeeping gene. For the reference gene, ΔΔCt was set to zero and and 2^{-0} equals one by definition, so the fold change in gene expression of the reference gene was equal to one (Livak et al., 2001). Data were collected and statistical analysis was assessed by the non-parametric Mann-Whitney U test with significance levels set at $P < 0.05$ (Figure 7.8, Appendix 7.2).

For the behavioural assay, raw data were subjected to arcsine transformation in order to obtain a normal distribution and the memory indexes of each genotype were subjected to a one-way ANOVA test followed by post-hoc analysis with the Tukey's HSD test. The one way ANOVA test was also use to calculate significant differences among the courtship indexes of sham males of each genotype. Significance was set at $P < 0.05$. All graphs are displayed as mean ± standard error.

3 RESULTS

3.1 Identification of genes transcriptionally regulated by *HDAC4*

In an effort to elucidate the impact of *HDAC4* on transcription and to identify possible gene targets, a transcriptome analysis was conducted on heads of transgenic flies overexpressing *HDAC4* in all neurons. It was previously shown that induced overexpression of *HDAC4* in the adult brain of *Drosophila* impaired LTM (Fitzsimons et al., 2013) therefore, in order to provide the same experimental conditions used in the LTM memory assay, the TARGET system (section 1.3.2) was used in combination with the *elav-GAL4* driver (Figure 3.1) to drive gene expression in all neurons (Koushika et al., 1996; Brand and Perrimon, 1993; McGuire et al., 2004). As *HDAC4* is involved in segmentation of the embryo (Zeremski et al., 2003) the TARGET system provided a means to overcome developmental effects caused by overexpression of *HDAC4* thus allowing evaluation of the effects of *HDAC4* on gene expression and memory in the adult brain.

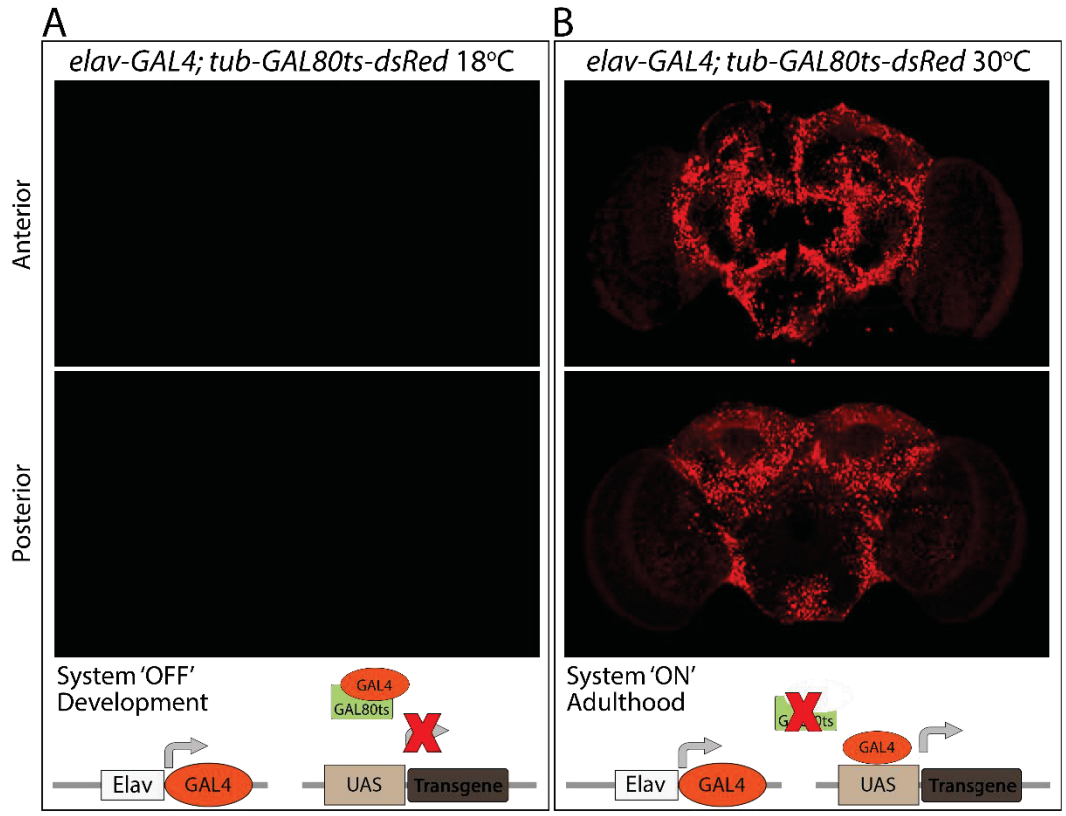

Figure 3.1 The *elav-GAL4; tub-GAL80^{ts}* construct drives transgene expression in all neurons during adulthood. (A) Confocal micrographs of anterior and posterior brains of flies grown at 18°C harbouring nuclear red fluorescent protein Redstinger (dsRed) driven by the *elav-GAL4; tub-GAL80^{ts}* driver. At 18°C transgene expression is not activated since the temperature sensitive

mutant GAL80^{ts} prevents GAL4 binding to the UAS (cartoon). (B) At 30°C GAL80^{ts} is non-functional and GAL4-mediated activation of the UAS transgene is activated (cartoon). Abbreviations: UAS = Upstream Activating Sequence; tub = tubulin.

Male flies harbouring the transgene construct *UAS-HDAC4OE* (in which the *HDAC4* open reading frame is fused to *UAS*) were crossed to females of the *elav-GAL4; tub-GAL80^{ts}*. In these flies GAL4 is expressed pan-neuronally through the *elav* promoter and GAL80^{ts} is expressed ubiquitously by the *tubulin* promoter. An illustration of the genetic crossing scheme used to generate the *HDAC4OE* and control flies is shown in Figure 3.2.

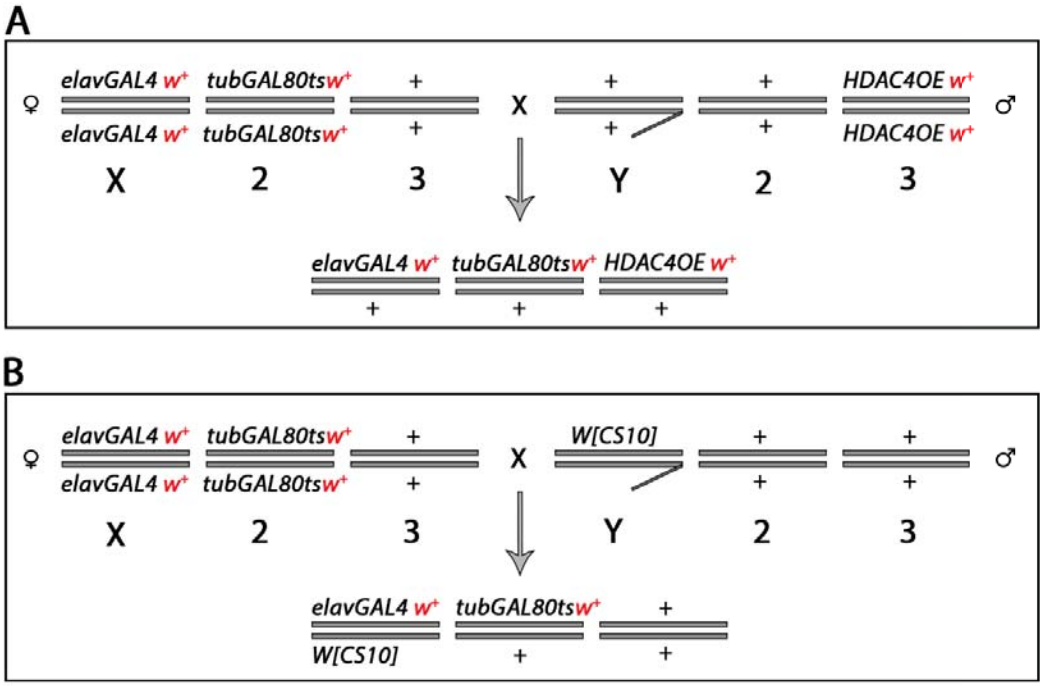

Figure 3.2 Representation of the genetic scheme to generate *HDAC4OE* and control flies for transcriptome analysis. Chromosomes are shown as gray lines and numbered with X and Y indicating the first chromosome (X for females and Y for males). Following the second chromosome (2) and the third chromosome (3). The mini *white* (*w+*) gene, a selectable marker of transgenesis, is highlighted in red. (A) Genetic cross between *elav-GAL4; tub-Gal80^{ts}* females and *UAS-HDAC4OE* males results in progeny that overexpresses *HDAC4* at 30°C. (B) Control cross in which wild type w^{CS10} flies were used instead of flies overexpressing *HDAC4*. The w^{CS10} wild type strain possesses a *w-* mutation in a wild-type Canton special (CS) strain genetic background which is the same genetic background as *HDAC4OE*.

Flies were raised at the temperature of 18°C during development. At this temperature, GAL80^{ts}, a temperature sensitive mutant, is active and inhibits GAL4 activity. Following eclosion, flies were transferred to 30°C to inactivate GAL80^{ts} permitting GAL4-mediated activation of the UAS transgene (McGuire et al., 2004).

Following isolation of RNA from heads, sequencing libraries were generated from three independent biological replicates from wild-type and flies overexpressing *HDAC4* and the samples were sequenced using a single-end strategy (section 2.5).

RNA sequencing (RNAseq) analysis resulted in a high quality percent alignment of the reads to the genome (>80%) for each replicate (Table 3.1). One of the three control samples displayed a different Fragments Per Kilobase of transcript per Million mapped (FPKM) distribution with respect to the other replicates, showing a smaller inter-quartile range and more outliers in the distribution (Figure 3.3A). However, the median value was still within the inter-quartile range of the other distribution and the other two control replicates reflected a similar distribution to the three overexpression (OE) replicates. The analysis was performed both including and excluding this control. Significant changes in transcript abundance were detected in 32 genes and 28 of these genes were still significantly differentially expressed when the analysis included the three controls (Figure 3.3B).

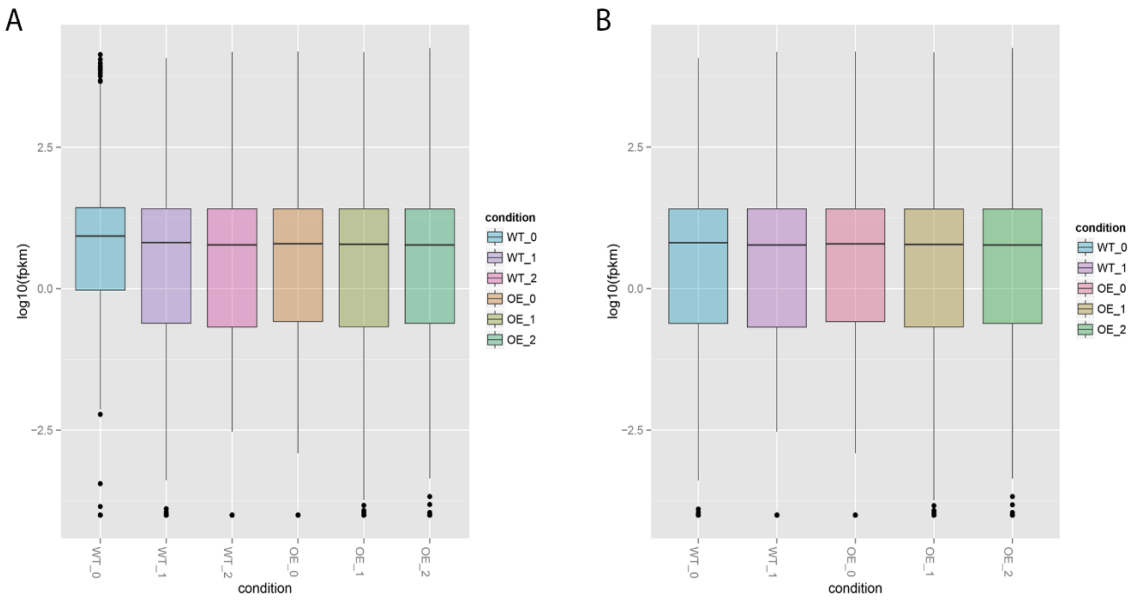

Figure 3.3 Boxplots showing the FPKM distribution of the sample replicates. Range of FPKM values represented as log10 transformed FPKM values for the replicates of both conditions wild-type and *HDAC4OE*. (A) Boxplot includes the excluded control indicated as WT_0 which

displays a different FPKM distribution compared to the other replicates. (B) Boxplot in which the equivocal wild-type control was excluded. Abbreviations: WT = wild-type, OE = overexpression.

Sample	Replicate	Alignment percentage
CS	1	83.5%
CS	2	88.3%
CS	3	87.5%
OE	1	88.7%
OE	2	86.3%
OE	3	86.3%

Table 3.1 Reads alignment percentages. High quality percent alignment were obtained for each replicate from the TopHat analysis over the *Drosophila* genome. The table includes the alignment percentage of the control that was excluded (control CS 1).

The analysis confirmed that *HDAC*4 was significantly overexpressed by nearly twofold and the *white (w)* gene was significantly overexpressed as well. This was expected since the *w* gene was used as an eye selectable marker for transgenesis and flies overexpressing *HDAC4* harboured three copies of *w* compared to the two copies harboured by control flies (Figure 3.2), validating the capacity of this methodology to detect changes.

However, global changes in gene expression were not observed since out of the approximately 17728 genes of the *Drosophila* genome (FlyBase FB2016_03 released May 26th, 2016), only 28 showed significant differential expression, with 13 genes showing down-regulation and 13 (not including *HDAC4* and the *w* gene) displaying up-regulation (Table 3.2). As the analysis was performed on whole heads, an evaluation of the expression pattern of these genes in the head, eyes and brain was undertaken using microarray data from Flyatlas (flyatlas.org), a free online resource that provides a comprehensive microarray data collection of gene expression in multiple tissues of *Drosophila melanogaster* (Chiantapalli et al., 2007; Robinson et al., 2013).

The RNA expression levels of each genes in the head, eye and brain are listed in Table 3.3. For some genes there was no information available about their expression levels in the brain (*Larval serum protein 2, Ornithine decarboxylase 1*) and for other genes, the expression level in the brain was <10, which is considered to be “no” expression by Flyatlas (*Odorant binding protein 99d, CG9701, CG4757, CG18473, Homogenitsate 1,2-dioxygenase, CG31205 CG3088, CG8329, CG8343, CG11211, CG9676*).

In order to prioritise genes for further analysis it was decided that only genes with a signal intensity > 10 would be considered as according to Flytlas, RNA expression levels which range between 0-10 are considered no expression, signals over 100 are considered abundant, and anything over 1000 as remarkable (Chintapalli et al., 2007). Similarly, this was the cut-off used in a previous study by Winbush and colleagues (2012) that performed an RNA sequencing analysis to detect gene expression changes associated with LTM of courtship rejection in *Drosophila* males. Genes that displayed RNA expression level > 10 were taken under consideration for further analysis and included: *CG6409, Laminin A, Carbonic anhydrase 2, Odornat binding protein 56b, Niemann-Pick type C-2g, Activity regulated cytoskeleton associated protein 1, UDP-glycosyltransferase 35b, CG9377, Short Spindle 7, CG6503,* and *Kekkon 2*.

Gene name	FlybaseID	log2(fold change)	P-value	Q-value	Molecular function/biological process
Odorant binding protein 99d/Obp99d	FBgn0039684	-1.67	5.00E-05	0.016069	Odorant binding/sensory perception of chemical stimulus.
Larval Serum Protein 2/ Lsp2	FBgn0002565	-1.37	5.00E-05	0.016069	Nutrient reservoir activity/synaptic target inhibition; motor neuron axon guidance.
CG9701	FBgn0036659	-1.34	5.00E-05	0.016069	Hydrolase activity/carbohydrate metabolic process.
CG4757	FBgn0027584	-1.27	5.00E-05	0.016069	Carboxylic ester hydrolase activity/unknown.
CG18473	FBgn0037683	-1.26	5.00E-05	0.016069	Hydrolase activity/catabolic process.
CG6409	FBgn0036106	-0.90	5.00E-05	0.016069	Unknown/GPI anchor biosynthetic process.
Laminin A/LanA	FBgn0002526	-0.76	5.00E-05	0.016069	Receptor binding/brain development, tissue morphogenesis.
Kekkon 2/kek2	FBgn0015400	-0.71	5.00E-05	0.016069	Unknown/sensory perception of pain.
Carbonic anhydrase 2/CAH2	FBgn0027843	-0.70	5.00E-05	0.016069	Carbonate dehydratase activity/one-carbon metabolic process.
Activity-regulated cytoskeleton associated protein 1/Arc1	FBgn0033926	-0.68	5.00E-05	0.016069	Nucleic acid binding/behavioural response to starvation.
Odorant binding protein 56d/Obp56d	FBgn0034470	-0.67	5.00E-05	0.016069	Odorant binding/olfactory behaviour.
Homogentisate 1,2-dioxygenase/hgo	FBgn0040211	-0.55	0.00015	0.04148	Homogentisate 1,2-dioxygenase activity/oxidation-reduction process.
CG31205	FBgn0051205	-0.54	0.00015	0.04148	Serine-type endopeptidase activity/proteolysis.
Short Spindle 7/ssp7	FBgn0052667	0.66	5.00E-05	0.016069	Unknown/mitotic spindle assembly.
CG6503	FBgn0040606	0.67	5.00E-05	0.016069	Unknown.
White*	FBgn0003996	0.67	5.00E-05	0.016069	Transmembrane signalling receptor activity/ eye pigment biosynthetic process
Pyrroline-5-carboxylate reductase-like 2/P5cr-2	FBgn0038516	0.68	5.00E-05	0.016069	Pyrroline-5-carboxylate reductase activity/proline biosynthetic process.
Ornithine decarboxylase1/Odc1	FBgn0013307	0.68	5.00E-05	0.016069	Ornithine decarboxylase activity/polyamine biosynthetic process.
CG3088	FBgn0036015	0.70	5.00E-05	0.016069	Unknown.
Niemann-Pick type C-2g/Npc2g	FBgn0039800	0.79	5.00E-05	0.016069	Sterol binding/mesoderm development.
CG8329	FBgn0036022	0.83	5.00E-05	0.016069	Serine-type endopeptidase activity/proteolysis.

CG8343	FBgn0040502	0.89	5.00E-05	0.016069	Carbohydrate binding, mannose binding/unknown.
UDP-glycosyltransferase 35b/Ugt35b	FBgn0026314	0.93	5.00E-05	0.016069	UDP-glycosyltransferase activity/UDP-glucose metabolic process.
CG9377	FBgn0032507	0.95	5.00E-05	0.016069	Unknown.
CG15068	FBgn0040733	1.02	5.00E-05	0.016069	Unknown.
CG11211	FBgn0033067	1.07	5.00E-05	0.016069	Mannose binding, carbohydrate binding/unkown.
Histone deacetylase 4/HDAC4	FBgn0041210	1.09	5.00E-05	0.016069	Histone deacetylation, regulation of transcription, long-term memory.
CG9676	FBgn0030773	1.17	5.00E-05	0.016069	Serine-type endopeptidase activity/proteolysis.

Table 3.2 Genes whose transcripts are significantly altered in abundance by overexpression of *HDAC4*. *HDAC4* as well as the *white* gene (*) were expected to be upregulated since these flies harboured overexpression of *HDAC4* and three copies of the *white* gene (selectable marker for transgenesis). Genotypes: HDAC4OE: *w[CS10]elav-GAL4/+; tub-GAL80^{ts}/+; HDAC4OE/+*. Control: *w[CS10]elav-GAL4/+; tub-GAL80^{ts}/+*.

Gene symbol	RNA expression level in the head	RNA expression level in the eye	RNA expression level in the brain
Obp99d	30.4	5.75	3
Lsp2	457.2	481.75	No informative data
CG9701	153.6	83.95	6
CG4757	750.8	652.4	8.7
CG18473	58.2	66.92	7.1
CG6409	3666.5	1384.125	43.6
LanA	132.8	29.47	79.2
kek2	18.7	20.725	155.8
CAH2	394.5	389.175	22.9
Arc1	669.1	136.57	512.3
Obp56d	4046	2102.4	71.1
Hgo	182.1	110.5	5.3
CG31205	189.9	20.9	2.6
ssp7	1469	1078.15	113.6
CG6503	3123.2	2289.225	152.9
P5cr-2	381.3	113.575	14.3
Odc1	559.1	255.825	No informative data
CG3088	4390.6	4.775	8.8
Npc2g	2108.8	1515.85	74
CG8329	4765.9	1.95	0.6
CG8343	4771.6	3.8	1.9
Ugt35b	895.7	293.075	1117.4
CG9377	481.4	No informative data	1191.6
CG15068	2653.4	1222.6	94.5
CG11211	2310.6	4.025	9.1
HDAC4	69.8	124.85	439.3
CG9676	2680.1	6.476	7

Table 3.3 RNA expression levels in *Drosophila* head, eyes and brain of the genes transcriptionally regulated by *HDAC4*. Microarray data from Flyatlas providing an estimate of the expression levels of each gene in the head, eyes and brain. Data collected from FlyBase, release FB2016_03 (flybase.org). 0-9.99 = no expression, 10-99.9 = low expression, 100-499.99 = moderate expression, 500-999.99 = high level of expression, > 999.99 = very high level of expression.

Overall, the analysis detected genes that function in the central nervous system, as well as in other adult head tissues and taken together these data suggest that the *HDAC4* has a minimal effect on global gene expression in the brain or that the experimental set up and conditions were not ideal for detecting such changes. However, a small subset of genes

that were altered in transcriptional abundance were detected and interaction of these genes with *HDAC4* is further investigated in section 3.2.

The modest number of genes found to be transcriptionally regulated by *HDAC4* may be partially due to the fact that in the brain HDAC4 tends to be mostly cytoplasmic under basal conditions (Chawla et al., 2003; Darcy et al., 2010) and its nuclear localisation may be limited to a small subsets of neurons therefore any transcriptional change cannot be detected by whole brain or head analysis. In addition, HDAC4 may possess functions outside the nucleus. For this reason a genetic screen was adopted in order to identify genes that may interact in the same molecular pathway as *HDAC4* in neurons, expanding the research beyond transcriptional regulation.

3.2 A genetic screen for modifiers of the *HDAC4*-induced rough eye phenotype

In order to detect *HDAC4* interacting genes, a rough eye enhancer phenotype screen was performed, which allows identification of genes that interact genetically with *HDAC4*, without prior knowledge of the nature of the interaction (Kaplow et al., 2009).

The compound eye of the fruit fly is an ideal model system for genetic analysis of neuronal pathways since it does not affect viability or fertility, it is easy to score phenotypically and it is rich in neuronal photoreceptors, thus genetic interactions occurring in the eye are likely to also occur in the brain. Wild-type eyes of *Drosophila* consist of an array of approximately 800 hexagonal ommatidia, with interommatidial mechanosensory bristles. The eye in young-adult flies displays an intense red pigmentation that slightly darkens with age. Figure 3.4 shows the eye phenotype of a wild-type fly.

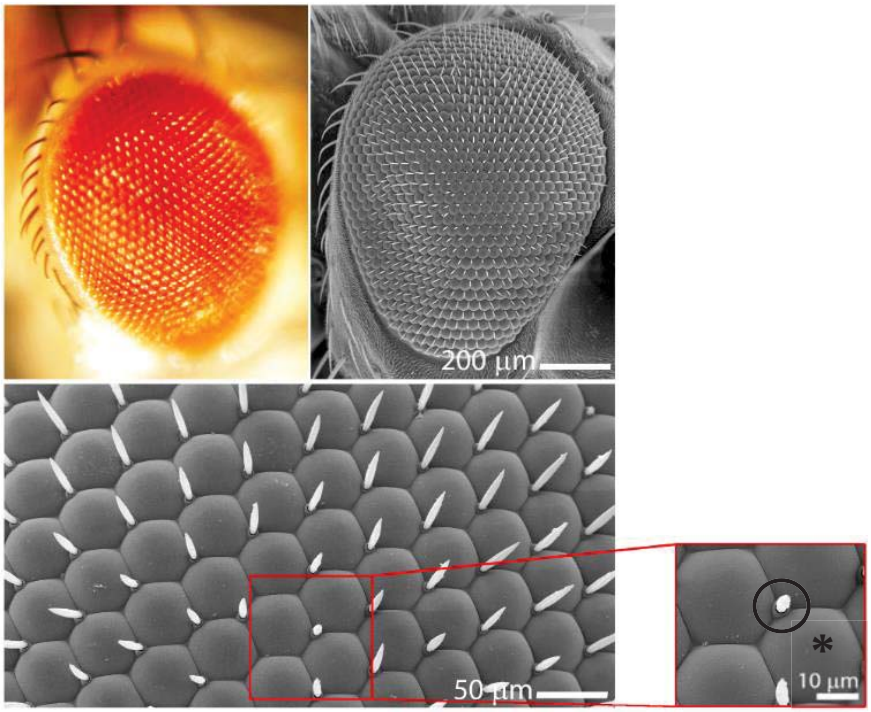

Figure 3.4 Wild-type eye of *Drosophila*. Stereomicrograph and scanning electron micrographs of wild-type eye of *Drosophila*. Bristles and ommatidia are indicated in the red panel by a circle and an asterisk respectively.

In order to perform genetic screens in the eye of *Drosophila*, expression or knockdown of the gene of interest must be induced in the eye and the most commonly used strategy makes use of the GAL4/UAS system in combination with the glass multimer reporter (GMR) eye-specific driver (Figure 3.5).

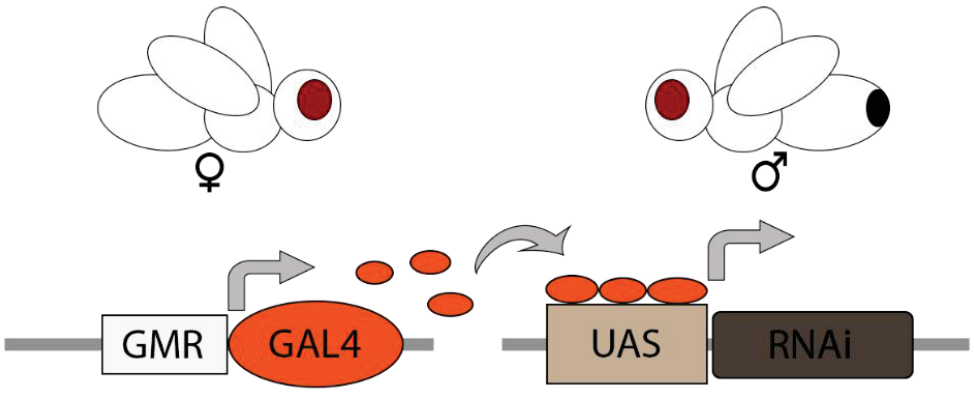

Figure 3.5 The GMR-GAL4/UAS system. The GAL4/UAS construct comprises two components: the yeast GAL4 transcription factor under the control of the GMR eye promoter, and

the UAS construct in which a gene of interest, i.e. double-strand (ds)-RNA, is cloned. A genetic cross between a female and a male is required in order to induce GAL4 dependent transcription of the UAS-RNAi transgene. Abbreviations: GMR = glass multimer reporter; UAS = upstream activating sequence; RNAi = RNA interference.

The rationale of this type of screen is that if two genes interact, the combination of the two can provoke a phenotype that is more severe than the eye phenotype of the individual genes suggesting the two genes have a synergistic effect on the phenotype. "Synergy occurs when the contribution of two mutations to the phenotype of a double mutant exceeds the expectations from the additive effects of the individual mutations" (Pérez-Pérez et al., 2009). For instance, if *HDAC4OE* inhibits function of a gene product required for eye development, then knockdown of this gene in combination with overexpression of *HDAC4* will result in a breakdown of this developmental process, i.e. severely impaired eye development, which would suggest the two genes act in the same genetic pathway (Figure 3.6).

A weak rough eye phenotype provides a convenient system to score for modifiers (enhancers or suppressors) of the rough eye phenotype and thus genes interacting in the same genetic pathway can be identified (Kaplow et al., 2009). It should be emphasised that this strategy does not provide detailed information about whether the genes physically interact or not.

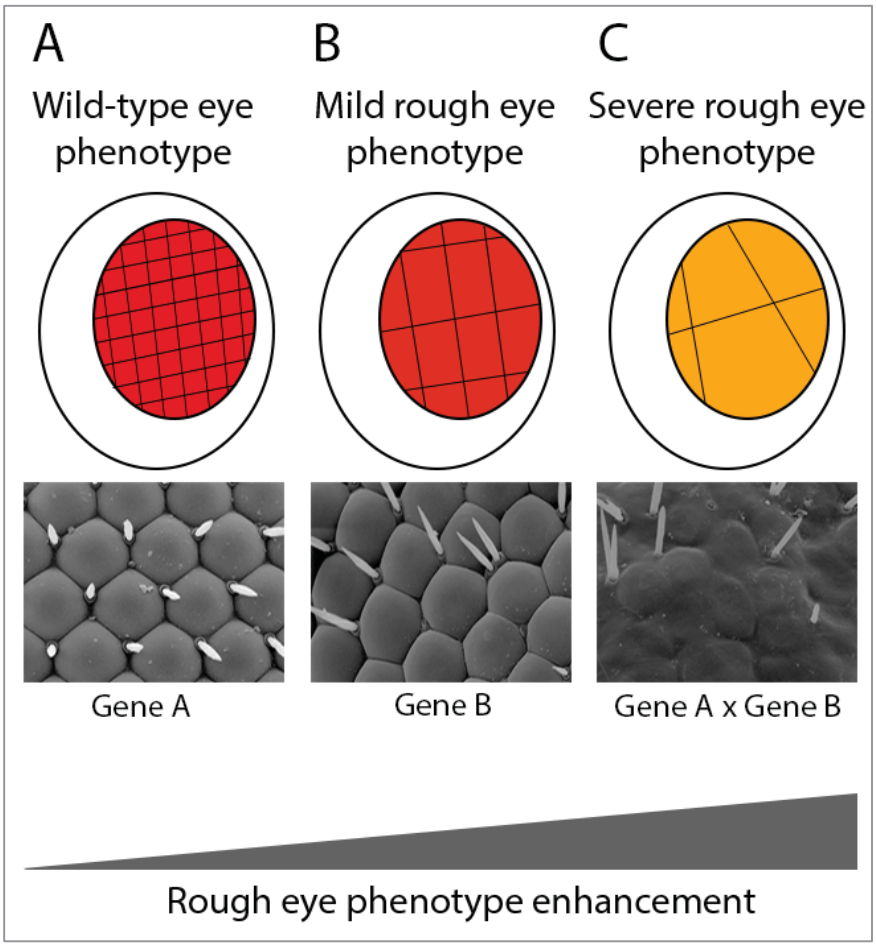

Figure 3.6 Cartoon showing the premise of the genetic screen for modifiers of the *HDAC4*-induced rough eye phenotype. Genetic screens are performed using the eye of *Drosophila* in order to identify genes that interact in the same genetic pathway. (A and B). Genes expressed individually result in a wild-type phenotype or in a mild rough eye phenotype. (C) Combination of gene A and gene B results in a severe rough eye phenotype. This suggests the genes may interact in the same genetic pathway, i.e. synergistic effect.

3.2.1 Development and validation of the method

Overexpression of *HDAC4* (*HDAC4OE*) in the eye photoreceptors was induced through the *GMR-GAL4/UAS* system and resulted in a mild rough eye phenotype with moderately irregular ommatidia, disorganisation of bristles and loss of pigmentation (Figure 3.7A). These flies served as the reference line in the actual screen since a mild rough eye phenotype can be scored for either suppression or enhancement of the rough phenotype, which would indicate a genetic interaction (Kaplow et al., 2009).

In control flies in which *HDAC4OE* was not induced, the *GMR-GAL4* driver did not result in phenotypic alterations of the eye. These flies displayed wild-type eye phenotypes characterised by a regular pattern of ommatidia and bristles (Figure 3.7B).

The severity of the eye phenotype was dependent on the dose of *HDAC4* since two copies of *HDAC4OE* resulted in a severe rough eye phenotype with complete loss of ommatidia, scattered distribution of bristles and a striking loss of pigmentation intensity and a smaller eye shape (Figure 3.7C).

In order to validate that the mild rough phenotype was caused by overexpression of *HDAC4* specifically rather than by non-specific effects, a genetic rescue study was conducted in which the line harbouring one copy of *HDAC4* was recombined with an *HDAC4* knockdown line and crossed to *GMR-GAL4*. This resulted in restoration of a wild-type eye phenotype (Figure 3.7D) meaning that the eye phenotype was a result of *HDAC4OE* and not caused by non-specific effects.

Since both the reference line and the RNAi stocks used for the screen contained an UAS sequence to allow *GAL4*-dependent transgene expression it is possible that two UAS constructs could titrate *GAL4* and result in decreased expression of *HDAC4* and/or the UAS-RNAi. Therefore, the *GMR-GAL4; UAS-HDAC4OE* line was crossed to two *UAS*-reporter genes (*UAS-CD8::GFP* and a *UAS-LacZ*). The resulting phenotypes were comparable to the reference line harbouring one copy of *HDAC4OE* indicating that an additional UAS sequence had no significant effect on the eye phenotype (Figure 3.7E and F).

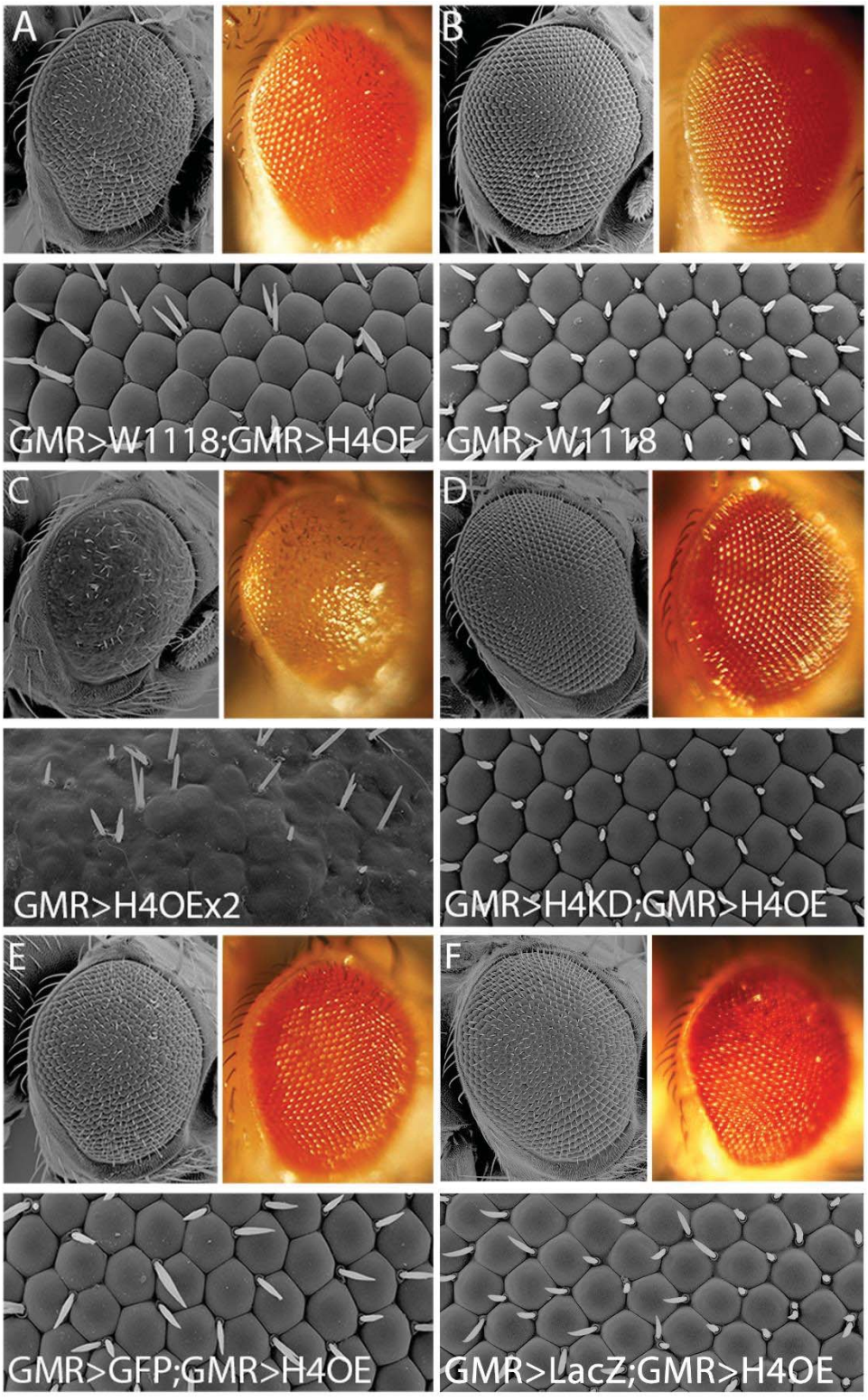

Figure 3.7 Eye images showing the impact of different dose of *HDAC4* on the eye surface phenotype and the validation of the screen. Stereomicrographs and scanning electron micrographs of *Drosophila* eyes. (A) Flies of the reference line harbouring one copy of *HDAC4OE* (*GMR-GAL4/+; UAS-HDAC4OE/+*) show a mild-rough eye phenotype. (B) Flies used as control for the *GMR-GAL4* driver display a normal eye phenotype (*GMR-GAL4/+*). (C)

A second copy of *HDAC4OE* enhances the rough eye phenotype (*GMR-GAL4/+; UAS-HDAC4OE/UAS-HDAC4OE*). (D) Co-expression of *UAS-HDAC4OE* and an RNAi hairpin targeted to *HDAC4* restores with wild-type eye phenotype (*GMR-GAL4/+; UAS-HDAC4OE/UAS-HDAC4KD*). (E-F) Co-expression of *UAS-HDAC4OE* with *UAS* reporter genes *GFP* and *LacZ* does not affect the eye phenotype (*GMR-GAL4/+; UAS-HDAC4OE/UAS-GFP* and *GMR-GAL4/+; UAS-HDAC4OE/UAS-LacZ).* Abbreviations: H4OE = *HDAC4* overexpression, H4KD = *HDAC4* knockdown; H4OEx2 = double copy of *HDAC4* overexpression.

The screen was performed on the F1 progeny obtained by crossing flies homozygous for *HDAC4* (*GMR-GAL4; UAS-HDAC4OE*) in the eye, to a panel of lines which were each homozygous for UAS-RNAi (Table 7.2, Appendix 7.1), available from the Vienna Drosophila Resource Centre (VDRC, Vienna, Austria) and the Bloomington Drosophila Stock Centre (BDSC, Indiana, USA). Ideally, an unbiased genome-wide RNAi screen would be performed, however due to the limited human resources, a total of 124 lines were scored. These lines were chosen based on literature review and information provided by databases such as DroID (Drosophila Interactions Database, http://www.droidb.org/), a comprehensive public resource for gene and protein interactions designed specifically for *Drosophila melanogaster*. DroID includes genetic interactions and experimentally detected protein–protein interactions acquired from the literature and from external databases, and predicted protein interactions based on experiments in other species (Murali et al., 2011). Genes known to have a role in synaptic plasticity, memory, chromatin regulation, as well as detected to interact with *HDAC4* in different model systems and/or in non-neuronal tissues were selected (Table 7.2, Appendix 7.1).

A qualitative scoring system was designed in order to assess whether a particular RNAi enhanced or suppressed the *HDAC4*-induced rough eye phenotype of the F1 progeny (Kaplow et al., 2009). The eye features, e.g. organisation of both ommatidia and bristles, pigmentation and shape, were visually evaluated and genes classified following the ensuing scheme:

a. suppressors of the rough eye phenotype, e.g. genes that improved the *HDAC4*-induced rough eye phenotype;
b. no effect, e.g. genes that did not result in a significant modification of the rough eye phenotype;

c. enhancers of the rough eye phenotype, e.g. genes that resulted in a more severe and dramatic phenotype with respect to eyes expressing *HDAC4* or the RNAi line individually (synergistic interactions)
d. RNAi lines altering the eye phenotype in absence of *HDAC4OE* were excluded from the analysis.

3.2.2 A genetic screen for modifiers of the *HDAC4*-rough eye phenotype detected genes involved in transcriptional regulation, cytoskeleton regulation and SUMOylation pathway

Initially, a subset of the genes whose expression changed upon overexpression of *HDAC4* (section 3.1), which consisted in those that were significantly expressed in the brain with a score of >10 according to Flyatlas (Winbush et al., 2012), were tested in the eye screen. None of them enhanced or suppressed the *HDAC4*-induced rough eye phenotype (Table 7.3, Appendix 7.1). This suggests that they either do not interact genetically with *HDAC4* or that the knockdown level of these RNAi lines was not sufficient to exert an effect on the eye phenotype. With regards to *Pyrroline-5-carboxylate reductase-like 2* and *CG15068*, analysis through the eye screen could not be performed due to unavailability of the specific RNAi strain from the stock centres.

Of the additional 124 RNAi lines analysed, four had to be excluded because of their strong effect on the eye phenotype in absence of *HDAC4OE* (Table 3.4). A total of 29 genes resulted in an enhancement of the rough eye phenotype hinting that those gene interacted in the same genetic pathway as *HDAC4* (Tables 3.5 and 3.6). Examples of rough eye phenotypes and corresponding controls are shown in Figure 3.8 A-F.

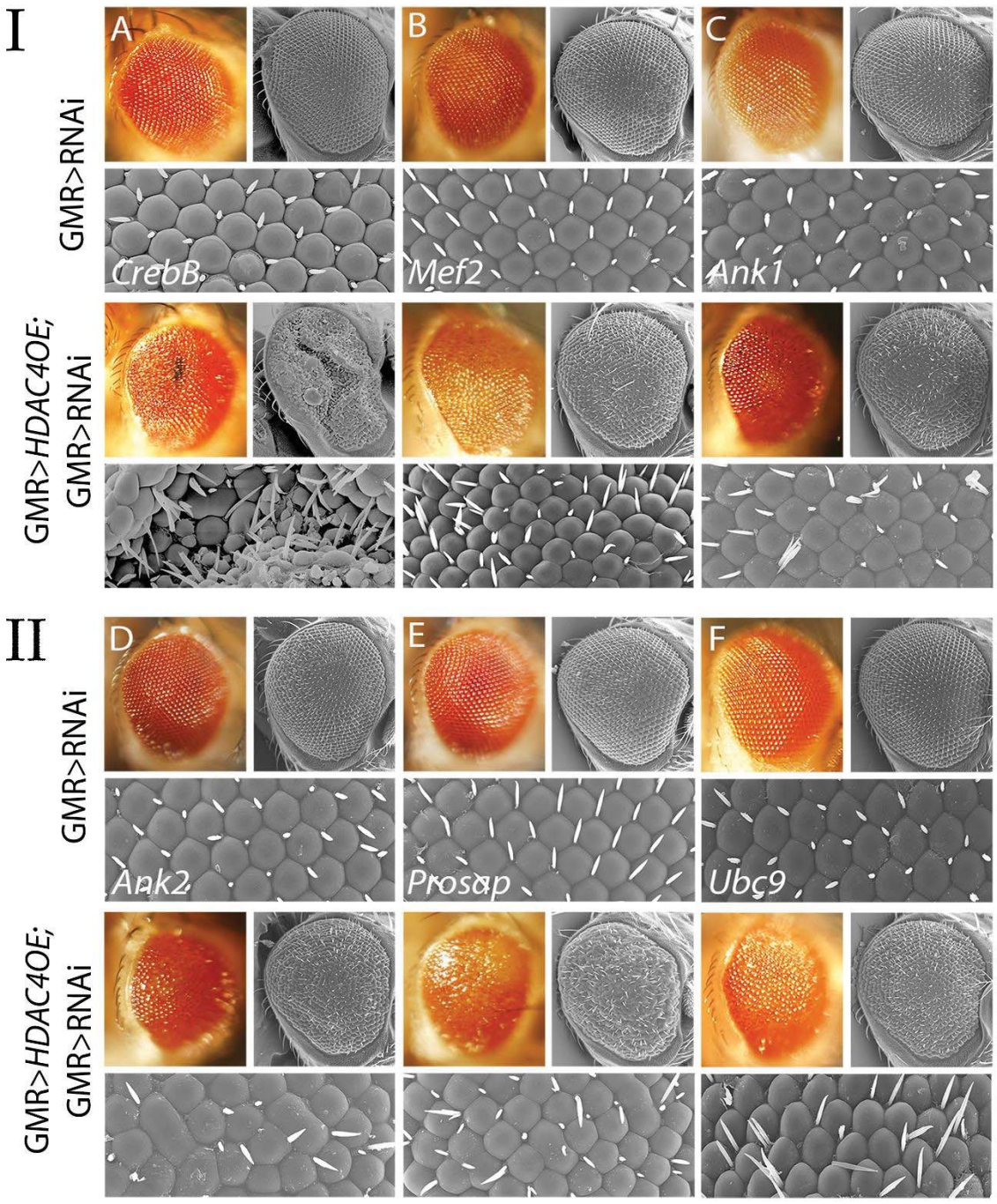

Figure 3.8 Enhancers of the *HDAC4*-induced rough eye phenotype. Stereomicrographs and scanning electron micrographs of the enhanced rough eye phenotypes. In both, panel I and II, the upper rows show *GMR-GAL4* induced expression of the RNAi lines individually and the lower rows show the phenotypes resulting from co-expression of the RNAi and *HDAC4*. The phenotype due to *GMR-GAL4* induced expression of one copy of *HDAC4* was enhanced by co-expression of the RNAi targeted to (A) *CrebB*; (B), *Mef2*; (C) *Ankyrin1 (Ank1)*; (D) *Ankyrin2 (Ank2)*; (E) *Prosap*; (F) *Ubc9.*

Of the genes that enhanced the rough eye phenotype, nine had been previously shown to interact with *HDAC4* in *Drosophila* tissues or in other organisms and thus were indicative of conserved interactions (Table 3.5). This provided validation of the effectiveness of the screen to identify *HDAC4* interactors. This group included genes encoding for transcription factors CrebB and the myocite-enhancer factor 2 (Mef2), transcription repressors Sin3A and Smrter, the molecular chaperone 14-3-3ζ which is known to mediate HDAC4 nuclear import and the histone acetyltransferase Gcn5. Interactions were also observed with the E2 SUMO-conjugating enzyme Lesswright also known as Ubc9, the E3 SUMO ligase nucleoporin Nup358 and the ankyrin repeat family member CG5846, the fly homolog of human RFXANK (Nie et al., 2015) shown to interact physically with HDAC4 through both *in vitro* MBP pull-down assays in SF9 cells and *in vivo* via co-immunoprecipitation procedures in human embryonic kidney 293 (HEK293) cells (Wang et al., 2005). The remaining twenty genes were suggestive of novel interactions and are listed in Table 3.6.

A more extensive analysis of the 29 putative *HDAC4* interactors was conducted using the Search Tool for the Retrieval of Interacting Genes/Proteins (STRING - http://string-db.org, version 10.0), an online database that provides visualisation of both predicted and known functional or physical protein interactions. STRING quantitatively integrates association data from diverse sources, e.g. previously published studies, high-throughput experiments and co-expression data (Szklarczyk et al., 2015). A network analysis of those candidates revealed evidence for direct or indirect interactions among many of the 29 genes that fall into one of three major classes which were: transcription factors and chromatin modifiers including *Smrter, Gcn5, Mef2, CrebB, Sin3A, Schnurri*, cytoskeleton regulators which included *14-3-3ζ, Amnesiac, Ankyrin, Ankyrin2, CG5846, Derailed, Highwire, Moesin, NetrinB, Prospap, RanBP21, Sra-1, Trio*, and members of the SUMOylation machinery, *Su(var)1-10, Ulp1, Lesswright (Ubc9),* and *Nup358* (Figure 3.9).

Gene name	Flybase ID	Molecular function/biological process
Twinstar	FBgn0011726	Actin binding/cellular component organization, actin filament polymerization.
CBP/p300	FBgn0261617	cAMP response element binding protein binding/regulation of transcription, cell cycle check point.
Notch	FBgn0004647	Transmembrane signalling receptor activity/ cell adhesion, neurological system process, learning and memory.
Sumo (Smt3)	FBgn0264922	Protein binding/central nervous system neuron development, dendritic spine development, protein sumoylation

Table 3.4 Genes excluded from further analysis after the rough eye phenotype screen. Genes that provoked a severe rough eye phenotype in absence of *HDAC4OE* were not taken under consideration for further analysis**.**

Gene name	Flybase ID	Molecular function/biological process
14-3-3 ζ	FBgn0004907	Protein binding/olfactory learning.
Cyclic-AMP response element binding protein B	FBgn0265784	Transcription factor activity/synapse organisation, long-term memory.
Gcn5	FBgn0020388	Histone acetyltransferase activity/dendrite morphogenesis, axon target recognition
Lesswright (Ubc9)	FBgn0010602	SUMO-conjugating enzyme/cell migration, cell localisation.
Myocyte enhancer factor2	FBgn0011656	Transcriptional factor activity/biological regulation, cardiovascular system development.
Nucleoporin 358Kd	FBgn0039302	Ran GTPase binding/protein import into nucleus; ventral cord development.
CG5846 (Rfxank)	FBgn0032171	Ankyrin repeat domain/unknown.
Sin3A	FBgn0022764	Transcription cofactor activity/regulation of developmental process.
Smrter	FBgn0265523	Transcription co-repressor activity/regulation of mitotic cell cycle, negative regulation of Notch signalling pathway.

Table 3.5 Conserved interactions detected by the *HDAC4*-induced rough eye phenotype screen. Genes that genetically interacted with *HDAC4* and that were previously found to interact with *HDAC4* in other tissues or organisms**.**

Gene name	Flybase ID	Molecular function/biological process
Amnesiac	FBgn0086782	Neuropeptide hormone activity, involved in memory, learning, cognition, response to stimulus and stress, associative learning.
Ankyrin1	FBgn0011747	Structural constituent of cytoskeleton/cytoskeletal anchoring at plasma membrane; signal transduction.
Ankyrin2	FBgn0261788	Structural constituent of cytoskeleton/regulation of synaptic transmission, maintenance of protein location, signal transduction, cell growth.
Crammer	FBgn0034443	Cysteine-type endopeptidase inhibitor activity/short-term memory, long-term memory.
Derailed	FBgn0015380	Protein tyrosine kinase activity/learning or memory, neurological system process.
Highwire	FBgn0030600	Ubiquitin-protein transferase activity/ response to axon injury, cell communication, adult behaviour, synapse organization.
IGF-II mRNA-binding protein	FBgn0262735	mRNA binding protein/positive regulation of axon regeneration, nervous system development, synaptic growth at neuromuscular junction.
Krasavietz	FBgn0250753	Translation initiation factor binding/ axon midline choice point recognition, long-term memory, neuron fate commitment.
Moesin	FBgn0011661	Actin binding/establishment or maintenance of bipolar cell polarity, male courtship behaviour, olfactory behaviour.
Netrin B	FBgn0015774	Unknown/ synaptic target attraction, axon guidance, dendrite guidance, synaptic target recognition, glial cell migration.
Prosap	FBgn0040752	GKAP/Homer scaffold activity/ postsynaptic density assembly.
RanBP21	FBgn0031051	Ran GTPase binding/ intracellular protein transport.
Rogdi	FBgn0036697	Unknown/learning and memory.
Scamp	FBgn0040285	Unknown/synaptic vesicle exocytosis, neuromuscular synaptic transmission, long-term memory.
Schnurri	FBgn0003396	Transcription factor activity/associative learning, peripheral nervous system development.
Specifically Rac1-associated protein 1	FBgn0038320	Rho-GTPase binding/axon guidance, regulation of synapse organisation, cell shape.
Suppressor of variegation 2-10	FBgn0003612	DEAD/H-box RNA helicase binding/neurogenesis, DNA conformation change, organ development.
Trio	FBgn0024277	Rho guanyl- nucleotide exchange factor activity/neurogenesis, brain development, axon guidance.
Ubiquitin activating enzyme 2	FBgn0029113	Small protein activating enzyme activity/protein sumoylation.
Ulp1	FBgn0027603	SUMO-specific protease activity/protein desumoylation, dendritic spine morphogenesis, axogenesis.

Table 3.6 Novel interactions detected via the *HDAC4*-induced rough eye phenotype screen.

Novel genes identified to genetically interact with *HDAC4*.

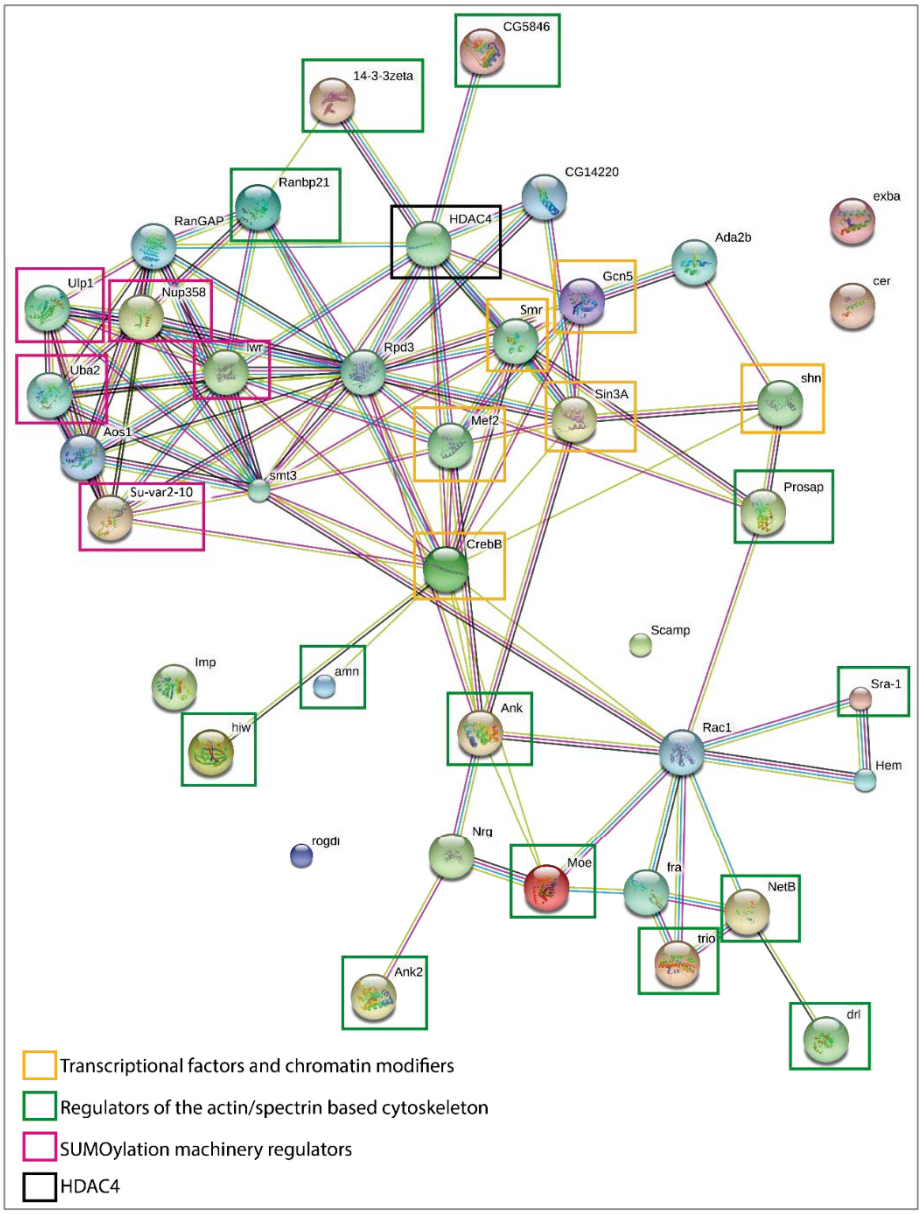

Figure 3.9 STRING analysis of the enhancers of the *HDAC4*-induced rough eye phenotype. Analysis of predicted interactive pathways among *HDAC4* and the candidates that enhanced the rough eye phenotype was performed using the STRING online database. The candidate genes were grouped in three major classes highlighted in yellow, green and pink indicating transcriptional factors and chromatin modifiers, regulators of the actin/spectrin cytoskeleton and SUMOylation machinery enzymes, respectively. *HDAC4* is highlighted in the black square.

The following studies presented in this thesis focus on examining the role of the candidate *HDAC4* interactors *Ankyrin1* and *Ankyrin2* in brain development and memory formation. The rationale for the selection of these genes is provided below (section 3.3).

However, the identification of several putative *HDAC4* interacting factors formed the basis of several new projects in the laboratory for which a brief description is provided below:

1. Investigating the interaction between *HDAC4* and *Mef2* in memory formation.

Several studies in mammalian cell culture, e.g. myoblasts, 293T cells and granule cortical neurons, have shown a direct physical interaction between MEF2 and HDAC4 and that HDAC4 represses MEF2 transcriptional activity via direct binding (Miska et al., 1999; Bolger et al., 2007; Cohen et al., 2009). In *Drosophila*, it was previously shown that Mef2 and HDAC4 co-localise in the mushroom body nuclei and the hypothesis of a genetic interaction between HDAC4 and Mef2 is supported by the evidence showing that Mef2 redistribute in the nuclei upon overexpression of HDAC4 (Fitzsimons et al., 2013). Further analysis will be performed to elucidate the significance of this association in the brain of *Drosophila melanogaster* as the focus of a PhD project.

2. Investigating the role of *Moesin* in brain development and memory formation.

Moesin is the sole member of the *Drosophila* ezrin, radixin, moesin protein family and serve as a linker factor between transmembrane proteins and the actin cytoskeleton. Preliminary data showed that wild-type levels of *Moesin* are required for proper LTM formation but not STM (P. S. Freymuth and H. L. Fitzsimons unpublished data) as previously shown for *HDAC4* (Fitzsimons et al., 2013). In addition, knockdown of *Moesin* in the mushroom body was found to severely impair development of the mushroom body, a region of the fly brain involved in memory formation (P. S. Freymuth and H. L. Fitzsimons unpublished data).

3. Investigating the role of the SUMOylation machinery in memory formation and its interaction with *HDAC4*.

Subsequent analysis conducted by Dr Fitzsimons detected that most of the *Drosophila* SUMOylation machinery enzymes, which are conserved and enriched in fly heads (Long and Griffith, 2000), also interacted with *HDAC4*. A growing body of evidence indicates that SUMOylation is a critical mechanism for the regulation of neuronal protein activity (Martin et al., 2007; Wilkinson and Henley, 2010) and for memory formation (Yang et al., 2012; Chen et al., 2014; Drisaldi et al., 2015). It was determined that knockdown of *Ubc9*, the sole E2-conjugating enzyme of *Drosophila* SUMOylation machinery, resulted in impaired brain development and LTM formation. In addition, *Ubc9* and *HDAC4* were shown to interact genetically during LTM formation (Schwartz et al., 2016).

3.3 Characterisation of *Ankyrin1* and *Ankyrin2* expression in the adult brain and their roles in brain development and memory formation

The rough eye phenotype screen led to the identification of several components of the actin/spectrin cytoskeleton, which is required to stabilise the neuronal architecture. Reorganisation of the actin cytoskeleton is a critical process that allows axon elongation, growth and arborisation of dendritic branches and this cytoskeletal plasticity is believed to be required for memory formation and storage (Fischer et al., 1998; Krucker et al., 2000; Matus, 2000; Lamprecht and LeDoux. 2004; Goellner et al., 2012). Among the cytoskeletal interactors identified, *Ankyrin1 (Ank1)* and *Ankyrin2 (Ank2)* were chosen for analysis of their potential role in brain development and memory formation. The main reason guiding this choice was the finding that HDAC4 harbours an ankyrin repeat binding domain which is highly conserved among vertebrates and invertebrates (Wang et al., 2005; McKinsey et al., 2006; Xu et al., 2012) suggesting that HDAC4 might bind to Ank1 and Ank2. In addition, two other ankyrin repeat proteins, namely Prosap and CG5846, were identified in the screen.

Several studies have shown that both loss of *Ank2* via double stranded RNA (dsRNA) and mutations of *Ank2* in *Drosophila* larvae resulted in retraction of synaptic boutons, reduction in terminal size, and disruption of neuronal excitability (Koch et al., 2008; Pielage et al., 2008). In addition, a study conducted in cultured primary neurons from mouse hippocampus showed that micro-RNA dependent down-regulation of ANKYRIN G (ANK-G), the closest homolog to *Drosophila* Ank2, resulted in axonal, synaptic and cognitive defects (Sun et al., 2014a, b). Furthermore, there is accumulating evidence that the *ANKYRIN3* gene (*ANK3)* is critical for normal neuronal functions. For instance mutations of human *ANK3* identified from genome wide association studies correlate with onset of neurocognitive disorders including bipolar disorder, autism spectrum disorders, schizophrenia and severe attention deficit hyperactivity disorder (Bi et al., 2012; Leussis et al., 2012; Zhang et al., 2014; Iqbal et al., 2013).

Despite these data, there has been a dearth of functional studies on the role of *Ank1* and *Ank2* in the adult brain of *Drosophila melanogaster*, therefore the aim of this study was to investigate their role in LTM formation and to determine whether an interaction with *HDAC4* is required for normal LTM formation.

3.3.1 Ankyrin2

3.3.1.1 Ankyrin2 is highly expressed throughout the fly brain and it is an axonal protein

To date, the expression and localisation pattern of Ank2 has been described in neuromuscular junction larval models (Koch et al., 2008; Pielage et al., 2008) and characterisation of Ank2 in the adult brain has not yet been assessed. To this end, immunohistochemistry on whole-mount brains was conducted using an antibody specific to *Drosophila* Ank2 (a kind gift from Dr Aberle). This antibody has been previously shown to bind specifically to the long isoform (L) of Ank2 (section 1.6) in the *Drosophila* neuromuscolar junction (Koch et al., 2008). Although specific, it was found to recognise a nuclear epitope whose identity has not been established (Koch et al., 2008).

In the adult brain, the antibody detected a broad expression profile for Ank2 including high localisation in the optic lobes and antennal lobes (Figure 3.10C), as well as in axon tracts and in the mushroom body lobes (Figure 3.10E). Ank2 was also highly concentrated in calyces, which are the dendritic fields of the mushroom body (Figure 3.10D). In addition, a punctuate pattern was observed in the nuclei of the Kenyon cells (Figure 3.10F), the intrinsic cell bodies of the mushroom body which project their axons anteriorly to form the mushroom body lobes.

The presence of Ank2 in the mushroom body of the *Drosophila* brain is of great interest as the mushroom body plays an essential role for LTM formation, as previously shown for *HDAC4* whose both overexpression and depletion in this structure impair LTM (Fitzsimons et al., 2013).

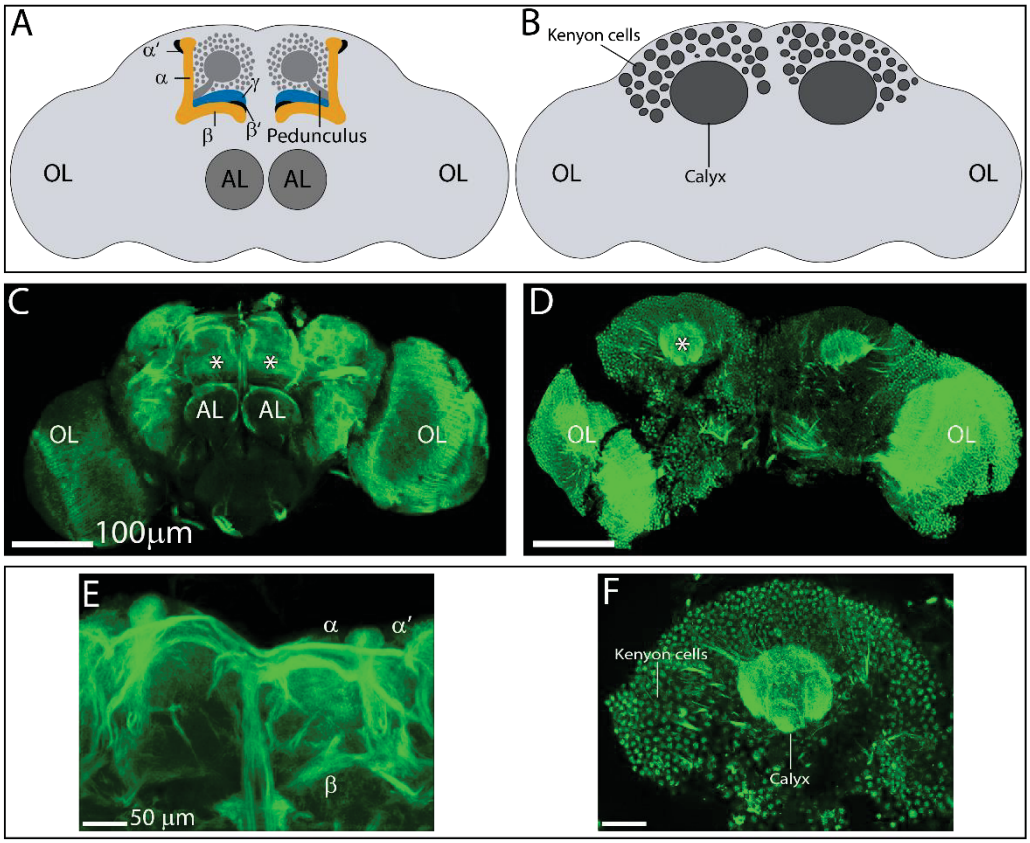

Figure 3.10 Ank2 is broadly expressed in the adult brain of *Drosophila*. (A) Schematic representation of the frontal brain region of *Drosophila* showing organisation of the mushroom body and other brain regions. Abbreviations: OL = optic lobe. AL = antennal lobe. (B) Schematic representation of the posterior brain region of *Drosophila* showing the calyces and the cell bodies of the Kenyon cells, the intrinsic neurons of the mushroom body. (C) Frontal maximum intensity projection through the brain showing extensive distribution of Ank2 in several regions of the brain including AL, OL, and at axon tracts with presumptive localisation at the mushroom body lobes (white asterisks). Zoom 2.3, objective 10X. (D) Posterior confocal maximum intensity projection through the brain. Asterisk indicates the calyx. Zoom 2.1, objective 10X. (E) Magnification of the anterior central brain indicating Ank2 distribution in the axon tracts and mushroom body lobes (in this image α, α' and β lobes are visible). Zoom 2.2, objective 40X in oil. (F) Magnification of one calyx and surrounding Kenyon cells nuclei. Zoom 1.6, objective 40X in oil.

In order to achieve a complete characterisation of Ank2 expression in the adult brain, additional immunohistochemical analyses on wild-type brains were conducted using several antibodies recognising markers of specific neuronal compartments including nuclei, axons and dendrites as well as glia.

Firstly, the expression pattern of Neuroglian (Nrg) and its localisation with respect to Ank2 was examined. Nrg is a neuronal adhesion molecule and the sole *Drosophila* L1-CAM element sharing homology to the vertebrate neuronal adhesion protein family members. Nrg mediates axon-axon interactions and enables axon guidance through the mushroom body (Siegenthaler et al., 2015). While a direct interaction between Ank2 and Nrg was demonstrated *in vivo* through co-immunoprecipitation assays in larval brain extracts (Enneking et al., 2013) and *in vitro* through yeast-two hybrid experiments (Bouley et al., 2000), the relative expression pattern of the two in the adult brain has not yet been examined.

Double labelling with anti-Nrg and anti-Ank2 revealed that Ank2 and Nrg localise in the same regions of the brain including the mushroom body lobes (Figure 3.11A) and the axonal regions surrounding the calyces (Figure 3.11B, white arrowheads). These axons possibly belong to the olfactory projection neurons which innervate the calyces of the mushroom body (Masuda-Nakagawa et al., 2010).

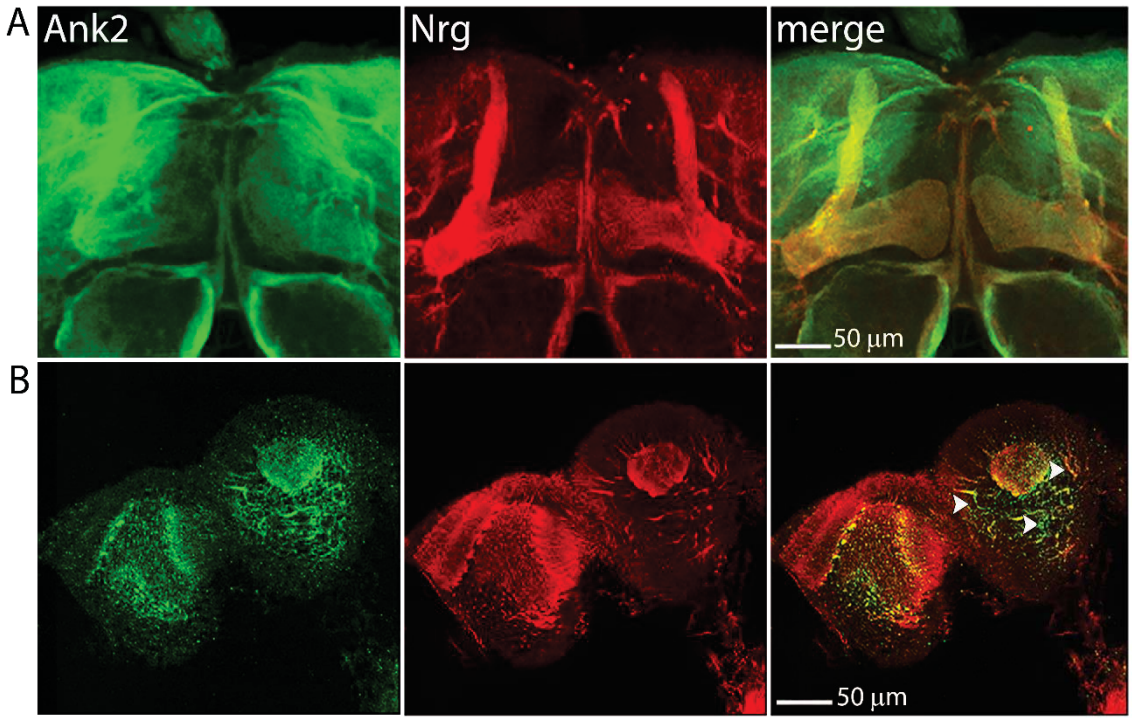

Figure 3.11 Ank2 co-localises with Nrg in the axons of the adult brain. (A) Frontal confocal projections through the brain showing localisation of Ank2 (green) and Nrg (red) in the mushroom body lobes. Zoom 4.7, objective 10X. (B) Posterior confocal single z-stack (1 µm) showing distribution of Ank2 (green) and Nrg (red) to the calyx. Both Ank2 and Nrg concentrate in the

axons of the projection neurons (white arrowheads) surrounding the calyx. Zoom 1.5, objective 40X in oil.

It has to be highlighted that protein expression level of Ank2 in the lobes of the mushroom body was variable among the brains analysed, however its distribution was consistent.

Hereafter, confocal images in this thesis are displayed as 'colour-blind friendly' confocal micrographs that are highly employed by the *Drosophila* community (Figure 3.12). The red and the green are widely used in the life science environment but these colours are unable to be distinguished by the majority of individuals affected by colour vision impairment. Replacing the red with the magenta can render the confocal images more readable and effective to any audience.

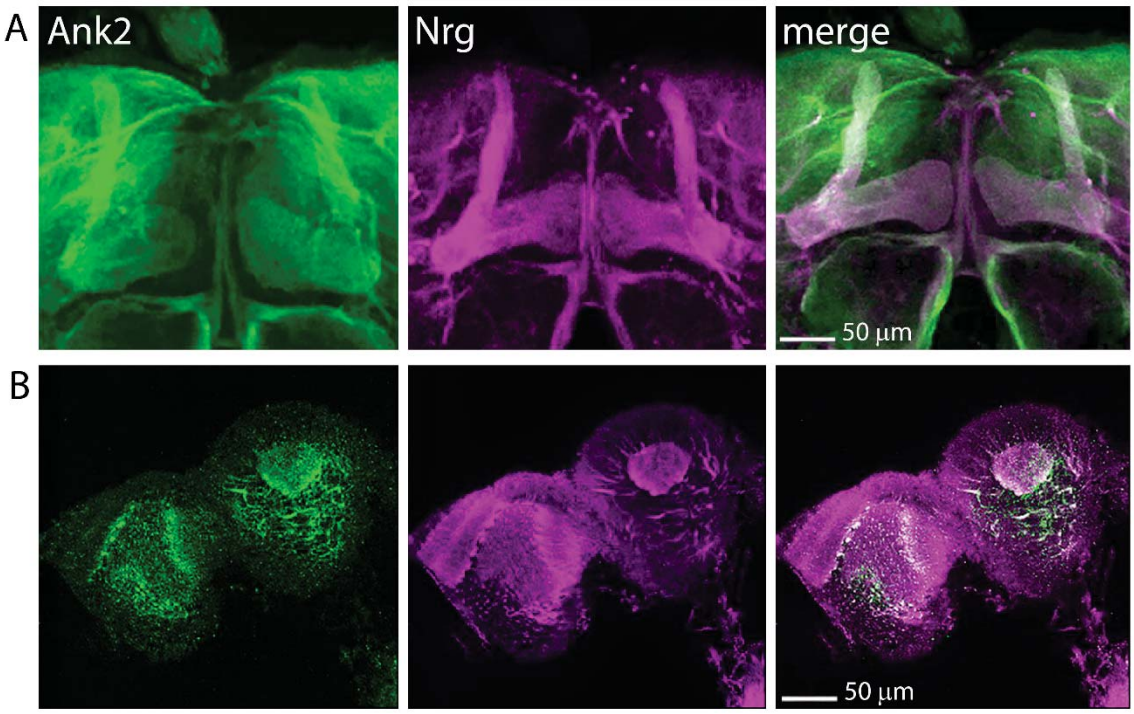

Figure 3.12 Colour-blind friendly version of Figure 3.11. This effect was obtained using Adobe Photoshop software. The contents belonging to the red channel were selected and copied into the blue channel, transforming the red data into magenta. The overlap between the green and the magenta generates white that can be easily visualised.

In order to confirm Ank2 axonal localisation an antibody targeting Futsch was adopted. Futsch is an axonal marker homologous to the vertebrate MAP1B microtubule-associated protein which localises to axons (Hummel et al., 2000) and double labelling with anti-Ank2 showed an overlapping pattern between Ank2 and Futsch both in the anterior and posterior portions of the brain (Figure 3.13). Concentration of Futsch and Ank2 was observed in the axons of the projection neurons surrounding the calyx and in four distinct regions of the lower area of the calyx (Figure 3.13B yellow asterisks). Those fascicles are believed to be the axons of the Kenyon cells that assemble into four bundles and fuse to form the peduncle, a tract that projects anteriorly and then ramifies into two branches of neurons that form the lobes of the mushroom body (Kurusu and Zinn, 2008).

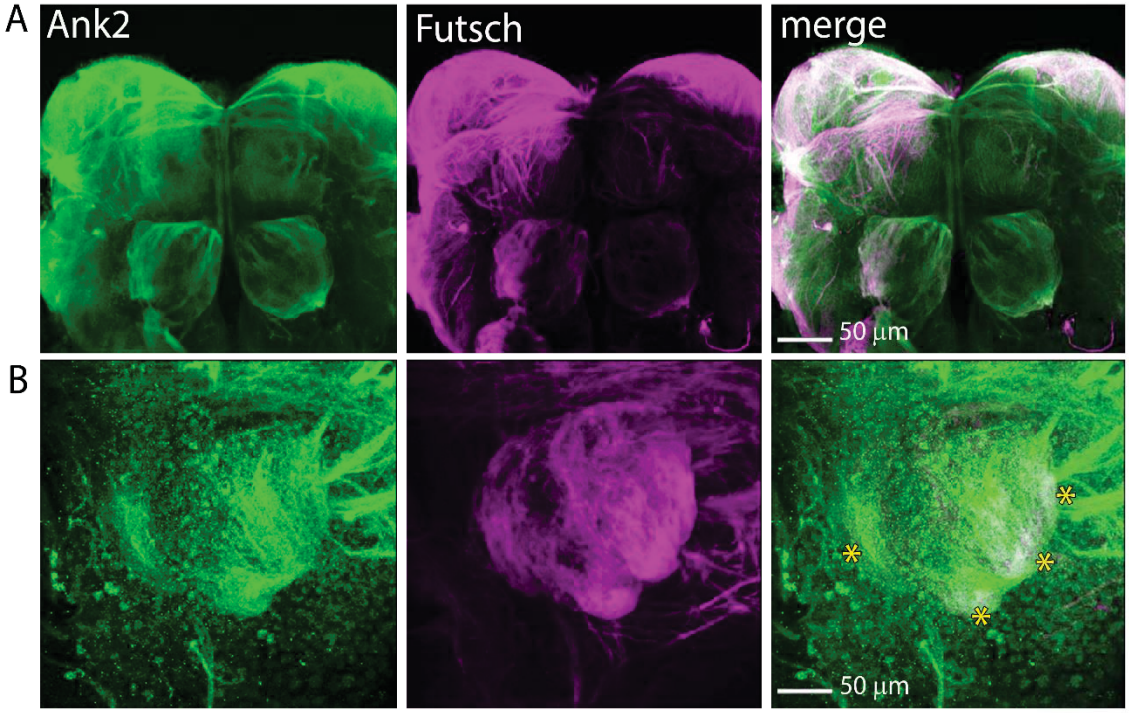

Figure 3.13 Ank2 localises to axons in the brain. (A) Frontal confocal projections at maximum intensity through the brain showing localisation of Ank2 (green) and Futsch (magenta). Zoom 1.8, objective 40X in oil. (B) Posterior confocal projection showing the calyx (dendritic region). Ank2 and Futsch concentrate in the axonal regions only. Asterisks indicate the axon bundles of the Kenyon cells where merge between Ank2 and Futsch occurs. Zoom 3, objective 63X in oil.

In order to verify whether Ank2 also localised to dendrites, double labelling with an antibody that recognises the post-synaptic density protein Disc-large 1 (Dlg-1) was conducted. *Dlg1* encodes for a protein called Discs Large 1, a MAGUK (Membrane

Associated Guanylate Kinase) family member, highly conserved homolog of mammalian PSD-95 and SAP97 (Maiya et al., 2012) which are involved in dendritic outgrowth and branching (Charych et al., 2006; Zhang et al., 2015). Dlg1 was detected in the dendritic field (the calyx) in distinctive domains called microglomeruli (Figure 3.14). Indeed, cells in the calyx are organised into an array of microglomeruli each comprising the large synaptic bouton of projection neurons from the antennal lobe surrounded by tiny postsynaptic neurites from intrinsic Kenyon cells (Leiss et al., 2009; Butcher et al., 2012). Dlg1 in the microglomeruli was interspersed by Ank2 positive axon tracts and no overlay between the two proteins was observed supporting the evidence of a preferential axonal localisation of Ank2 in the adult fly brain.

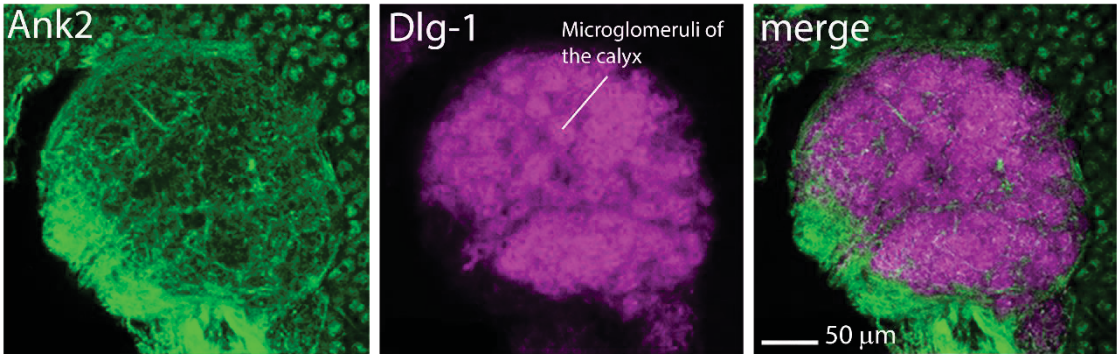

Figure 3.14 Ank2 does not localise in the dendritic regions of the *Drosophila* brain. Single plane (1 µm) of the posterior side of the brain showing the calyx, i.e. the dendritic field. Ank2 (green) is present in the axons surrounding the calyx and does not co-localise with the dendritic marker Dlg-1 (magenta). Zoom 4.9, objective 63X in oil.

It was noticed that anti-Ank2 immunostaining indicated a partial localisation of Ank2 in the nuclei of the Kenyon cells. In order to investigate this further, analyses were performed with anti-Elav that targets an RNA-binding protein localised to the nucleus (Koushika et al., 1996) and it is used as a neuronal nuclear marker.

In the posterior region of the brain, where the nuclei of the Kenyon cells are clearly visible, Elav is present in the neuronal nuclei in contrast to the axonal distribution of Ank2 (Figure 3.15A and B). However, in the Kenyon cells, Ank2 is also present in the nuclei but the lack of overlay suggest they do not overlap in the nucleus (Figure 3.15C).

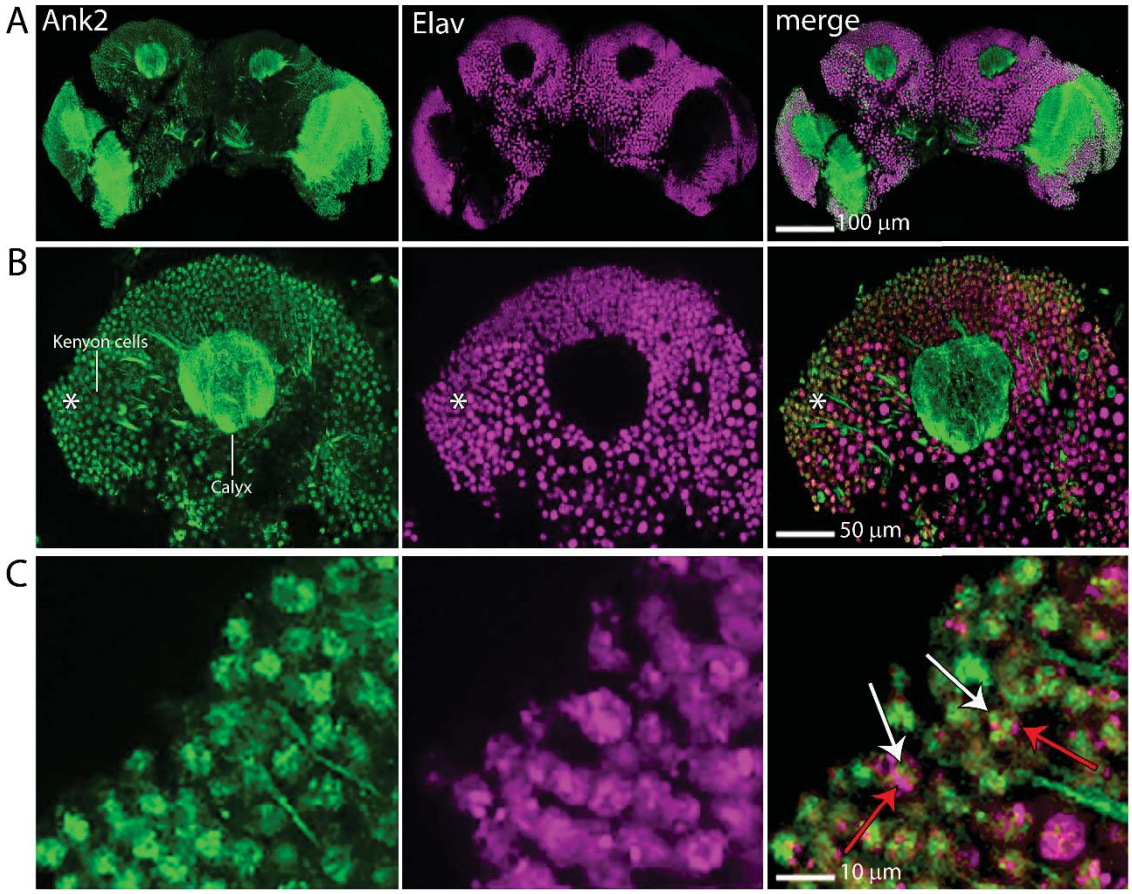

Figure 3.15 Ank2 localises to distinct nuclear compartment in the nuclei of the Kenyon cells. (A) Posterior confocal z-stack (1 µm) of the posterior side of the brain showing distribution of Ank2 (green) and Elav (magenta) in the nuclei. Zoom 1.3, objective 20X. (B) A posterior single confocal z-stack (1 µm) magnifying the calyx and the Kenyon cells. Zoom 2.1, objective 40X in oil. (C) Magnification of a subset of Kenyon cells showing the nuclear expression pattern of Ank2 (white arrows) and Elav (red arrows). No overlay is observed between Ank2 and Elav in the Kenyon cell nuclei.

As with mammalian neurons, *Drosophila* neurons are sheathed by glial cells that mediate key aspects of neuronal development and function including axon pathfinding, modelling of synaptic connections and recycling of synaptic neurotransmitter (Freeman at al., 2006; Awasaki et al., 2008; Awasaki and Lee, 2011). To identify the glial cells, mature brains were stained with an antibody against a protein named Reversed polarity (Repo), a transcription factor specifically expressed in all glial cells (Berger et al., 2007). No overlap between Ank2 and Repo was observed, confirming the specific neuronal expression pattern of Ank2 (Figure 3.16).

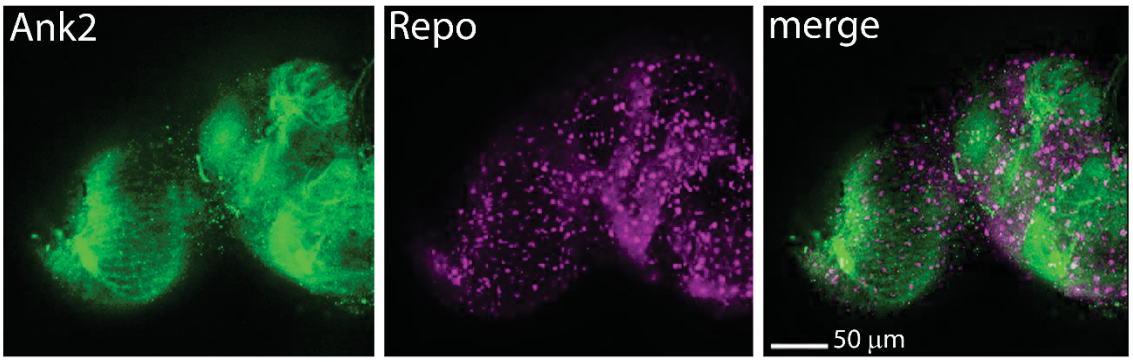

Figure 3.16 Ank2 is not present in glial cells . Frontal confocal projection of half hemisphere of the brain showing expression of Ank2 (green) and glial marker Repo (magenta). Zoom 2.5, objective 20X.

3.3.1.2 *Ankyrin2* is required for normal development of the mushroom body

Long-term courtship memory is contingent upon intact architecture of the mushroom body (McBride et al., 1999). Given the expression of Ank2 in the mushroom body, its role in regulating development of this structure was investigated, since alterations of the mushroom body lobes caused by decreased expression of *Ank2* could have a negative impact on LTM formation. In this case, to avoid developmental effects, any investigation into the role of *Ank2* in LTM would require manipulation of *Ank2* in the adult brain via the TARGET system (section 3.1).

The effect of *Ank2* knockdown on brain development was analysed in detail via anti-Fasciclin II (anti-FasII) immunohistochemistry. FasII is a cell adhesion molecule that is highly expressed in the mushroom body and participates in axonal pathfinding, fasciculation and divergence in the *Drosophila* nervous system (Fushima and Tsujimura, 2007). Antibodies specific for FasII have been revealed to be valuable resources to characterise the anatomy of the mushroom body lobes (Crittenden et al., 1998). FasII exhibits a complex expression pattern, being detected at high levels in the α and β lobes, low levels in γ lobe and not at all in the α′ and β′ lobes (Crittenden et al., 1998) and is currently commonly used marker to visualise mushroom body lobes architecture in immunohistochemical analysis.

For immunohistochemical analysis of mushroom body development *elav-GAL4* females were crossed to *UAS-Ank2*RNAi males and raised at room temperature, i.e. 22°C, resulting in pan-neuronal expression of RNAi. Prior the analysis, knockdown of *Ank2* was confirmed by qPCR (Figure 7.7 and 7.8, Appendix 7.2) using at least three biological replicates from cDNA preparations derived from heads of flies in which *UAS-Ank2*RNAi was expressed via the pan-neuronal *elav-GAL4* driver.

Following immunohistochemistry with FasII antibody, brains were visualised under confocal microscope. A variety of phenotypic defects were observed, with brains presenting one or more of the following morphological alterations of the lobes including, thin lobes, outgrowth and guidance defects with lobes branching in the wrong direction or not properly elongated, e.g. shorter or longer occasionally resulting in lobes fusion, and lack of one or more lobes. Representative images are shown below (Figure 3.17). Approximately 37% of the brain hemispheres displayed abnormal morphology e.g thin lobes (Figure 3.17, micrographs C, D, E, G, H, J, K arrowheads), and 37% of the hemisphere exhibited outgrowth defects of the α, β and γ lobes (Figure 3.17, micrographs B, F, G, H, I, J, K arrows). In a few brains, the β lobes from the two hemispheres converged resulting in a fusion of the lobes (Figure 3.17, micrographs F, G, I, J, red dotted circle) and in 6% of hemispheres, absence of γ lobes was observed (Figure 3.17, micrograph L, asterisks).

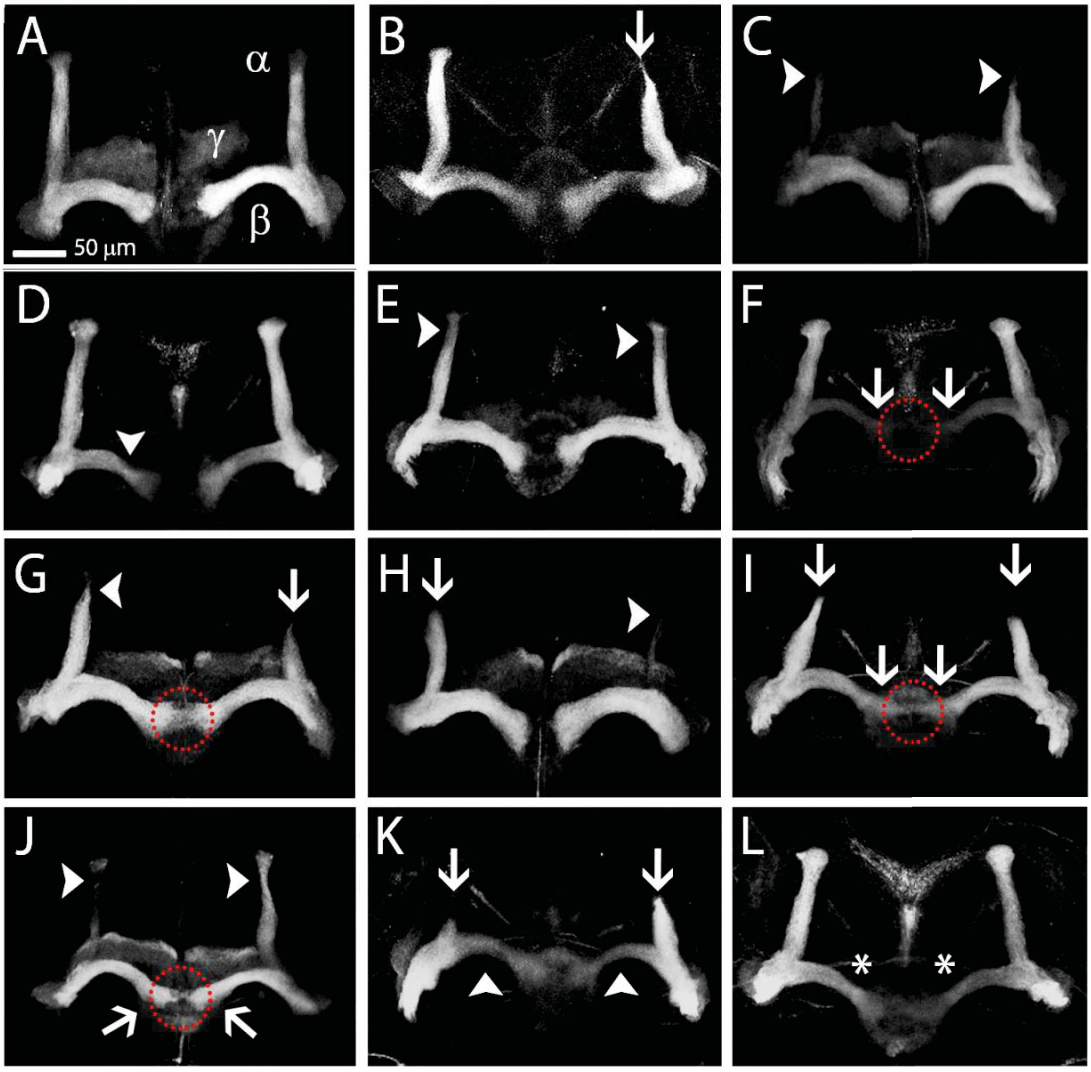

M

Ank2 knockdown phenotypes	N = 30
Outgrowth and guidance defects	37%
Lobes fusion	13%
Abormal morphology	37%
Lobe missing	6%

Figure 3.17 *Ank*2 knockdown phenotypes at 22°C. Immunohistochemistry with anti-FasII on whole-mount brains reveals morphological defects of the mushroom body lobes resulting from *elav-GAL4* driven expression of *UAS-Ank2*RNAi at 22°C. Images are frontal projections of confocal z-stacks under a 40X objective in oil with a zoom range between 1-1.6. Phenotypic alterations consisted of the following traits: outgrowth and guidance defects indicated by a white

arrow, lobes fusion indicated by a red dotted circle, thinner lobes indicated by a white arrowhead and missing γ lobes indicated by a white asterisk. (A) Wild-type brain. (B-L) *Ank2* knockdown brains. (M). Table summarising the mushroom body morphological defects. The percentage was calculated from the total number of brain hemispheres examined (N).

Subsequently, pan-neuronal depletion of *Ank2* was tested at the higher temperature of 25°C, as GAL4 activity is temperature dependent and more severe phenotypes were expected. In addition, this was also the temperature at which male flies would be tested in the memory assay.

In this case, the majority of the brain hemispheres, approximately 40%, exhibited loss of one or two lobes (Figure 3.18, micrographs B, D, E, F, G, H, J, asterisks). Around 23% of the hemispheres displayed outgrowth defects with lobes that did not completely elongate or that fused with the lobe in the opposite hemisphere (Figure 3.18, micrographs D, E, F, I, L, arrows, fusion of the lobes indicated by a red dotted circle) and 23% showed thinner lobes (Figure 3.18, micrograph C, F, G, H, J, arrowheads).

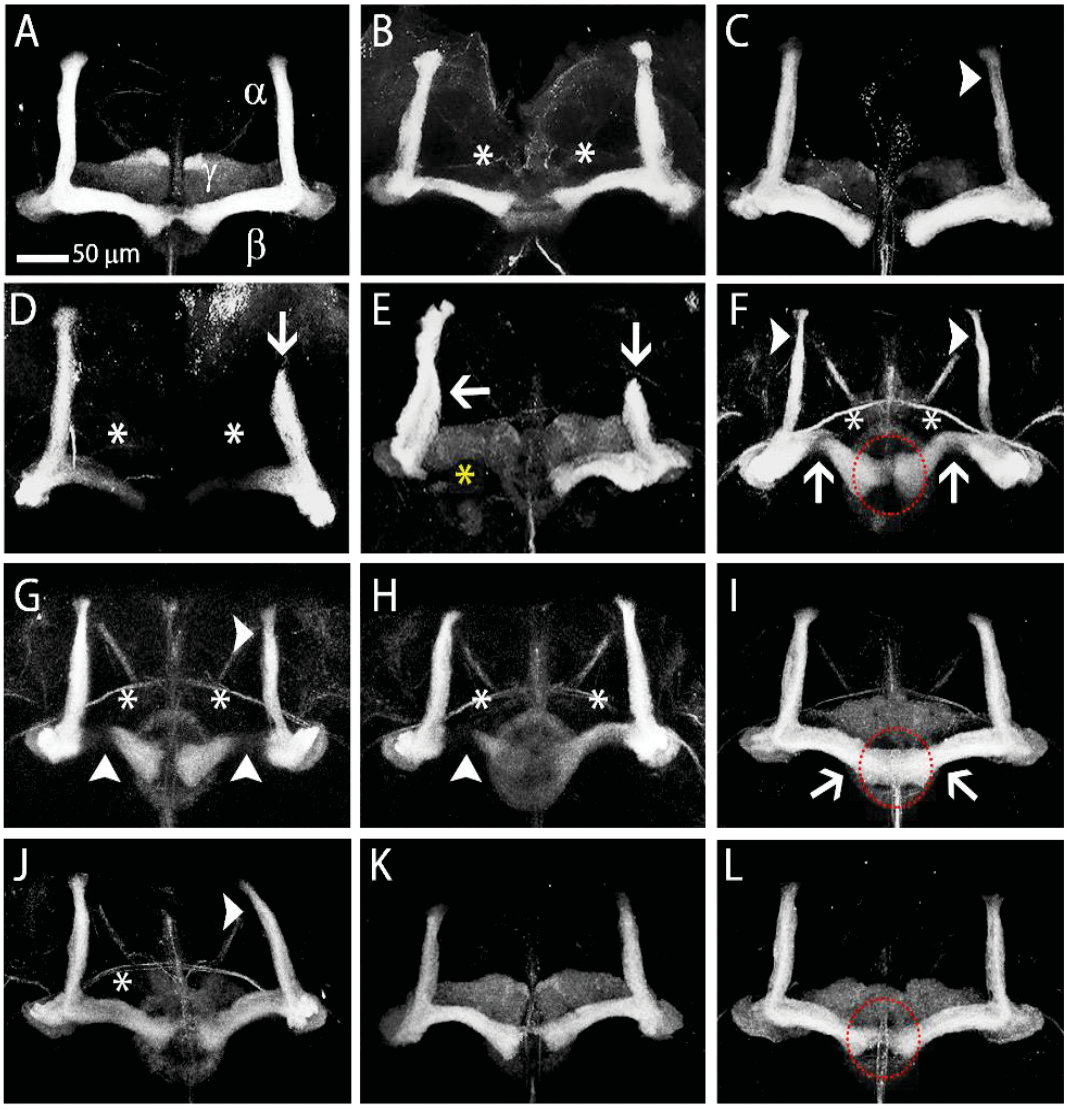

M

Ank2 knockdown phenotypes	N = 30
Outgrowth and guidance defects	23%
Lobes fusion	10%
Abormal morphology	23%
Lobe missing	40%

Figure 3.18 *Ank*2 knockdown phenotypes at 25°C. Immunohistochemistry with anti-FasII on whole-mount brains reveals morphological defects of the mushroom body lobes resulting from *elav-GAL4* driven expression of *UAS-Ank2*RNAi at 25°C. Images are projections of confocal z-stacks under a 40X objective in oil with a zoom range between 1-1.6. Phenotypic alterations consisted of the following traits: outgrowth and guidance defects indicated by a white arrow, lobes fusion indicated by a red dotted circle, thinner lobes indicated by a white the arrowhead and missing lobes indicated by asterisks, white for γ lobes, yellow for β lobes. (A) Wild-type brain.

(B-L). *Ank2* knockdown brains (M) Table summarising the mushroom body morphological defects. The percentage was calculated from the total number of brain hemispheres examined (N).

In order to investigate the extent to which *Ank2* depletion could affect mushroom body lobe development, flies expressing pan-neuronal *UAS-Ank2*RNAi were grown at the higher temperature of 27°C to allow a higher degree of GAL4 activity. The resulting phenotypes of the mushroom body lobes were rather severe and in most extreme cases loss of all lobes and formation of ball-like structures was observed (Figure 3.19, micrograph I). Approximately 62% of the brain hemispheres showed thinner lobes (Figure 3.19, micrographs B, C, D, E, F, G, arrowheads), 50% showed outgrowth defects (Figure 3.19, micrographs B, C, D, F, G, H, I) and 50% missed one or more lobes (Figure 3.19, micrographs B, E, F, H, I, asterisks).

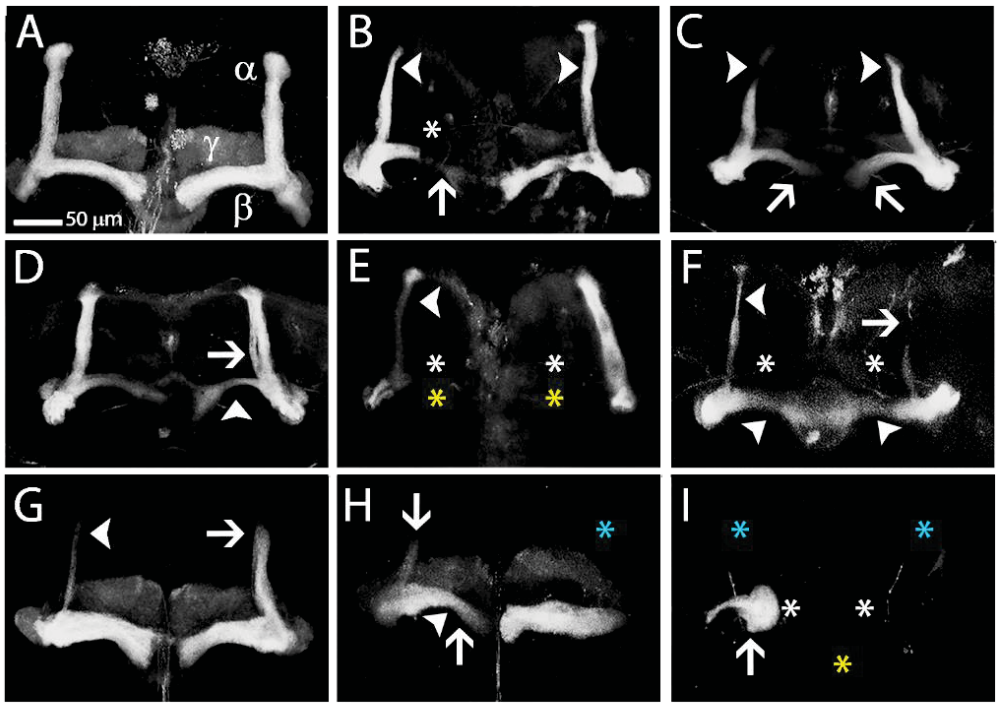

J

Ank2 knockdown phenotypes	N = 16
Outgrowth and guidance defects	50%
Lobes fusion	0%
Abormal morphology	62%
Lobe missing	50%

Figure 3.19 *Ank*2 knockdown phenotypes at 27°C. Immunohistochemistry with anti-FasII on whole-mount brains reveals morphological defects of the mushroom body lobes resulting from *elav-GAL4* driven expression of *UAS-Ank2*RNAi at 27°C. Images are projections of confocal z-stacks under a 40X objective in oil with a zoom range between 1-1.6. Phenotypic alterations consisted of the following traits: outgrowth and guidance defects indicated by a white arrow, thinner lobes indicated by a white arrowhead and missing lobes indicated by asterisks, white for γ lobes, yellow for β lobes and blue for α lobes. (A) Wild-type brain. (B-I) *Ank2* knockdown brains. (J) Table summarising the mushroom body morphological defects. The percentage was calculated from the total number of brain hemispheres examined (N).

3.3.1.3 *Ankyrin2* is required for long-term memory formation both during development and in adulthood

It was previously shown that knockdown of *Ank2* in the mushroom body could impair one hour STM formation in the courtship suppression assay (Iqbal et al., 2013) and pan-neuronal knockdown of *Ank2* resulted in impairment of three hour olfactory memory (Walkinshaw et al., 2015). However, no evidence has yet been provided with respect to the possible role of *Ank2* in brain development and in LTM (> three hour memory).

In the previous section (section 3.3.1.2), a critical role of *Ank2* in mushroom body development was demonstrated and since integrity of these structures is required for regular associative learning and memory formation (McBride et al., 1999), an evaluation of whether such morphological alterations resulted in defects in LTM formation was conducted.

*UAS-Ank2*RNAi males were crossed to *elav-GAL4* females in order to promote *Ank2* knockdown in all neurons of the brain and 24 hour LTM was estimated by subjecting male flies to the repeat training courtship suppression assay (section 1.3.3). This associative memory test evaluates the courtship activity of a male exposed to a previously mated and unreceptive female. In such conditions a male learns that he has been rejected and as a result suppresses his courtship activity towards female flies he is subsequently presented with. After seven hours of training males form a stable LTM that lasts for at least 24 hours (Keleman et al., 2007; Fitzsimons et al., 2011; Fitzsimons et al., 2013). After this time, each male is placed with a new freshly mated (unreceptive) female and a courtship index is calculated by dividing the amount of time each male spends courting by the total duration of the observation period (Reza et al., 2013).

A memory index can be calculated as the ratio between the courtship index of each tested fly by the mean courtship index value of control flies (sham) that were not housed with a mated female in the training session. A range of values is obtained between zero indicating the highest memory score possible, to one meaning memory is impaired and no different from untrained sham controls (Ejima and Griffith, 2010). Normal memory is generally characterised by a memory index of 0.5-0.7 (Fitzsimons et al., 2011, 2013).

3.3.1.3.1 Depletion of *Ankyrin2* during development impairs long-term memory formation but does not affect learning and immediate recall of memory

To test for the influence of *Ank2* on LTM, females harbouring the pan-neuronal *elav-GAL4* driver were crossed to either *UAS-Ank2*RNAi or wild-type males of the CS wild-type line. In addition wild-type CS females were crossed to *UAS-Ank2*RNAi males as a control for the *UAS-Ank2*RNAi line itself.

Pan-neuronal knockdown of *Ank2* resulted in a significant and severe loss of LTM formation compared to control genotypes (ANOVA, post-hoc Tukey's HSD, $P < 0.001$, Figure 3.20A). An important aspect in these memory assay that requires consideration is that knockdown of a specific gene could possibly alter the courtship behaviour itself thus rendering it difficult to determine whether the effect on memory is specific to the processes required for memory or to a reduced courtship activity, which could alter the males capacity to learn and form new memories. In order to control this aspect, the courtship activity of sham males was compared. Those males are used as control for the courtship activity since during the testing phase they are coupled with a mated female for the first time and would court most of the time, displaying a courtship index of approximately one (~ 0.9-1). Comparison of the courtship activity of sham males of each genotype did not result in statistical differences (Figure 3.20B) therefore impaired memory formation was not caused by a flaw in the ability to court.

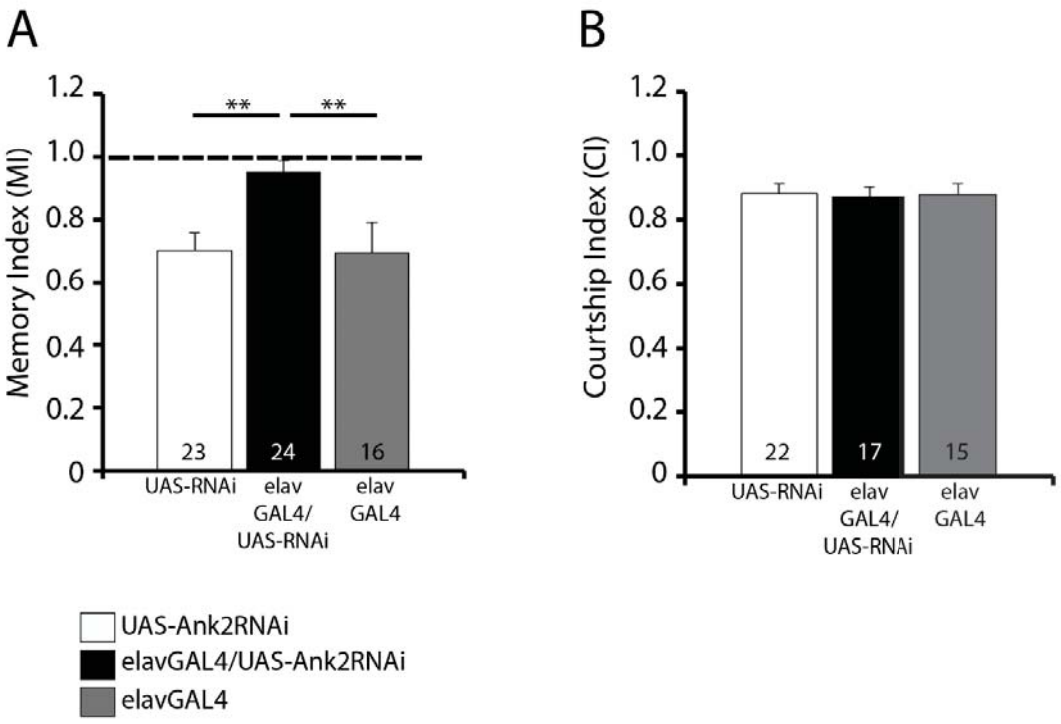

Figure 3.20 *Elav-GAL4* pan neuronal knockdown of *Ank2* in the brain during development abolishes LTM formation. (A) Flies expressing *UAS-Ank2*RNAi in whole brain neurons (black bar) showed significant impairment of LTM compared to control genotypes ank2KD (white bar) and elavGAL4 (gray bar) (ANOVA, post-hoc Tukey's HSD, ** $P < 0.01$), with a score of approximately one indicating memory no different than a sham male. (B) Courtship activity of sham males was not altered by *elav-GAL4* mediated expression of *Ank2*RNAi (ANOVA, $P = 0.869$). Numbers within bars indicate the number of animals analysed. Genotype abbreviations: UAS-AnkRNAi = *UAS-Ank2RNAi/+*. elavGAL4/ UAS-Ank2RNAi = *elav-GAL4/Y; UAS-Ank2RNAi/+*. elavGAL4 = *elav-GAL4/Y*.

It was previously shown that the ablation of mushroom body structures does not cause detrimental effects on learning and immediate recall of memory (zero to two minutes after training) in the courtship conditioning assay (McBride et al., 1999), meaning that although these structures are not required for these early memory processes, they are essential for consolidation of short-term and long-term memories (McBride et al., 1999). To examine a possible role of *Ank2* in learning and immediate recall of memory, flies harbouring pan-neuronal knockdown of *Ank2* were subjected to a one hour training session and a learning index (LI) was assessed as the ratio between the final and initial ten minutes of the training session. For immediate memory assessment, flies were tested

immediately after (zero minutes) the training session (Ejima and Griffith, 2010). Flies with intact learning are expected to decrease their courtship activity over the one hour training with a resulting learning index in the range of 0.2-0.6 (Ejima and Griffith, 2010). In both assays, there was no difference in learning and immediate memory between controls (white and gray bars) and *UAS-Ank2*RNAi flies (black bar) (Figure 3.21). The knockdown of *Ank2* appeared to improve the learning and memory performance. However, no statistical differences were measured, suggesting *Ank2* is not required for learning and immediate recall of memory.

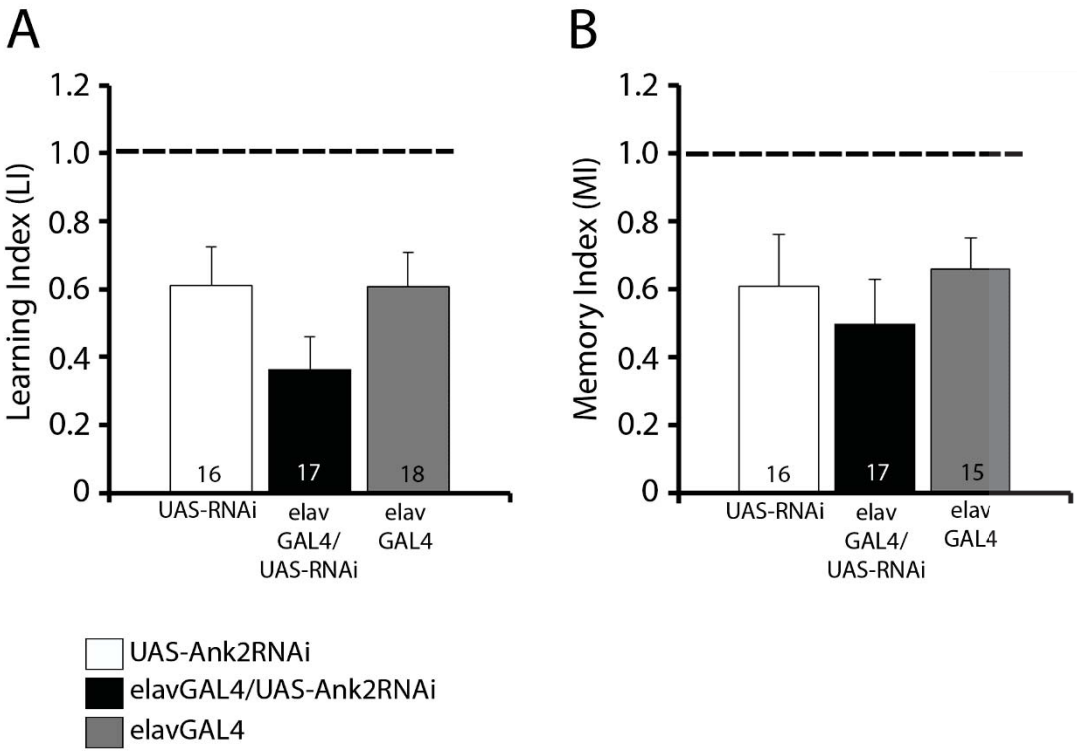

Figure 3.21 *Elav-GAL4* pan-neuronal knockdown of *Ank2* throughout development has no impact on learning and immediate memory (A) Learning index. Flies in which *Ank2* was knocked-down in all neurons of the brain, displayed normal abilities to learn (ANOVA, P = 0.251). (B) No impairment to the immediate retrieval of memory was observed in flies harbouring *elav-GAL4* mediated knockdown of *Ank2* (ANOVA, P = 0.819). Numbers within bars indicate the number of animals analysed. Genotype abbreviations: UAS-Ank2RNAi = *UAS-Ank2RNAi/+*. elavGAL4/UAS-Ank2RNAi = *elav-GAL4/Y; UAS-Ank2RNAi/+*. elavGAL4 = *elav-GAL4/Y*.

These results suggest that while *Ank2* is not involved in earlier phases of the memory process, it may be involved in LTM specifically. However, it is yet to be determined if the LTM deficit is a result of impaired mushroom body development or due to a distinct role in LTM.

3.3.1.3.2 Knockdown of *Ankyrin2* in the adult brain impairs long-term memory

3.3.1.3.2.1 Decreased expression of *Ankyrin2* in all neurons of the brain impairs long-term memory formation

In order to obviate the effect of decreased *Ank2* expression on development and to test the memory of flies with normal morphology of the mushroom body, the TARGET system was used to induce *UAS-Ank2*RNAi expression in the adult brain specifically (section 3.1). Pan-neuronal knockdown of *Ank2* was induced in all neurons of the brain with the *elav-GAL4* driver and gene expression was restricted to adulthood with the TARGET system which induces gene expression in a temperature regulated fashion (section 3.1).

Elav-GAL4; tub-GAL80^{ts} females were crossed to *UAS-Ank2*RNAi and wild-type CS males and raised at the permissive temperature of 18°C at which GAL80^{ts} mediated-inactivation of GAL4 is active. At the same time, wild-type CS females were crossed to *UAS-Ank2*RNAi males, in order to generate a control for the *UAS-Ank2*RNAi line and also raised at 18°C. Seventy-two hours after eclosion, male flies from the F1 progeny were collected individually and transferred to 30°C to induce RNAi expression. After three days, males were tested in the courtship suppression assay (section 2.17).

Adult-specific knockdown of *Ank2* resulted in impairment of LTM formation (Figure 3.22A, ANOVA, post-hoc Tukey's HSD, $P < 0.05$) while sham males showed normal courtship activity with no significant differences among genotypes (Figure 3.22B) therefore the memory phenotype was not determined by the inability of the males to court normally.

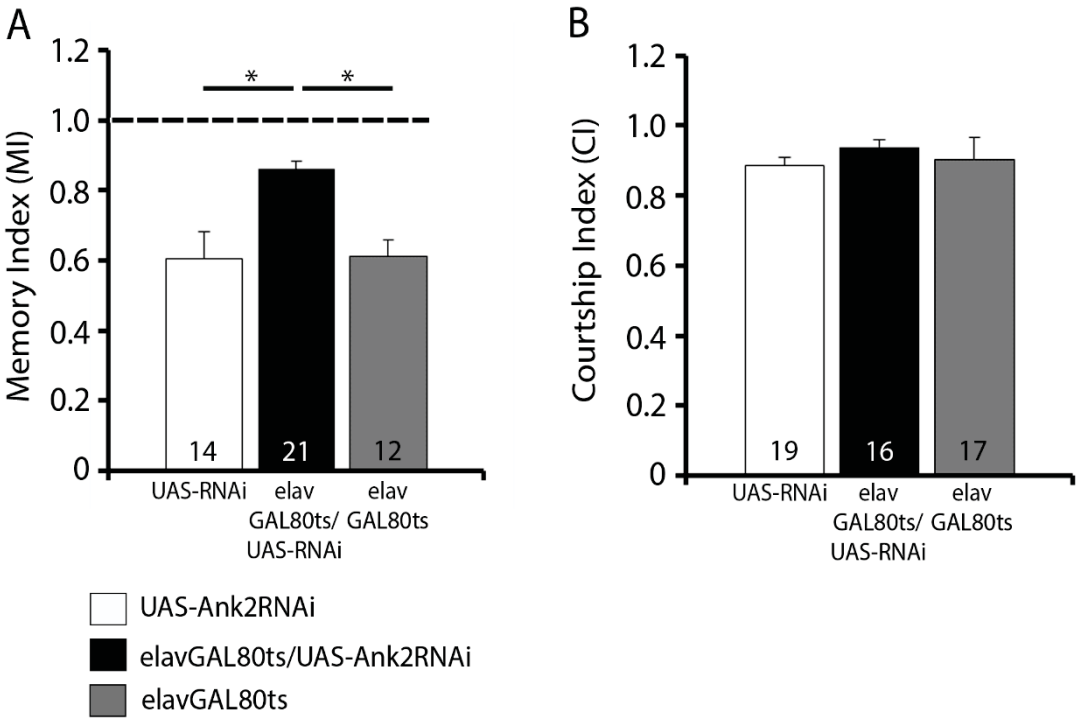

Figure 3.22 Pan-neuronal knockdown of *Ank2* induced during adulthood impairs LTM formation. (A) Flies expressing *UAS-Ank2*RNAi in the adult brain (black bar) showed impairment of LTM when compared to control genotypes ank2KD (white bar) and elavGAL4 (gray bar) (ANOVA, post-hoc Tukey's HSD, * $P < 0.05$). (B) The courtship activity of sham males was not affected by knockdown of *Ank2* (ANOVA, $P = 0.187$). Numbers within bars indicate the numbers of animals tested. Genotype abbreviations: UAS-Ank2RNAi = *UAS-Ank2RNAi/+*. elavGAL80^{ts}/UAS-Ank2RNAi = *elav-GAL4/Y; tub-GAL80^{ts}/UAS-Ank2RNAi.* elavGAL80^{ts}: *elav-GAL4/Y; tub-GAL80^{ts}/+*.

To confirm that *Ank2* knockdown was not induced at the temperature of 18°C, e.g. TARGET system "OFF", a subset of flies were grown 18°C and kept at the same temperature for two days after eclosion and subsequently subjected to whole-mount brain dissection for immunohistochemistry analysis with anti-FasII. No evident morphological defects were detected in the mushroom body of these flies compared to wild-type flies (Figure 3.23) confirming that the subjects analysed in behavioural assays possessed normal anatomy of the mushroom body lobes, hence the memory impairment was not a result of malformation of the mushroom body.

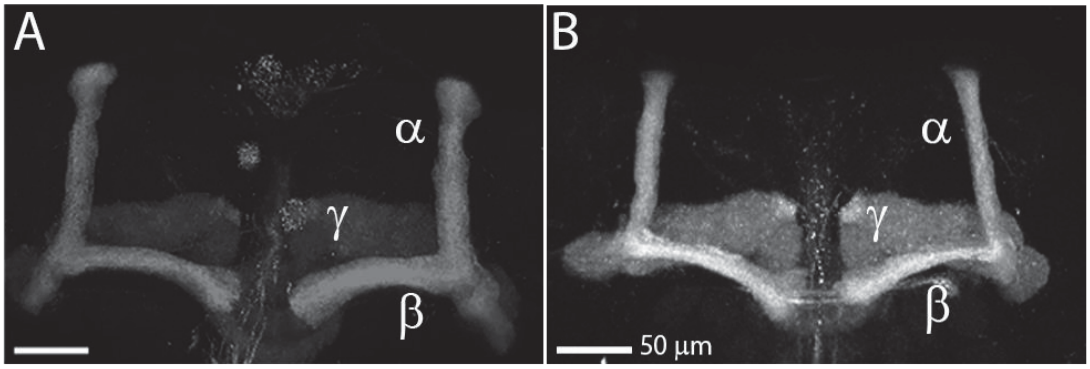

Figure 3.23 Pan-neuronal knockdown of *Ank2* is not induced by the TARGET system during development. Flies subjected to courtship suppression assay to test for *Ank2* knockdown effects on LTM during adult stage were also subjected to anti-FasII immunohistochemistry to confirm that GAL4-dependent activation of *UAS-Ank2*RNAi was not induced during development. Flies were grown and kept at 18°C after eclosion and anti-FasII immunohistochemistry of whole-mount brains was conducted. (A) Representative confocal micrograph of mushroom body lobes derived from control fly. (B) Representative confocal micrograph of mushroom body lobes from flies harbouring the TARGET system and *UAS-Ank2*RNAi at 18°C.

3.3.1.3.2.2 Knockdown of *Ankyrin2* in the mushroom body impairs long-term memory formation

Since LTM memory is known to depend on mushroom body architecture and integrity (McBride et al., 1999), knockdown of *Ank2* was induced specifically in the mushroom body rather than in all neurons to determine whether expression of *Ank2* in this compartment is required for memory formation.

The three classes of Kenyon cells (α/β; α'/β' and γ) that form the mushroom body lobes are not identical and differ in gene expression, neurotransmitter systems and roles in behavioural function (Lee et al., 1999; Akalal et al., 2006; Aso et al., 2009; Spindler and Hartenstein, 2010; Kunz et al., 2012). To achieve a complete characterisation of the role of *Ank2* in all classes of Kenyon cells, well characterised mushroom body-*GAL4* drivers were used that fall into four categories: drivers labelling all lobes (*OK107-GAL4* and *MB247-GAL4*), γ lobes (*1471-GAL4* and *NP1131-GAL4*), α/β lobes (*c739-GAL4*), α'/β' lobes (*c305a-GAL4*). All GAL4 drivers used in this experimental procedure were expressed with *tub-GAL80^{ts}* (TARGET system) to induce transgene expression in the adult in order to avoid developmental effects of *Ank2* knockdown.

To characterise the role of *Ank2* in the mushroom body, the *OK107-GAL4* driver was initially selected since it drives robust expression in all of the mushroom body. However, it does drive low level of expression in regions outside the mushroom body including the optic lobes (OL), the pars intercerebralis (PI), the antennal lobes (AL) and the subesophageal ganglion (SOG) (Figure 3.24). *OK107-GAL4* driven expression of *UAS-Ank2*RNAi in the adult brain resulted in complete loss of LTM formation (Figure 3.25A, ANOVA, post-hoc Tukey's HSD, $P < 0.001$) without impairing the courtship activity of sham males (Figure 3.25B). This suggests a mushroom body-specific role for *Ank2* in LTM although this driver mediates expression at a lower level in other brain regions.

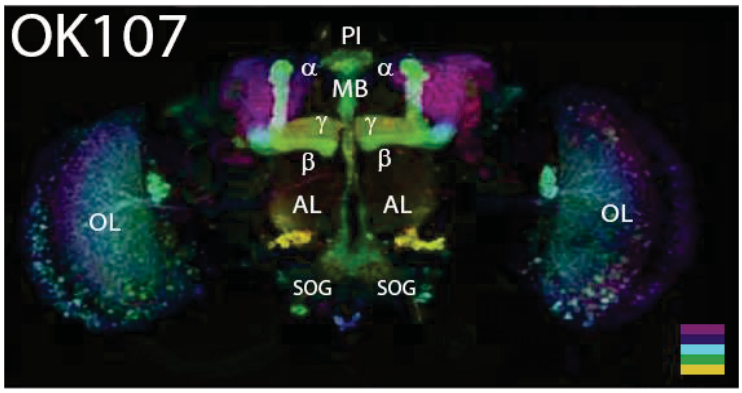

Figure 3.24 *OK107-GAL4* driver labelling profile. Confocal micrographs of brains showing GFP expression mediated by *OK107-GAL4* driver. Aso et al., 2009. Used under CC BY 3.0 (http://creativecommons.org/licenses/by/3.0), "OK107" inscription and colour scale were modified from the original source. *OK107-GAL4* driver strongly and uniformly labels all regions of the mushroom body. Outside the mushroom body, a strong signal is observed in the optic lobes (OL), antennal lobes (AL), pars intercerebralis (PI), and cells of the subesophageal ganglion (SOG). The applied colour represents the depth from anterior (yellow), to posterior (purple).

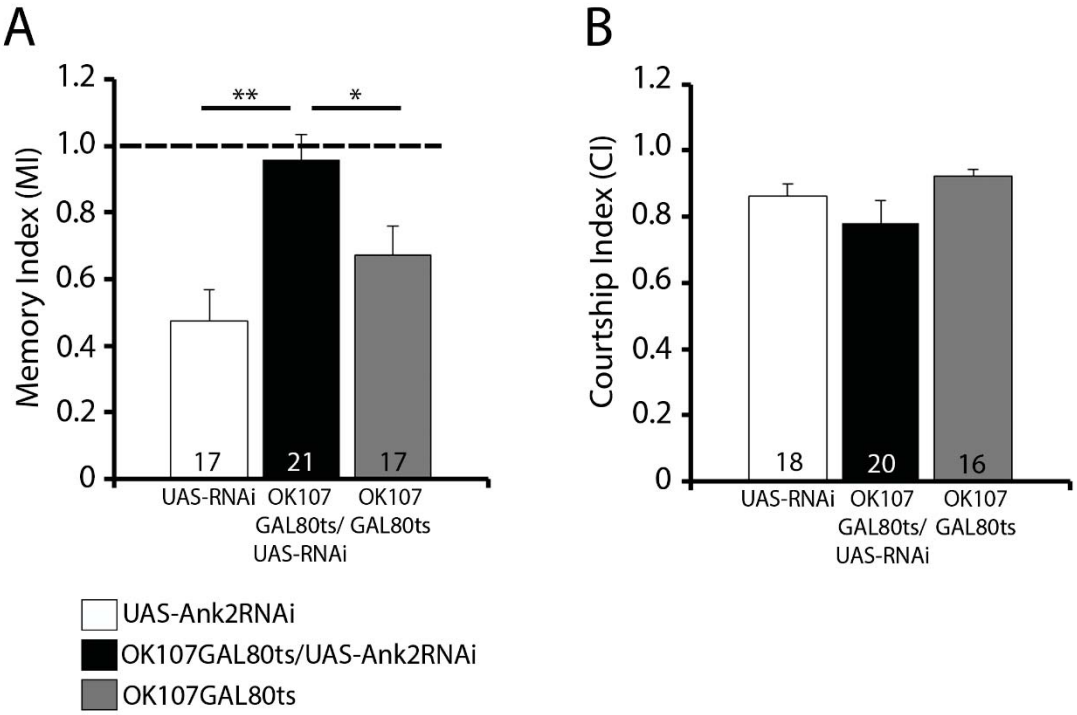

Figure 3.25 Decreased expression of *Ank2* in the mushroom body severely compromises LTM formation in adult flies. (A) Flies in which *Ank2* was knocked-down in all regions of mushroom body (black bar) showed impairment of LTM (ANOVA, post-hoc Tukey's HSD, * $P < 0.05$; ** $P < 0.01$). (B) Courtship activity of sham males was not impaired by *OK107-GAL4* driven knockdown of *Ank*2 (ANOVA, $P = 0.161$). Numbers within bars indicate the number of animals tested. Genotype abbreviations: UAS-Ank2RNAi = *UAS-Ank2RNAi/+*. OK107GAL80^{ts}/UAS-Ank2RNAi = *tub-GAL80^{ts}/UAS-Ank2RNAi; OK107-GAL4/+*. OK107GAL80^{ts} = *tub-GAL80^{ts}/+; OK107-GAL4/+*.

In order to limit transgene expression mainly to the mushroom body lobes, the *MB247-GAL4* driver was used which strongly labels the α/β and γ neurons, and the α'/β' neurons to a weaker degree with minimal expression outside the mushroom body (Figure 3.26).

MB247-GAL4 driven expression of *UAS-Ank2*RNAi resulted in an extremely significant aberration of LTM formation (Figure 3.27A, ANOVA, post-hoc Tukey's HSD, $P < 0.0001$) indicating that its expression in the α/β and γ neurons is important for memory formation. Courtship activity was evaluated and no statistical differences existed among sham males of each genotype meaning that the memory impairment was not caused by deficits in the ability to court (Figure 3.27B).

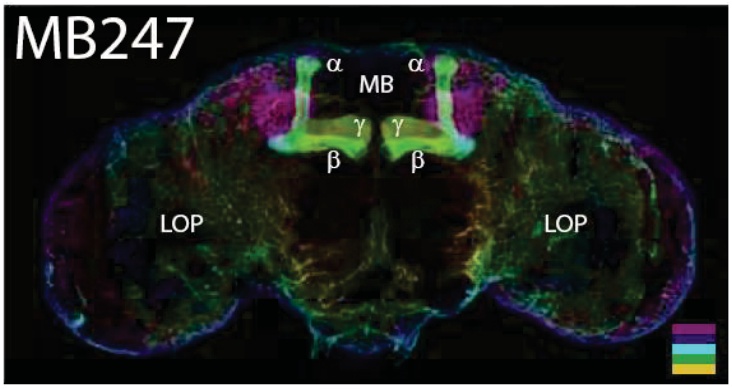

Figure 3.26 *MB247-GAL4* driver expression profile. Confocal micrographs of brains showing GFP expression mediated by *MB247-GAL4* driver. Aso et al., 2009. Used under CC BY 3.0 (http://creativecommons.org/licenses/by/3.0), "MB247" inscription and colour scale were modified from the original source. *MB247-GAL4* strongly labels the α/β and γ neurons with very low background expression. Expression in the α'/β' is weaker than in the other α/β subdivisions. Additional expression is detected in the cells in the lobula plate (LOP) and surface glia. The applied colour illustrates the depth from anterior (yellow) to posterior (purple).

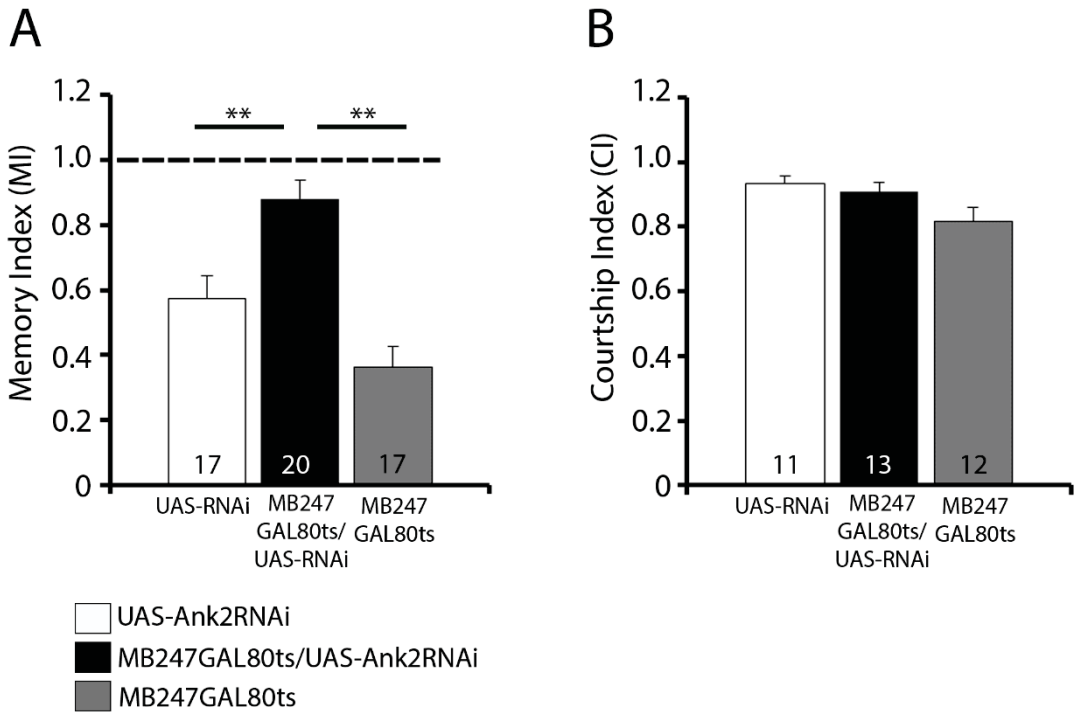

Figure 3.27 RNAi-mediated decreased expression of *Ank2* in α/β and γ lobes negatively affects LTM formation in adult flies. (A) Flies in which *Ank2* was knocked-down in the α/β and γ lobes of the mushroom body (black bar) showed significant impairment of LTM with respect to the control genotypes (white and gray bars) (ANOVA, post hoc Tukey's HSD, ** P <0.01). (B) No significant differences in the courtship activity of sham males were detected (ANOVA, post-

hoc Tukey's HSD, P = 0.453) meaning that the courtship activity is not impaired by knockdown of *Ank2*. Numbers within bars indicate the number of animals tested. Genotype abbreviations: UAS-Ank2RNAi = *UAS-Ank2RNAi/+*. MB247GAL80^{ts}/UAS-Ank2RNAi= *tub-GAL80^{ts}/UAS-Ank2RNAi; MB247-GAL4/+*. MB247GAL80^{ts} = *tub-GAL80^{ts}/+; MB247-GAL4/+*.

3.3.1.3.2.3 *Ankyrin2* is required in the γ lobes for long-term memory formation

In order to restrict *UAS-Ank2*RNAi expression to the γ neurons of the mushroom body, the *1471-GAL4* driver was employed even though it drives expression in some other regions including the antennal lobes, the antennal nerves, the pars intercerebralis and the subesophageal ganglion (Figure 3.28). Flies in which *Ank2* expression was depleted in the γ lobes were tested in the courtship suppression assay. These flies displayed a low memory index of approximately 0.8, however no significant differences were observed in comparison to control flies (Figure 3.29A, ANOVA, P = 0.0558). The courtship activity of sham males was not compromised (Figure 3.29B).

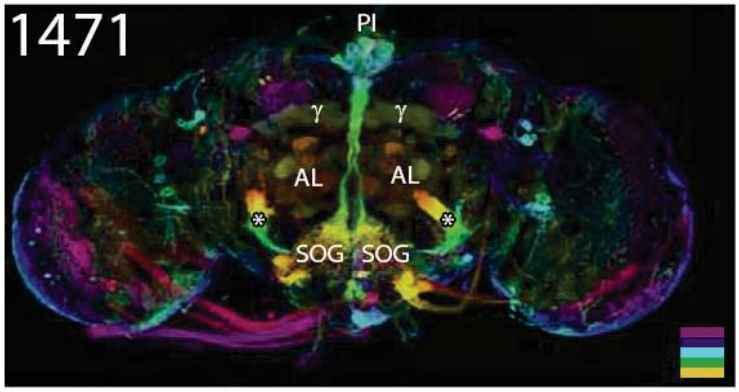

Figure 3.28 *1471-GAL4* driver expression profile. Confocal micrographs of brains showing GFP expression mediated by *1471-GAL4* driver. Aso et al., 2009. Used under CC BY 3.0 (http://creativecommons.org/licenses/by/3.0), "1471" inscription and colour scale were modified from original source. In the mushroom body, *1471-GAL4*-mediated expression of GFP is restricted in the γ neurons. *1471-GAL4* also labels a broad range of neuropils outside of the mushroom body, including the pars intercerebralis (PI), the antennal lobes (AL), the antennal nerves (indicated by an asterisk), the SOG. The applied colour illustrates the depth from anterior (yellow) to posterior (purple).

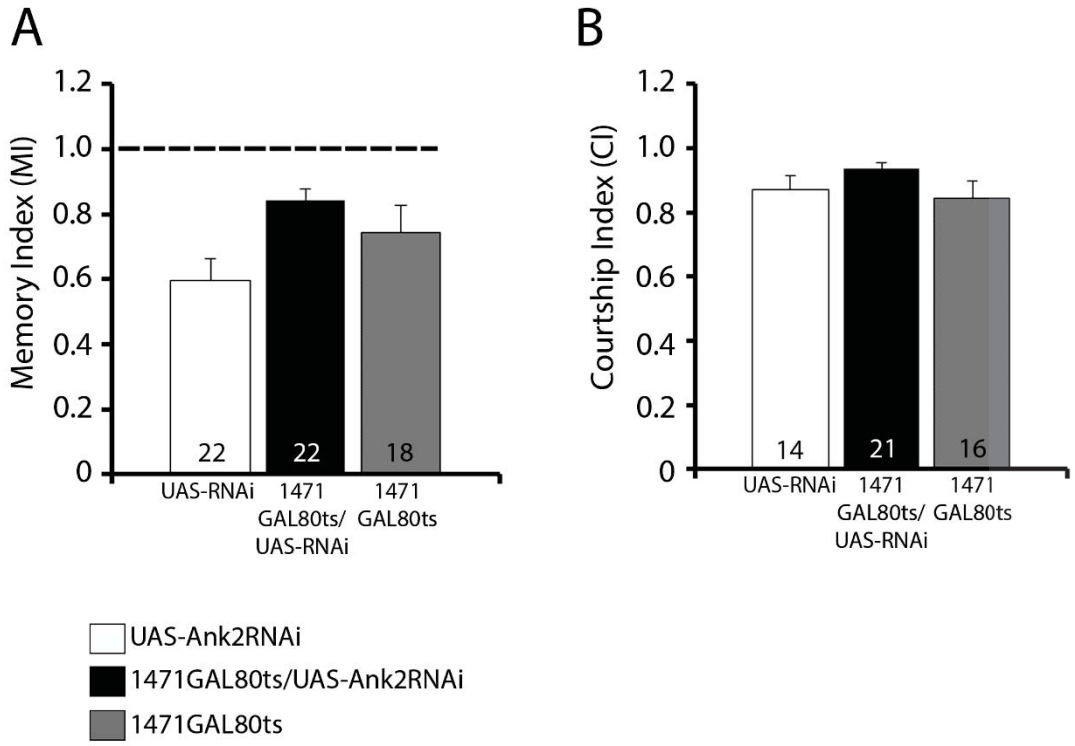

Figure 3.29 *Ank2* knockdown driven by *1471-GAL4* in the γ neurons does not affect LTM significantly. (A) Flies in which *Ank2* knockdown was mediated by the *1471-GAL4* driver in the γ lobes of the mushroom body (black bar), did not show impairment of LTM (ANOVA post hoc Tukey's HSD, P = 0.0558). (B) No significant differences in courtship activity among sham males of each group were detected (ANOVA, P = 0.109). Numbers within bars indicate the amount of animals tested. Genotype abbreviations: UAS-Ank2RNAi = *UAS-Ank2RNAi/+*. 1471GAL80^{ts}/UAS-Ank2RNAi = *tub-GAL80^{ts}/1471-GAL4, UAS-Ank2RNAi*. 1471GAL80^{ts} = *tub-GAL80^{ts}/1471-GAL4*.

As the *1471-GAL4* driver expresses only weakly in the γ lobes, a different γ lobe driver, *NP1131-GAL4,* was adopted. This driver promotes strong expression in the γ lobes, although very low expression is observed in α'/β' lobes and elsewhere in the brain including the subesophageal ganglion, the ellipsoid body (EB) and the pars intercerebralis (Figure 3.30). *NP1131-GAL4* driven expression of *UAS-Ank2*RNAi in the adult brain significantly impaired memory formation with a memory index of approximately one (Figure 3.31A, ANOVA, post-hoc Tukey's HSD, $P < 0.01$) whereas the courtship activity of sham males was not disrupted (Figure 3.31B) suggesting that the memory defects were not determined by an impairment of courtship activity of male flies.

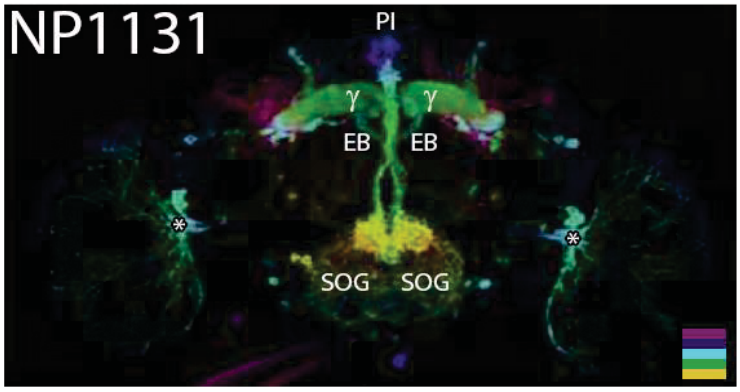

Figure 3.30 *NP1131-GAL4* driver expression profile. Confocal micrographs of brains showing GFP expression mediated by *NP1131-GAL4* driver. Aso et al., 2009. Used under CC BY 3.0 **(**http://creativecommons.org/licenses/by/3.0), "NP1131" inscription and colour scale were modified from original source. Additional expression is visible in the ellipsoid body (EB), subesophageal ganglion (SOG), pars intercerebralis (PI), large interneurons connecting the optic lobes and the central brain (asterisks), and other cells distributed in the brain. The applied colour illustrates the depth from anterior (yellow) to posterior (purple).

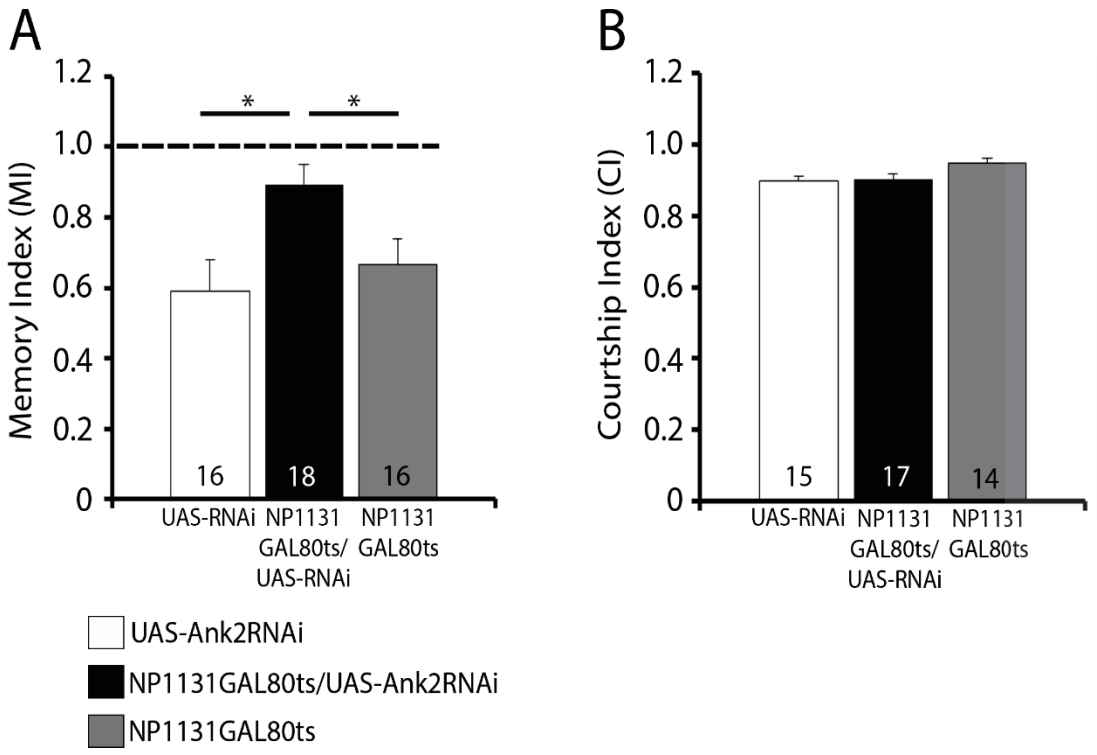

Figure 3.31 *NP1131-GAL4; tub-GAL80ts* driven expression of *UAS-Ank2*RNAi impairs LTM formation. (A) Flies in which *UAS-Ank2*RNAi was induced in the γ lobes (black bar) showed impairment of LTM in comparison to the control genotypes (white and gray bars)

(ANOVA, post-hoc Tukey's HSD, * P < 0.05). (B) Courtship activity of sham males was not impaired by *Ank2*RNAi driven by *NP1131-GAL4* driver (ANOVA, P = 0.085). Numbers within bars indicate the number of animals analysed. Genotype abbreviations: UAS-Ank2RNAi = *UAS-Ank2RNAi/+*. NP1131GAL80^{ts}/UAS-Ank2RNAi = *tub-GAL80^{ts}/NP1131-GAL4, UAS-Ank2RNAi*. NP1131GAL80^{ts} = *tub-GAL80^{ts}/ NP1131-GAL4*.

The *c739-GAL4* driver was adopted to restrict knockdown of *Ank2* predominantly to the α/β neurons, although other neuropils outside the mushroom body are labelled including local interneurons in the antennal lobes and neurons projecting from/to the optic lobes (Figure 3.32). The α/β neurons are believed to play adult specific roles since they develop after puparium formation (Lee et al, 1999). Interestingly, they are among the largest group of neurons and their axons are the most densely packed (Lee et al, 1999).

RNAi-mediated depletion of *Ank2* in the α/β neurons did not result in LTM impairment (ANOVA, P = 0.196) and courtship activity among sham males of each genotype was not statistically significant (ANOVA, P = 0.16). Overall, this result suggests that *Ank2* is not required for normal memory formation in these neurons (Figure 3.33). However, it has to be highlighted that despite a statistical difference in courtship activity was not measured flies in which the *UAS-Ank2*RNAi construct was not expressed, displayed variable courtship activity (Figure 3.33B, white bar).

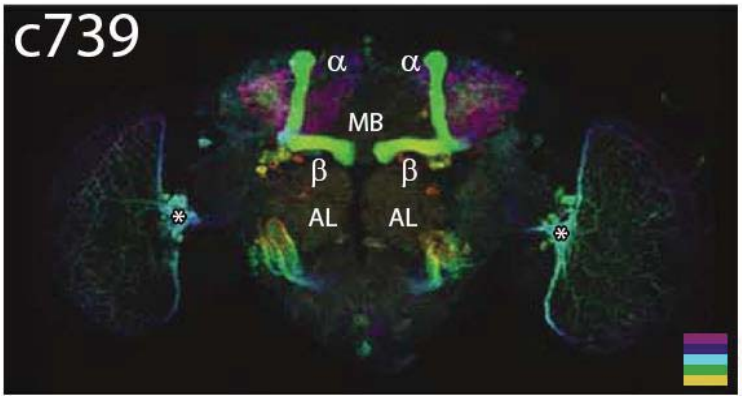

Figure 3.32 *c739-GAL4* driver expression profile. Confocal micrographs of brains showing GFP expression mediated by *c739-GAL4* driver. Aso et al., 2009. Used under CC BY 3.0 (http://creativecommons.org/licenses/by/3.0), "c739" inscription and colour scale were modified from original source. *c739-GAL4* strongly innervates the entire α/β lobes. Outside the mushroom body, it labels elements in a wide range of neuropils, including local interneurons in the antennal

lobes (AL), a cluster of neurons projecting from/to the optic lobes (asterisks), and many other cells throughout the brain. The applied colour illustrates the depth from anterior (yellow) to posterior (purple).

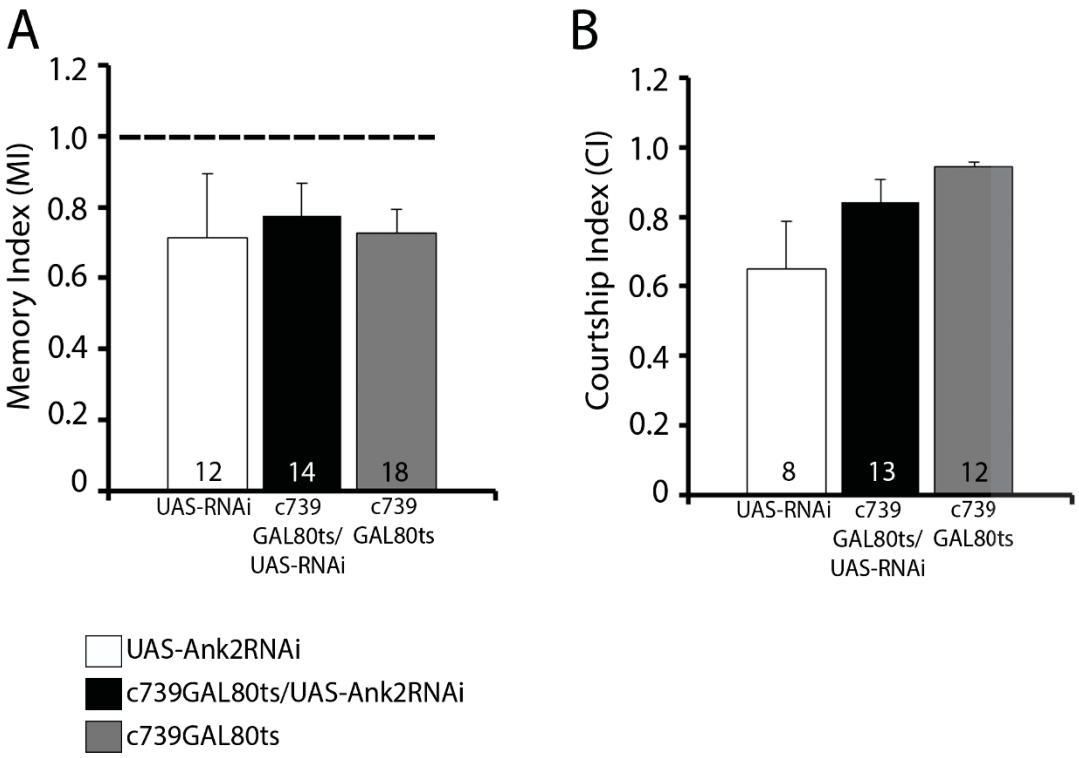

Figure 3.33 Knockdown of *Ank2* in α/β neurons does not affect LTM formation. (A) Flies expressing *UAS-Ank2*RNAi in α/β lobes did not show LTM impairment (ANOVA, P = 0.196). (B) No significant differences were observed among the courtship activity of sham males (ANOVA, P = 0.16) meaning that the courtship activity was not impaired by knockdown of *Ank2* in those neurons. Numbers within bars indicate the number of animals tested. Genotype abbreviations: UAS-Ank2RNAi = *UAS-Ank2RNAi/+*. c739GAL80^{ts}/UAS-Ank2RNAi = *tub-GAL80^{ts}/c739-GAL4, UAS-Ank2RNAi*. c739GAL80^{ts} = *tub-GAL80^{ts}/c739-GAL4*.

To selectively drive *Ank2*RNAi in α'and β' lobes the *c305a-GAL4* driver was employed and memory was assessed through the courtship conditioning assay. This driver also targets several other region of the brain including the antennal lobes, the ellipsoid body and the subesophageal ganglion (Figure 3.34). Flies harbouring knockdown of *Ank2* in the α'and β' lobes showed robust LTM, with a memory index of approximately 0.4 (Figure 3.35A, ANOVA, P = 0.371) therefore *Ank2* is not required in this subset of mushroom body neurons for normal LTM formation.

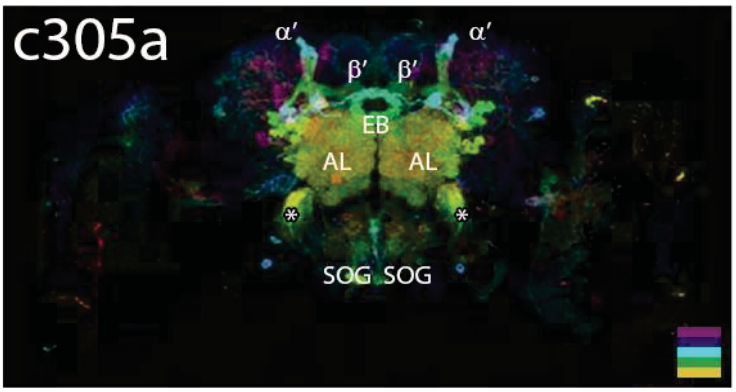

Figure 3.34 *c305a-GAL4* driver expression profile. Confocal micrographs of brains showing GFP expression mediated by *c305a-GAL4* driver. Aso et al., 2009. Used under CC BY 3.0 (http://creativecommons.org/licenses/by/3.0), "c305a" inscription was modified from original source. Outside the mushroom body, *c305a-GAL4* labels several neuropils including the antennal lobes (AL), the ellipsoid body (EB), large paired neurons originating (asterisk) from the subesophageal ganglion (SOG) and many other cells throughout the brain. The applied colour illustrates the depth from anterior (yellow) to posterior (purple).

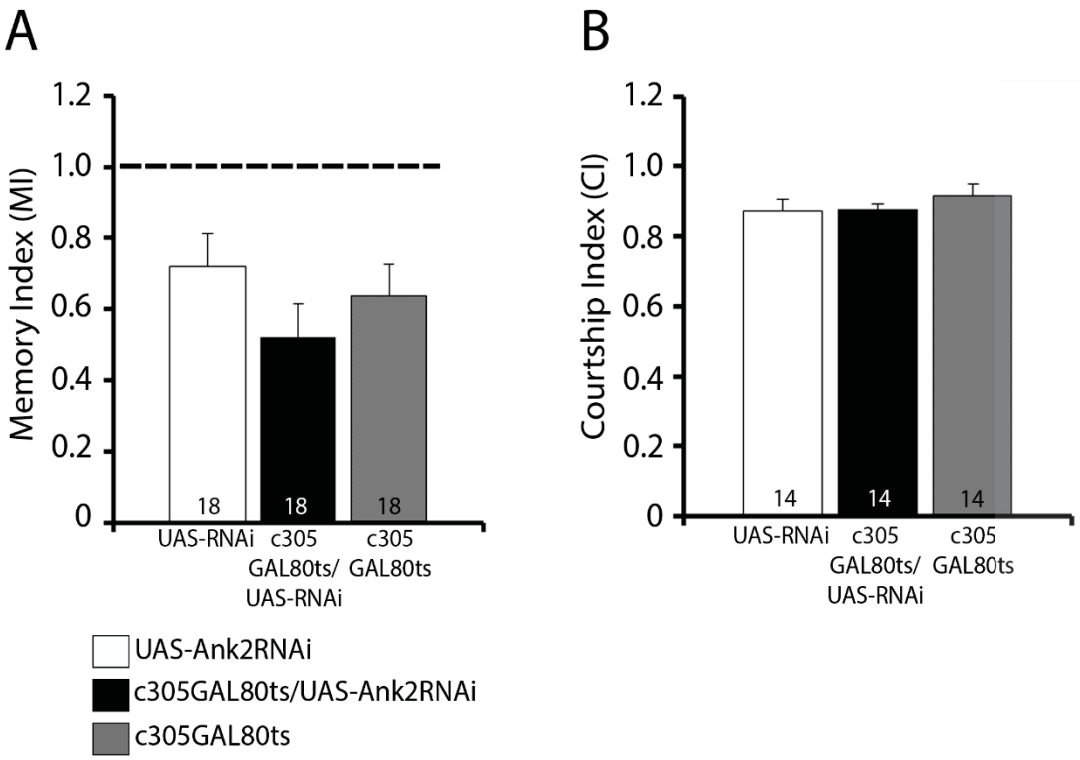

Figure 3.35 Knockdown of *Ank2* does not affect LTM formation in α'/β' neurons. (A) Flies expressing *UAS-Ank2*RNAi in the α'/β' lobes of the mushroom body did not show LTM impairment (ANOVA, P = 0.371). (B) No significant differences were observed among the courtship activity of sham males (ANOVA, P = 0.151) meaning that the courtship activity was

not impaired by knockdown of *Ank2* in those neurons. Numbers within bars indicate the number of animals analysed. Genotype abbreviations: UAS-Ank2RNAi = *UAS-Ank2KD/+*. C305aGAL80^{ts}/UAS-Ank2RNAi = *tub-GAL80^{ts}/c305-GAL4, UAS-Ank2KD.* c305aGAL80^{ts} = *tub-GAL80^{ts}/c305a-GAL4.*

In summary, taken together these data show that in the adult brain, wild-type levels of *Ank2* are required in the mushroom body, specifically in the γ lobes, for normal LTM formation.

3.3.2 Ankyrin1

Knockdown of *Ank1* was found to enhance the *HDAC4*-induced rough eye phenotype, therefore an investigation on its role on brain development and memory formation was conducted in view of the fact that a full characterisation of the role of *Ank1* in the fly nervous system has not been carried out so far. A recent study showed enrichment of Ank1 in a specific region of the Kenyon cells that the authors referred to as axon initial segment (AIS)-like region of the *Drosophila* neurons. Mammalian neurons possess a compartment known as the axon initial segment consisting of specific cytoskeletal and cell adhesion proteins that functions as a diffusion barrier that limits the exchange of membrane proteins between the somato-dendritic and axonal compartments, as well as between the proximal and distal segments of the axon (Wright and Zinn, 2009). Trunova and colleagues, found an AIS-like region in the *Drosophila* brain, in the γ lobes specifically where an enrichment of Ankyrin1 and ion channels was detected as a unique and distinct region within these lobes of the mushroom body (Trunova et al., 2011). These findings suggest Ank1 may play important roles in the nervous system.

3.3.2.1 Ankyrin1 is localised in the mushroom body lobes and calyces

Since an antibody for *Drosophila* Ank1 was not available, to visualise Ank1 subcellular localisation in the adult brain a transgenic line was generated that expressed Ank1 with a C-terminal MYC epitope (section 2.10.5) and an antibody against MYC was used to visualise Ank1MYC.

UAS-Ank1MYC expression was induced in the brain with the *elav-GAL4* pan-neuronal driver and flies were raised at 25°C. Distribution of Ank1MYC could be clearly

distinguished in the lobes of the mushroom body (Figure 3.36B white arrowheads and D) in line with Trunova et al., study (2011) where distribution of Ank1 was observed in the mushroom body, specifically in the γ neurons of 3rd instar larvae. Distribution of Ank1MYC was also detected in the calyces, the dendritic field of the mushroom body (Figure 3.36C white asterisks). A high concentration was observed in the axon bundles (Figure 3.36E asterisks) that project towards the anterior portion of the brain. In addition, MYC staining appeared to concentrate in the cytoplasm of Kenyon cells (Figure 3.36E dotted white circle).

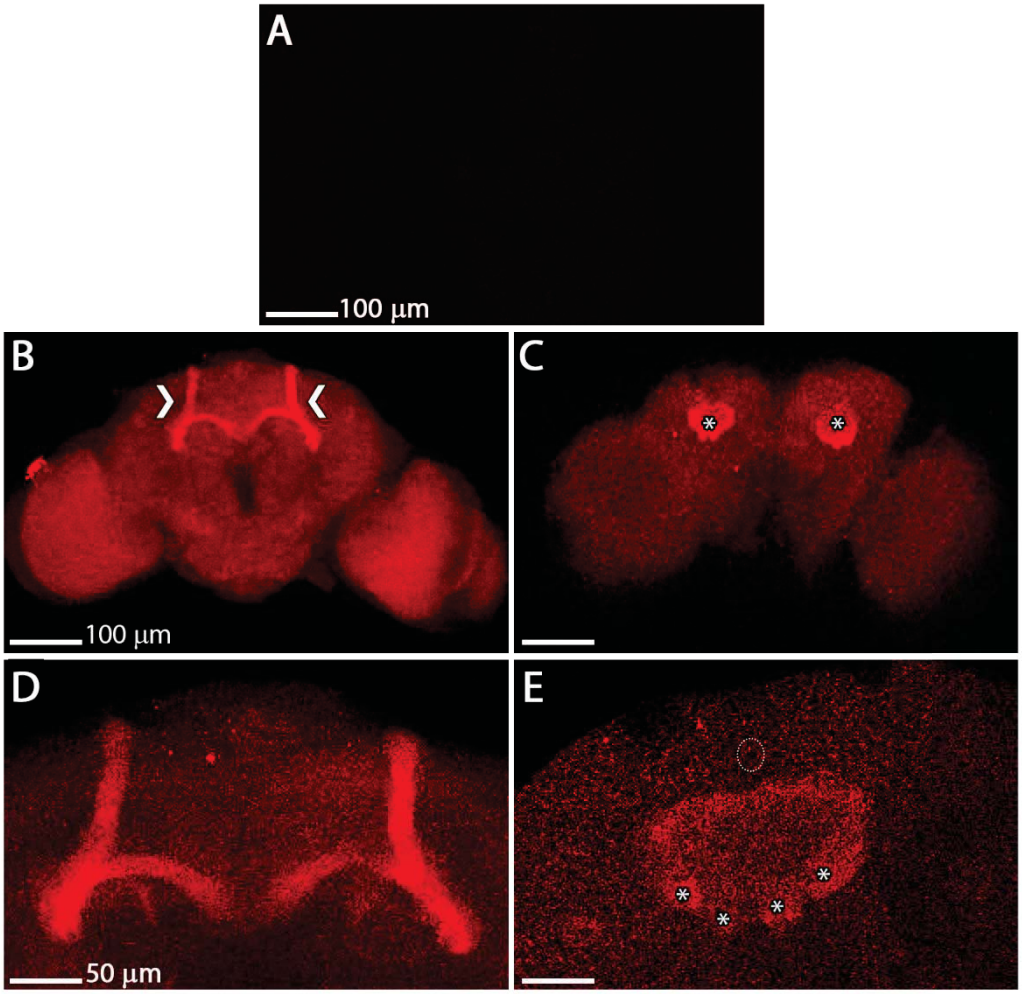

Figure 3.36 Ank1 localises in the mushroom body lobes and in the calyces. Whole-mount brain confocal projections of *elav-GAL4; UAS-Ank1MYC* brains stained with anti-MYC. (A) Wild-type brains were used as negative controls to show absence of MYC staining. (B) Anterior portion of brain showing MYC staining in the lobes of the mushroom body (white arrowheads). (C) Posterior side of the brain displaying MYC staining in the calyces (white asterisks). (D) Magnification of the mushroom body lobes. (E) Magnification of the calyx in the posterior side

of the brain showing Ank1MYC expression pattern with high concentration in the axon bundles (asterisks) that project towards the anterior portion of the brain. MYC staining appears to concentrate in the cytoplasm of Kenyon cells (dotted white circle).

3.3.2.2 Expression of *Ankyrin1* is dispensable for development of the mushroom body lobes

The role of *Ank1* in mushroom body development was examined by inducing knockdown of *Ank1* the fly brain throughout development using the *elav-GAL4* pan-neuronal driver and immunohistochemistry performed with the mushroom body marker FasII. Flies were raised at 25°C in order to test whether at this temperature, the same used for behavioural assays, knockdown of *Ank1* had any impact on development of the mushroom body. Prior to the analysis, knockdown of *Ank1* was verified by qPCR (Figure 7.7 and 7.8, Appendix 7.2) using at least three biological replicates from cDNA preparations derived from heads of flies in which RNAi of *Ank1* was induced through the pan-neuronal *elav-GAL4* driver.

Immunohistochemical analysis revealed brains with normal lobe architecture, suggesting that Ank1 is not involved in development of the mushroom body (Figure 3.37). However, a very mild effect on the morphology of the lobes was observed in brains of flies raised at higher temperature, i.e. higher GAL4 activity (Figure 3.38) indicating that Ank1 does play a role in mushroom body development although the phenotype is much milder than that caused by knockdown of *Ank2* (section 3.3.1.1). Possibly, the *Ank1*RNAi line is not as effective as the *Ank2*RNAi line.

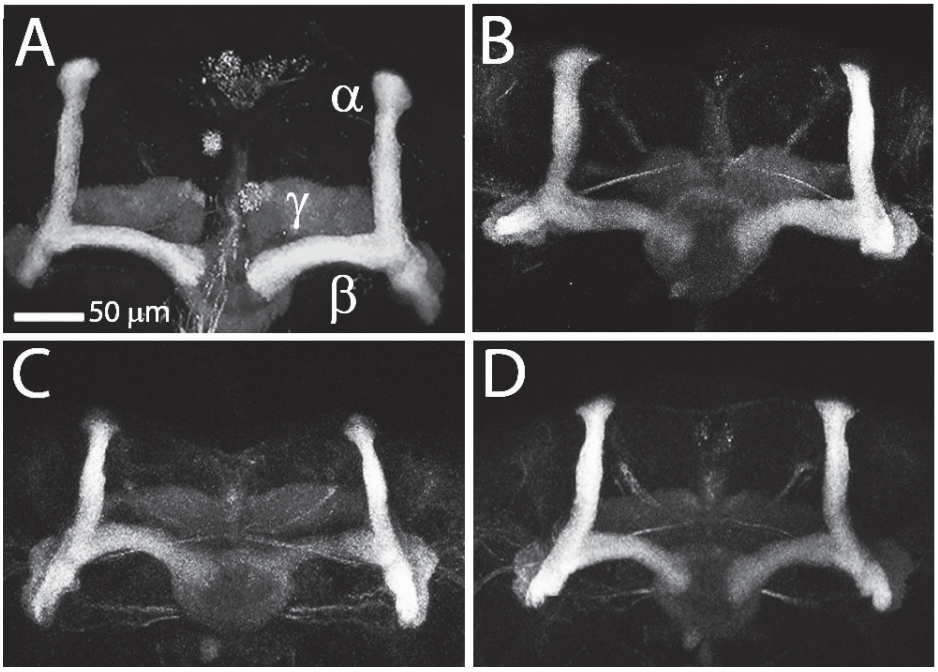

Figure 3.37 *Ank1* knockdown phenotypes at 25°C. Immunohistochemistry with anti-FasII on whole-mount brains reveals no morphological defects of the mushroom body lobes resulting from *elav-GAL4* driven expression of *UAS-Ank1*RNAi at 25°C. Images are projections of confocal z-stacks under 40X in oil objective, zoom range 1-1.6. Flies were grown at the temperature of 25°C to investigate whether knockdown of *Ank1* could affect mushroom body lobe development. Several brains were observed and they all showed normal lobe structures and morphologies.

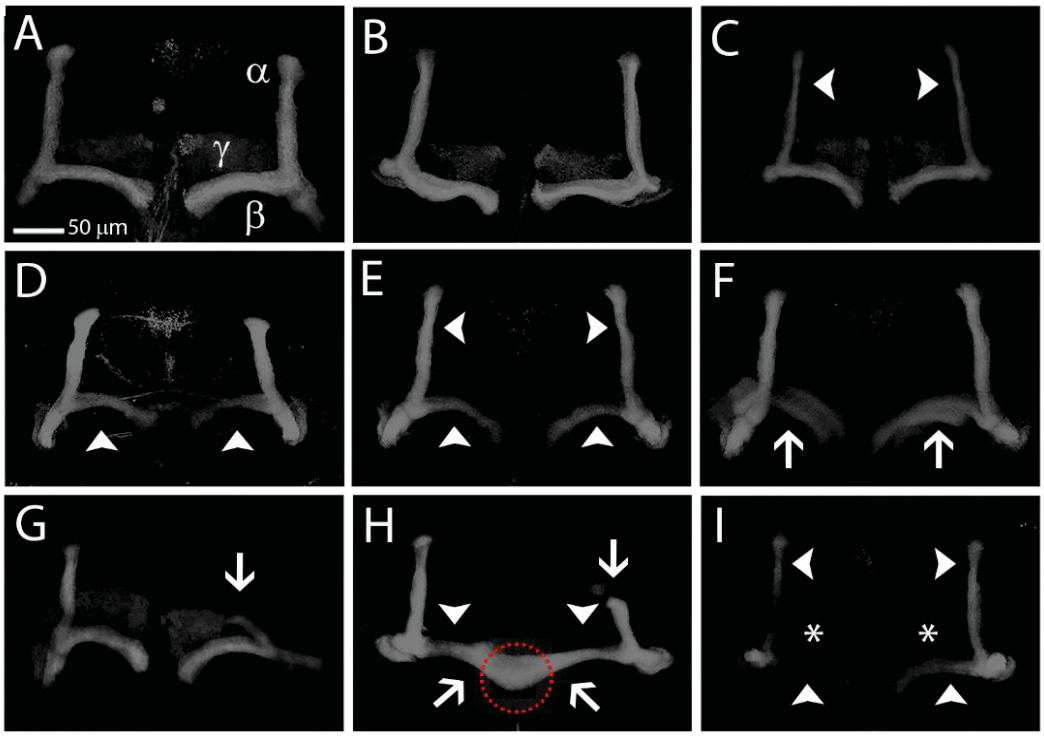

J

Ank1 knockdown phenotypes	**N = 20**
Outgrowth and guidance defects	25%
Lobes fusion	5%
Abormal morphology	50%
Lobe missing	10%

Figure 3.38 *Ank1* knockdown phenotypes at 27°C. Immunohistochemistry with anti-FasII on whole-mount brains reveals mild morphological defects of the mushroom body lobes resulting from *elav-GAL4* driven expression of *UAS-Ank1*RNAi at 27°C. Images are projections of confocal z-stacks under 40X in oil objective, zoom range 1-1.6. The phenotypes observed were the following: thinner lobes (white arrowheads), outgrowth and guidance defects (white arrows), lobes fusion (red dotted circle) and missing lobes indicated by the asterisk. (A) Wild-type brain. (B-I) *Ank1* knockdown brains. (J) Table summarising the mushroom body morphological defects. The percentage was calculated from the total number of brain hemispheres examined (N).

3.3.2.3 Depletion of *Ankyrin1* during development is not required for long-term memory formation

To study the effect of *Ank1* loss on LTM formation, knockdown of *Ank1* was induced in the fly brain throughout development using the *elav-GAL4* pan-neuronal driver and its effect on LTM assessed by the courtship suppression assay. Flies harbouring knockdown of *Ank1* did not show significant impairment of neither LTM formation nor of courtship activity (Figure 3.39) and the memory index was around 0.4, which corresponds to a good memory performance, suggesting an 'improvement' of LTM formation. However, this result was not significant in comparison to the controls (Figure 3.39A, white and gray bars) suggesting that this gene may not be involved in LTM formation.

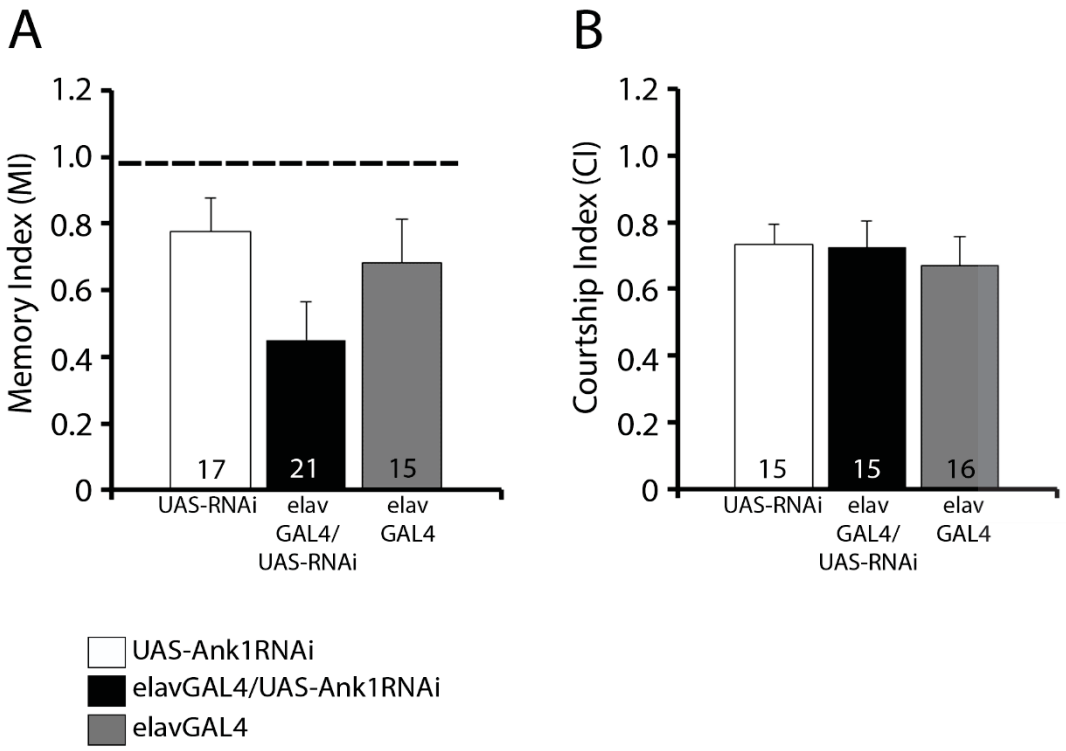

Figure 3.39 Decreased expression of *Ank1* during development does not impair LTM formation. (A) Flies in which *Ank1* was depleted in the entire brain during development (black bar) did not show impairment of LTM (ANOVA, P = 0.075). (B) Graph showing the courtship index, i.e. the time males spent courting during the observation period. No significant difference among sham males of each genotype was detected (ANOVA, P = 0.923) meaning that the courtship activity is not impaired by knockdown of *Ank1*. Numbers within bars indicate the number of animals tested. Genotype abbreviations: UAS-Ank1RNAi = *UAS-Ank1RNAi/+*. elavGAL4/UAS-Ank1RNAi = *elav-GAL4/Y; UAS-Ank1RNAi/+*. elavGAL4 = *elav-GAL4/Y*.

In light of these results, no further characterisation of *Ank1* was carried out and the following sections of this thesis focus on the investigation of the interaction between *HDAC4* and *Ank2*.

3.4 Investigation of the relationship between HDAC4 and Ankyrin2

The aim of this study was to gain a better understanding of the mechanisms through which *HDAC4* regulates memory by identifying genes that interact in its genetic pathway in *Drosophila*. In the previous section, a full characterisation of *Ank2* in the adult brain of *Drosophila* was presented, providing new insights into the role of this gene in brain development and memory formation. These results depicted intriguing similarities in *Ank2* knockdown and *HDAC4* overexpression phenotypes. For instance, overexpression of *HDAC4* was previously shown to impair LTM in *Drosophila* (Fitzsimons et al., 2013) to the same extent as shown in this study for *Ank2* and furthermore in both cases the phenotypes were mediated through manipulation of gene expression in the γ lobes.

Interestingly, mammalian HDAC4 is known to possess an ankyrin repeat-binding domain which is recognised by ankyrin repeat-containing proteins such as RFXANK and ANKRA (Wang et al., 2005; McKinsey et al., 2006; Xu et al., 2012; Nie et al., 2015) and this region is highly conserved between humans and *Drosophila* with an identity of 76.5% (Figure 3.40).

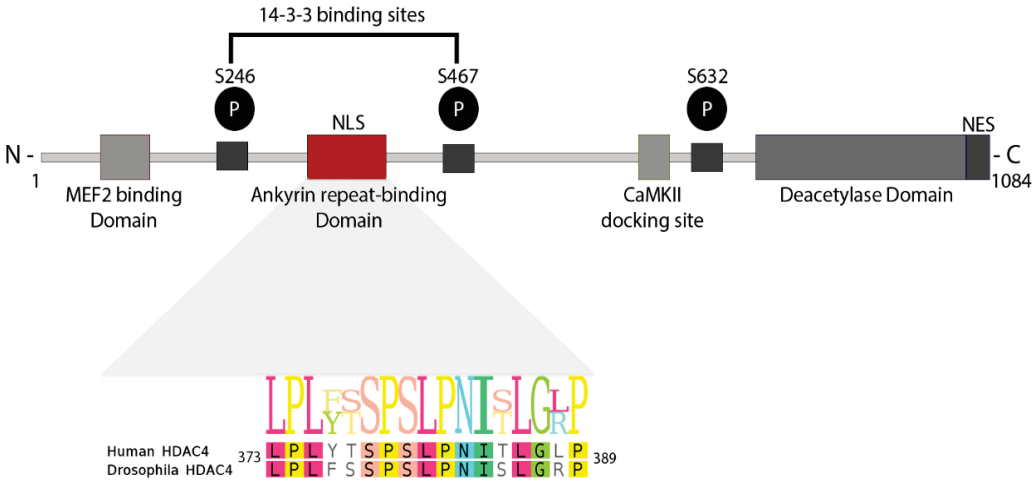

Figure 3.40 HDAC4 harbours an ankyrin-repeat-binding domain. Mammalian HDAC4 contains an ankyrin repeat-binding region highly conserved in *Drosophila* HDAC4 with an

identity of 76.5% which increases to 94.1% when a Blosum 62 substitution matrix (BLSM62) is applied to generate a more accurate alignment. Alignment was performed using Geneious software version 7.1.9.

In addition, both *HDAC4* and *ANK3*, the human homologue of *Drosophila Ank2*, have been implicated in autism. *HDAC4* was recently found to be significantly overexpressed in the brain of autistic subjects (Nardone et al., 2014) and through whole-genome sequencing on patients affected by autism spectrum disorders, three different missense mutations were identified in the *ANK3* gene (Bi et al., 2012) suggesting an association between *ANK3* and autism spectrum disorder susceptibility. This evidence indicate that an interaction between *Ank2* and *HDAC*4 warrants further investigation and to this end, three approaches were undertaken. Initially, immunohistochemistry was performed to determine whether Ank2 and HDAC4 are distributed to the same regions of the fly brain. Subsequently, a GST pull-down assay was conducted to examine whether a physical interaction between HDAC4 and Ank2 occurs at the ankyrin repeat-binding region of HDAC4 protein and finally, behavioural tests were performed to determine whether a genetic interaction occurs between *HDAC4* and *Ank2* during LTM formation.

3.4.1 HDAC4 co-localises with Ankyrin2 in mushroom body lobes

In order to determine whether Ank2 and HDAC4 localise to the same brain regions, immunohistochemistry was performed on whole mount brains from flies in which overexpression of *HDAC4* was induced during adulthood with *elav-GAL4; tub-GAL80^{ts}* to avoid developmental effects. It has to be highlighted that since an antibody specific for *Drosophila* HDAC4 was not available, a previously characterised FLAG tagged HDAC4 transgene was used to visualise HDAC4 subcellular localisation via FLAG antibody (Fitzsimons et al., 2013).

This analysis revealed a substantial overlapping pattern of distribution between Ank2 and HDAC4, both concentrating in the α/β and γ lobes of the mushroom body (Figure 3.41A). A matching pattern of expression was also observed in the posterior side of the brain in the four axonal bundles that project frontally and that give rise to the lobes (Figure 3.41B, yellow asterisks). Ank2 was mostly distributed to the axons that surround the calyx (Figure 3.41B, white arrows), while HDAC4 distribution was detected in the cell bodies (Figure 3.41B white arrowheads).

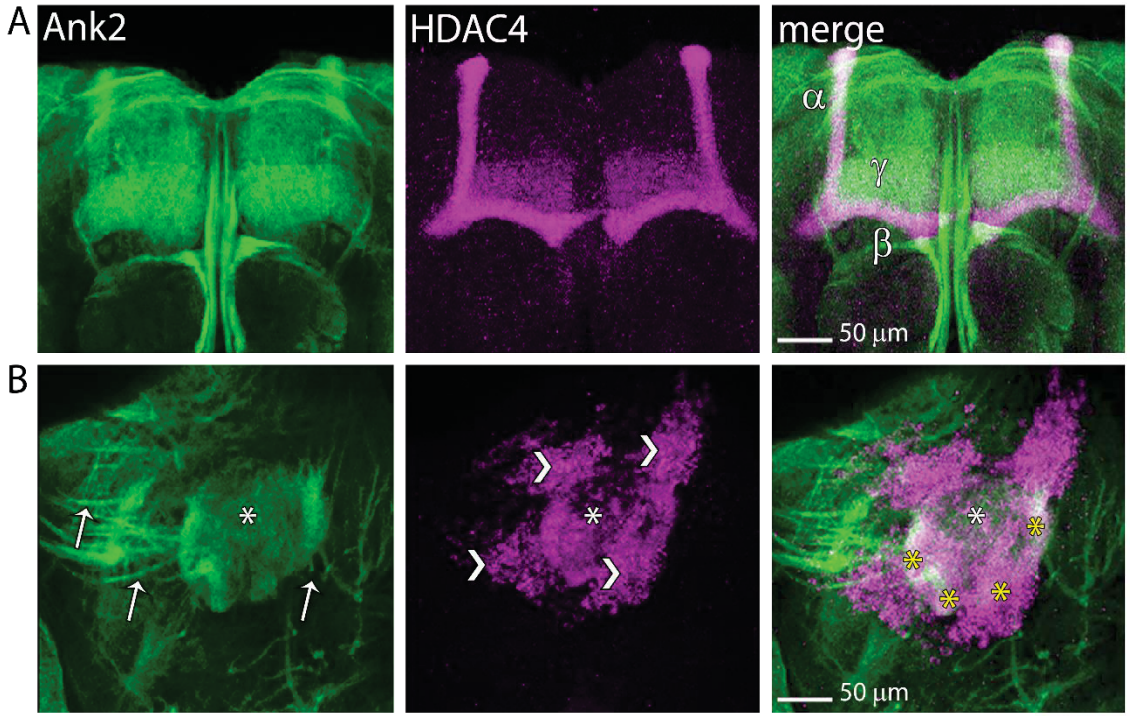

Figure 3.41 Ank2 and HDAC4 are located in the same brain regions. (A) Frontal confocal projections through the brain showing expression pattern profile of Ank2 (green) and HDAC4 (magenta). Zoom 3.6, objective 20X. (B) Posterior confocal projections through the brain showing expression of Ank2 (green) and HDAC4 (magenta) in the calyces (white asterisk) and in the axon bundles (yellow asterisks). Zoom 6.1, objective 20X.

To further characterise HDAC4 localisation in the brain and its relation to Ank2, a co-labelling was performed with an anti-Nrg antibody. As the association between Nrg and Ank2 is well characterised and conserved between flies and vertebrates (Goosens et al., 2011) with both shown to localise in the same brain regions in adult brains (section 3.3.1.1), immunohistochemistry was performed to determine whether also HDAC4 co-localises with Nrg in the fly brain.

The *Drosophila* genome presents one gene encoding for a single L1-CAM element, Nrg, sharing homology to all four vertebrate immunoglobulin protein family members L1, CHL1, NrCAM (neuronal CAM), and Neurofascin. Nrg is an integral membrane glycoprotein, member of the Ig family, expressed on a variety of cell types in the *Drosophila* embryo including glial and neuronal cell bodies (Bieber et al., 1989), implicated in different aspects of neuronal differentiation and development, such as neurite outgrowth, axon guidance and myelination, synaptogenesis, and neuronal migration (Davis & Bennett, 1994; Hortsch et al., 1998; Needham et al., 2001;

Godenschwege et al., 2006; Martin et al., 2008; Goosens et al., 2011; Kudumala et al., 2013; Enneking et al., 2013; Siegenthaler et al., 2015).

Of interest is the central ankyrin interacting motif, FIGQY, highly conserved among all vertebrate L1 family proteins and *Drosophila* Nrg (Hortsch et al., 2009) and required for binding of Ank2 (which hypothetically may also interact with the ankyrin repeat binding region of HDAC4). It has been previously shown that phosphorylation of the tyrosine residue within the FIGQY domain negatively regulates the binding of ankyrins to Nrg (Garver et al., 1997; Tuvia et al., 1997; Zhang et al., 1998) leading to pathological phenotypes in mammals as well as severe synaptic defects in *Drosophila* (Goosens et al., 2011; Kudumala et al., 2013).

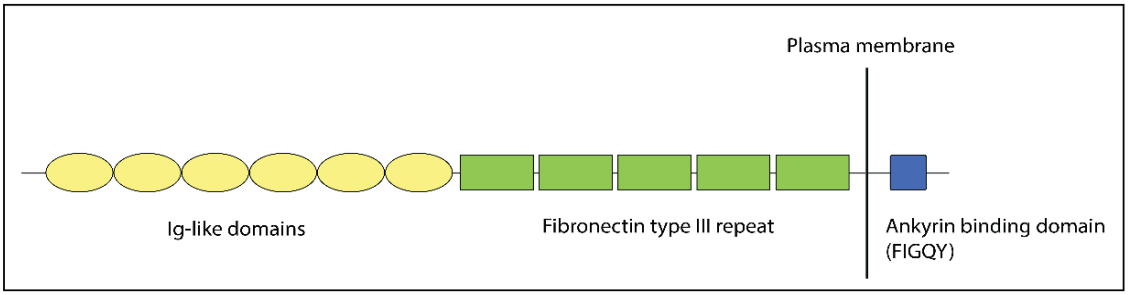

Figure 3.42 Schematic representation of Nrg structural domains. IgCAMs usually consist of 6 Ig-domains, 3–5 fibronectin type III domains, a transmembrane domain, and an intracellular tail. The extracellular domain of L1 family proteins mediates cell–cell adhesion via homophilic and heterophilic interactions (Hortsch et al., 2000; Enneking et al., 2013). The intracellular tail contains distinct protein–protein interaction domains potentially controlling the localization and function of L1 proteins (Dubreuil et al., 1996; Hortsch et al., 2009).

Brains overexpressing *HDAC4-FLAG*, were labelled with anti-FLAG and anti-Nrg and intense co-localisation of HDAC4 and Nrg was observed, largely in the lobes of the mushroom body (Figure 3.43). This was suggestive of a possible interactive pathway among HDAC4, Ank2 and Nrg.

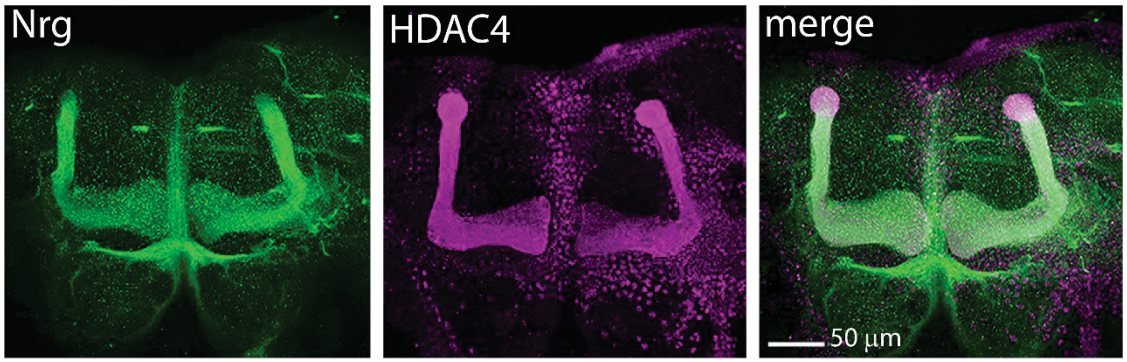

Figure 3.43 HDAC4 strongly co-localises with Nrg in the lobes of the mushroom body. Frontal confocal projections through the brain showing expression pattern profile of Nrg (green) and HDAC4 (magenta). Zoom 1.7, objective 40X in oil.

3.4.2 *HDAC4* is required for normal development of the mushroom body lobes

To determine whether *HDAC4* affects brain development, overexpression of *HDAC4* was induced with *elav-GAL4* pan-neuronal driver. A FasII antibody was used to label the lobes of the mushroom body (section 3.3.1.2) and immunohistochemistry revealed profound morphological deficits with acute outgrowth defects (Figure 3.44, white arrows), thinner lobes (Figure 3.44, white arrowhead) and loss of at least one lobe in all brains analysed (Figure 3.44, asterisks). Remarkably the immunoreactivity of FasII increased in the central complex upon overexpression of *HDAC4* (Figure 3.44, red arrows). The central complex is a group of unpaired and interconnected neuropils across the midline of the *Drosophila* brain (Figure 3.44, midline indicated with a red uppercase M). The central complex is both a sensory integration and a motor control centre involved in locomotor control, visual memory and spatial orientation (reviewed by Pfeiffer and Homberg, 2014). This region of the fly brain has been proposed to share homology with vertebrate cerebellum, for motor coordination and balance, and with basal ganglia with which it shares similar programs of gene expression and regulation and a similar neurotransmitter system with a rich supply of GABAergic and dopaminergic neurons (Strausfeld and Hirth, 2013; Pfeiffer and Homberg, 2014).

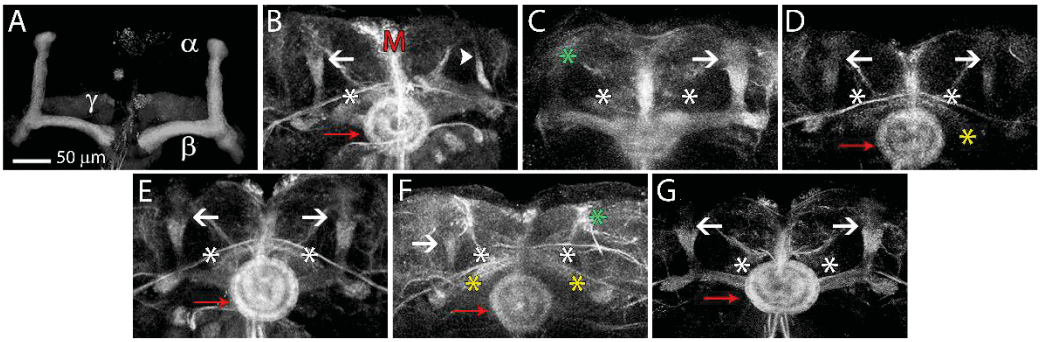

H

HDAC4 overexpression phenotypes	N = 12
Outgrowth and guidance defects	75%
Abormal morphology	8%
Lobe missing	91%
Prominent CC (N=6 brains)	83%

Figure 3.44 *HDAC4* overexpression phenotypes. Immunohistochemistry with anti-FasII on whole-mount brains reveals severe morphological defects of the mushroom body lobes resulting from *elav-GAL4* driven expression of *UAS-HDAC4OE* at 25°C. (A) Wild-type brain. (B-G) Micrographs showing mushroom body phenotypic defects upon pan-neuronal overexpression of *HDAC4*. White arrows indicate outgrowth and guidance defects, white arrowhead indicates lobes with a thinner shape. Asterisks indicate lobe loss (white = γ lobes, green = β lobes, yellow = α lobes). The central complex is indicated with a red arrow and the midline with a red M. Images are projections of confocal z-stacks, zoom range between 1-1.6, objective 40X in oil. Scale bar = 50 µm. (H). Table summarising the mushroom body lobe phenotypes. The percentage was calculated from the total number of brain hemispheres examined (N), except for brains showing a prominent central complex for which the percentage was calculated on the total number of brains analysed since the central complex is not a bilateral structure as the mushroom body. Abbreviations: CC = central complex

Similarly, as shown in section 3.3.1.2, knockdown of *Ank2* in developing brain resulted in impaired mushroom body lobe structures and comparable effects could be observed with the most severe phenotypes of *Ank2*RNAi resembling those of *HDAC4OE* (Figure 3.45).

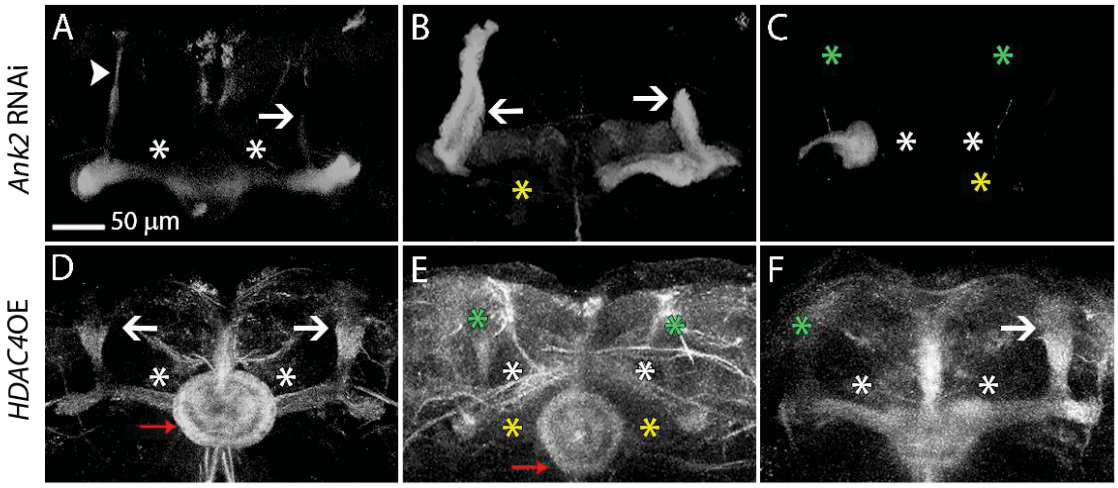

Figure 3.45 Knockdown of *Ank2* and overexpression of *HDAC4* have similar detrimental effects on mushroom body lobe development. Immunohistochemistry with anti-FasII on whole-mount brains reveals similar severe morphological defects of the mushroom body lobes resulting from *elav-GAL4* driven expression of *UAS-Ank2*RNAi (A-B-C) and of *UAS-HDAC4OE* (D-E-F) at 25°C. Images are projections of confocal z-stacks. Scale bar = 50 µm. White arrows = outgrowth and guidance defect, white arrowheads = thinner lobes; asterisks = loss of lobes (green = β; yellow = α; white = γ); red arrow = central complex.

Since Ank2 and HDAC4 co-localise in the same brain regions and they both regulate development of the lobes, an epistasis study was performed with a line harbouring both knockdown of *Ank2* and overexpression of *HDAC4* (*UAS-Ank2*RNAi/*UAS-HDAC4OE*), in order to investigate whether the combination of the two genes could enhance the phenotypic defects caused by the genes individually. An illustration of the genetic scheme performed to generate flies for this experimental procedure is shown in Figure 3.46.

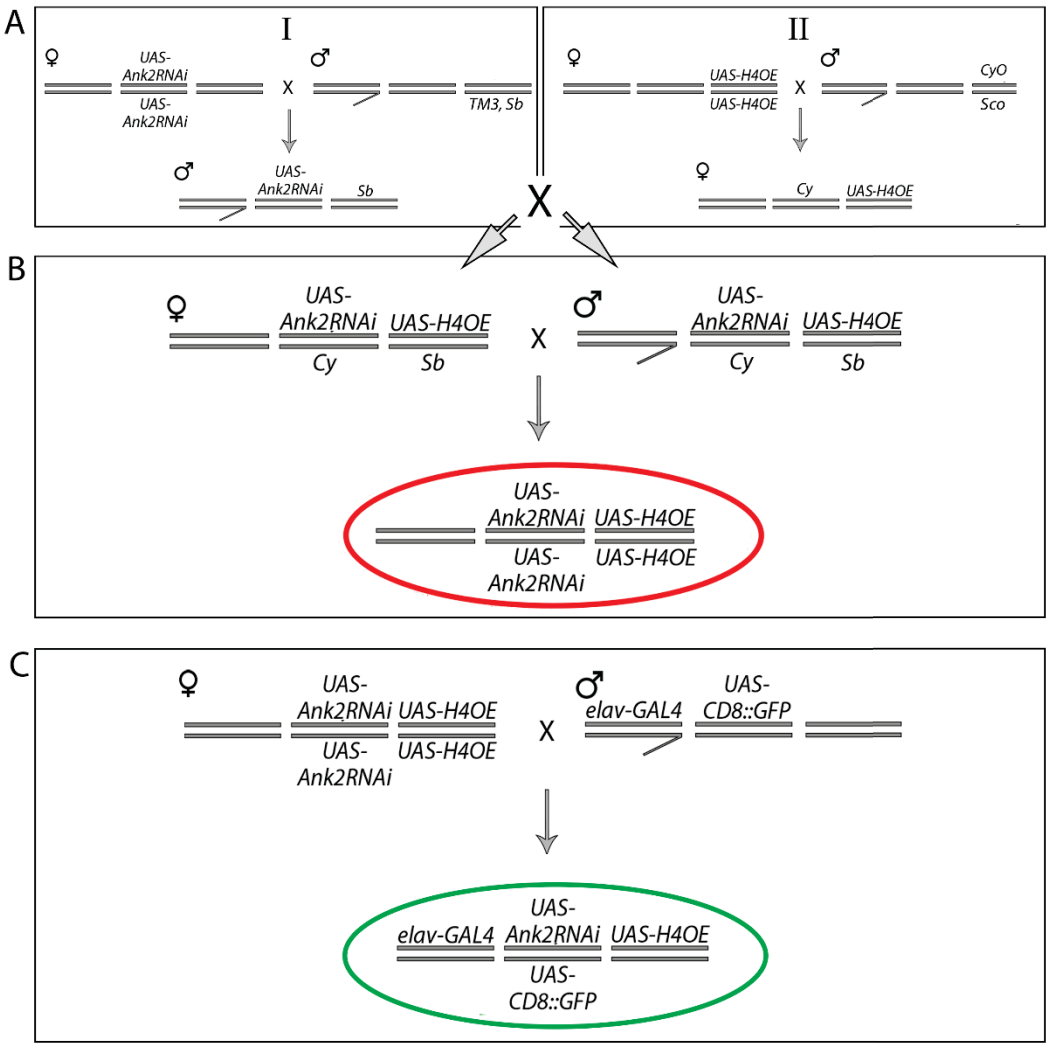

Figure 3.46 Illustration of the genetic mating scheme employed to generate the *UAS-Ank2*RNAi; *UAS-HDAC4OE* fly line for epistasis studies. (A) In order to recombine *Ank2* and *HDAC4* in the same fly line, stocks carrying a balancer chromosome were used. Balancer chromosomes prevent recombination (as they are the products of multiple, nested chromosomal inversions that prevent synapsis between homologous chromosomes) and contain a dominant phenotypic marker that allows traceability of the chromosomes through several crosses to ensure the correct progeny are selected. (A-I) Homozygous *UAS-Ank2*RNAi flies were crossed to *Sb*/TM3 flies, a third chromosome balancer line with stubble bristles (Sb) marker and Sb progeny were selected. (A-II) homozygous *UAS-HDAC4OE* flies were crossed to CyO/Sco with Curly wings (Cy) marker. Cy progeny were selected. The two selected stocks were then crossed in order to generate (B) heterozygous progeny harbouring both *Ank2*RNAi and *HDAC4OE*, whose presence was indicated by the stubble bristles and curly wings phenotype. Flies which presented both dominant markers simultaneously were inter-crossed to generate recombinant *UAS-Ank2*RNAi; *UAS-HDAC4OE*. Therefore, absence of both markers would mean that *UAS-Ank2*RNAi; *UAS-HDAC4OE* doubly recombinant line was generated (red circle). (C). This line

was finally crossed to the *elav-Gal4; UAS-CD8::GFP* line in order to promote expression of *UAS-Ank2*RNAi; *UAS-HDAC4OE* in all neurons of the brain and to be able to perform immunohistochemistry with anti-GFP and anti-FasII. Abbreviations: *H4O*E = HDACOE; *TM3* = 3rd multiply-inverted 3; *Sb* = stubble; *CyO* = Curly of Oister; *Sco* = scutoid; *Cy* = curly.

In principle, when the individual expression of a gene results in mild anatomical alterations of the lobes, if two genes interact then the combination of the two would produce an enhancement of the irregular lobe phenotypes.

Figure 3.47D shows brains in which simultaneous knockdown of *Ank2* and overexpression of *HDAC4* was induced through the pan-neuronal driver *elav-GAL4*. This was co-expressed with CD8::GFP, a plasma membrane-targeted GFP which allows for visualisation of GFP in neuronal processes and in brain structures (Fitzsimons et al., 2013), and is commonly used for anatomical studies on *Drosophila* brains.

In order to evaluate for synergistic effects, brains were raised at 18°C to limit the phenotypic effects caused by *HDAC4* and *Ank2* when expressed individually. At 18°C GAL4 is less active and thus less severe phenotypes are expected. Immunohistochemistry with anti-FasII and anti-GFP was conducted. *UAS-Ank2*RNAi*; UAS-HDAC4OE* brains did not show immunoreactivity in the region of the mushroom body lobes, suggesting that a complete loss of axons occurred. In particular, the FasII signal was entirely absent in these brains, while it was still visible in brains expressing *UAS-HDAC4OE* and *UAS-Ank2*RNAi individually (Figure 3.47B and C respectively). However, drawing a clear interpretation of these results was difficult even at 18°C as brains overexpressing *HDAC4* showed a very weak, almost non-detectable GFP signal and minimal FasII inensity (Figure 3.47B), indicating severe loss of mushroom body structures therefore rendering it hard to distinguish between synergistic and additive effects. “Synergy occurs when the contribution of two mutations to the phenotype of a double mutant exceeds the expectations from the additive effects of the individual mutations” (Pérez-Pérez et al., 2009).

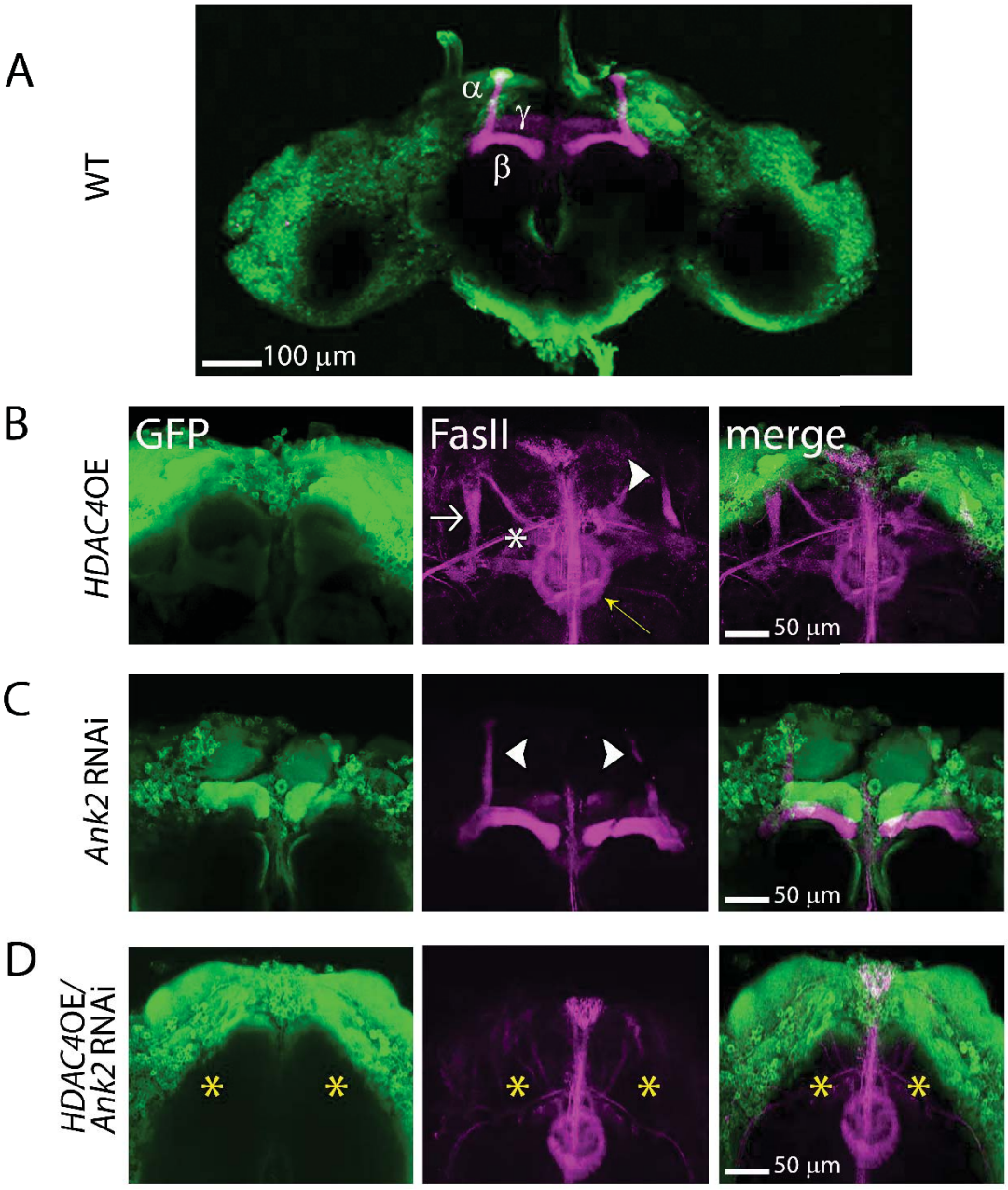

Figure 3.47 Combination of *Ank2* knockdown and *HDAC4* overexpression in the developing brain causes additive effects to the mushroom body lobe phenotype. Confocal projections through the brain showing the mushroom body lobe architecture with anti-GFP and anti-FasII staining. (A) Whole wild-type brain under 10X objective. α, β and γ lobes are indicated. (B) Confocal projections through a brain expressing pan-neuronal *UAS-HDAC4*OE. The white arrow indicates outgrowth defects, the white arrowhead indicates a thin lobe, the white asterisk indicates lack of γ lobe and the yellow arrow indicates the central complex. (C) Confocal projections through a brain expressing *UAS-Ank2*RNAi. Thinner lobes are indicated by a white arrowhead. (D) Confocal projections through a brain with simultaneous knockdown of *Ank2* and overexpression of *HDAC4*. Yellow asterisks indicate loss of all lobes of the mushroom body.

Brains B-D were mounted under a 40X objective in oil. Genotype abbreviations: elavGAL4-CD8::GFP;WT = *elav-GAL4/Y; UAS-CD8::GFP/+*. elavGAL4-CD8::GFP; HDAC4OE = *elav-GAL4/Y; UAS-CD8::GFP/+; UAS-HDAC4OE/+*. elavGAL4-CD8::GFP; ank2KD = *elav-GAL4/Y; UAS-CD8::GFP/UAS-Ank2RNAi*. elavGAL4-CD8::GFP;HDAC4OE/ank2KD = *elav-GAL4/Y; UAS-CD8::GFP/UAS-Ank2RNAi, UAS-HDAC4OE.*

3.4.3 Investigation of a physical interaction between HDAC4 and Ankyrin2

HDAC4 and Ank2 share many similar characteristics, such as co-localisation in the same brain regions, both are required for proper mushroom body lobe development and both, when depleted individually, significantly impair LTM during adulthood and this effect is restricted to the γ neurons specifically (for HDAC4 study see Fitzsimons et al., 2013). Furthermore, HDAC4 harbours an ankyrin repeat-binding domain which mediates direct interaction with ankyrin-repeat containing proteins ANKRA and RFXANK in mammalian cell culture studies (Wang et al., 2005; McKinsey et al., 2006; Xu et al., 2012; Nie et al., 2015). From these observations, it was hypothesised that a physical interaction between Ank2 and HDAC4 may occur in *Drosophila*. To this end, a GST pull-down assay was performed where a fusion construct between the ankyrin repeat-binding region of HDAC4 and a glutathione S-transferase (GST) epitope was generated then expressed (section 2.10.6 and 2.15). Since the prey Ank2 is too long (400 kDa) to clone and the Ank2 antibody was shown not to be suitable for western blotting, a GFP fusion Ank2 line created by H. Matsubayashi and M. T. Yamamoto (Kyoto Drosophila Centre) was employed. This construct harbours an artificial GFP exon with minimum splicing signals and its own translational start site (Figure 3.48A white curved arrow). Insertion into an intron results in an in frame fusion of the GFP between the exons of the target gene.

Prior to the GST pull-down, PCR analysis of the Ank2-EGFP line was successfully conducted to confirm the presence of the EGFP insert into the *Ank2* gene (Figure 3.48C).

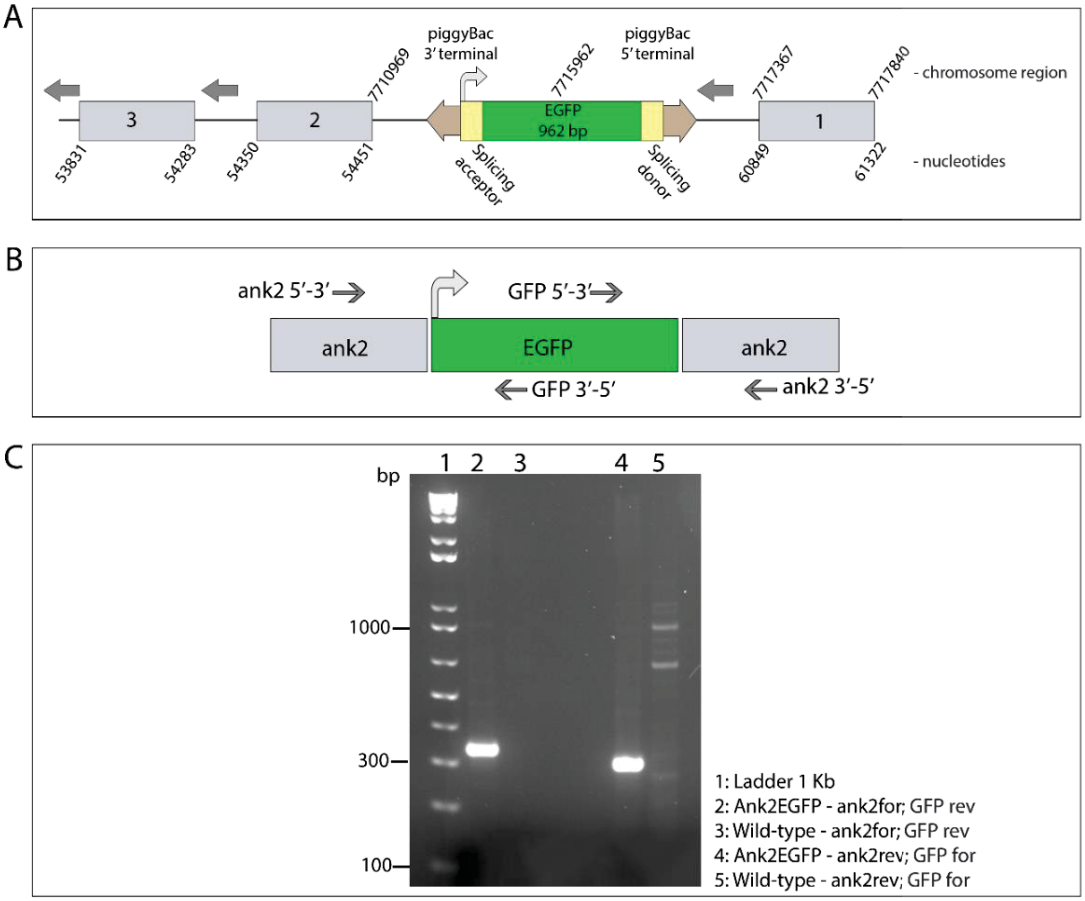

Figure 3.48 PCR Confirmation of EGFP insert into the Ank2-EGFP line of *Drosophila*. (A) Schematic representation of the *Ank2* gene. Three exons (1, 2, 3) are shown and the EGFP insert in position 7715962 of Chromosome 3L is represented. A piggyTrap transposon contains an artificial GFP exon with minimum splicing signals and contains its own translational start (white curved arrow). Dark gray arrows represents the direction of the *Ank2* gene with exons numbered 1, 2, 3. (B) Primers set was designed in order to cover the EGFP tag and the *Ank2* flanking regions in the forward and reverse direction. (C) A PCR was performed using genomic DNA from the Ank2-EGFP strain. No bands were expected in the wild-type control whereas bands of approximately 333 bp and of 294 bp were expected for the GFP reverse primer and GFP forward primer orientation respectively in the Ank2-EGFP samples (lanes 2 and 4).

Cytoplasmic lysates produced from bodies of transgenic flies harbouring the *Ank2*-EGFP gene were analysed by western blotting to determine the presence of Ank2-EGFP in these lysates. The blot revealed two bands at 75 kDa (Figure 3.49). According to Flybase release R6.11, the GFP insert is located within the intron of the smallest isoform of Ank2, isoform E, which measures around 90 kDa. The bands detected were clear, not

visible in the control lane, thus it is likely that the antibody binds to smaller splice variants of the Ank2 protein, for which a very complex composition of splicing variants has been shown previously (Hortsch et al., 2002, section 1.6). It is also possible that the bands may derive from posttranslational products.

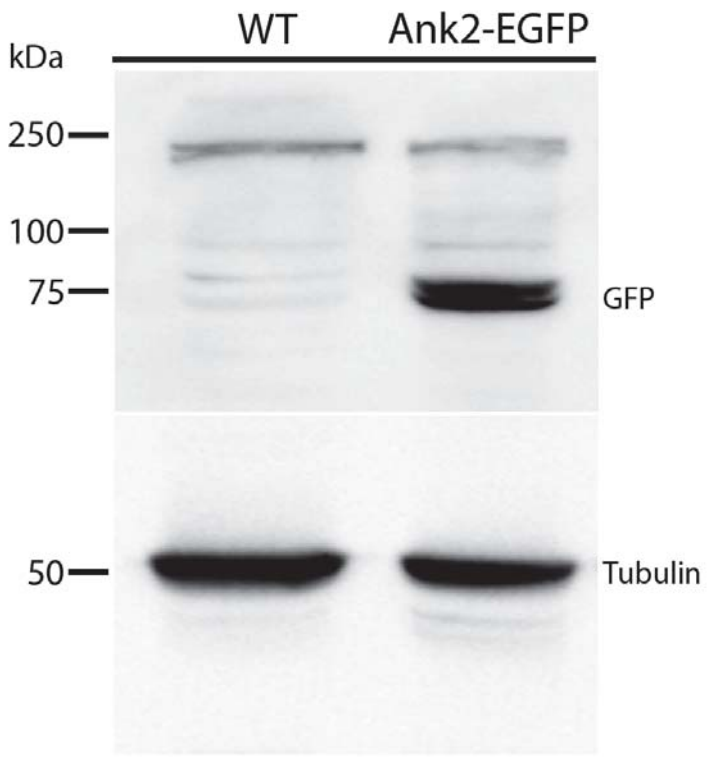

Figure 3.49 Western blotting showing Ank2-EGFP. Whole bodies from theAnk2-EGFP strain were subjected to SDS-PAGE and western blotting in order to visualise Ank2 with a GFP antibody. Two bands of approximately 75 kDa were detected. Anti-GFP at 1:20,000 was used. A strip and re-blot procedure was performed to detect tubulin which was used as the loading control, anti-tubulin 1:500. Detection of the GFP blot was conducted using ECL select whereas detection of tubulin was conducted using ECL Plus.

The pull-down reaction was performed by binding purified HDAC4-GST protein to the glutathione-sephorose-agarose beads, then adding Ank2-EGFP cytoplasmic lysates followed by detection of Ank2-EGFP by western blotting using the anti-GFP antibody. Negative controls were used with the aim to monitor non-specific interactions with the GST tag or glutathione-sephorose-agarose beads. The expected band of 75 kDa was detected in the Ank2-EGFP input lane. No bands of that size were observed in the five control lanes, whereas a band of 75 kDa was detected when Ank2-EGFP and HDAC4-

GST were both present (Figure 3.50A). A preliminary conclusion was drawn that HDAC4 and Ank2 interact through the ankyrin repeat-binding region of HDAC4. However, this pull-down needs to be repeated to confirm this interaction. In addition, it is not possible to conclude that the interaction is direct since a cytoplasmic cell lysate was used rather than purified Ank2 protein, so it is possible that an intermediate product may be involved in mediating such an interaction. The use of a purified Ank2 would be of value to confirm a direct physical interaction.

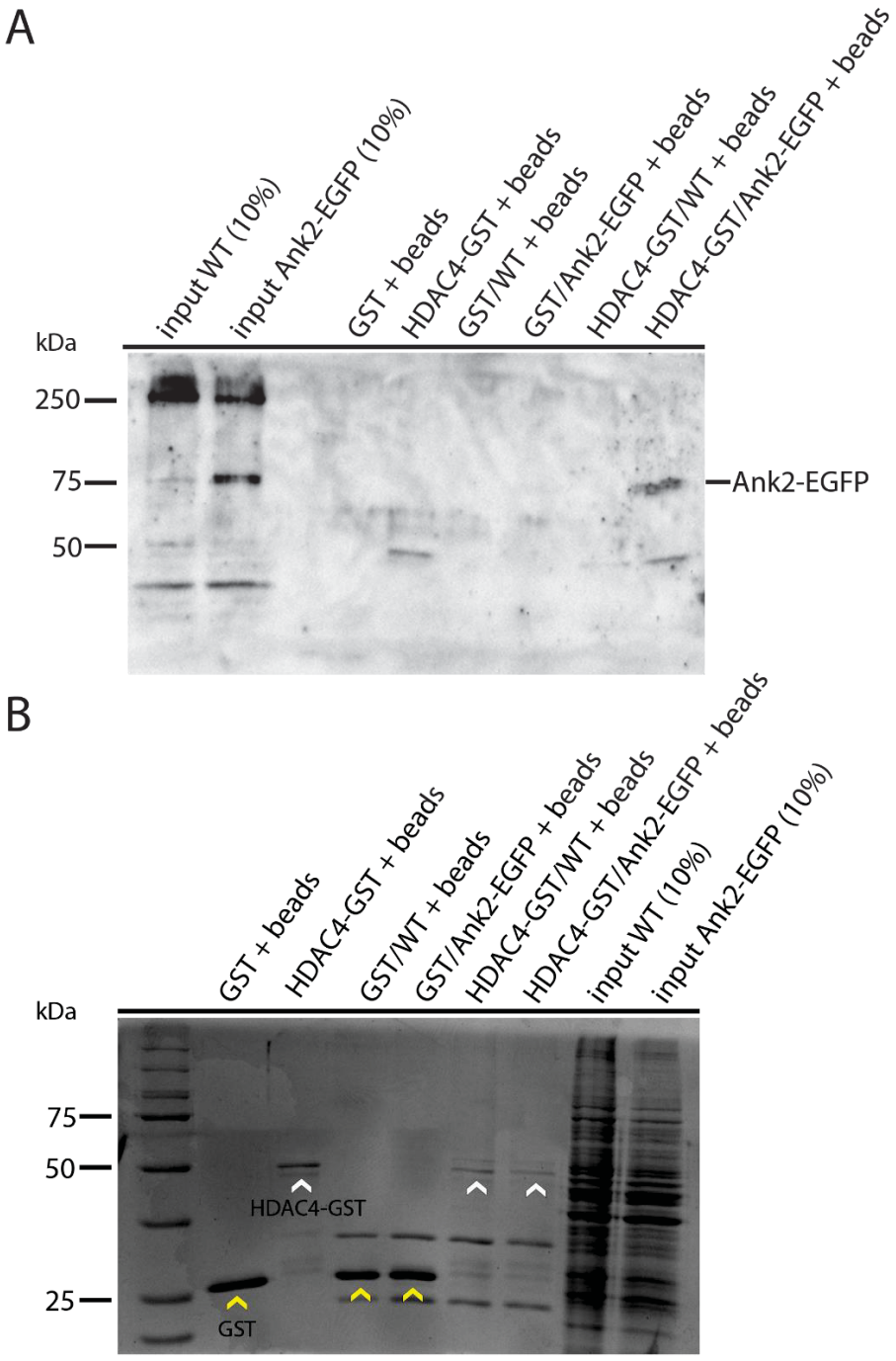

Figure 3.50 GST pull-down assay to investigate potential physical interaction between HDAC4 and Ank2. (A) A GST pull-down assay was performed using cytoplasmic extracts of *Drosophila* bodies derived from the Ank2-EGFP strain. Wild-type controls (WT) and Ank2-EGFP extracts (input 10%) were mixed with both glutathione beads alone (GST/WT and GST/Ank2-EGFP) and with glutathione beads coated with HDAC4 ankyrin repeats-binding domain (HDAC4-GST/WT and HDAC4-GST/Ank2-EGFP). GST and HDAC4-GST were also tested without lysates as negative controls to verify binding to GST or glutathione-sephorose-4B beads and incubated with NEB buffer (GST and HDAC4-GST). Samples were recovered by

centrifugation and analysed by SDS-PAGE and western blotting using an anti-GFP antibody (1:5,000) to detect Ank2-EGFP. (B) Coomassie blue staining experiment was performed at the same time as SDS-PAGE and western blotting procedures, on the same samples, to verify the presence of the GST epitope alone at 26 kDa (yellow arrowheads) and the fusion construct HDAC4-GST at 50 kDa (white arrowheads).

3.4.4 Examining an interaction between *HDAC4* and *Ankyrin2* in long-term memory formation in *Drosophila*: preliminary data

In parallel to the protein binding analysis, an epistasis study was undertaken to determine whether a genetic interaction between *HDAC4* and *Ank2* occurs during LTM formation. To this end, a fly line simultaneously expressing *UAS-Ank2*RNAi and *UAS-HDAC4OE* was generated (section 3.4.2, Figure 3.46) and evaluated in the courtship suppression assay. Such an approach, was successfully adopted by Dr Fitzsimons in a previous study that showed impairment of LTM formation in flies co-expressing *UAS-Ubc9*RNAi and *UAS-HDAC4OE* driven in the mushroom body by the *OK107-GAL4; tub-GAL80ts* promoter, suggesting these two genes interact in the mushroom body during LTM formation process (Schwartz et al., 2016). Flies co-expressing *UAS-Ank2*RNAi and *UAS-HDAC4OE* were crossed to *MB247-GAL4; tub-GAL80ts* driver lines, to both enable induction of expression during adulthood and to restrict their expression to the α/β and γ lobes of the mushroom body as the *MB247-GAL4* driver specifically labels those brain regions (Aso et al., 2009). Since the *MB247-GAL4* driven expression of either *UAS-Ank2*RNAi or *UAS-HDAC4OE* was previously shown to cause LTM defects at 30°C (section 3.3.1.3.2.2 for Ank2 and Fitzsimons et al., 2013 for *HDAC4OE*), for this experimental procedure flies were raised at 18°C and transferred to 24°C after eclosion, to induce an intermediate expression level of the TARGET system. Since the TARGET system is temperature sensitive it was contemplated that at 24°C, the expression of *UAS-Ank2*RNAi and *UAS-HDAC4OE* would decrease by approximately half and that this may provide a context in which expression was insufficient to impair LTM, which would allow assessment of a genetic interaction between the two genes (Schwartz et al., 2016). This was previously shown by Dr Fitzsimons (Schwartz et al., 2016) who used a luciferase assay to determine the optimal temperature at which *OK107-GAL4* would drive intermediate expression of *Ubc9*RNAi and *HDAC4OE* (Schwartz et al., 2016). This work

demonstrated that 24°C was the optimal temperature and was adopted to conduct the preliminary experiments herein presented. However, it has to be noted that since *OK107-GAL4* and *MB247-GAL4* are different drivers, they may possess a different strength in promoting gene expression, thus a luciferase assay to verify the optimal temperature at which *MB247-GAL4* mediates half expression of both, *UAS-Ank2*RNAi and *UAS-HDAC4OE,* should be performed.

In the graphs below (Figure 3.51A) it can be observed that at 24°C individual expression of *UAS-Ank2*RNAi resulted in a good memory performance with a memory index of approximately 0.66 (Figure 3.51, dark gray bar) while flies overexpressing *HDAC4* resulted in a low memory performance with a memory index of 0.85 (Figure 3.51, blue bar). This suggests that although expression was only half-induced the levels of *HDAC4OE* were still sufficient to induce impairment LTM. However, the *UAS-Ank2*RNAi*; UAS-HDAC4OE* combination genotype (Figure 3.51, black bar) resulted in a robust impairment of LTM formation (memory index = 1.02, ANOVA, post-hoc Tukey's HSD, $P < 0.05$), which is significant in comparison to flies harbouring only the *Ank2* knockdown individually (Figure 3.51, dark gray bar, $P < 0.05$). Controls were used to test the driver alone (Figure 3.51, light gray bar) and the *UAS-Ank2*RNAi*; UAS-HDAC4OE* line in absence of the *MB247-GAL4; tub-GAL8ts* driver, i.e. not induced (Figure 3.51, white bar).

To optimise such an assay, flies can be raised at lower temperature e.g. 22°C, to try decreasing the expression levels of *HDAC4OE* without further decreasing the knockdown levels of *Ank2*. Alternatively, a different driver can be tested, such as the *OK107-GAL4* driver (Schwartz et al., 2016).

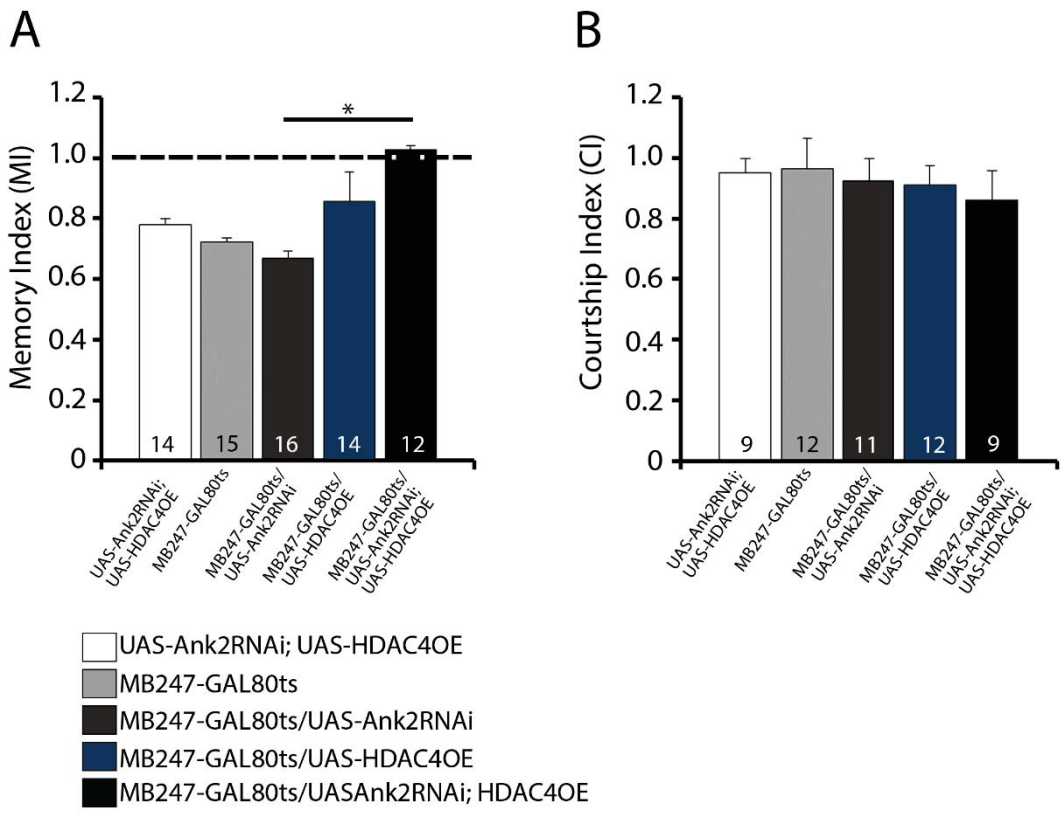

Figure 3.51 Putative role of *HDAC4* and *Ank2* in the regulation of 24 hours courtship memory. (A) Combination of *HDAC4* overexpression and *Ank2* knockdown in the fly brain resulted in impairment of LTM (ANOVA, post-hoc Tukey's HSD * $P < 0.05$). Significance was measured between flies expressing *UAS-Ank2*RNAi; *UAS-HDAC4OE* in the mushroom body lobes and flies expressing *UAS-Ank2*RNAi individually (* $P < 0.05$). (B) Courtship activity of sham flies was unaffected (ANOVA $P = 0.294$). Numbers within bars indicate the number of animals analysed. Genotype abbreviations: UAS-Ank2RNAi; UAS-HDAC4OE = *UAS-Ank2RNAi; UAS-HDAC4OE*. MB247-GAL80^{ts} = *tubGAL80^{ts}/+; MB247-GAL4/+*. MB247-GAL80^{ts}/UAS-Ank2RNAi = *tubGAL80^{ts}/UAS-Ank2RNAi; MB247-GAL4/+*. MB247-GAL80^{ts}/UAS-HDAC4OE = *tubGAL80^{ts}/+; MB247-GAL4/UAS-HDAC4OE*. MB247GAL80^{ts}/UAS-Ank2RNAi; UAS-HDAC4OE = *tubGAL80^{ts}/UAS-Ank2RNAi; MB247-GAL4/UAS-HDAC4OE*.

4 DISCUSSION

4.1 Identification of genes that interact with *HDAC4*

4.1.1 Transcriptome analysis in the head of *Drosophila* reveals that *HDAC4* does not have a global effect on gene expression

In an effort to advance the understanding on the mechanisms of action through which *HDAC4* regulates LTM, the focus of this study was to identify upstream regulators or downstream targets of the molecular pathway in which *HDAC4* acts. As HDAC4 is a demonstrated transcriptional regulator (Miska et a., 1999; Grozinger and Schreiber, 2000; Huang et al., 2000; Kao et al., 2000; Vega et al., 2004; Li et al., 2012; Sando et al., 2012) and since it is able to shuttle between the nucleus and the cytoplasm, a transcriptome analysis was performed to detect whether in *Drosophila* neuronal nuclei, *HDAC4* mediates transcriptional changes. The experimental set up was designed in order determine whether the LTM impairment observed in flies overexpressing *HDAC4* in all neurons of the brain (Fitzsimons et al., 2013) could be related to transcriptional changes induced by *HDAC4OE*. Very few changes in transcription were detected.

A limitation of this approach, could reside in the fact that sequencing was performed on cDNA of RNA isolated from whole heads rather than from the brain tissue specifically, likely resulting in a decreased sensitivity to detect global changes. The analysis was however able to detect significant differential transcriptional changes in 28 genes compared to wild-type samples, including both *HDAC4* and the *white* gene. A further explanation that could account for the minimal effect on transcription is that HDAC4 is predominantly cytoplasmic and localises in a small subset of nuclei, most of which are in the Kenyon cells of the mushroom body (P. S. Freymuth personal communication).

Isolation of those neuronal nuclei would be a valuable approach to limit the transcriptional profiling to the single nuclei of the mushroom body, distinguished from the rest of the cells by expression of a tag such as green fluorescent protein (GFP) (Deal and Henikoff., 2010). A strategy named INTACT (isolation of nuclei tagged in specific cell types) could be adopted to genetically tag nuclei in the brain and purify them from the total pool through affinity isolation. Isolated nuclei can be used for applications such as gene expression analysis and chromatin immunoprecipitation. Weake and colleagues described a protocol specific for *Drosophila*, in which the GAL4/UAS binary expression system is used to genetically label the nuclei of cells of interest with a nuclear envelope-

localized EGFP tag. The EGFP-tagged nuclei can then be isolated using antibodies against GFP that are coupled to magnetic beads (Ma and Weake, 2014).

Despite the above mentioned limitations, these results were in line with microarray studies in which manipulation of *HDAC4* did not yield significant changes in global gene expression in the mouse hippocampus (Kim et al., 2012). However, capability of HDAC4 to regulate transcription was shown in a study by Sando and colleagues (2012) who reported that expression of a nuclear restricted form of *HDAC4* in mouse primary cortical neurons resulted in differential transcript abundance of a subset of genes essential for synaptic function, meaning that *HDAC4* is capable of regulating transcription when present into the nucleus. Of the genes found to be transcriptionally regulated by *HDAC4* in this study, only a few were significantly expressed in the brain, including *Activity regulated cytoskeleton associated protein 1 (Arc1), Kekkon 2* and *Laminin A*.

Kekkon 2 is expressed in neurons and it is a member of a class of genes highly conserved from invertebrates to humans (MacLaren et al., 2004) that encodes transmembrane proteins with six leucine-rich repeats and a single immunoglobulin loop (LIG family) (Musacchio and Perrimon, 1996). *Kekkon 2* was identified in a microarray screen for genes whose transcriptional activity is regulated by neuronal excitability (Guan et al., 2005). It was found that *Kekkon 2* is enriched in axons and synaptic terminal of the *Drosophila* larvae and that its absolute levels are required to regulate synaptic varicosity number, as both increased and decreased levels of expression of this gene caused a reduction in the number of boutons at the neuromuscular junction, suggesting a role for *Kekkon 2* in synaptic plasticity (Guan et al., 2005). Interestingly, a conserved Kekkon 2-like mammalian member of the LIG family named AMIGO/Alivin was shown to be subjected to activity-dependent transcriptional regulation and to promote neurite outgrowth (Kuja-Panula et al., 2003), suggesting the possibility of a conserved role in activity-dependent modification of synaptic connectivity (MacLaren et al., 2004).

Laminin is a glycoprotein complex of the extracellular matrix, which has been shown to promote neurite outgrowth *in vitro* (Kuhn et al., 1995) and further studies showed that extracellular matrix containing Laminin A is required for the normal pathfinding by the ocellar pioneer axons in *Drosophila* (García-Alonso et al., 1996). Laminin A localises at the synaptic clefts and its overexpression in the postsynaptic region results in decreased growth of the neuromuscular junction (Tsai et al., 2012).

Arc1 is one of three *Drosophila* homologs of mammalian activity-regulated cytoskeleton-associated protein (ARC). In mammals *ARC* is an immediate-early gene

essential for synaptic plasticity and possible implications in onset of Alzheimer's disease have been recently suggested in mouse model of Alzheimer's disease, where intraneuronal amyloid-β expression in the CA3 region of the hippocampus correlated with increased neuronal activation leading to impairments in synaptic function and memory processes (Morin et al., 2016). However, in *Drosophila*, an *Arc* null mutant did not display synaptic plasticity defects at the larval neuromuscular junction nor impairments in memory formation, although behavioural data were limited to immediate memory recall (zero to two minutes after training) and to two hour STM of courtship conditioning. LTM was not evaluated (Mattaliano et al., 2007). Interestingly, *Arc* expression is positively regulated by *Mef2* in neurons (Flavell et al., 2006) and an interaction between HDAC4 and MEF2 is known to occur in neuronal nuclei with HDAC4 repressing MEF2 transcriptional activity (Li et al., 2012) suggesting that decreased levels of *Arc1* in the fly head may result from negative regulation of *Mef2* activity by *HDAC4.*

In summary, these genes are potential *HDAC4* targets and further investigation on the interaction between these genes and *HDAC4* and their roles in brain development and memory formation, may shed light on the molecular pathway through which *HDAC4* regulates such processes.

4.1.2 Transcription factors, SUMOylation machinery enzymes and cytoskeletal regulators interact with *HDAC4*

Given the number of genes transcriptionally regulated by *HDAC4* and its mostly cytoplasmic localisation, a genetic rough eye phenotype screen was performed with the aim to identify genes that interacted with *HDAC4* through both transcriptional and non-transcriptional mechanisms.

Eleven of the genes found in the transcriptome analysis were tested in the rough eye phenotype screen but did not result in a significant enhancement or suppression of the *HDAC4*-induced rough eye phenotype. Several reasons could be responsible for this result, such as the likelihood that the RNAi levels in these lines were not sufficient to knockdown expression of the target gene in the eye or, alternatively they may not interact with *HDAC4* as suggested by the RNAseq data. In light of this, it would be recommended using paired-end over single-end sequences in differential expression studies since the effect of paired-end against single-end strategy was found to have a great impact in terms

of false positives (González and Joly, 2013). In addition, qPCR experiments can be performed to verify the transcriptome results and to confirm that the RNAi efficiently knocked-down the target genes.

However, out of an additional 124 lines analysed, 29 genes were identified to genetically interact with *HDAC4* and were clustered into three major classes according to their role in the cell. These included transcription factors/chromatin regulators, members of the SUMOylation machinery and regulators of the actin/spectrin cytoskeleton. It has to be highlighted that the genes detected by the screen all caused enhancement, not suppression, of the rough eye phenotype suggesting *HDAC4* may act upstream of the putative genetic pathway with these candidates. In agreement, in a recent proteomic study on hippocampus of mouse models of Alzheimer's disease and normal aging, HDAC4 was a top predicted upstream regulator mediating protein abundance changes of proteins implicated in the onset of memory deficits common to Alzheimer's disease and normal aging (Neuner et al., 2016).

4.1.2.1 The rough eye phenotype screen detected conserved interactions in the *HDAC4* genetic pathway

Some of the genes identified by the screen were already known to associate with *HDAC4* in other tissues or animal models and some were known to have a role in memory formation, providing validation of the efficacy of the screen to identify interactions and that those interactions are conserved across the animal kingdom. HDAC4 has been previously found to interact with some of the transcriptional regulators identified in the screen. These include Smrter, which has been previously found to directly interact with HDAC4 in a yeast-two hybrid assay (Kao et al., 2000). Smrter is the homolog of human SMRT/N-CoR, which is a co-repressor complex with HDAC activity provided by association between the deacetylase activating domain of SMRT/N-CoR with class I HDAC3 (Guenther et al., 2001). The catalytic domain of HDAC4 interacts with HDAC3 via SMRT/N-CoR and this complex acts as transcriptional repressor in HEK293 cells and in the human cervical cancer cell line HeLa (Fischle et al., 2002). Interestingly, a non-canonical system for HDAC4 nuclear export was demonstrated in rat cortical neurons. Soriano and colleagues (2013) showed that while a mutant form of HDAC4 lacking its N-terminal phosphorylation sites is constitutively nuclear, co-expression with SMRT

renders it exportable in a manner that is independent from CaMK-dependent phosphorylation. SMRT possesses a domain named RD3 which mediates HDAC4 translocation. Disruption of the association between RD3 and HDAC4 prevents nuclear export of HDAC4. SMRT thus provides a platform for an alternative shuttling pathway in response to SMRT exporting signals such as synaptic activity or inhibition of HDAC3 through inhibitors (Soriano et al., 2013). The nuclear export may result in a relief of transcriptional repression operated by this complex. It would be interesting to examine in the brain whether a link between this process and neurological functions exist, given that regulation of HDAC4's subcellular distribution is a primary mechanism for control of its transcriptional activity.

HDAC4 was also found to interact genetically with another transcriptional co-repressor, Sin3A. HDAC4 was previously found to co-immunoprecipitate with SIN3A in the fibroblast-like COS1 cell line (Nakagawa et al., 2006). Sin3A regulates chromatin remodelling through interaction with transcription factors (Silverstein and Ekwall, 2005) and is part of a complex composed of DNA-binding proteins, histone modification enzymes and other adaptor proteins involved in a wide range of biological activities including cell cycle regulation, DNA replication, apoptosis and modifications of chromatin (Dannenberg et al. 2005). In another genetic eye screen performed in *Drosophila* to detect modifiers of Amyloid-beta (Aβ) toxicity, mutants of *HDAC4* and *Sin3A* were both found to enhance Aβ induced rough eye phenotype suggesting a role in Aβ-induced neuronal toxicity (Cao et al., 2008).

The transcription factors CrebB and Mef2 were identified in the screen and they have both been shown to immunoprecipitate with HDAC4 in cerebellar extracts of mice homozygous null for the *ATM* (*ATM*$^{-/-}$) gene, mutations of which result in the neurodegenerative disease ataxia telangiectasia. In *ATM* $^{-/-}$ mice, HDAC4 translocates into the nucleus where it represses MEF2 and CREBB transcriptional activity suggesting HDAC4 may play a role in disease progression (Li et al., 2012). Furthermore, HDAC4 and Mef2 have been shown to co-localise in the nuclei of the Kenyon cells in the *Drosophila* brain, although significance and physiological role of such association in *Drosophila* has still to be determined (Fitzsimons et al., 2013).

MEF2 is a target of class IIa HDACs and it has been demonstrated that the interaction between HDAC4 and MEF2 results in the repression of MEF2 activity and negative regulation of developmental programs including myoblast differentiation (Miska et al., 1999; McKinsey et al., 2000a) and chondrocyte hypertrophy (Vega et al., 2004). In

vertebrates, MEF2 is a family of transcription factors composed of four distinct genes, *MEF2-A*, *B*, *C* and *D* which regulate synapse development and neuronal survival (Mao et al., 1999; Flavell et al., 2006; Shalizi et al., 2005; Flavell et al., 2008a, 2008b; Barbosa et al., 2008; Simon et al., 2008; Cole et al., 2012). Interestingly several genes found to be targets of *MEF2* have been implicated in human neurological disorders such as epilepsy and autism spectrum disorders (Flavell et al., 2008a, b). In addition, mutations in the *MEF2-C* gene have been linked to severe intellectual disabilities and epilepsy conditions (Zweier et al., 2010). Previous studies conducted by Barbosa and colleagues (2008) demonstrated that a brain specific knock-out of *Mef2-C* in the hippocampus of adult mice caused impairments in hippocampus dependent memory and brain-specific deletion of *Mef2-A* and *Mef2-D* both individually and in combination did not result in specific impairments of learning, memory and in the number of dendritic spines (Akhtar et al., 2012). However, it was shown that increased levels of isoforms A and D in dentate gyrus and amygdala blocked learning-induced increases in spine density, spatial-memory formation and disrupted fear-memory formation (Cole et al., 2012) whereas decreasing MEF2 function in such regions facilitated the formation of spatial and fear memory.

Taken together these data highlight the importance of *Mef2* in plasticity and memory and suggests that *HDAC4* may influence memory via repression of *Mef2* transcriptional activity. Lending support to this theory is a study in which genome-wide mRNA profiling showed that in cortical neurons both HDAC4 and MEF2 regulate at least six genes involved in synaptic function including *Homer1*, *Lgi1*, *Prkca*, *Syngap*, *Rgs2*, and *Mapk8* (Sando et al, 2012). Expression of these genes was repressed by *HDAC4* and activated by *Mef2* in similar experimental settings suggesting that these genes are involved in a strict and fine control of transcriptional regulation.

Clearly, the role of *Mef2* in memory formation is complex and context dependent as is the relationship between *HDAC4* and *Mef2*. Indeed, HDAC4 requires binding to MEF2 to translocate into the nucleus where it represses MEF2 transcriptional activity, thus MEF2 regulates the subcellular distribution of its own repressor. It is likely that impairment of memory by overexpression of *Mef2* (Cole et al., 2012) may be in part due to increased concentration of HDAC4 in the nucleus and consequent repression of MEF2 transcriptional activity.

How the interplay between these proteins is coordinated to regulate memory formation is intriguing and the focus of future research, where the interaction both physical and genetic with Mef2 can be evaluated by a series of protein-protein interaction assays e.g.

pull-down, co-immunoprecipitation, as well as behavioural assays in flies harbouring both overexpression of *HDAC4* and depletion of *Mef2* induced in the brains of adult flies. In addition, the role of RNAi-induced *Mef2* depletion in the fruit fly can also be assessed in the courtship conditioning assay to measure its effect on LTM formation in a *Drosophila* model system.

4.1.2.2 Novel interactions were detected by the *HDAC4*-induced rough eye phenotype screen

Novel interactions with other transcriptional regulators were identified, including *Schnurri* and *Rogdi*. *Schnurri* encodes a zinc finger transcription factor homologous to the human major histocompatibility complex-binding proteins 1 and 2, which have been shown to harbour common variant single-nucleotide polymorphisms associated with schizophrenia (Takao et al., 2013). SCHNURRI has been found to localise in several brain regions including hippocampus, cortex, and cerebellum (Fukuda et al, 2002). In *Drosophila*, *Schnurri* is down-regulated during consolidation of courtship memory suggesting a role for this gene in specific time frames during the process of LTM formation (Winbush et al., 2012).

The exact function of the protein encoded by *Rogdi* is unknown, however this gene is highly conserved and has orthologs in many species, including *Drosophila melanogaster*. It shows particularly high expression levels in various human brain regions (Brandon and Sawa, 2011) and it has been reported that a non-sense mutation in the human homolog causes the neurodevelopmental disorder Kohlschutter-Tonz syndrome (Mory et al., 2012; Schossig et al., 2012).

Interestingly, both *Rogdi* and *Schnurri* were previously identified in a screen for *Drosophila* olfactory memory mutants, with transposon insertions in both genes resulting in severely impaired 24 hour memory without affecting learning (Dubnau et al., 2003). In this same study *Krasavietz*, which was also found in the eye screen, was identified as a memory gene since null mutants displayed defects in memory formation. The finding that these genes, which are involved in memory, interact with *HDAC4* further suggests a role for *HDAC4* in memory and warrants a more profound investigation.

4.1.2.3 *HDAC4* interacts with the SUMOylation machinery

Almost all components of the *Drosophila* SUMOylation machinery were detected through the eye screen. SUMOylation is a reversible post-translational modification carried out by an enzymatic pathway that mediates covalent attachment of a small ubiquitin-like modifier (SUMO) polypeptide to a lysine residue of a target protein. This results in regulation of activity, stability and intracellular localisation of the protein (Wilkinson et al., 2010). SUMO has been linked to nucleocytoplasmic shuttling and specific proteins require SUMOylation for their nuclear import or export (Meulmeester and Melchior, 2008). A growing body of evidence indicates that SUMOylation has a critical role in both nuclear and extranuclear domains and it is implicated in neuropathological conditions (Martin et al., 2007). Indeed, SUMO proteins have been detected within inclusion bodies (cellular deposits containing abnormal aggregated proteins) in various neurodegenerative diseases such as Huntington's disease, Parkinson's disease and Alzheimer's disease (Dorval and Fraser, 2007; Eckermann, 2013; Krumova and Weishaupt, 2013; Guerra de Souza et al., 2016).

The SUMOylation machinery is conserved in *Drosophila* (Talamillo et al., 2008) and is enriched in the adult central nervous system where it is required for normal neuronal function (Long and Griffith, 2000). The screen detected most of the enzymes involved in the SUMOylation process including the E1- Ubiquitin activating enzyme 2, the E2-Conjugating enzyme Ubc9, the E3-Ligase su(var)1-10 along with the nuclear pore complex protein Nup358 and the SUMO protease Ulp1 which mediates desumoylation of the SUMOylated substrates. In view of these data, the role of SUMOylation enzymes in *Drosophila* brain development and memory formation was explored further by Dr Fitzsimons. This analysis focused on Ubc9 which was previously shown to physically interact with HDAC4 in human bone osteosarcoma epithelial cells (U2O2) (Zhao et al., 2005). Pan-neuronal RNAi-depletion of *Ubc9* in the brain of *Drosophila* resulted in impaired mushroom body lobe development and decay of LTM (Schwartz et al., 2016).

Importantly, an increasing number of SUMOylated substrates are being identified including MEF2, whose SUMOylation at lysine residue K395 in mouse fibroblasts and myoblasts results in a reduction of its transcriptional activity (Riquelme et al., 2006), CREBB has also been shown to be SUMOylated at lysine residues K271 and K290 in the hippocampus of rats after water maze spatial training resulting in enhancement of spatial learning and memory (Chen et al., 2014). Noteworthy is the fact that both Mef2 and

CrebB were detected in the screen. ARC1 has been found to be SUMOylated in mammals resulting in dendritic and cytoskeletal localisation of ARC1 (Bramham et al., 2010). Interestingly *Arc1* was one of the genes found to be transcriptionally regulated by *HDAC4* in this study and an earlier study by Dejean and colleagues (Kirsh et al., 2002) showed that HDAC4 can be SUMOylated by either RANBP2 or PIAS, mammalian homologues of *Drosophila* Nup358 and su(var)1-10, both found in the screen. However, global changes in SUMOylation were not observed in flies overexpressing *HDAC4* in the neurons and changes in SUMOylation of candidate proteins such as Mef2 and CrebB which have been shown to interact with HDAC4 (Miska et al., 1999; Li et al., 2012) and are SUMO targets (Grégoire and Yang, 2005; Grégoire et al., 2005; Zhao et al., 2005; Chen et al., 2014) were not detected through co-immunoprecipitation assays, likely because SUMOylation changes mediated by HDAC4 are restricted to distinct regions of the brain. On the other hand, *Drosophila* brains harbouring simultaneous overexpression of *HDAC4* and knockdown of *Ubc9* during adulthood resulted in a significant impairment of LTM formation in the courtship suppression assay, suggesting that a functional interaction between these genes is important for LTM (Schwartz et al., 2016).

In light of these data, a hypothetical model has been proposed in which Ubc9 SUMOylates HDAC4 that as a result shuttles into the nucleus and represses Mef2 transcriptional activity. Since *Mef2* regulates *Arc1* activity (Flavell et al., 2006), lower *Mef2* expression may lead to decreased levels of Arc1 protein leading to synaptic plasticity and memory impairments. To evaluate such a hypothesis it would be necessary to measure SUMOylation of HDAC4 and a mass spectrometry approach would be a valuable strategy as well as purification of the intended targets for pull-downs assays (Riquelme et al., 2006).

4.1.2.4 HDAC4 interacts with regulators of the cytoskeleton

The largest group of genes that enhanced the *HDAC4*-induced rough eye phenotype was composed of regulators of the actin/spectrin cytoskeleton such as *Trio, NetrinB, Derailed, Ankyrin, Ankyrin2,* and *Moesin,* suggesting that *HDAC4* might regulate memory through interaction with genes involved in remodelling the actin/spectrin cytoskeleton, a phenomenon which is believed to regulate the structural changes that underpin learning and memory (Fischer et al., 1998; Engert and Bonhoeffer, 1999; Bailey

and Kandel, 1993; Krucker et al., 2000; Matus, 2000; Lamprecht and LeDoux. 2004; Leiss et al., 2009b; Goellner and Aberle, 2012; Ojelade et al., 2013).

Actin is highly concentrated in dendritic spines (Figure 4.1), small membranous extensions of dendrites which form a bridge between the axons and dendrites of neurons and that have been indicated as the regions where memories are stored (Segal, 2005).

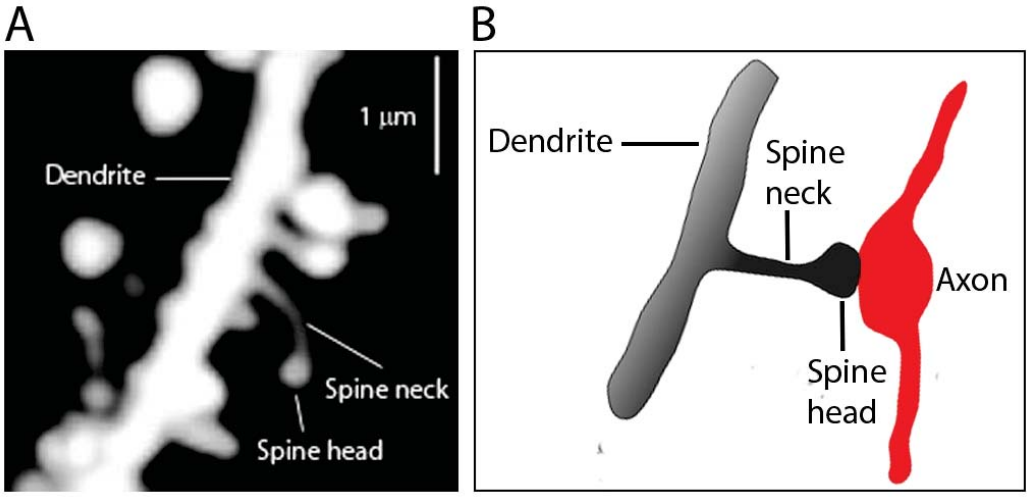

Figure 4.1 Dendritic spine location and morphology. Dendritic spines are extensions of dendrites that link the dendrites to the axons and are believed to be the regions of the neurons where memories are stored. (A) Laser scanning two photon microscope showing spines on a dendrite of a medium spiny striatal neuron. The image was obtained by expressing Enhanced Green Fluorescent Protein (EGFP). (B) Cartoon representing the schematic organisation and morphology of dendritic spines connecting to an axon. For both images, the copyright holders release this work into the public domain and grant the right to use this image for any purpose.

A large body of evidence indicates that polymerisation/depolymerisation or alterations of the underlying actin cytoskeleton are responsible for the spine structural changes required for synaptic plasticity and memory formation (Grove et al., 2004; Shuai et al., 2010; Hotulainen and Hoogenraad, 2010; Lamprecht, 2011; Ojelade et al., 2013; Lamprecht, 2014).

The actin cytoskeleton is also located in axons where it regulates vesicle transport, axonal morphogenesis, guidance to synaptic targets, axonal shape, branching and regeneration (Letourneau, 2009). In addition, actin serves as a scaffold protein to recruit and maintain specific proteins at the axonal domain such as sodium channels thereby

indirectly regulating neurotransmitter release (Sankaranarayanan et al., 2003). It was also shown that, opposite to mammals, inhibition of actin polymerisation within the mushroom body of the honeybee enhanced associative olfactory memory (Ganeshina et al., 2012). Spectrin is localised in both the pre and post-synaptic cytoskeleton and can interact with actin filaments forming an actin/spectrin cytoskeletal network. Spectrin mediates recruitment of ion channels, cell-adhesion molecules and adaptor proteins (such as ankyrins) at specific loci of the membrane and provides support to cell shape and architecture (Lai et al., 2006; Pielage et al., 2006; Xu et al., 2013). For instance, loss of pre-synaptic spectrin in the *Drosophila* neuromuscular junction was shown to cause disorganisation of synaptic cell-adhesion molecules culminating in axonal transport defects (Pielage et al., 2006).

Both *Trio* and *NetrinB* are required for normal axon outgrowth and guidance, and Trio-null cortical neurons fail to extend neurites in response to *Netrin1*, the mammal homologue of *Drosophila NetrinB* (Briançon-Marjollet et al., 2008).

The cytoskeletal adaptor protein Moesin was also identified in the screen. Through DNA microarray analyses *Moesin* was shown to be upregulated during olfactory memory formation (Dubnau et al., 2003) and in the same study *Moesin* was also identified as a candidate memory gene since disruption of this gene resulted in memory impairments in an aversive olfactory conditioning assay. In addition, genomic analysis revealed an upregulation of *Moesin* upon forced nuclear retention of HDAC4 in cultured cortical neurons, which conflicts with the well-characterised transcriptional repression activity operated by HDAC4 (Sando et al., 2012).

Preliminary data were generated which showed that knockdown of *Moesin* in the mushroom body resulted in complete loss of LTM formation (P. S. Freymuth and H. L. Fitzsimons unpublished data) and a previous study showed that it is required for development of the mushroom body (Siegenthaler et al., 2015). Moreover, depletion of *Moesin* expression levels was found to alter dendritic arborisation growth and morphology (P. S. Freymuth and H. L. Fitzsimons unpublished data). Future studies will involve investigation of the interaction between *HDAC4* and *Moesin* in LTM and brain development.

Derailed is a receptor tyrosine kinase expressed in neurons that project through the anterior commissural tract in the *Drosophila* embryonic ventral nerve cord including interneurons and a small number of motor neurons (Bonkowsky et al., 1999; Yoshikawa et al., 2003). Derailed localises to the growth cones and axons of these neurons as they

extend towards the anterior commissure suggesting it is involved in axon guidance (Bonkowsky et al., 1999; Yoshikawa et al., 2003). Derailed may exhibit similar functions in the adult nervous system where it is required for proper projections within the mushroom body (Moreau-Fauvarque et al., 1998; Simon et al., 1998). *Derailed* was also found to localise to the proximal segment of axons in *Drosophila* cultured embryonic neurons, contributing to the axonal membrane compartmentalisation together with receptors Roundabout 2 and Roundabout 3 which were found at the distal segment of the axons (Katsuki et al., 2009). Derailed is therefore involved in maintenance of intra-axonal compartmentalisation by forming a diffusion barrier in neurons that limits the exchange of proteins between the distinct axon domains (Katsuki et al., 2009; Rasband et al., 2010).

This is intriguing since the notion of a diffusion barrier in the proximal axon segment is well known in mammalian neurons, which possess a compartment known as the axon initial segment. This compartment consists of specific cytoskeletal and cell adhesion proteins, including ANK-G the closest homologue to *Drosophila* Ank2 and L1CAM molecules that are homologues of *Drosophila* Nrg. In cultured hippocampal neurons, the axon initial segment functions as a diffusion barrier that limits the exchange of membrane proteins between the somato-dendritic and axonal compartments, as well as between the proximal and distal segments of the axon (Wright and Zinn, 2009).

The axon initial segment-like region in the *Drosophila* brain, has been suggested to localise at the γ neurons since an enrichment of Ank1 and ion channels were detected as a unique and distinct region within these lobes of the mushroom body (Trunova et al., 2011). Interestingly, *Ank1* as well as *Ank2* were found in the screen, with *Ank2* also found to play a key role in maintaining the diffusion barrier at the neuromuscular junction of *Drosophila* and in the dendrites of class I dorsal dendritic arborisation neurons (Yamamoto et al., 2006; Luna and Rolls, 2010; Enneking et al., 2013).

The closest mammalian homolog of *Drosophila Ank2* is *ANK3,* which encodes for the ANK-G protein. *ANK3* is required for axon initial segment stability through organisation of ion channels and recruitment of specific proteins such as neuronal adhesion molecules (L1CAMs). Decreased levels of expression of *ANK3* were shown to lead to axon firing impairment and lack of neuronal specificity with axons acquiring dendritic features in cultured hippocampal neurons from a mouse model of Alzheimer's disease (Sun et al., 2014b). These data suggest that loss of ANK-G disrupts the diffusion barrier in the axon initial segment.

Genome-wide association studies have revealed that cognitive disorders including Alzheimer's disease, schizophrenia and autism, all correlate with mutations in the *ANK3* gene (Leussis et al., 2012; Zhang et al., 2014, Bi et al., 2012) and interestingly HDAC4 has also been implicated in all of these disorders (Kim et al., 2010; Nardone et al., 2014, Neuner et al., 2016; Shen et al., 2016). Intriguing, mammalian HDAC4 has been shown to harbour an ankyrin repeats-binding domain and to physically interact with the ankyrin repeat containing proteins RFXANK and ANKRA2 in mammalian HEK293 cells (Wang et al., 2005; McKinsey et al., 2006; Xu et al., 2012). The *Drosophila* homolog of RFXANK, CG5846, was also identified in the rough eye phenotype screen. It can be speculated that *HDAC4* and *Ank2* may interact through this domain, which is highly conserved across vertebrates and invertebrates, and may mediate maintenance of neuronal stability and functioning. Remarkably, Prosap, another ankyrin repeat containing protein was also identified through the screen. Prosap is the ortholog of the mammalian *PROSAP/SHANK* family known to be implicated in the pathogenesis of autism and autism spectrum disorders (Arons et al., 2012).

4.1.3 Limitations of the analysis

In summary, the results presented in this thesis indicate that *HDAC4* interacts with genes belonging to different classes including transcriptional regulators, cytoskeleton regulators and the SUMOylation machinery. HDAC4 may regulate LTM by SUMOylation mechanisms affecting for instance *Mef2*, *CrebB* and *Arc1* localisation and activities with consequences to the transcriptional machinery necessary for LTM consolidation and through interaction with cytoplasmic elements regulating actin and spectrin dynamics and thus indirectly influencing dendritic spine growth and neurotransmitter release processes. Despite the molecular differences between axons and dendrites, HDAC4 may belong to both neuronal subdomains and could mediate differential responses depending on which substrate it may recruit and bind. Therefore, further studies are required to detect HDAC4 targets in order to elucidate its function in neurons.

Although the screen identified several genes known to interact with *HDAC4* in other organisms or tissues therefore validating the capacity of this model to detect genetic

interactions, limitations reside in the fact that this was a candidate screen rather than an unbiased genome-wide screen for which resources were not available.

Although RNAi-based screens are widely used and an advantageous methodology to study gene function, it must be acknowledged that inaccurate results such as false positives and negatives can occur. A source of false positives is represented by off-target effects, which are determined by dsRNAs having sequence similarity to mRNAs not intended as targets. The VDRC stock centre provides two libraries of RNAi lines, the GD and the KK library with the latter designed to result in lower off-target effects compared to the GD library. The KK library is based on φC31-mediated transgenes with a single defined insertion site of the UAS-RNAi transgene whereas the GD strains are generated via P-element mediated transgenesis which results in semi-random insertions into the genome (Yamamoto-Hino and Goto, 2013; VDRC-stockcenter.vdrc.at).

Where possible, lines used in the screen were chosen from the KK library in order to limit the possibility of off-target effects. Another strategy that was adopted to overcome such limitations was to evaluate candidate genes using more than one dsRNA for the same gene, since each dsRNA is homologous to a different mRNA region of the gene targeted and thus not likely to affect the same non-target mRNA (Perrimon et al., 2010; Yamamoto-Hino and Goto, 2013). For the genes of interest, i.e. the ones used for further analysis including *Ubc9, Ank1* and *Ank2*, independent RNAi lines were evaluated in a second round of screening to provide confirmation of the positive result. False negatives can be due to the limited expression or inefficacy of the RNAi to bind its target, caused by the insertion site of the UAS-RNAi construct (Yamamoto-Hino and Goto, 2013) which may result in poor knockdown of the target mRNA (Dietzl et al., 2007). In addition, in order to verify the phenotypes observed, The VDRC recently announced a collection of new UAS-RNAi lines using short hairpin microRNA technology that will extend and complement the current VDRC RNAi collection based on longer dsRNA inverted repeat technology. These lines include short hairpins RNAs containing a 21 bp targeting sequence embedded into a microRNA backbone and have been shown to be very effective for gene knockdown in both the germline and somatic tissues (Ni et al., 2009; VDRC-stockcenter.vdrc.at/) and would represent a valuable resource to perform further verification screens.

4.1.4 Future directions

Since the nature of the interaction between the candidates found in the eye screen and HDAC4 is not known, it would be worthwhile directing research aimed at characterising the nuclear and cytoplasmic functions of HDAC4. This could be achieved by exploring the roles of specific subcellular localisation mutants of HDAC4 in *Drosophila*. For instance, human HDAC4 (hHDAC4) and *Drosophila melanogaster* HDAC4 (DmHDAC4) mutants exist and could be used to dissect nuclear and cytoplasmic roles of HDAC4. Nuclear restricted hHDAC4 (hHDAC4 3SA) contains substitutions of three serine residues (S246/467/632) with alanines. This prevents CaMKII-dependent phosphorylation that is required for 14-3-3 binding and HDAC4 cytoplasmic retention (Backs et al., 2006). The cytoplasmic restricted mutant possesses a point mutation at amino acid L175, shown to be critical for MEF2 binding and consequent HDAC4 nuclear import (Wang and Yang, 2001). Substitution with alanine (L175A) is enough to impair association between HDAC4 and MEF2 and determine predominant cytoplasmic localisation of HDAC4 (Wang and Yang, 2001). The *Drosophila* nuclear mutant form of HDAC4 contains the N-terminal NLS but it is deprived of the C-terminal NES while the cytoplasmic restricted mutant possess a point mutation whereby a leucine is substituted with an alanine at position 168 (L168A), preventing HDAC4-Mef2 association and therefore nuclear import.

Future work would look at the role of cytoplasmic versus nuclear HDAC4 to assess their effect in LTM formation. In addition, a natural evolution of this study would be to test these variants in the rough eye phenotype screen and investigate which genes are targeted by the different mutants and if DmHDAC4 and hHDAC4 have an overlapping array of interactors. Also, localisation studies through immunohistochemistry as well as protein-protein interaction assays could be adopted in order to test for physical interactions with candidates and these mutants of HDAC4.

Moreover, analysis of the nuclear role of HDAC4 could be performed as previously described (section 4.1.1) by using the INTACT technique to tag the Kenyon cell nuclei and isolate them to investigate the transcriptional changes induced by overexpression of wild-type *HDAC4* throughout the brain. This would be a key analysis to perform since it would reproduce the experimental conditions in which LTM defects were reported upon pan-neuronal overexpression of *HDAC4* throughout the entire brain and would abet to

determine whether the detrimental effects on LTM formation are linked to transcriptional activity in a subset of nuclei.

In conclusion, the findings herein presented validate the eye screening as a reliable system to identify potential new *HDAC4* interacting factors thereby providing valuable and encouraging resources to conduct further investigation on the role of *HDAC4* and its interacting candidates in memory formation.

4.2 Analysis of the roles of *Ankyrin2* and *Ankyrin1* in mushroom body development and long-term memory formation

4.2.1 Ankyrin2 is broadly distributed within the adult brain

Ankyrins are structural proteins that connect transmembrane proteins to the actin/spectrin cytoskeleton and play a pivotal role in maintaining architectural stability and polarity of the cells. The results of this study provide novel insight into the role of *Drosophila Ank2* in the adult brain of *Drosophila melanogaster*.

A full characterisation of the Ank2 expression profile in the adult brain was conducted revealing widespread localisation of Ank2 throughout the brain with high concentration in the optic lobes, antennal lobes and mushroom body. Within the mushroom body, Ank2 was concentrated in the lobes, which are comprised of axonal bundles. This was consistent with studies on embryonic and third instar larvae in which Ank2 was detected in the axons (Hortsch et al., 2002; Koch et al., 2008; Pielage et al., 2008). Particularly in the periactive zone of the neuromuscular junction (Koch et al., 2008), an area that surrounds the active zone (site of neurotransmitter release) and that regulates synaptic development (Sone et al., 2000).

4.2.2 *Ankyrin2* is required for maturation of the mushroom body lobes and long-term memory formation

Given that Ank2 was observed to be highly distributed in the brain, its role in brain development was subsequently evaluated. Pan-neuronal knockdown of *Ank2* resulted in severe anatomical alterations of the mushroom body lobes, ranging from morphological deformities characterised by a thinner shape (e.g. restricted dimensions of the axonal tract), to more dramatic conditions in which axonal guidance and growth were impaired

and loss of one or more lobes occurred. Similarly, studies from Pielage and colleagues (2008) and Koch and colleagues (2008), showed that Ank2 is required for synapse stability since both dsRNA-mediated knockdown and mutation of *Ank2* resulted in severe morphological defects of the neuromuscular junction, synaptic disassembly and retraction, disruption of neuronal excitability (Pielage et al., 2008), withdrawal of synaptic boutons, disruption of the presynaptic active zone and disintegration of the microtubule (Koch et al., 2008). Moreover, absence of axonal Ank2 through chromosome deletion was shown to be lethal (Hortsch et al., 2002).

Data collected in this thesis showed that *Ank2* is an important mediator of mushroom body lobe development, a structure required for normal LTM formation therefore it was valuable to examine its role in memory formation. It was unsurprising that these flies also showed impaired memory. However, *Ank2* was not required to establish normal learning and immediate memory (zero to two minute memory) since these traits were not compromised by pan-neuronal knockdown of *Ank2*. This was in line with a previous study in which decreased expression of *Ank2* in the mushroom body did not result in defects of learning capacities but caused significant impairment to one hour STM in the courtship conditioning (Iqbal et al., 2013). Similarly, pan-neuronal knockdown of *Ank2* impaired three hour memory when tested in the olfactory conditioning (Walkinshaw et al., 2015). The lack of effect on learning, immediate memory and courtship activity suggests that *Ank2* plays a role in specific phases of memory rather than exerting effects on global neurological functions. Whether *Ank2* plays a role in the biological processes required for LTM or whether the LTM defects were due to impaired brain development was assessed via restricted knockdown of *Ank2* to adulthood using the TARGET system. In this study, a role for *Ank2* in regulating LTM formation independently of developmental processes was shown, with flies displaying LTM deficits when *Ank2*RNAi was induced in the adult phase specifically.

In order to determine whether *Ank2* expression was required in the mushroom body for normal memory formation, the impact of *Ank2* on individual subregions of the mushroom body was tested and revealed that the memory defects within this region could be ascribed to the γ neurons. The non-mushroom body expression driven by *NP1131-GAL4* partially overlaps with that of *c305a-GAL4* and *1471-GAL4*, suggesting that expression of *UAS-Ank2*RNAi in these brain areas does not contribute to the memory deficit and the only brain region that always correlates with impairment of LTM is the γ lobe. However it is likely that other regions of the brain contribute to the memory

phenotype observed in *Ank2* knockdown flies and future studies could examine the role of mushroom body extrinsic neurons that could possibly be involved in memory formation including for instance projection neurons, dopamine neurons or output neurons (Aso et al., 2014b; Guvren-Ozkan and Davis, 2014). This finding was significant since it was previously shown that overexpression of *HDAC4* in the γ lobes, resulted in impairments of LTM in *Drosophila* (Fitzsimons et al., 2013) indicating that HDAC4 and Ank2 are required in the same cells providing further support for an interaction.

The γ lobes are the first neurons to develop, during third instar larvae (Lee et al., 1999; Aso et al., 2009) and may play a major role in earlier stages of larval life but they can also change their network patterns in adult life (Lee et al., 1999) and contribute to brain plasticity and memory-related processes. For instance, mutation of the cytoplasmic polyadenylation element-binding protein Orb2 resulted in deficits of LTM. Cytoplasmic polyadenylation element-binding proteins are believed to contribute to the protein synthesis processes underlying changes in synaptic efficacy (Keleman et al., 2007). Restoration of Orb2 in the γ lobes selectively resulted in rescue of LTM formation after one training session, suggesting that these neurons are likely involved in regulating synaptic plasticity and memory traits.

Through functional optical imaging *in vivo* it was shown that the γ neurons of *Drosophila* respond with axonal calcium influx when subjected to aversive odour conditioning (Akalal et al., 2010) resulting in the formation of a robust LTM lasting 48 hours. Moreover, γ neuron calcium-influx was blocked by expressing a repressor of CrebB or a CamKII RNAi. Taken together these results suggest that that the γ neurons represent an area of the brain where protein synthesis is required and hence where LTM may take place.

4.2.2.1 Future directions

These results reveal that *Ank2* plays an essential role in LTM and add new insights to previous vertebrate studies that describe this gene as a master regulator of brain development, neurogenesis and neuroprotection (Leussis et al., 2012; Iqbal et al., 2013; Sun et al., 2014a, 2014b; Durak et al., 2015). *Ank2* is the closest *Drosophila* homolog to human *ANK3*. *ANK3* was identified to be a risk gene for neuropsychiatric disorders including bipolar disorder, schizophrenia, autism spectrum disorder and for cognitive

disorders such as Alzheimer's disease (Tesli et al., 2011; Bi et al., 2012; Leussis et al., 2012; Rueckert et al., 2013; Santuccione et al., 2013; Zhang et al., 2014; Sun et al., 2014a; Cassidy et al., 2014). A possible explanation for the importance of *ANK3* may reside in the fact that the protein for which it encodes, ANK-G, is an essential component of the proximal portion of the axon (Zhou et al., 1998; Kole et al., 2008; Hedstrom et al., 2008; Jones et al., 2014; Yoshimura et al., 2014).

It would be of interest to determine whether knockdown of *Ank2* results in alteration of the *Drosophila* axon initial segment-like region. Interestingly, a study showed that the medium isoform of Ank2, Ank2-M, is distributed in axons and dendrites of class I dorsal dendritic arborisation neurons (Yamamoto et al., 2006). These neurons are a subfamily of multidendritic sensory neurons in the peripheral nervous system of *Drosophila* larvae that are highly used to study dendritic development (Shimono et al., 2009; Jan and Jan, 2010). RNAi-induced depletion of *Ank2* in this subset of neurons in the larval abdominal hemisegment was sufficient to induce axons to acquire dendritic traits (Yamamoto et al., 2006) suggesting an essential role for *Ank2* in the regulation of somatodendritic-axonal separation in *Drosophila* (Yamamoto et al., 2006).

Confocal imaging on third instar larvae brains, in which the axon initial segment-like compartment was previously characterised and located to the γ lobes (Trunova et al., 2011) was performed but this attempt was unsuccessful as the γ region was extremely difficult to image in both control and *Ank2*RNAi-induced flies. Likely, the driver was not sufficiently strong to label the γ neurons or the brains were not correctly positioned on the slide.

However, it would be valuable to re-attempt this analysis since it could be hypothesised that the memory defects induced by *Ank2* depletion depend on the structural instability of the cell. The decreased expression of *Ank2* may cause dysregulation of the distribution and recruitment of the *Drosophila* axon initial segment-like region associated proteins and this would have devastating consequences for cell polarity, axonal transport and action potential firing leading to neurological flaws. It would be interesting to evaluate whether Ank2 is distributed throughout this region and determine if reduced *Ank2* expression alters the morphology of such area and/or the localisation of markers of the axon initial segment, such as Nrg, for which a good antibody is available.

Furthermore, the specific role/s of Ank2 are yet to be completely determined, since the diverse splicing isoforms are distributed differently within the nervous system. Indeed, short isoforms are restricted to cell bodies whereas long isoforms have been detected

specifically in the axons (Hortsch et al., 2002; Pielage et al., 2008; Koch et al., 2008). Extra-long isoforms have been detected in the axons as well as in cell bodies (Koch et al., 2008) and a nuclear distribution of Ank2-L was detected in adult brains in this study.

In summary, in this study compelling evidence for the role of *Ank2* in LTM formation was provided. The critical role this protein plays in LTM combined with intellectual disability phenotypes resulting from mutation of *ANK3* in humans, suggests that further study of its role in cognition is warranted.

4.2.3 Ankyrin1 is distributed in the mushroom body and it is not dispensable for brain development and long-term memory formation.

In this study, the role of *Ank1* was also examined. In contrast to *Ank2* which is selectively expressed in the nervous system, *Ank1* is ubiquitously expressed.

In section 3.2, it was reported that knockdown of *Ank1* in the eye of *Drosophila* enhanced the *HDAC4*-induced rough eye phenotype and therefore further investigations on its role on brain development and memory formation were conducted. Besides, a full characterisation of the role of *Ank1* in the fly nervous system has not been reviewed so far. A recent study on third instar larval brains, showed localisation of an Ank1-GFP fusion protein at the axon initial segment-like compartment, in the γ neurons (Trunova et al., 2011).

In this thesis, it was shown that pan-neuronal knockdown of *Ank1* did not result in impairment of LTM formation and very mild effect on mushroom body lobes development were observed, with phenotypic alterations less severe than the ones caused by pan-neuronal knockdown of *Ank2*.

This could be attributed to different reasons. For instance the RNAi line may not be sufficiently effective to knockdown the target genes and thus influence LTM and mushroom body development or, even though in vertebrates ankyrins do not have redundant functions (Mohler et al., 2004; Cunha and Mohler, 2009), redundancy in the fly nervous system may exist and *Ank2* may provide for the lack of *Ank1* preserving normal LTM and compensating for the loss of *Ank1* during mushroom body development. This could be examined by generating a line harbouring a double knockdown of both *Ank1* and *Ank2* to test in the courtship suppression assay and for FasII immunohistochemistry of developing brains. Although *Ank1*RNAi did not influence

memory, it would be important to further explore its role in the *Drosophila* nervous system since Ank1 is present in the axon initial segment-like region of *Drosophila* (Trunova et al., 2011), it seems to be involved in brain development (section 3.3.2.2) and to elucidate whether possible redundancy roles between *Ank1* and *Ank2* exist.

4.3 Investigating the interaction between HDAC4 and Ankyrin2

The data herein presented provided evidence that *HDAC4* and *Ank2* genetically interact in the eye (section 3.2), they both are involved in brain development (sections 3.3.1.2 and 3.4.2) and LTM (section 3.3.1.3 and Fitzsimons et al., 2013) with *Ank2* knockdown and *HDAC4OE* resulting in similar phenotypes. Therefore, further investigation of a potential physical and functional interaction was carried out.

4.3.1 HDAC4 and Ankyrin2 co-localise in the axons of the mushroom body as well as with Neuroglian suggesting a possible interaction among these factors

Initially, co-localisation studies were performed to examine the relative distribution of Ank2 and HDAC4 in the brain. Confocal micrographs showed a robust overlap in the distribution of HDAC4 and Ank2 in the lobes of the mushroom body (axonal regions).

In a separate study HDAC4 was shown to localise as punctate foci in the nucleus of the Kenyon cells (Fitzsimons et al., 2013) and similarly in this study, Ank2 was observed to localise in specific nuclear regions in the Kenyon cells (section 3.3.1.1). It would be interesting to study whether co-localisation occurs in the nucleus between these two proteins and if overexpression of HDAC4 influences Ank2 distribution. Indeed, it has been demonstrated that in mammalian cell culture HDAC4 can form a complex with RFXANK through its ankyrin repeat-binding domain and that this complex responds to cell signalling by shuttling from the cytoplasm to the nucleus where it mediates silencing of *Major Histocompability Complex II* promoter activation (McKinsey et al., 2006), suggesting a non-canonical pathway for HDAC4 nuclear import and regulation of gene transcription independent of MEF2 binding. It would be of interest to examine such an aspect in the fly brain as well through more in-depth immunohistochemical analyses.

HDAC4 was also found to localise to the same subcellular region as Nrg, which co-localise with Ank2, opening questions about a possible genetic pathway involving *Ank2*, *Nrg* and *HDAC4*. The Ank2-Nrg association is well characterised in both vertebrates and fruit flies and it has been shown to be essential for the regulation of synaptic plasticity, axonal elongation and growth (Davis & Bennett, 1994; Hortsch et al., 1998; Needham et al., 2001; Godenschwege et al., 2006; Hortsch et al., 2009; Martin et al., 2008; Cunha et al., 2009; Goossens et al., 2011; Kudumala et al., 2013; Enneking et al., 2013; Siegenthaler et al., 2015). This hypothetical complex may cooperate in regulating molecular composition at the proximal region of the axons, where the interaction between Nrg and Ank2 is a prerequisite for the structural integrity of the axon initial segment. In addition, studies on primary cultures of rat hippocampal neurons, showed that recruitment of NF186, the mammalian homolog of *Drosophila* Nrg, at the axon initial segment is dependent on prior accumulation of ANK-G, human homolog of *Drosophila* Ank2 (Dzhashiashvili et al., 2007).

One possible hypothesis is that HDAC4 may bind Ank2 through its ankyrin repeats-binding region negatively influencing association between Ank2 and Nrg, thus preventing Ank2-dependent Nrg recruitment at the axon initial segment, eventually leading to deficits to cell architecture and polarity. To assess this possibility, a preliminary immunohistochemistry assay should be performed to observe whether HDAC4 localises at the axon initial segment-like brain region of *Drosophila*, which has been previously detected at the γ lobes (Trunova et al., 2011). It is likely that HDAC4 resides in this region of the fly brain since memory analyses determined that depletion of *HDAC4* at the γ neurons impairs LTM formation and moreover, a supporting evidence to this hypothesis is the fact that the eye screen revealed a genetic interaction between *HDAC4* and *Derailed*, which is known to localise at the proximal segment of axons and it is required to maintain somato-dendritic compartmentalisation by forming a barrier similar to vertebrate axon initial segment (Katsuki et al., 2009; Rasband et al., 2010).

As previously described for *Ank2* (section 4.2.3.1), an attempt to determine whether HDAC4 and Ank2 localise at the axon initial segment-like region of *Drosophila*, was carried out by inducing *HDAC4OE* in the γ neurons and brains were dissected from third instar larvae (Trunova et al., 2011). The experimental procedure was not successful since γ lobes were not detected under confocal microscope. However, it would be worthwhile to repeat this experiment to determine whether Nrg, Ank2 and HDAC4 distribute in this region, whose structural instability and dysfunction may contribute to the onset of

neuropsychiatric developmental disorders such as schizophrenia, bipolar disorder and autism spectrum disorder (Buffington and Rasband, 2011). Also more detailed analysis could be performed, such as testing for a physical interaction between Nrg and HDAC4 as well as memory tests to determine whether *Nrg* is involved in LTM formation and if a genetic interaction with *HDAC4* occurs during this process. Moreover, the hypothesis for an interaction with Nrg was also supported by the fact that the intracellular domain of Nrg not only possesses an ankyrin-binding region but also an Ezrin-Radixin-Moesin domain, which mediates binding of Moesin and this association is necessary for proper axon guidance within the mushroom body (Siegenthaler et al., 2015). *Moesin* was found in the eye screen to genetically interact with *HDAC4* and data were reported on a critical role for *Moesin* in mushroom body development and LTM formation (P. S. Freymouth and H. L. Fitzsimons unpublished data).

Taken together these data suggest that HDAC4 may interact with Ank2, with a possible interaction with Nrg, to form a ternary complex. It is possible that this association is fundamental for normal neuronal functions. However further studies are required to investigate the nature and importance of this putative interaction.

4.3.2 A pull-down assay suggests a physical interaction between Ankyrin2 and HDAC4 ankyrin repeat-binding domain

In order to determine whether HDAC4 and Ank2 physically interact, GST pull-down assays were performed. These experiments revealed a possible physical interaction between Ank2 and HDAC4. However, these initial experiments indicated the interaction was weak or unstable and requires optimisation of pull-down or co-immunoprecipitation analysis.

If this is a weak or transient interaction, such an issue could be addressed by covalently crosslinking the interacting proteins prior to pull-down, in order to seize and strengthen the interaction. Crosslinking reagents can provide the means for capturing protein-protein complexes by covalently bonding them together as they interact. The rapid reactivity of the common functional groups on crosslinkers allows even transient interactions to be frozen in place or weakly interacting molecules to be captured in a complex stable enough for isolation and characterization (Thermo Scientific Pierce Protein Interaction technical handbook, version 2, pages 24-30, 2010).

It is also possible that the accomplished result is a false-positive despite a carefully designed experiment including controls which would have suggested a false-positive outcome. A unique band was observed in the HDAC4-GST/Ank2-EGFP lane at the expected size and no bands were observed in the controls, including the ones in which the cytoplasmic lysate from Ank2-EGFP flies was incubated and pulled-down with GST alone, suggesting the signal was not due to an unspecific binding of Ank2 to the GST tag.

The GST-pull down assay was preferred over co-immunoprecipitation analysis because of a lack of antibodies properly working on blots. Indeed, a line harbouring HDAC4-YFP is available and could be used for co-immunoprecipitation procedures as shown in a previous study where such assay was conducted to detect interaction between HDAC4 and Ubc9 (Schwartz et al., 2016). A GFP antibody could be employed and wild-type lysates as a prey to detect Ank2 would be easily available. However, the Ank2 antibody did not successfully work on blots, potentially due the fact that it may recognise big isoforms of Ank2 (<400 kDa) that were not detected even through adaptation of the SDS-PAGE and western blotting procedure to the detection of big proteins (e.g. the gel concentration was decreased from 10% to 7% and the proteins were run at a lower voltage for at least two hours to allow bigger proteins to migrate over the stacking gel).

However, the GST pull-down assay was performed by using a cytoplasmic lysate derived from bodies of flies expressing an Ank2-EGFP protein so a direct interaction would not be determined by such an experimental set up. It would be necessary to use a purified Ank2 product (recently amplified and ready to be used) and determine whether a direct interaction between HDAC4 ankyrin repeat domain and the ankyrin repeat region of the Ank2 protein occurs. Limiting the binding reaction to those components will clarify whether a direct physical association between Ank2 and HDAC4 occurs.

However, a general limitation to these biochemical approaches exists in that it involves studying the protein interaction in isolation without including the competing protein interactions that can occur within cells. An *in vivo* light microscopy approach for detecting protein interactions may be considered, using the multiphoton Flurescence Lifetime Imaging Microscopy (FLIM) in combination with the Fluorescence Resonance Energy Transfer (FRET) strategy. In FRET experiments, the potential binding partners are labelled with fluorophores that are spectrally different, in a way that the emission spectrum of the donor molecule overlaps the excitation spectrum of the acceptor molecule. If the molecular partners are in close contact, the donor transfers its energy to

the acceptor which will emit a fluorescence photon while the fluorescence lifetime of the donor decreases (Llères et al., 2007; Becker 2012).

4.3.3 *HDAC4* and *Ankyrin2* may interact during long-term memory formation.

In order to evaluate the synergistic effects between *HDAC4* and *Ank2* during LTM formation, flies were generated in which *HDAC4* was overexpressed and *Ank2* was knocked-down in the mushroom body. The TARGET system was used to modulate the level of expression such that it was approximately intermediate-maximal expression for each gene. It was expected that this would not result in severe memory deficits due to inadequate transgene expression and hence if a genetic interaction occurred this would result in synergistic detrimental effects on LTM in the *UAS-Ank2*RNAi*; UAS-HDAC4OE* fly line, in comparison to *UAS-HDAC4OE* and *UAS-Ank2*RNAi individually. However, at 24°C, *HDAC4OE* individually was still sufficiently strong to impair LTM formation. These data suggest that a potential synergystic effect may exist, since simultaneous expression of *UAS-HDAC4OE* and *UAS-Ank2*RNAi resulted in a severe depletion of LTM formation significant with respect to *UAS-Ank2*RNAi individually. However, the memory deficits in flies overexpressing HDAC4 means that it cannot be determined whether this was a real genetic interaction or an additive effect.

Subsequent analyses could be performed decreasing the temperature at which flies are raised from 24°C to 22°C, which would possibly decrease *UAS-HDAC4OE* expression levels without dramatically affecting *Ank2* expression levels which at 24°C appear to be appropriate for such an assay. Once this procedure is optimised, further memory tests could similarly be performed to analyse whether a functional interaction between *Nrg* and *HDAC4* occurs, using flies harbouring simultaneous knockdown of *Nrg* and overexpression of *HDAC4*. However, a prior characterisation of *Nrg* knockdown on LTM would be necessary since this has not been assessed so far.

In summary, evidence for a potential physical and functional interaction between HDAC4 and Ank2 was provided, although further studies are required to confirm this. Nevertheless, the similar phenotypes and localisation of these two proteins supports the necessity to further investigate and elucidate the potentiality of this genetic association as a possible mechanism of action through which *HDAC4* regulates memory formation. Such a mechanism could possibly reside in the association of HDAC4 and Ank2 at the

plasma membrane resulting in regulation of axonal and dendritic architecture, which may alter remodelling of the cytoskeleton affecting neurotransmitter release and/or dendritic growth and ultimately memory formation.

5 SUMMARY AND FUTURE PERSPECTIVES

In an effort to advance the understanding on the mechanisms of action through which *HDAC4* regulates LTM, the focus of this study was to identify upstream regulators or downstream targets of the *HDAC4* molecular pathway and to investigate the role of these interactors in brain development and LTM formation.

HDAC4 was found to interact genetically with transcriptional regulators, components of the SUMOylation machinery and cytoskeletal regulators including *Ank2*, which has subsequently been shown to be crucial for mushroom body axons maturation and LTM formation to the same extent as *HDAC4*. These findings are suggestive of a cytoplasmic role for HDAC4 in the regulation of LTM through remodelling of the cytoplasm underpinning axon and dendritic functionality. This would be in line with the well-demonstrated predominant distribution of HDAC4 in the cytoplasm but the nuclear role of HDAC4 in the context of memory regulation should not be put aside, since HDAC4 is an established transcription regulator repressing expression of genes critical for memory formation (Li et al., 2012; Sando et al., 2012; Neuner et al., 2016). Although minimal changes in global transcription were detected upon overexpression of *HDAC4*, this does not preclude the possibility that *HDAC4* transcriptionally regulates *Ank2* and the other genes identified in the screen in a subset of nuclei in the brain.

Moreover, several questions were raised which have opened new research avenues to be pursued in the future. The major findings presented in this thesis and the future directions to undertake in order to elucidate *HDAC4* mechanism of action are summarised below.

5.1 Overexpression of *HDAC4* in the whole fly head has minimal effect on global changes in gene expression.

As *HDAC4* is a demonstrated transcriptional regulator (Miska et a., 1999; Grozinger and Schreiber, 2000; Huang et al., 2000; Kao et al., 2000; Vega et al., 2004; Li et al., 2012; Sando et al., 2012) and since it is able to shuttle between the nucleus and the cytoplasm, a transcriptome analysis was performed to detect whether *HDAC4* mediates transcriptional changes. The experimental set up was designed in order to verify whether the LTM impairment observed in flies overexpressing *HDAC4* in all neurons of the brain (Fitzsimons et al., 2013) could be related to transcriptional changes induced by *HDAC4OE*. Overexpression of *HDAC4* in the fly head did not result in global changes in gene expression, possibly because only a subset of nuclei may present HDAC4 and thus

the analysis was not able to detect changes. The INTACT procedure, which allows isolation of tagged nuclei, would permit a more accurate measurement of gene expression restricted to neuronal nuclei, a subset of which would exhibit HDAC4 localisation and such nuclei will be isolated and used for RNAseq analysis. This approach would provide a more compelling answer to whether *HDAC4* regulates transcription of genes involved in LTM in the fly brain.

5.2 A genetic screen for modifiers of the *HDAC4*-induced rough eye phenotype detected genes involved in transcription, SUMOylation and cytoskeletal organisation

Since minimal effects on gene expression were reported in flies overexpressing *HDAC4* in neurons, a different strategy was undertaken to detect interacting genes beyond transcription. As overexpression of *HDAC4* in the eye photoreceptors resulted in a mild rough eye phenotype, this was used as a 'readout' for *HDAC4* function when other genes were down-regulated through RNAi in the eye simultaneously to *HDAC4OE*. Enhanced or decreased severity of the *HDAC4*-induced rough eye phenotype suggested a genetic interaction between the gene and *HDAC4*. This assay detected genes belonging to three major categories, namely, transcription factors, SUMOylation machinery and cytoplasm organisers. Among this latter category, further experiments were conducted on *Ank2*.

In addition, the eye screen results opened new exciting research fronts in the laboratory with analyses on the interaction between HDAC4 and the SUMOylation machinery enzymes, with focus on Ubc9 (Schwartz et al., 2016), transcription factor Mef2, and transmembrane protein Moesin.

The genetic screen suggested that HDAC4 may operate through multiple mechanisms of action in the regulation of memory including a program through which *HDAC4* may inhibit transcription of genes required for memory formation such as *CrebB* (found in the screen); SUMOylation enzymes recently found to have critical roles in memory and learning (Schwartz et al., 2016), and regulators and interactors of the cytoskeleton involved in axon and dendritic growth and remodelling, phenomenon believed to be at the basis of synaptic plasticity and memory.

Future research will evaluate the specific roles of nuclear and cytoplasmic HDAC4 through the use of subcellular mutants that can be tested in the courtship suppression

memory assay, and possibly in genetic screen which would abet the detection of specific *HDAC4* interactive factors belonging to either the nuclear or cytoplasmic subdomain.

5.3 Ankyrin2 is a cytoplasmic protein required for *Drosophila* mushroom body development and long-term memory formation in both developing and post-mitotic phases

Among cytoplasmic effectors, this thesis focused on the roles of *Ank2* as no studies have been conducted to date on its role on LTM and adult brain functions. Depletion of *Ank2* in the developing brains resulted in a robust impairments of mushroom body axon development as well as significant impairments of LTM formation. Similarly, when *Ank2*RNAi was induced specifically in the adult brains, LTM defects were observed indicating a specific role in memory formation independent of brain development with a specific role of the γ neurons as previously shown for HDAC4 (Fitzsimons et al., 2013).

5.4 A preliminary study on a putative interaction between Ankyrin2 and HDAC4

The in-depth study carried out on *Ank2* reported a series of phenotypes shared between *Ank2* knockdown and *HDAC4OE*, with both critical for normal mushroom body lobe development and LTM formation notably when genetic manipulation of both genes was restricted to the γ lobes. In addition, the finding that HDAC4 possess an ankyrin repeat-binding domain supported the hypothesis of a physical interaction and this led to more specific, although preliminary, investigations on a putative interaction.

GST pull-down assays and courtship conditioning assay provided beginning data on a physical as well as a genetic interaction between Ank2 and HDAC4. These observations opened several questions but also exciting research avenues that will provide more compelling evidence and that will allow to draw a conclusive picture.

In conclusion, understanding the roles of *HDAC4* and its genetic pathway in both the nucleus and in the cytoplasm will help to further elucidate its role in LTM and such studies would not only advance our understanding on the sophisticated and intricate molecular pathway underlying memory formation but would as well provide the basis to possibly expand these studies on mammalian models and proteomic research studies, with

the ultimate goal to design and establish drugs that would ameliorate the *HDAC4*-induced cognitive deficits.

6 References

Abel, T., & Lattal, K. M. (2001). Molecular mechanisms of memory acquisition, consolidation and retrieval. *Current Opinion in Neurobiology*, **11**, 180-187.

Abel, T., & Zukin, R. S. (2009). Epigenetic targets of HDAC inhibition in neurodegenerative and psychiatric disorders. *Current Opinion in Pharmacology*, **8**, 57–64.

Abel, T., Martin, K. C., Bartsch, D., & Kandel, E. R. (1998). Memory suppressor genes: inhibitory constraints on the storage of long-term memory. *Science*, **279**, 338-41.

Akalal, D. B., Yu, D., & Davis, R. L. (2010). A late-phase, long-term memory trace forms in the gamma neurons of Drosophila mushroom bodies after olfactory classical conditioning. *Journal of Neuroscience*, **30**, 16699-16708.

Akhtar, M. W., Kim, M. S., Adachi, M., Morris, M. J., Qi, X., Richardson, J. A., Bassel-Duby, R., Olson, E. N., Kavalali, E. T., & Monteggia, L. M. (2012). In vivo analysis of MEF2 transcription factors in synapse regulation and neuronal survival. *Plos One*, **7**, e34863.

Alarcon, J. M., Malleret, G., Touzani, K., Vronskaya, S., Ishii, S., Kandel, E. R., & Barco, A. (2004). Chromatin acetylation, memory, and LTP are impaired in CBP+/- mice: a model for the cognitive deficit in Rubinstein-Taybi syndrome and its amelioration. *Neuron*, **42**, 947-959.

Alberini, C. M. (2009). Transcription factors in long-term memory and synaptic plasticity. *Physiological Reviews*, **89**, 121-145.

Alberini, C. M., Ghirardl, M., Metz, R., & Kandel, E. R. (1994). C/EBP is an immediate-early gene required for the consolidation of long-term facilitation in Aplysia, *Cell*, **76**, 1099-1114.

American Psychiatric Association. (2013). Diagnostic and statistical manual of mental disorders (5th ed.). Washington DC.

Arons, M. H., Thynne, C. J., Grabrucker, A. M., Li, D., Schoen, M., Cheyne, J. E., Boeckers, T. M., Montgomery, J. M., & Garner, C. C. (2012). Autism-associated mutations in ProSAP2/Shank3 impair synaptic transmission and neurexin–neuroligin-mediated transsynaptic signaling. *The Journal of Neuroscience*, **32**, 14966–14978.

Aso, Y., Grubel, K., Busch, S., Friedrich, A. B., Siwanowicz, I., & Tanimoto, H. (2009). The mushroom body of adult Drosophila characterized by GAL4 drivers. *Journal of Neurogenetics*, **23**, 156-172.

Aso, Y., Hattori, D., Yu, Y., Johnston, R. M., Iyer, N. A., Ngo, T-TB, Dionne, H., Abbott, L. F., Axel, R., Tanimoto, H., & Rubin, G. M. (2014a). The neuronal architecture of the mushroom body provides a logic for associative learning. *eLife*, **3**, e04577.

Aso, Y., Sitaraman, D., Ichinose, T., Kaun, K. R., Vogt, K., Belliart-Guérin, G., Plaçais, P-Y., Robie, A. A., Yamagata, N., Schnaitmann, C., Rowell, W. J., Johnston, R. M., Ngo, T-TB., Chen, N., Korff, W., Nitabach, M. N., Heberlein, U., Preat, T., Branson, K. M., Tanimoto, H., & Rubin, G. M. (2014b). Mushroom body output neurons encode valence and guide memory-based action selection in Drosophila. *eLife*, **3**, 04580.

Awasaki, T., & Lee, T. (2011). New tools for the analysis of glial cell biology in Drosophila. *Glia*, **59**, 1377-1386.

Awasaki, T., Lai, S. L., Ito, K., & Lee, T. (2008). Organization and postembryonic development of glial cells in the adult central brain of Drosophila. *Journal of Neuroscience*, **28**, 13742-13753.

Bahari-Javan, S., Maddalena, A., Kerimoglu, C., Wittnam, J., Held, T., Bähr, M., Burkhardt, S., Delalle, I., Kügler, S., Fischer, A., & Sananbenesi, F. (2012). HDAC1 Regulates Fear Extinction in Mice. *The Journal of Neuroscience*, **32**, 5062-5073.

Bailey, C. H., & Kandel, E. R. (1993). Structural changes accompanying memory storage. *Annual Review of Physiology*, **55**, 397-426.

Backs, J., Song, K., Bezprozvannaya, S., Chang, S., & Olson, E. N. (2006). CaM kinase II selectively signals to histone deacetylase 4 during cardiomyocyte hypertrophy. *Journal of Clinical Investigation*, **116**, 1853–1864.

Barbosa, A. C., Kim, M. S., Ertunc, M., Adachi, M., Nelson, E. D., McAnally, J., Richardson, J. A., Kavalali, E. T., Monteggia, L. M., Bassel-Duby, R., Olson, E. N. (2008). MEF2C, a transcription factor that facilitates learning and memory by negative regulation of synapse numbers and function. *Proceedings of the National Academy of Sciences*, **105**, 9391-9396.

Barco, A., Bailey, C. H., & Kandel, E. R. (2006). Common molecular mechanisms in explicit and implicit memory. *Journal of Neurochemistry*, **97**, 1520-1533.

Becker, W. (2012), Fluorescence lifetime imaging – techniques and applications. *Journal of Microscopy*, **247**, 119–136.

Bellen, H. J., Tong, C., & Tsuda, H. (2010). 100 years of Drosophila research and its impact on vertebrate neuroscience: a history lesson for the future. *Nature Review Neuroscience*, **11**, 514-522.

Bender, K. J., & Trussell, L. O. (2012). The physiology of the axon initial segment. *Annual Review of Neuroscience*, **35**, 249-265.

Benfenati, F. (2007). Synaptic plasticity and the neurobiology of learning and memory. *Acta Biomedica*, **79**, 58-66.

Bennett, V. (1978). Purification of an active proteolytic fragment of the membrane attachment site for human erythrocyte spectrin. *The Journal of Biological Chemistry*, **253**, 2292–2299.

Bennett, V., & Baines, A. J. (2001). Spectrin and ankyrin-based pathways: Metazoan inventions for integrating cells into tissues. *Physiological Reviews*, **81**, 1353–1392.

Berger, C., Renner, S., Lüer, K., & Technau, G. M. (2007). The commonly used marker ELAV is transiently expressed in neuroblasts and glial cells in the Drosophila embryonic CNS. *Developmental Dynamics*, **236**, 3562-3568.

Bertos, N. R., Wang, A. H., & Yang, X.-J. (2001). Class II histone deacetylases: structure, function, and regulation. *Biochemistry and Cell Biology*, **79**, 243-252.

Bi, C., Wu, J., Jiang, T., Liu, Q., Cai, W., Yu, P., Cai, T., Zhao, M., Jiang, Y. H., & Sun, Z. S. (2012). Mutations of ANK3 identified by exome sequencing are associated with autism susceptibility. *Human Mutation*, **33**, 1635-1638.

Bieber, A. J., Snow, P. M., Hortsch, M., Patel, N. H., Jacobs, J. R., Traquina, Z. R., Schilling, J., & Goodman, C. S. (1989). Drosophila neuroglian: a member of the immunoglobulin superfamily with extensive homology to the vertebrate neural adhesion molecule L1. *Cell*, **59**, 447-460.

Bier, E. (2005). Drosophila, the golden bug, emerges as a tool for human genetics. *Nature Reviews: Genetics*, **6**, 9-23.

Bischof, J., Maeda, R. K., Hediger, M., Karch, F., & Basler, K. (2007). An optimized transgenesis system for Drosophila using germ-line-specific phiC31 integrases. *Proceedings of the National Academy of Sciences of the United States of America*, **104**, 3312-3317.

Bogart, K., & Andrews, J. (2006). Extraction of total RNA from Drosophila. CGB Technical Report 2006-10. The Center for Genomics and Bioinformatics, Indiana University, Bloomington, Indiana.

Bolger, T. A., & Yao, T. P. (2005). Intracellular trafficking of histone deacetylase 4 regulates neuronal cell death. *Journal of Neuroscience*, **25**, 9544-9553.

Bolger, T. A., Zhao, X., Cohen, T. J., Tsai, C. C., & Yao, T. P. (2007). The neurodegenerative disease protein ataxin-1 antagonizes the neuronal survival function of myocyte enhancer factor-2. *Journal of Biological Chemistry*, **282**, 29186-29192.

Bonkowsky, J. L., Yoshikawa, S., O'Keefe, D. D., Scully, A. L., & Thomas, J. B. (1999). Axon routing across the midline controlled by the Drosophila Derailed receptor. *Nature*, **402**, 540-544.

Bottomley, M. J., Lo Surdo, P., Di Giovine, P., Cirillo, A., Scarpelli, R., Ferrigno, F., Jones, P., Neddermann, P., De Francesco, R., Steinkuhler, C., Gallinari, P., & Carfi, A. (2008). Structural and functional analysis of the human HDAC4 catalytic domain reveals a regulatory structural zinc-binding domain. *Journal of Biological Chemistry*, **283**, 26694-26704.

Bouley, M., Tian, M. Z., Paisley, K., Shen, Y. C., Malhotra, J. D., & Hortsch M. (2000). The L1-type cell adhesion molecule neuroglian influences the stability of neural ankyrin in the Drosophila embryo but not its axonal localization. *The Journal of Neuroscience*, **20**, 4515-4523.

Bramham, C. R., Alme, M. N., Bittins, M., Kuipers, S. D., Nair, R. R., Pai, B., Panja, D., Schubert, M., Soule, J., Tiron, A., & Wibrand, K. (2010). The Arc of synaptic memory. *Experimental Brain Research*, **200**, 125-140.

Brand, A. H., & Perrimon, N. (1993). Targeted gene expression as a means of altering cell fates and generating dominant phenotypes. *Development*, **118**, 401-415.

Brandl, A., Heinzel, T., & Kramer, O. H. (2009). Histone deacetylases: salesmen and customers in the post-translational modification market. *Biology of the Cell*, **101**, 193-205.

Brandon, N. J., & Sawa, A. (2011). Linking neurodevelopmental and synaptic theories of mental illness through DISC1. *Nature Review Neurosci*ence, **12**, 707-22.

Bredy, T. W., & Barad, M. (2008). The histone deacetylase inhibitor valproic acid enhances acquisition, extinction, and reconsolidation of conditioned fear. *Learning & Memory*, **15**, 39–45.

Briançon-Marjollet, A., Ghogha, A., Nawabi, H., Triki, I., Auziol, C., Fromont, S., Piché, C., Enslen, H., Chebli, K., Cloutier, J-F., Castellani, V., Debant, A., & Lamarche-Vane, N. (2008). Trio mediates netrin-1-induced rac1 activation in axon outgrowth and guidance. *Molecular and Cellular Biology*, **28**, 2314–2323.

Broide, R. S, Redwine, J. M., Aftahi, N., Young, W., Bloom, F. E. & Winrow, C. J. (2007) Distribution of histone deacetylases 1-11 in the rat brain. *Journal of Molecular Neuroscience*, **31**, 47-58.

Buffington, S. A., & Rasband, M. N. (2011). The axon initial segment in nervous system disease and injury. *European Journal of Neuroscience*, **34**, 1609-1619.

Buggy, J. J., Sideris, M. L., Mak, P., Lorimer, D. D., Mcintosh, B., & Clark, J. M. (2000). Cloning and characterization of a novel human histone deacetylase, HDAC8. *Biochemical Journal*, **350**, 199-205.

Busto, G. U., Cervantes-Sandoval, I., & Davis, R. L. (2010). Olfactory Learning in Drosophila. *Physiology*, **25**, 338–346.

Butcher, N. J., Friedrich, A. B., Lu, Z., Tanimoto, H., & Meinertzhagen, I. A. (2012). Different classes of input and output neurons reveal new features in microglomeruli of the adult Drosophila mushroom body calyx. *Journal of Comparative Neurology*, 10, 2185-2201.

Cao, W., Song, H. J., Gangi, T., Kelkar, A., Antani, I., Garza, D., & Konsolaki, M. (2008). Identification of novel genes that modify phenotypes induced by Alzheimer's beta-amyloid overexpression in Drosophila. *Genetics*, **178**, 1457-1471.

Cassidy, C., Buchy, L., Bodnar, M., Dell'Elce, J., Choudhry, Z., Fathalli, F., Sengupta, S., Fox, R., Malla, A., Lepage, M., Iyer, S., & Joober, R. (2014). Association of a risk allele of ANK3 with cognitive performance and

cortical thickness in patients with first-episode psychosis. *Journal of Psychiatry & Neuroscience*, **39**, 31–39.

Castellucci, V., Pinsker, H., Kupfermann, I., & Kandel, E. R. (1970). Neuronal mechanisms of habituation and dishabituation of the gill-withdrawal reflex in Aplysia. *Science*, **167**, 1745-1748.

Charych, E. I., Akum, B. F., Goldberg, J. S., Jörnsten, R. J., Rongo, C., Zheng, J. Q., & Firestein, B. L. (2006). Activity-independent regulation of dendrite patterning by postsynaptic density protein PSD-95. *The Journal of Neuroscience*, **26**, 10164-10176.

Chawla, S., Vanhoutte, P., Arnold, F. J. L., Huang, C. L. H., & Bading, H. (2003). Neuronal activity-dependent nucleocytoplasmic shuttling of HDAC4 and HDAC5. *Journal of Neurochemistry*, **85**, 151-159.

Chen, C. C., Wu, J. K., Lin, H. W., Pai, T. P., Fu, T. F., Wu, C. L., Tully, T., & Chiang, A. S. (2012). Visualizing long-term memory formation in two neurons of the Drosophila brain. *Science*, **335**, 678-685.

Chen, Y.-C., Hsu, W.-L., Ma, Y.-L., Tai, D. J. C., & Lee, E. H. Y. (2014). CREB SUMOylation by the E3 ligase PIAS1 enhances spatial memory. *The Journal of Neuroscience*, **34**, 9574-9589.

Chintapalli, V. R., Wang, J., & Dow, J. A. (2007). Using FlyAtlas to identify better Drosophila melanogaster models of human disease. *Nature Genetics*, **39**, 715-720.

Cho, Y., Griswold, A., Campbell, C., & Min, K. T. (2005). Individual histone deacetylases in Drosophila modulate transcription of distinct genes. *Genomics*, **86**, 606-617.

Cohen, T. J., Barrientos, T., Hartman, Z. C., Garvey, S. M., Cox, G. A., & Yao, T. P. (2009). The deacetylase HDAC4 controls myocyte enhancing factor-2-dependent structural gene expression in response to neural activity. *FASEB Journal*, **23**, 99-106.

Cole, C. J., Mercaldo, V., Restivo, L., Yiu, A. P., Sekeres, M. J., Han, J. H., Vetere, G., Pekar, T., Ross, P. J., Neve, R. L., Frankland, P. W., & Josselyn, S. A. (2012). MEF2 negatively regulates learning-induced structural plasticity and memory formation. *Nature Neuroscience*, **15**, 1255-1264.

Crittenden, J. R., Efthimios, M. C., Skoulakis, K-A. H., Kalderon, D., & Davis, R. L. (1998). Tripartite mushroom body architecture revealed by antigenic markers. Learning and memory, **5**, 38-51.

Cunha, S. R., & Mohler, P. J. (2009). Ankyrin protein networks in membrane formation and stabilization. *Journal of Cellular and Molecular Medicine*, **13**, 4364–4376.

Dannenberg, J.-H., David, G., Zhong, S., van der Torre, J., Wong, W. H., & DePinho, R. A. (2005). mSin3A corepressor regulates diverse transcriptional networks governing normal and neoplastic growth and survival. *Genes & Development*, **19**, 1581–1595.

Darcy, M. J., Calvin, K., Cavnar, K., & Ouimet, C. C. (2010). Regional and subcellular distribution of HDAC4 in mouse brain. *Journal of Comparative Neurology*, **518**, 722-740.

Davis, J. Q., Bennett, V. (1994). Ankyrin binding activity shared by the neurofascin/L1/NrCAM family of nervous system cell adhesion molecules. *The Journal of Biological Chemistry*, **269**, 27163-27166.

Davis, R. L. (1993). Mushroom bodies and Drosophila learning, *Neuron*, **11**, 1-14.

Davis, R. L. (2005). Olfactory memory formation in Drosophila: from molecular to systems neuroscience. *Annual Review Neuroscience*, **28**, 275-302.

Day, J. J., & Sweatt, J. D. (2011). Epigenetic Mechanisms in Cognition. *Neuron*, **70**, 813-829.

De Belle, J. S., & Heisenberg, M. (1994). Associative odor learning in Drosophila abolished by chemical ablation of mushroom bodies. *Science*, **263**, 692-695.

De Ruijter, A. J. M., van Gennip, A. H., Caron, H. N., Kemp, S., & van Kuilenburg, A. B. P. (2003). Histone deacetylases (HDACs): characterization of the classical HDAC family. *Biochemical Journal*, **370**, 737–749.

Deal, R. B., & Henikoff, S. (2010). A simple method for gene expression and chromatin profiling of individual cell types within a tissue. *Developmental Cell*, **18**, 1030-1040.

DeFelipe, J. (2006). Brain plasticity and mental processes: Cajal again. *Nature Review Neuroscience*, **7**, 811-817.

del Valle Rodríguez, A., Didiano, D., & Desplan, C. (2012). Power tools for gene expression and clonal analysis in Drosophila. *Nature Methods*, **9**, 47-55.

Delcuve, G. P., Khan, D. H., & Davie, J. R. (2012). Roles of histone deacetylases in epigenetic regulation: emerging paradigms from studies with inhibitors. *Clinical Epigenetics*, **4**, 1-13.

Dietz, K. C., & Casaccia, P. (2010). HDAC inhibitors and neurodegeneration: at the edge between protection and damage. *Pharmacological Research*, **62**, 11-17.

Dietzl, G., Chen, D., Schnorrer, F., Su, K. C., Barinova, Y., Fellner, M., Gasser, B., Kinsey, K., Oppel, S., Scheiblauer, S., Couto, A., Marra, V., Keleman, K., & Dickson, B. J. (2007). A genome-wide transgenic RNAi library for conditional gene inactivation in Drosophila. *Nature*, **448**, 151-156.

Dillon, M. E., Wang, G., Garrity, P. A., & Hueya, R. B. (2009). Review: Thermal preference in Drosophila. *Journal of Thermal Biology*, **34**, 109-119.

Dorval, V., & Fraser, P. E. (2007). SUMO on the road to neurodegeneration. *Biochimica et Biophysica Acta - Molecular Cell Research*, **1773**, 694-706.

Drisaldi, B., Colnaghi, L., Fioriti, L., Rao, N., Myers, C., Snyder, A. M., Metzger, D. J., Tarasoff, J., Konstantinov, E., Fraser, P. E., Manley, J. L., & Kandel, E. R. (2015). SUMOylation is an inhibitory constraint that regulates the prion-like aggregation and activity of CPEB3. *Cell Reports*, **11**, 1694-1702.

Dubnau, J., Chiang, A.S., Grady, L., Barditch, J., Gossweiler, S., McNeil, J., Smith, P., Buldoc, F., Scott, R., Certa, U., Broger, C., & Tully, T. (2003). The staufen/pumilio pathway is involved in Drosophila long-term memory. *Current Biology*, **13**, 286–296.

Dubreuil, R. R., MacVicar, G., Dissanayake, S., Liu, C., Homer, D., & Hortsch, M. (1996). Neuroglian-mediated cell adhesion induces assembly of the membrane skeleton at cell contact sites. *The Journal of Cell Biology*, **133**, 647-655.

Duffy, J. B. (2002). GAL4 system in Drosophila: a fly geneticist's Swiss army knife. *Genesis*, **34**, 1-15.

Dujardin, F. (1850). Memoire sur le systeme nerveux des insects. Title translation: Thesis on the nervous system of the insect. *Annales des Sciences Naturelles*, **14**, 195–206.

Dukas, R. (2008). Evolutionary biology of insect learning. *Annual Review of Entomology*, **53**, 145-160.

Dunwell, T. L., & Pfeifer, G. P. (2014). Drosophila genomic methylation: new evidence and new questions. *Epigenomics*, **6**, 459–461.

Durak, O., de Anda, F. C., Singh, K. K., Leussis, M. P., Petryshen, T. L., Sklar, P., & Tsai, L. –H. (2015). Ankyrin-G regulates neurogenesis and Wnt signaling by altering the subcellular localization of β-catenin. *Molecular Psychiatry*, **20**, 388-397.

Dzhashiashvili, Y., Zhang, Y., Galinska, J., Lam, I., Grumet, M., & Salzer, J. L. (2007). Nodes of Ranvier and axon initial segments are ankyrin G-dependent domains that assemble by distinct mechanisms. *Journal of Cell Biology*, **177**, 857-870.

Eckermann, K. (2013). SUMO and Parkinson's Disease. *Neuromolecular Medicine*, **15**, 737-759.

Ejima, A., & Griffith, L. C. (2007). Measurement of courtship behavior in Drosophila melanogaster. *Cold Spring Harbor Protocols*, **2007**.

Ejima, A., & Griffith, L. C. (2010). Assay for courtship suppression in Drosophila. *Cold Spring Harbor Protocols*, **2011**.

Ejima, A., Smith, B. P. C., Lucas, C., Levine, J. D., & Griffith, L. C. (2005). Sequential learning of pheromonal cues modulates memory consolidation in trainer-specific associative courtship conditioning. *Current Biology*, **15**, 194–206.

Engert, F., & Bonhoeffer, T. (1999). Dendritic spine changes associated with hippocampal long-term synaptic plasticity. *Nature*, **399**, 66-70.

Enjin, A., Zaharieva, E. E., Frank, D. D, Mansourian, S., Suh, G. S., Gallio, M., & Stensmyr, M. C. (2016). Humidity sensing in Drosophila. *Current Biology*, **26**, 1352-1358.

Enneking, E. M., Kudumala, S. R., Moreno, E., Stephan, R., Boerner, J., Godenschwege, T. A., & Pielage, J. (2013). Transsynaptic coordination of synaptic growth, function, and stability by the L1-type CAM Neuroglian. *PLoS Biology*, **11**, e1001537.

Fahrbach, S. E. (2006). Structure of the mushroom bodies of the insect brain. *Annual Review Entomology*, **51**, 209-232.

Fischer, J. A., Giniger, E., Maniatis, T., & Ptashne, M. (1988). GAL4 activates transcription in Drosophila. *Nature*, **332**, 853–856.

Fischer, M., Kaech, S., Knutti, D., & Matus, A. (1998). Rapid actin-based plasticity in dendritic spines. *Neuron*, **20**, 847-854.

Fischle, W., Dequiedt, F., Fillion, M., Hendzel, M. J., Voelter, W., & Verdin, E. (2001). Human HDAC7 histone deacetylase activity is associated with HDAC3 in vivo. *The Journal of Biological Chemistry*, **276**, 35826-35835.

Fischle, W., Dequiedt, F., Hendzel, M. J., Guenther, M. G., Lazar, M. A., Voelter, W., & Verdin, E. (2002). Enzymatic activity associated with class II HDACs is dependent on a multiprotein complex containing HDAC3 and SMRT/N-CoR. *Molecular Cell*, **9**, 45-57.

Fitzsimons, H. L. (2015). The Class IIa histone deacetylase HDAC4 and neuronal function: Nuclear nuisance and cytoplasmic stalwart? *Neurobiology of Learning and Memory*, **123**, 149-158.

Fitzsimons, H. L., & Scott, M. J. (2011). Genetic modulation of Rpd3 expression impairs long-term courtship memory in Drosophila. *PloS One*, **6**, e29171.

Fitzsimons, H. L., Schwartz, S., Given, F. M., & Scott, M. J. (2013). The histone deacetylase HDAC4 regulates long-term memory in Drosophila. *Plos One*, **8**, e83903.

Flavell, S. W., & Greenberg, M. E. (2008a). Signaling mechanisms linking neuronal activity to gene expression and plasticity of the nervous system. *Annual Review of Neuroscience*, **31**, 563-590.

Flavell, S. W., Cowan, C. W., Kim, T.-K., Greer, P. L., Lin, Y., Paradis, S., Griffith, E. C., Hu, L. S., Chen, C., & Greenberg, M. E. (2006). Activity-Dependent Regulation of MEF2 Transcription Factors Suppresses Excitatory Synapse Number. *Science*, **311**, 1008-1012.

Flavell, S. W., Kim, T. K., Gray, J. M., Harmin, D. A., Hemberg, M., Hong, E. J., Markenscoff-Papadimitriou, E., Bear, D. M., & Greenberg, M. E. (2008b). Genome-wide analysis of MEF2 transcriptional program reveals synaptic target genes and neuronal activity-dependent polyadenylation site selection. *Neuron*, **60**, 1022–1038.

Flexner, J. B., Flexner, L. B., & Stellar, E. (1963). Memory in mice as affected by intracerebral puromycin. *Science*, **141**, 57-59.

Foglietti, C., Filocamo, G., Cundari, E., De Rinaldis, E., Lahm, A., Cortese, R., & Steinkuhler, C. (2006). Dissecting the biological functions of Drosophila

histone deacetylases by RNA interference and transcriptional profiling. *Journal of Biological Chemistry*, **281**, 17968-17976.

Freeman, M. R., & Doherty, J. (2006). Glial cell biology in Drosophila and vertebrates. *Trends in Neurosciences*, **29**, 82-90.

Fukuda, S., Yamasaki, Y., Iwaki, T., Kawasaki, H., Akieda, S., Fukuchi, N., Tahira, T., & Hayashi, K. (2002). Characterization of the biological functions of a transcription factor, c-mycintron binding protein 1 (MIBP1). *Journal of Biochemistry*, **131**, 349-357.

Fushima, K., & Tsujimura, H. (2007). Precise control of fasciclin II expression is required for adult mushroom body development in Drosophila. *Development, Growth and Differentiation*, **49**, 215-227.

Ganeshina, O., Erdmann, J., Tiberi, S., Vorobyev, M., & Menzel, R. (2012). Depolymerization of actin facilitates memory formation in an insect. *Biology Letters*, **8**, 1023–1027.

Gao, L., Cueto, M. A., Asselbergs, F., & Atadja, P. (2002). Cloning and functional characterization of HDAC11, a novel member of the human histone deacetylase family. *Journal of Biological Chemistry*, **277**, 25748-25755.

Garcia-Alonso, L., Fetter, R. D., & Goodman, C. S. (1996). Genetic analysis of laminin A in Drosophila: extracellular matrix containing laminin A is required for ocellar axon pathfinding. *Development*, **122**, 2611-2621.

Garver, T. D., Ren, Q., Tuvia, S., & Bennett, V. (1997). Tyrosine phosphorylation at a site highly conserved in the l1 family of cell adhesion molecules abolishes ankyrin binding and increases lateral mobility of neurofascin. *The Journal of Cell Biology*, **137**, 703–714.

Giralt, A., Puigdellívol, M., Carretón, O., Paoletti, P., Valero, J., Parra-Damas, A., Saura, C. A., Alberch, J., & Ginés, S. (2012). Long-term memory deficits in Huntington's disease are associated with reduced CBP histone acetylase activity. *Human Molecular Genetics*, **21**, 1203-1216.

Glozak, M. A., Sengupta, N., Zhang, X., & Seto, E. (2005). Acetylation and deacetylation of non-histone proteins. *Gene*, **363**, 15-23.

Godenschwege, T. A., Kristiansen, L. V., Uthaman, S. B., Hortsch, M., & Murphey, R. K. (2006). A conserved role for Drosophila Neuroglian and human L1-CAM in central-synapse formation. *Current Biology*, **16**, 12-23.

Goellner, B. & Aberle, H. (2012). The synaptic cytoskeleton in development and disease. *Developmental Neurobiology*, **72**, 111–125.

González, E. & Joly, S. (2013). Impact of RNA-seq attributes on false positive rates in differential expression analysis of de novo assembled transcriptomes. *BMC Research Notes*, **6**, 503.

Goossens, T., Kang, Y. Y., Wuytens, G., Zimmermann, P., Callaerts-Vegh, Z., Pollarolo, G., Islam, R., Hortsch, M., & Callaerts, P. (2011). The Drosophila L1CAM homolog Neuroglian signals through distinct pathways to control different aspects of mushroom body axon development. *Development*, **138**, 1595-1605.

Gräff, J., & Tsai, L. H. (2013). The potential of HDAC inhibitors as cognitive enhancers. *Annual Review of Pharmacology and Toxicology*, **53**, 311-330.

Grégoire, S., & Yang, X.-J. (2005). Association with class IIa histone deacetylases upregulates the sumoylation of MEF2 transcription factors. *Molecular and Cellular Biology*, **25**, 2273-2287.

Grégoire, S., Tremblay, A. M., Xiao, L., Yang, Q., Ma, K., Nie, J., Mao, Z., Wu, Z., Giguère, V., & Yang, X. J. (2005). Control of MEF2 transcriptional activity by coordinated phosphorylation and sumoylation. *The Journal of Biological Chemistry*, **281**, 4423-4433.

Gregoretti, I. V., Lee, Y. M., & Goodson, H. V. (2004). Molecular evolution of the histone deacetylase family: functional implications of phylogenetic analysis. Journal of *Molecular Biology*, **338**, 17-31.

Grove, M., Demyanenko, G., Echarri, A., Zipfel, P. A., Quiroz, M. E., Rodriguiz, R. M., Playford, M., Martensen, S. A., Robinson, M. R., Wetsel, W. C., Maness, P. F., & Pendergast, A. M. (2004). Abi2-deficient mice exhibit defective cell migration, aberrant dendritic spine morphogenesis, and deficits in learning and memory. *Molecular and Cellular Biology*, **24**, 10905-10922.

Grozinger, C. M. & Schreiber, S. L. (2000). Regulation of histone deacetylase 4 and 5 and transcriptional activity by 14-3- 3-dependent cellular localization. *Proceedings of the National Academy of Sciences of the United States of America*, **97**, 7835-7840.

Grozinger, C. M., Hassig, C. A., & Schreiber, S. L. (1999). Three proteins define a class of human histone deacetylases related to yeast Hda1p. *Proceedings*

of the National Academy of Sciences of the United States of America, **96**, 4868-4873.

Guan, J. S., Haggarty, S. J., Giacometti, E., Dannenberg, J. H., Joseph, N., Gao, J., Nieland, T. J., Zhou, Y., Wang, X., Mazitschek, R., Bradner, J. E., DePinho, R. A., Jaenisch, R., & Tsai, L. H. (2009). HDAC2 negatively regulates memory formation and synaptic plasticity. *Nature*, **459**, 55-60.

Guan, Z., Saraswati, S., Adolfsen, B., & Littleton, J. T. (2005). Genome-wide transcriptional changes associated with enhanced activity in the drosophila nervous system. *Neuron*. **48**, 91–107.

Guenther, M. G., Barak, O., & Lazar, M. A. (2001). The SMRT and N-CoR Corepressors Are Activating Cofactors for Histone Deacetylase 3. *Molecular and Cellular Biology*, **21**, 6091-6101.

Guerra de Souza, A. C., Prediger, R. D. & Cimarosti, H. (2016), SUMO-regulated mitochondrial function in Parkinson's disease. *Journal of Neurochemistry*, **137**, 673–686.

Guven-Ozkan, T., & Davis, R. L. (2014). Functional neuroanatomy of Drosophila olfactory memory formation. *Learning & Memory*, **21**, 519–526.

Haggarty, S. J., & Tsai, L. H. (2011). Probing the role of HDACs and mechanisms of chromatin-mediated neuroplasticity. *Neurobiology of Learning and Memory*, **96**, 41-52.

Hall, J. (1994). The mating of a fly. *Science*, **264**, 1702-1714.

Han, P. L., Levin, L. R., Reed, R. R., & Davis, R. L. (1992). Preferential expression of the Drosophila rutabaga gene in mushroom bodies, neural centers for learning in insects. *Neuron*, **9**, 619--627.

Hardeland, R. (1971). Lighting conditions and mating behavior in Drosophila. The *American Naturalist*, **105**, 198-200.

Hawkins, R. D., Kandel, E. R., & Bailey, C. H. (2006). Molecular mechanisms of memory storage in Aplysia. *The Biological Bulletin*, **210**, 174-191.

Hedstrom, K. L., Ogawa, Y., & Rasband, M. N. (2008). AnkyrinG is required for maintenance of the axon initial segment and neuronal polarity. *Journal of Cell Biology*, **183**, 635-640.

Heisenberg, M., Borst, A., Wagner, S., & Byers, D. (1985). Drosophila mushroom body mutants are deficient in olfactory learning. *Journal of Neurogenetics*, **2**, 1–30.

Henikoff, S; Henikoff, J. G. (1992). Amino acid substitution matrices from protein blocks. *Proceedings of the National Academy of Sciences of the United States of America*, 89, 10915-10919.

Ho, V. M., Lee, J. A., & Martin, K. C. (2011). The cell biology of synaptic plasticity. *Science*, **334**, 623-628.

Hortsch, M. (2000). Structural and functional evolution of the L1 family: are four adhesion molecules better than one? *Molecular and Cellualr Neurosciences*, **15**, 1-10.

Hortsch, M., Diahann, H., Jyoti, D. M., Sherry, C., Jason, F., Gregory, J., & Dubreuil, R. R. (1998). Structural requirements for outside-in and inside-out signaling by Drosophila neuroglian, a member of the l1 family of cell adhesion molecules. *The Journal of Cell Biology*, **142**, 251–261.

Hortsch, M., Nagaraj, K., & Godenschwege, T. A. (2009). The interaction between L1-type proteins and ankyrins--a master switch for L1-type CAM function. *Cellular & Molecular Biology Letters*, **14**, 57-69.

Hortsch, M., Paisley, K. L., Tian, M. Z., Qian, M., Bouley, M., & Chandler, R. (2002). The axonal localization of large Drosophila ankyrin2 protein isoforms is essential for neuronal functionality. *Molecular and Cellular Neuroscience*, **20**, 43-55.

Hotulainen, P., & Hoogenraad, C. C. (2010). Actin in dendritic spines: connecting dynamics to function. *Journal of Cell Biology*, **189**, 619-629.

Huang, E. Y., Zhang, J., Miska, E. A., Guenther, M. G., Kouzarides, T., & Lazar, M. A. (2000). Nuclear receptor corepressors partner with class II histone deacetylases in a Sin3-independent repression pathway. *Genes and Development*, **14**, 45-54.

Hummel, T., Krukkert, K., Roos, J., Davis, G., & Klämbt, C. (2000). Drosophila Futsch/22C10 is a MAP1B-like protein required for dendritic and axonal development. *Neuron*, **26**, 357-370.

Ichinose, T., Aso, Y., Yamagata, N., Abe, A., Rubin, G. M., & Tanimoto, H. (2015). Reward signal in a recurrent circuit drives appetitive long-term memory formation. *eLife*, **4**, e10719.

Iqbal, Z., Vandeweyer, G., van der Voet, M., Waryah, A. M., Zahoor, M. Y., Besseling, J. A., Roca, L. T., Vulto-van Silfhout, A. T., Nijhof, B., Kramer, J. M., Van der Aa, N., Ansar, M., Peeters, H., Helsmoortel, C., Gilissen,

C., Vissers, L. E., Veltman, J. A., de Brouwer, A. P., Frank Kooy, R., Riazuddin, S., Schenck, A., van Bokhoven, H., & Rooms, L. (2013). Homozygous and heterozygous disruptions of ANK3: at the crossroads of neurodevelopmental and psychiatric disorders. *Human Molecular Genetics*, **22**, 1960-1970.

Ito, K., Awano, W., Suzuki, K., Hiromi, Y., & Yamamoto, D. (1997). The Drosophila mushroom body is a quadruple structure of clonal units each of which contains a virtually identical set of neurones and glial cells. *Development*, **124**, 761-771.

Ito, K., Suzuki, K., Estes, P., Ramaswami, M., Yamamoto, D., & Strausfeld, N. J. (1998). The organization of extrinsic neurons and their implications in the functional roles of the mushroom bodies in Drosophila melanogaster Meigen. *Learning & Memory*, **5**, 52–77.

Jackson, G. R. (2008). Guide to understanding Drosophila models of neurodegenerative diseases. *PLoS Biology*, **6**, e53.

Jan, Y.-N., & Jan, L. Y. (2010). Branching out: mechanisms of dendritic arborization. *Nature Reviews Neuroscience*, **11**, 316–328.

Jones, S. L., Korobova, F., & Svitkina, T. (2014). Axon initial segment cytoskeleton comprises a multiprotein submembranous coat containing sparse actin filaments. *Journal of Cell Biology*, **205**, 67-81.

Kandel, E. R. (2001). The molecular biology of memory storage: a dialogue between genes and synapses. *Science*, **294**, 1030-1038.

Kandel, E. R. (2004). The Molecular biology of memory storage: a dialog between genes and synapses. *Bioscience Reports*, **24**, 475-522.

Kandel, E. R. (2012). The molecular biology of memory: cAMP, PKA, CRE, CREB-1, CREB-2, and CPEB. *Molecular Brain*, **5**, 14.

Kandel, E. R., & Spencer, W. A. (1968). Cellular neurophysiological approaches in the study of learning. *Physiological Review*, **48**, 65-134.

Kao, H. Y., Downes, M., Ordentlich, P. & Evans, R. M. (2000). Isolation of a novel histone deacetylase reveals that class I and class II deacetylases promote SMRT-mediated repression. *Genes and Development*, **14**, 55–66.

Kao, H. Y., Verdel, A., Tsai, C. C., Simon, C., Juguilon, H., & Khochbin, S. (2001). Mechanism for nucleocytoplasmic shuttling of histone deacetylase 7. *The Journal of Biological Chemistry*, **276**, 47496-47507.

Kaplow, M. E., Mannava, L. J., Pimentel, A. C., Fermin, H. A., Hyatt, V. J., Lee, J. J., & Venkatesh, T. R. (2009). A genetic modifier screen identifies multiple genes that interact with drosophila rap/fzr and suggests novel cellular roles. Journal of Neurogenetics, 21, 105-151.

Katsuki, T., Ailani, D., Hiramoto, M., & Hiromi, Y. (2009). Intra-axonal patterning: intrinsic compartmentalization of the axonal membrane in Drosophila neurons. *Neuron*, **64**, 188-199.

Keleman, K., Kruttner, S., Alenius, M., & Dickson, B. J. (2007). Function of the Drosophila CPEB protein Orb2 in long-term courtship memory. *Nature Neuroscience*, **10**, 1587-1593.

Keleman, K., Vrontou, E., Krüttner, S., Yu, J. Y., Kurtovic-Kozaric, A., & Dickson, B. J. (2012). Dopamine neurons modulate pheromone responses in Drosophila courtship learning. *Nature*, **489**, 145-149.

Kim, H. F., Ghazizadeh, A., & Hikosaka, O. (2014). Separate groups of dopamine neurons innervate caudate head and tail encoding flexible and stable value memories. *Frontiers in Neuroanatomy*, **8**, 120.

Kim, M. S., Akhtar, M. W., Adachi, M., Mahgoub, M., Bassel-Duby, R., Kavalali, E. T., Olson, E. N., & Monteggia, L. M. (2012). An essential role for histone deacetylase 4 in synaptic plasticity and memory formation. *Journal of Neuroscience*, **32**, 10879-10886.

Kim, T., Park, J. K., Kim, H. –J., Chung, J.-H., & Kim, J. W. (2010). Association of histone deacetylase genes with schizophrenia in Korean population. *Psychiatry Research*, **178**, 266-269.

Kim, Y.-C., Lee, H.-G., & Han, K.-A. (2007). D1 Dopamine Receptor dDA1 is required in the mushroom body neurons for aversive and appetitive learning in Drosophila. *The Journal of Neuroscience*, **27**, 7640-7647.

Kirsh, O., Seeler, J. S., Pichler, A., Gast, A., Müller, S., Miska, E., Mathieu, M., Harel-Bellan, A., Kouzarides, T., Melchior, F., & Dejean, A. (2002). The SUMO E3 ligase RanBP2 promotes modification of the HDAC4 deacetylase. *The EMBO Journal*, **21**, 2682-2691.

Kitamoto, T. (2001). Conditional modification of behavior in Drosophila by targeted expression of a temperature-sensitive shibire allele in defined neurons. *Journal of Neurobiology*, **47**, 81-92.

Kleefstra, T., Schenck, A., Kramer, J. M., & van Bokhoven, H. (2014). The genetics of cognitive epigenetics. *Neuropharmacology*, **80**, 83-94.

Koch, I., Schwarz, H., Beuchle, D., Goellner, B., Langegger, M., & Aberle, H. (2008). Drosophila ankyrin 2 is required for synaptic stability. *Neuron*, **58**, 210-222.

Kole, M. H., Ilschner, S. U., Kampa, B. M., Williams, S. R., Ruben, P. C., & Stuart, G. J. (2008). Action potential generation requires a high sodium channel density in the axon initial segment. *Nature Neuroscience*, **11**, 178-186.

Kordeli, E., Lambert, S., & Bennett, V. (1995). AnkyrinG. A new ankyrin gene with neural-specific isoforms localized at the axonal initial segment and node of Ranvier. *The Journal of Biological Chemistry*, **270**, 2352-2359.

Korzus, E., Rosenfeld, M. G., Mayford, M. (2004). CBP histone acetyltransferase activity is a critical component of memory consolidation, *Neuron*, **42**, 961-972.

Koushika, S. P., Lisbin, M. J., & White, K. (1996). ELAV, a Drosophila neuron-specific protein, mediates the generation of an alternatively spliced neural protein isoform. *Current Biology*, **6**, 1634-1641.

Krucker, T., Siggins, G. R., & Halpain, S. (2000). Dynamic actin filaments are required for stable long-term potentiation (LTP) in area CA1 of the hippocampus. *Proceedings of the National Academy of Sciences*, **97**, 6856-6861.

Krumova, P., & Weishaupt, J. H. (2013). Sumoylation in neurodegenerative diseases. *Cellular and Molecular Life Sciences*, **70**, 2123-2138.

Kudumala, S., Freund, J., Hortsch, M., & Godenschwege, T. A. (2013). Differential effects of human L1CAM mutations on complementing guidance and synaptic defects in Drosophila melanogaster. *PloS One*, **8**, e76974.

Kuhn, T. B., Schmidt, M. F., & Kater, S. B. (1995). Laminin and fibronectin guideposts signal sustained but opposite effects to passing growth cones. *Neuron*, **14**, 275-285.

Kuja-Panula, J., Kiiltomäki, M., Yamashiro, T., Rouhiainen, A., & Rauvala, H. (2003). AMIGO, a transmembrane protein implicated in axon tract development, defines a novel protein family with leucine-rich repeats. *The Journal of Cell Biology*, **160**, 963-973.

Kunz, T., Kraft, K. F., Technau, G. M., & Urbach, R. (2012). Origin of Drosophila mushroom body neuroblasts and generation of divergent embryonic lineages. *Development*, **139**, 2510-2522.

Kurusu, M., & Zinn, K. (2008). Receptor tyrosine phosphatases regulate birth order-dependent axonal fasciculation and midline repulsion during development of the Drosophila mushroom body. *Molecular and Cellular Neuroscience*, **38**, 53-65.

Lahm, A., Paolini, C., Pallaoro, M., Nardi, M. C., Jones, P., Neddermann, P., Sambucini, S., Bottomley, M. J., Lo Surdo, P., Carfí, A., Koch, U., De Francesco, R., Steinkühler, C., & Gallinari, P. (2007). Unraveling the hidden catalytic activity of vertebrate class IIa histone deacetylases. *Proceedings of the National Academy of Sciences*, **104**, 17335-17340.

Lai, H. C., & Jan, L. Y. (2006). The distribution and targeting of neuronal voltage-gated ion channels. *Nature Reviews: Neuroscience*, **7**, 548-562.

Lamprecht, R. (2011). The roles of the actin cytoskeleton in fear memory formation. *Frontiers in Behavioral Neuroscience*, **5**, 39.

Lamprecht, R. (2014). The actin cytoskeleton in memory formation, *Progress in Neurobiology*, **117**, 1-19.

Lamprecht, R., & LeDoux, J. (2004). Structural plasticity and memory. *Nature Reviews Neuroscience*, **5**, 45-54.

Lattal, K. Matthew; Barrett, Ruth M.; Wood, Marcelo A. (2007). Systemic or intrahippocampal delivery of histone deacetylase inhibitors facilitates fear extinction. *Behavioral Neuroscience*, **121**, 1125-1131.

Lee, T., Lee, A., & Luo, L. (1999). Development of the Drosophila mushroom bodies: sequential generation of three distinct types of neurons from a neuroblast. *Development*, **126**, 4065-4076.

Leiss, F., Groh, C., Butcher, N. J., Meinertzhagen, I. A., & Tavosanis, G. (2009a). Synaptic organization in the adult Drosophila mushroom body calyx. *The Journal of Comparative Neurology*, **517**, 808-824.

Leterrier, C. & Dargent, B. (2014). No Pasaran! Role of the axon initial segment in the regulation of protein transport and the maintenance of axonal identity. *Semininars in Cell & Developmental Biology*, **27**, 44-51.

Letourneau, P. C. (2009). Actin in axons: stable scaffolds and dynamic filaments. *Results and Problems in Cell Differentiation*, **48**, 65-90.

Leussis, M. P., Madison, J. M., & Petryshen, T. L. (2012). Ankyrin 3: genetic association with bipolar disorder and relevance to disease pathophysiology. *Biology of Mood & Anxiety Disorders*, **2**, 1-13.

Levenson, J. M., & Sweatt, J. D. (2005). Epigenetic mechanisms in memory formation. *Nature Reviews: Neuroscience*, **6**, 108-118.

Levenson, J. M., O'Riordan, K. J., Brown, K. D., Trinh, M. A., Molfese, D. L., & Sweatt, J. D. (2004). Regulation of histone acetylation during memory formation in the hippocampus. *Journal of Biological Chemistry*, **279**, 40545-40559.

Li, J., Chen, J., Ricupero, C. L., Hart, R. P., Schwartz, M. S., Kusnecov, A., & Herrup, K. (2012). Nuclear accumulation of HDAC4 in ATM deficiency promotes neurodegeneration in ataxia telangiectasia. *Nature Medicine*, **18**, 783-790.

Li, X., Song, S., Liu, Y., Ko, S. H., & Kao, H. Y. (2004). Phosphorylation of the histone deacetylase 7 modulates its stability and association with 14-3-3 proteins. *The Journal of Biological Chemistry*, **279**, 34201-34208.

Liu, Y., Zhang, Y., & Wang, J. H. (2014). Crystal structure of human Ankyrin G death domain. *Proteins*, **82**, 3476-3482.

Livak, K. J., & Schmittgen, T. D. (2001). Analysis of relative gene expression data using real-time quantitative PCR and the 2(-Delta Delta C(T)) Method. *Methods*, **25**, 402-408.

Llères, D., Swift, S. & Lamond, A. I. (2007). Detecting protein-protein interactions in vivo with fret using multiphoton fluorescence lifetime imaging microscopy (FLIM). *Current Protocols in Cytometry*, **42**, 12.10.1–12.10.19.

Long, X., & Griffith, L. C. (2000) Identification and characterization of a SUMO-1 conjugation system that modifies neuronal calcium/calmodulin-dependent protein kinase II in Drosophila melanogaster. *The Journal of Biological Chemistry*, **275**, 40765–40776.

Lucio-Eterovic, A. K., Cortez, M. A., Valera, E. T., Motta, F. J., Queiroz, R. G., Machado, H. R., Carlotti, C. G., Neder, L., Scrideli, C. A., & Tone, L. G. (2008). Differential expression of 12 histone deacetylase (HDAC) genes in astrocytomas and normal brain tissue: class II and IV are hypoexpressed in glioblastomas. *BMC Cancer*, **8**, 1-10.

Luna, E., & Rolls, M. (2010). Diffusion barriers in Drosophila neuron. *The Penn State McNair Journal*, **16**, 65-73.

Ma, J., & Weake, V. M. (2014). Affinity-based isolation of tagged nuclei from Drosophila tissues for gene expression analysis. *Journal of Visualized Experiments*, **85**, 51418.

Mackay, T. F., & Anholt, R. R. (2006). Of flies and man: Drosophila as a model for human complex traits. *Annual Review of Genomics and Hum Genetics*, **7**, 339-367.

MacLaren, C. M., Evans, T. A., Alvarado, D., & Duffy J. B. (2004). Comparative analysis of the kekkon molecules, related members of the LIG superfamily. *Development, Genes and Evolution*, **214**, 360–366.

Maiya, R., Lee, S., Berger, K. H., Kong, E. C., Slawson, J. B., Griffith, L. C., Takamiya, K., Huganir, R. L., Margolis, & B., Heberlein, U. (2012). DlgS97/SAP97, a neuronal isoform of discs large, regulates ethanol tolerance. *Plos One*, **11**, e48967.

Majdzadeh, N., Morrison, B. E., & D'Mello, S. R. (2008). Class II HDACs in the regulation of neurodegeneration. *Frontiers in Bioscience*, **13**, 1072-1082.

Mao, Z., Bonni, A., Xia, F., Nadal-Vicens, M., & Greenberg, M. E. (1999). Neuronal activity-dependent cell survival mediated by transcription factor MEF2. *Science*, **286**, 785-790.

Marinesco, S., & Carew, T. J. (2002). Serotonin release evoked by tail nerve stimulation in the CNS of Aplysia: characterization and relationship to heterosynaptic plasticity. *The Journal of Neuroscience*, **22**, 2299-2312.

Martin, S., Wilkinson, K. A., Nishimune, A., & Henley, J. M. (2007). Emerging extranuclear roles of protein SUMOylation in neuronal function and dysfunction. *Nature Reviews Neuroscience*, **8**, 948-959.

Martin, V., Mrkusich, E., Steinel, M. C., Rice, J., Merritt, D. J., & Whitington, P. M. (2008). The L1-type cell adhesion molecule Neuroglian is necessary for maintenance of sensory axon advance in the Drosophila embryo. *Neural Development*, **3**, 10.

Masuda-Nakagawa, L. M., Awasaki, T., Ito, K., O'Kane, C. J. (2010). Targeting expression to projection neurons that innervate specific mushroom body calyx and antennal lobe glomeruli in larval Drosophila. *Gene Expression Patterns*, **10**, 328-337.

Mattaliano, M. D., Montana, E. S., Parisky, K. M., Littleton, J. T., & Griffith, L. C. (2007). The Drosophila ARC homolog regulates behavioral responses to starvation. *Molecular and Cellular Neurosciences*, **36**, 211–221.

Matus, A. (2000). Actin-based plasticity in dendritic spines. *Science*, **290**, 754-758.

Mayford, M., Siegelbaum, S. A., & Kandel, E. R. (2012). Synapses and memory storage. *Cold Spring Harbor Perspectives in Biology*, **a005751**.

McBride, S. M. J., Giuliani G., Choi, C., Krause, P., Correale, D., Watson, K., Baker, G., & Siwicki, K. K. (1999). Mushroom body ablation impairs short-term memory and long-term memory of courtship conditioning in Drosophila melanogaster. *Neuron*, 24, 967-977.

McGuire, S. E., Mao, Z., & Davis, L. R. (2004). Spatiotemporal gene expression targeting with the TARGET and gene-switch systems in Drosophila. *Signal Transduction Knowledge Environment*, **220**, p16.

McKinsey, T. A., Kuwahara, K., Bezprozvannaya, S., & Olson, E. N. (2006). Class II histone deacetylases confer signal responsiveness to the ankyrin-repeat proteins ANKRA2 and RFXANK. *Molecular Biology of the Cell*, **17**, 438–447.

McKinsey, T.A., Zhang, C.L., & Olson, E.N. (2000b). Activation of the myocyte enhancer factor-2 transcription factor by calcium/calmodulin-dependent protein kinase-stimulated binding of 14-3-3 to histone deacetylase 5. *Proceedings of the National Academy of Sciences of the United States of America*, **97**, 14400–14405.

McKinsey, T.A., Zhang, C.L., & Olson, E.N. (2001). Identification of a signal responsive nuclear export sequence in class II histone deacetylases. *Molecular and Cellular Biology*, **21**, 6312–6321.

McKinsey, T.A., Zhang, C.L., Lu, J., & Olson, E.N. (2000a). Signal-dependent nuclear export of a histone deacetylase regulates muscle differentiation. *Nature*, **408**, 106–111.

McQuown, S. C., Barrett, R. M., Matheos, D. P., Post, R. J., Rogge, G. A., Alenghat, T., Mullican, S. E., Jones, S., Rusche, J. R., Lazar, M. A., & Wood, M. A. (2011b). HDAC3 is a critical negative regulator of long-term memory formation. *Journal of Neuroscience*, **31**, 764-774.

Mehren, J. E., Ejima, A., & Griffith, L. C. (2004). Unconventional sex: fresh approaches to courtship learning. *Current Opinion in Neurobiology*, **14**, 745-750.

Meinertzhagen, I. A., Emsley, J. G. & Sun, X. J. (1998), Developmental anatomy of the Drosophila brain: neuroanatomy is gene expression. *Journal of. Comparative Neurology*, **402**, 1–9.

Meulmeester, E., & Melchior, F. (2008). Cell biology: SUMO. *Nature*, **452**, 709-711.

Mielcarek, M., Landles, C., Weiss, A., Bradaia, A., Seredenina, T., Inuabasi, L., Osborne, G. F., Wadel, K., Touller, C., Butler, R., Robertson, J., Franklin, S. A., Smith, D. L., Park, L., Marks, P. A., Wanker, E. E., Olson, E. N., Luthi-Carter, R., van der Putten, H., Beaumont, V., & Bates, G. P. (2013a). HDAC4 reduction: a novel therapeutic strategy to target cytoplasmic huntingtin and ameliorate neurodegeneration. *PLoS Biology*, **11**, e1001717.

Mielcarek, M., Seredenina, T., Stokes, M. P., Osborne, G. F., Landles, C., Inuabasi, L., Franklin, S. A., Silva, J. C., Luthi-Carter, R., Beaumont, V., & Bates, G. P. (2013b). HDAC4 does not act as a protein deacetylase in the postnatal murine brain in vivo. *PloS One*, **8**, e80849.

Mielcarek, M., Zielonka, D., Carnemolla, A., Marcinkowski, J. T., & Guidez, F. (2015). HDAC4 as a potential therapeutic target in neurodegenerative diseases: a summary of recent achievements. *Frontiers in Cellular Neuroscience*, **9**, 42.

Miki, Y. H., & Satoshi, G. (2013). In vivo RNAi-based screens: studies in model organisms. *Genes*, **4**, 646-665.

Ministry of Health. 2013. New Zealand Framework for Dementia Care. Wellington: Ministry of Health (www.health.govt.nz).

Miska, E. A., Karlsson, C., Langley, E., Nielsen, S. J., Pines, J., & Kouzarides, T. (1999). HDAC4 deacetylase associates with and represses the MEF2 transcription factor. *The EMBO Journal*, **18**, 5099-5107.

Miska, E. A., Langley, E., Wolf, D., Karlsson, C., Pines, J., & Kouzarides, T. (2001). Differential localization of HDAC4 orchestrates muscle differentiation. *Nucleic Acids Research*, **29**, 3439–3447.

Mohler, P. J., Gramolini, A. O., & Bennett, V. (2002). Ankyrins. *Journal of Cell Science*, **115**, 1565-1566.

Mohler, P. J., Splawski, I., Napolitano, C., Bottelli, G., Sharpe, L., Timothy, K., Priori, S. G., Keating, M. T., & Bennett, V. (2004). A cardiac arrhythmia syndrome caused by loss of ankyrin-B function. *Proceedings of the National Academy of Sciences of the United States of America*, **101**, 9137–9142.

Moreau-Fauvarque, C., Taillebourg, E., Boissoneau, E., Mesnard, J., & Dura, J. M. (1998). The receptor tyrosine kinase gene linotte is required for neuronal pathway selection in the Drosophila mushroom bodies. *Mechanisms of Development*, **78**, 47-61.

Morin, J. P., Cerón-Solano, G., Velázquez-Campos, G., Pacheco-López, G., Bermúdez-Rattoni, F., & Díaz-Cintra, S. (2016). Spatial memory impairment is associated with intraneural amyloid-β immunoreactivity and dysfunctional arc Expression in the hippocampal-CA3 region of a transgenic mouse model of Alzheimer's Disease. *Journal of Alzheimer's Disease*, **51**, 69-79.

Morris, M. J., & Monteggia, L. M. (2013). Unique functional roles for class I and class II histone deacetylases in central nervous system development and function. *International Journal of Developmental Neuroscience*, **31**, 370-381.

Morrison, B. E., Majdzadeh, N., & D'Mello, S. R. (2007). Histone deacetylases: focus on the nervous system. *Cellular and Molecular Life Sciences*, **64**, 2258-2269.

Mortazavi, A, Williams, B. A., McCue, K., Schaeffer, L., & Wold, B. (2008). Mapping and quantifying mammalian transcriptomes by RNA-Seq. Nature Methods, 5, 621-628.

Mory, A., Dagan, E., Illi, B., Duquesnoy, P., Mordechai, S., Shahor, I., Romani, S., Hawash-Moustafa, N., Mandel, H., Valente, E. M., Amselem, S., & Gershoni-Baruch, R. (2012). A nonsense mutation in the human homolog of Drosophila rogdi causes Kohlschutter–Tonz syndrome. *American Journal of Human Genetics*, **90**, 708–714.

Murali, T., Pacifico, S., Yu, J., Guest, S., Roberts, G. G., & Finley, R. L. (2011). DroID 2011: a comprehensive, integrated resource for protein,

transcription factor, RNA and gene interactions for Drosophila. *Nucleic Acids Research*, **39**, D736–D743.

Musacchio, M. & Perrimon, N. (1996). The Drosophila kekkon genes: novel members of both the leucine-rich repeat and immunoglobulin superfamilies expressed in the CNS. *Developmental Biology*, **178**, 63–76.

Nakagawa, T., & Guarente, L. (2011). Sirtuins at a glance. *Journal of Cell Science*, **124**, 833-838.

Nakagawa, Y., Kuwahara, K., Harada, M., Takahashi, N., Yasuno, S., Adachi, Y., Kawakami, R., Nakanishi, M., Tanimoto, K., Usami, S., Kinoshita, H., Saito, Y., & Nakao, K. (2006). Class II HDACs mediate CaMK-dependent signaling to NRSF in ventricular myocytes. *Journal of Molecular and Cellular Cardiology*, **41**, 1010-1022.

Nardone, S., Sams, D. S., Reuveni, E., Getselter, D., Oron, O., Karpuj, M., & Elliott, E. (2014). DNA methylation analysis of the autistic brain reveals multiple dysregulated biological pathways. *Translational Psychiatry*, **4**, e433.

Needham, L. K., Thelen, K., & Maness, P. F. (2001) Cytoplasmic domain mutations of the L1 cell adhesion molecule reduce L1-ankyrin interactions. *The Journal of Neruoscience*, **21**, 1490–1500.

Neuner, S. M., Wilmotta, L. A., Hoffmannb, B. R., Mozhuic, K., & Kaczorowskia, C. C. (2016). Hippocampal proteomics defines pathways associated with memory decline and resilience in normal aging and Alzheimer's disease mouse models. *Behavioural Brain Research*, article in press.

Ni, J. Q., Liu, L. P., Binari, R., Hardy, R., Shim, H. S., Cavallaro, A., Booker, M., Pfeiffer, B. D., Markstein, M., Wang, H., Villalta, C., Laverty, T. R., Perkins, L. A., & Perrimon, N. (2009). A Drosophila resource of transgenic RNAi lines for neurogenetics. *Genetics*, **182**, 1089-1100.

Nie, J., Xu, C., Jin, J., Aka, J. A., Tempel, W., Nguyen, V., You, L., Weist, R., Min, J., Pawson, T., & Yang, X. J. (2015). Ankyrin repeats of ANKRA2 recognize a PxLPxL motif on the 3M syndrome protein CCDC8. *Structure*, **23**, 700-712.

Nighorn, A., Healy, J. M., & Davis, R. L. (1991). The cyclic AMP phosphodiesterase encoded by the Drosophila dunce gene is concentrated in the mushroom body neuropil. *Neuron*, **6**, 455–467.

Ogawa, Y., & Rasband, M. N. (2008). The functional organization and assembly of the axon initial segment, *Current Opinion in Neurobiology*, **18**, 307-313.

Ojelade, S. A., Acevedo, S. F., & Rothenfluh, A. (2013). The role of the actin cytoskeleton in regulating drosophila behavior. *Reviews in the Neurosciences*, **24**, 471–484.

Okano, H., Hirano, T., & Balaban, E. (2000). Learning and memory. *Proceedings of the National Academy of Sciences of the United States of America*, **97**, 12403–12404.

Otto, E., Kunimoto, M., McLaughlin, T., & Bennet, V. (1991). Isolation and characterization of cDNAs encoding human brain ankyrins reveal a family of alternatively spliced genes. *The Journal of Cell Biology*, **114**, 241–253.

Pandey, U. B., & Nichols, C. D. (2011). Human disease models in Drosophila melanogaster and the role of the fly in therapeutic drug discovery. *Pharmacological Reviews*, **63**, 411-436.

Peixoto, L., & Abel, T. (2013). The role of histone acetylation in memory formation and cognitive impairments. *Neuropsychopharmacology*, **38**, 62-76.

Penney, J., & Tsai, L. H. (2014). Histone deacetylases in memory and cognition. *Science Signaling*, **7**, re12.

Pérez-Pérez, J. M., Candela, H., & Micol, J. L. (2009). Understanding synergy in genetic interactions. *Trends in Genetics*, **25**, 368-376.

Perrimon, N., Ni, J.-Q., & Perkins, L. (2010). In vivo RNAi: today and tomorrow. *Cold Spring Harbor Perspectives in Biology*, **2**, a003640.

Perttunen, V., & Erkkilä, H. (1952). Humidity reaction in Drosophila melanogaster. *Nature*, **169**, 278-279.

Pfeiffer, K., & Homberg, U. (2014). Organization and functional roles of the central complex in the insect brain. *Annual Review of Entomology*, **59**, 165-184.

Phelps, C. B., & Brand, A. H. (1998). Ectopic gene expression in Drosophila using GAL4 system. *Methods*, **14**, 367-379.

Pielage, J., Cheng, L., Fetter, R. D., Carlton, P. M., Sedat, J. W., & Davis, G. W. (2008). A presynaptic giant ankyrin stabilizes the NMJ through regulation of presynaptic microtubules and transsynaptic cell adhesion. *Neuron*, **58**, 195-209.

Pielage, J., Fetter, R. D., & Davis, G. W. (2006). A postsynaptic spectrin scaffold defines active zone size, spacing, and efficacy at the Drosophila neuromuscular junction. *Journal of Cell Biology*, **175**, 491-503.

Pitman, J. L., DasGupta, S., Krashes, M. J., Leung, B., Perrat, P. N., & Waddell, S. (2009). There are many ways to train a fly. *Fly*, **3**, 3.

Prince, M., Wimo, A., Guerchet, M., Ali, G-C., Wu, Y-T., & Prina, M., (2015). World Alzheimer Report 2015. The global impact of dementia. An analysis of prevalence, incidence, cost and trends. London, Alzheimer's Disease International.

Quinn, W. G., Harris, W. A., & Benzer, S. (1974). Conditioned behavior in Drosophila melanogaster. *Proceedings of the National Academy of Sciences of the United States of America*, **71**, 708–712.

Rasband, M. N. (2010). The axon initial segment and the maintenance of neuronal polarity. *Nature Reviews: Neuroscience*, **11**, 552-562.

Reza, M. A., Mhatre, S. D., Morrison, J. C., Utreja, S., Saunders, A. J., Breen, D. E., & Marenda, D. R. (2013). Automated analysis of courtship suppression learning and memory in Drosophila melanogaster. *Fly (Austin)*, **7**, 105-111.

Rieger, D., Fraunholz, C., Popp, J., Bichler, D., Dittmann, R., & Helfrich-Förster, C. (2007). The fruit fly Drosophila melanogaster favors dim light and times its activity peaks to early dawn and late dusk. *Journal of Biological Rhythms*, **22**, 387-399.

Riemensperger, T., Kittel, R. J., & Fiala, A. (2016). Optogenetics in Drosophila Neuroscience. In A. Kianianmomeni (Ed.), Optogenetics: Methods and Protocols (pp. 167-175). New York, NY: Springer New York.

Riquelme, C., Barthel, K. K. B., & Liu, X. (2006). SUMO-1 modification of MEF2A regulates its transcriptional activity. *Journal of Cellular and Molecular Medicine*, **10**, 132–144.

Robinson, S. W., Herzyk, P., Dow, J. A., & Leader, D. P. (2013). FlyAtlas: database of gene expression in the tissues of Drosophila melanogaster. *Nucleic Acids Research*, **41,** 744-750.

Ronan, J. L., Wu, W., & Crabtree, G. R. (2013). From neural development to cognition: unexpected roles for chromatin. *Nature Reviews: Genetics*, **14**, 347-359.

Roth, T. L., & Sweatt, J. D. (2009). Regulation of chromatin structure in memory formation. *Current Opinion in Neurobiology*, **19**, 336-342.

Roth, T. L., Roth, E. D., & Sweatt, J. D. (2010). Epigenetic regulation of genes in learning and memory. *Essays in Biochemistry*, **48**, 263-274.

Ruberto, G., Vassos, E., Lewis, C. M., Tatarelli, R., Girardi, P., Collier, D., & Frangou, S. (2011). The cognitive impact of the ANK3 risk variant for bipolar disorder: initial evidence of selectivity to signal detection during sustained attention. *PloS One*, **6**, e16671.

Rubtsov, A. M., & Lopina, O. D. (2000). Ankyrins. *FEBS Letters*, **482**, 1-5.

Rueckert, E. H., Barker, D., Ruderfer, D., Bergen, S. E., O'Dushlaine, C., Luce, C. J., Sheridan, S. D., Theriault, K. M., Chambert, K., Moran, J., Purcell, S. M., Madison, J. M., Haggarty, S. J., & Sklar, P. (2013). Cis-acting regulation of brain-specific ANK3 gene expression by a genetic variant associated with bipolar disorder. *Molecular Psychiatry*, **18**, 922-929.

Sambrook, J., & Russell, D. W. (2006). Detection of protein-protein interactions using the GST fusion protein pulldown technique. *Cold Spring Harbor Protocols*, **2006**, pdb.prot3757.

Sando, R., 3rd, Gounko, N., Pieraut, S., Liao, L., Yates, J., 3rd, & Maximov, A. (2012). HDAC4 governs a transcriptional program essential for synaptic plasticity and memory. *Cell*, **151**, 821-834.

Sang, T.-K., & Jackson, G. R. (2005). Drosophila models of neurodegenerative disease. *NeuroRx*, **2**, 438–446.

Sankaranarayanan, S., Atluri, P. P., & Ryan, T. A. (2003). Actin has a molecular scaffolding, not propulsive, role in presynaptic function. *Nature Neuroscience*, **6**, 127-135.

Santuccione, A. C., Merlini, M., Shetty, A., Tackenberg, C., Bali, J., Ferretti, M. T., McAfoose, J., Kulic, L., Bernreuther, C., Welt, T., Grimm, J., Glatzel, M., Rajendran, L., Hock, C., & Nitsch, R. M. (2013). Active vaccination with ankyrin G reduces beta-amyloid pathology in APP transgenic mice. *Molecular Psychiatry*, **18**, 358-368.

Sarkar, S. (2013). Drosophila melanogaster: a promising system for neurobiology research. *Advanced Techniques in Biology & Medicine*, **1**, e101.

Schmitt, M., & Matthies, H. (1979). Biochemical studies on histones of the central nervous system. III. Incorporation of [14C]-acetate into the histones of

different rat brain regions during a learning experiment. *Acta Biologica et Medica Germanica*, **38**, 683, 689.

Schossig, A., Wolf, N. I., Fischer, C., Fischer, M., Stocker, G., Pabinger, S., Dander, A., Steiner, B., Tönz, O., Kotzot, D., Haberlandt, E., Amberger, A., Burwinkel, B., Wimmer, K., Fauth, C., Grond-Ginsbach, C., Koch, M. J., Deichmann, A., von Kalle, C., Bartram, C. R., Kohlschütter, A., Trajanoski, Z., & Zschocke, J. (2012). Mutations in ROGDI Cause Kohlschütter-Tönz Syndrome. *The American Journal of Human Genetics*, **90**, 701-707.

Schwaerzel, M., Monastirioti, M., Scholz, H., Friggi-Grelin, F., Birman, S., & Heisenberg, M. (2003). Dopamine and octopamine differentiate between aversive and appetitive olfactory memories in Drosophila. *The Journal of Neuroscience*, **23**, 10495-10502.

Schwartz, S., Truglio, M., Scott, M. J., & Fitzsimons, H. L. (2016). Long-term memory in Drosophila is influenced by the histone deacetylase HDAC4 interacting with the SUMO-conjugating enzyme Ubc9. *Genetics*, **203**, 1249-1264.

Sedgwick, S. G., Smerdon, S. J. (1999). The ankyrin repeat: a diversity of interactions on a common structural framework. *Trends in Biochemical Sciences*, **24**, 311 – 316.

Segal, M. (2005). Dendritic spines and long-term plasticity. *Nature Reviews: Neuroscience*, **6**, 277-284.

Shalizi, A. K., & Bonni, A. (2005). Brawn for brains: the role of MEF2 proteins in the developing nervous system. *Current Topic in Developmental Biology*, **69**, 239-266.

Shen, X., Chen, J., Li, J., Kofler, J., & Herrup, K. (2016). Neurons in vulnerable regions of the Alzheimer's disease brain display reduced ATM signaling. (2016). *Eneuro*, 3, 0124-15.

Shimono, K., Fujimoto, A., Tsuyama, T., Yamamoto-Kochi, M., Sato, M., Hattori, Y., Sugimura, K., Usui, T., Kimura, K.-i., & Uemura, T. (2009). Multidendritic sensory neurons in the adult Drosophila abdomen: origins, dendritic morphology, and segment- and age-dependent programmed cell death. *Neural Development*, **4**, 1-21.

Shuai, Y., Lu, B., Hu, Y., Wang, L., Sun, K., & Zhong, Y. (2010). Forgetting is regulated through rac activity in Drosophila. *Cell*, **140**, 579-589.

Siegel, R. W., & Hall, J. C. (1979). Conditioned responses in courtship behavior of normal and mutant Drosophila. *Proceedings of the National Academy of Sciences of the United States of America*, **76**, 3430–3434.

Siegenthaler, D., Enneking, E. M., Moreno, E., & Pielage, J. (2015). L1CAM/Neuroglian controls the axon-axon interactions establishing layered and lobular mushroom body architecture. *Journal of Cell Biology*, **208**, 1003-1018.

Silverstein, R. A., & Ekwall, K. (2005). Sin3: a flexible regulator of global gene expression and genome stability. *Current Genetics*, **47**, 1-17.

Simon, A. F., Boquet, I., Synguelakis, M. & Preat, T. (1998). The Drosophila putative kinase linotte (derailed) prevents central brain axons from converging on a newly described interhemispheric ring. *Mechanisms of Development*, **76**, 45–55.

Simon, D. J., Madison, J. M., Conery, A. L., Thompson-Peer, K. L., Soskis, M., Ruvkun, G. B., Kaplan, M. J., & Kim, J. K. (2008). The microRNA miR-1 regulates a MEF-2 dependent retrograde signal at neuromuscular junctions. *Cell*, **133**, 903–915.

Siwicki, K. K., Riccio, P., Ladewski, L., Marcillac, F., Dartevelle, L., Cross, S. A., & Ferveur, J-F. (2005). The role of cuticular pheromones in courtship conditioning of Drosophila males. *Learning and Memory*, **12**, 636-645.

Sobotzik, J. M., Sie, J. M., Politi, C., Del Turco, D., Bennett, V., Deller, T., & Schultz, C. (2009). AnkyrinG is required to maintain axo-dendritic polarity in vivo. *Proceedings of the National Academy of Sciences of the United States of America*, **106**, 17564-17569.

Sone, M., Suzuki, E., Hoshino, M., Hou, D., Kuromi, H., Fukata, M., Kuroda, S., Kaibuchi, K., Nabeshima, Y., & Hama, C. (2000). Synaptic development is controlled in the periactive zones of Drosophila synapses. *Development*, **127**, 4157-4168.

Soriano, F. X., Chawla, S., Skehel, P., & Hardingham, G. E. (2013). SMRT-mediated co-shuttling enables export of class IIa HDACs independent of their CaM kinase phosphorylation sites. *Journal of Neurochemistry*, **124**, 26-35.

Stefanko, D. P., Barrett, R. M., Ly, A. R., Reolon, G. K., & Wood, M. A. (2009). Modulation of long-term memory for object recognition via HDAC inhibition. *Proceedings of the National Academy of Sciences of the United States of America*, **106**, 9447-9452.

Strausfeld, N. J., & Hirth, F. (2013). Deep homology of arthropod central complex and vertebrate basal ganglia. *Science*, **340**, 157-161.

Sun, X., Wu, Y., Gu, M., & Zhang, Y. (2014a). miR-342-5p decreases ankyrin G levels in Alzheimer's disease transgenic mouse models. *Cell Report*, **6**, 264-270.

Sun, X., Wu, Y., Gu, M., Liu, Z., Ma, Y., Li, J., & Zhang, Y. (2014b). Selective filtering defect at the axon initial segment in Alzheimer's disease mouse model. *Proceedings of the National Academy of Sciences of the United States of America*, **111**, 14271-14276.

Suster, M. L., Seugnet, L., Bate, M., & Sokolowski, M. B. (2004). Refining GAL4-driven transgene expression in Drosophila with a GAL80 enhancer-trap. *Genesis*, **39**, 240-245.

Szklarczyk, D., Franceschini, A., Wyder, S., Forslund, K., Heller, D., Huerta-Cepas, J., Simonovic, M., Roth, A., Santos, A., Tsafou, K. P., Kuhn, M., Bork, P., Jensen, L. J., & von Mering, C. (2015). STRING v10: protein-protein interaction networks, integrated over the tree of life. *Nucleic Acids Research*, **43**, D447-52.

Takahashi-Fujigasaki, J., & Fujigasaki, H. (2006). Histone deacetylase (HDAC) 4 involvement in both Lewy and Marinesco bodies. *Neuropathology and Applied Neurobiology*, **2**, 562-6.

Takao, K., Kobayashi, K., Hagihara, H., Ohira, K., Shoji, H., Hattori, S., Koshimizu, H., Umemori, J., Toyama, K., Nakamura, H. K., Kuroiwa, M., Maeda, J., Atsuzawa, K., Esaki, K., Yamaguchi, S., Furuya, S., Takagi, T., Walton, N. M., Hayashi, N., Suzuki, H., Higuchi, M., Usuda, N., Suhara, T., Nishi, A., Matsumoto, M., Ishii, S., & Miyakawa, T. (2013). Deficiency of Schnurri-2, an MHC enhancer binding protein, induces mild chronic inflammation in the brain and confers molecular, neuronal, and behavioral phenotypes related to schizophrenia. *Neuropsychopharmacology*, **38**, 1409–1425.

Talamillo, A., Sanchez, J., & Barrio, R. (2008) Functional analysis of the SUMOylation pathway in Drosophila. *Biochemical SocietyTransaction*, **36**, 868–873.

Tesli, M., Koefoed, P., Athanasiu, L., Mattingsdal, M., Gustafsson, O., Agartz, I., Rimol, L. M., Brown, A., Wirgenes, K. V., Smorr, L. L., Kahler, A. K., Werge, T., Mors, O., Mellerup, E., Jonsson, E. G., Melle, I., Morken, G., Djurovic, S., & Andreassen, O. A. (2011). Association analysis of ANK3 gene variants in nordic bipolar disorder and schizophrenia case-control samples. *American Journal of Medical Genetics. Part B: Neuropsychiatric Genetics*, **156B**, 969-974.

Thermo Scientific Pierce (2010). Protein Interaction technical handbook, version 2, Thermo Fisher Scientific Inc.

Tompkins, L., Siegel, R. W., Gailey, D. A., & Hall, J. C. (1985). Conditioned courtship in Drosophila and its mediation by association of chemical cues. *Behavior Genetics*, **13**, 565-578.

Touhara, K., & Vosshall, L. B. (2009). Sensing odorants and pheromones with chemosensory receptors, *Annual Review of Physiology*, **71**, 307-332.

Trapnell, C., Roberts, A., Goff, L., Pertea, G., Kim, D., Kelley, D. R., Pimentel, H., Salzberg, S. L., 5 Rinn, J. L., & Pachter, L. (2012). Differential gene and transcript expression analysis of RNA-seq experiments with TopHat and Cufflinks. *Nature Protocols*, **7**, 562–578.

Trunova, S., Baek, B., & Giniger, E. (2011). Cdk5 regulates the size of an axon initial segment-like compartment in mushroom body neurons of the Drosophila central brain. *Journal of Neuroscience*, **31**, 10451-10462.

Tsai, P. I., Wang, M., Kao, H. H., Cheng, Y. J., Lin, Y. J., Chen, R. H., & Chien, C. T. (2012). Activity-dependent retrograde laminin A signaling regulates synapse growth at Drosophila neuromuscular junctions. *Proceedings of the National Academy of Sciences of the United States of America*, **109**, 17699-17704.

Tully, T., & Quinn, W. G. (1985). Classical conditioning and retention in normal and mutant Drosophila melanogaster. *Journal of Comparative Physiology A*, **157**, 263-277.

Tuvia, S., Garver, T. D., & Bennett, V. (1997). The phosphorylation state of the FIGQY tyrosine of neurofascin determines ankyrin-binding activity and

patterns of cell segregation. *Proceedings of the National Academy of Sciences of the United States of America*, **94**, 12957–12962.

Van der Voet, M., Nijhof, B., Oortveld, M. A., & Schenck, A. (2014). Drosophila models of early onset cognitive disorders and their clinical applications. *Neuroscience & Biobehavioral Reviews*, **46 Pt 2**, 326-342.

Vang, L. L., Medvedev, A. V., & Adler, J. (2012). Simple ways to measure behavioral responses of Drosophila to stimuli and use of these methods to characterize a novel mutant. *PloS One*, **7**, e37495.

Vega, R. B, Matsuda, K., Oh, J., Barbosa, A. C, Yang, X., Meadows, E., McAnally, J., Pomajzl, C., Shelton, J. M, Richardson, J. A, Karsenty, G., & Olson, E. N. (2004). Histone deacetylase 4 controls chondrocyte hypertrophy during skeletogenesis. *Cell*, **119**, 555-566.

Verdin, E., Dequiedt, F., & Kasler, H. G. (2003). Class II histone deacetylases: versatile regulators. *Trends in Genetics*, **19**, 286-293.

Vinayak, P., Coupar, J., Hughes, E., Fozdar, P., Kilby, J., Garren, E.,Yoshii, T., & Hirsh, J. (2013). Exquisite light sensitivity of Drosophila melanogaster cryptochrome. *PLOS Genetics*, **9**, e1003615.

Volmar, C. H., & Wahlestedt, C. (2015). Histone deacetylases (HDACs) and brain function. *Neuroepigenetics*, **1**, 20-27.

Walkinshaw, E., Gai, Y., Farkas, C., Richter, D., Nicholas, E., Keleman, K., & Davis, R. L. (2015). Identification of genes that promote or inhibit olfactory memory formation in Drosophila. *Genetics*, **199**, 1173-1182.

Wang, A. H., & Yang, X. J. (2001). Histone deacetylase 4 possesses intrinsic nuclear import and export signals. *Molecular and Cellular Biology*, **21**, 5992-6005.

Wang, A. H., Bertos, N. R., Vezmar, M., Pelletier, N., Crosato, M., Heng, H. H., Th'ng, J., Han, J., & Yang, X.-J. (1999). HDAC4, a human histone deacetylase related to yeast HDA1, is a transcriptional corepressor. *Molecular and Cellular Biology*, **19**, 7816–7827.

Wang, A. H., Grégoire, S., Zika, E., Xiao, L., Li, C. S., Li, H., Wright, K. L., Ting, J. P., Yang, X. J. (2005). Identification of the ankyrin repeat proteins ANKRA and RFXANK as novel partners of class IIa histone deacetylases. *The Journal of Biological Chemistry*, **280**, 29117-29127.

Wang, A. H., Kruhlak, M. J., Wu, J., Bertos, N. R., Vezmar, M., Posner, B. I., Bazett-Jones, D. P. & Yang X. J. (2000). Regulation of histone deacetylase 4 by binding of 14-3-3 proteins. *Molecular and Cellular Biology*, **18**, 6904-6912

Wang, H., & Zeng, X. (2000). Analysing protein–protein interactions using a GST-fusion protein to pull down the interacting target from the cell lysate. *Technical Tips Online*, **5**, 26-30.

Wang, W. H., Cheng, L. C., Pan, F. Y., Xue, B., Wang, D. Y., Chen, Z., & Li, C. J. (2011). Intracellular trafficking of histone deacetylase 4 regulates long-term memory formation. *Anatomical Record (Hoboken)*, **294**, 1025-1034.

Wilkinson, K. A., & Henley, J. M. (2010). Mechanisms, regulation and consequences of protein SUMOylation. *The Biochemical Journal*, **428**, 133–145.

Williams, S. R., Aldred, M. A., Der Kaloustian, V. M., Halal, F., Gowans, G., McLeod, D. R., Zondag, S., Toriello, H. V., Magenis, R. E., & Elsea, S. H. (2010). Haploinsufficiency of HDAC4 causes brachydactyly mental retardation syndrome, with brachydactyly type E, developmental delays, and behavioral problems. *American Journal of Human Genetics*, **87**, 219-228.

Winbush, A., Reed, D., Chang, P. L., Nuzhdin, S. V., Lyons, L. C., & Arbeitman, M. N. (2012). Identification of gene expression changes associated with long-term memory of courtship rejection in Drosophila males. *G3 (Bethesda)*, **2**, 1437-1445.

Wright, A. P., & Zinn, K. (2009). Guidance receptors find their places in the axonal order. *Neuron*, **64**, 150–152.

Xu, C., Jin, J., Bian, C., Lam, R., Tian, R., Weist, R. You, L., Nie, J., Bochkarev, A., Tempel, W., Tan, C., Wasney, G. A., Vedadi, M., Gish, G. D., Arrowsmith, C. H., Pawson, T., Yank, X. J. & Min, J. (2012). Sequence-specific recognition of a PxLPxI/L motif by an ankyrin repeat tumbler lock. *Science Signaling*, **5**, ra39.

Xu, K., Zhong, G., & Zhuang, X. (2013). Actin, spectrin and associated proteins form a periodic cytoskeletal structure in axons. *Science*, **339**, 452-456.

Yamagata, N., Ichinose, T., Aso, Y., Plaçais, P.-Y., Friedrich, A. B., Sima, R. J., Preat, T., Rubin, G. M., & Tanimoto, H. (2015). Distinct dopamine

neurons mediate reward signals for short- and long-term memories. *Proceedings of the National Academy of Sciences of the United States of America*, **112**, 578–583.

Yamamoto-Hino, M., & Goto, S. (2013). In vivo RNAi-based screens: studies in model organisms. *Genes*, **4**, 646–665.

Yang, M. Y., Armstrong, J. D., Vilinsky, I., Strausfeld, N. J., & Kaiser, K. (1995). Subdivision of the drosophila mushroom bodies by enhancer-trap expression patterns, *Neuron*, **15**, 45-54.

Yang, Q. G., Wang, F., Zhang, Q., Xu, W. R., Chen, Y. P., & Chen, G. H. (2012). Correlation of increased hippocampal Sumo3 with spatial learning ability in old C57BL/6 mice. *Neuroscience Letters*, **518**, 75-79.

Yang, X. J., & Grégoire, S. (2005). Class II histone deacetylases: from sequence to function, regulation, and clinical implication. *Molecular and Cellular Biology*, **25**, 2873-2884.

Yasunaga, M., Ipsaro, J. J., & Mondragon, A. (2012). Structurally similar but functionally diverse ZU5 domains in human erythrocyte ankyrin. *Journal of Molecular Biology*, **417**, 336-350.

Yoshikawa, S., McKinnon, R. D., Koel, M., & Thomas, J. B. (2003). Wnt-mediated axon guidance via the Drosophila Derailed receptor. *Nature*, **422**, 583-588.

Yoshimura, T., & Rasband, M. N. (2014). Axon initial segments: diverse and dynamic neuronal compartments. *Current Opinion in Neurobiology*, **27**, 96-102.

Zars, T. (2000). Behavioral functions of the insect mushroom bodies, *Current Opinion in Neurobiology*, **10**, 790-795.

Zeremski, M., Stricker, J. R., Fischer, D., Zusman, S. B., & Cohen, D. (2003). Histone deacetylase dHDAC4 is involved in segmentation of the Drosophila embryo and is regulated by gap and pair-rule genes. *Genesis*, **35**, 31-38.

Zhang, C., Cai, J., Zhang, J., Li, Z., Guo, Z., Zhang, X., Lu, W., Zhang, Y., Yuan, A., Yu, S., & Fang, Y. (2014). Genetic modulation of working memory deficits by ankyrin 3 gene in schizophrenia. *Progress in Neuro-Psychopharmacology and Biological Psychiatry*, **50**, 110-115.

Zhang, L., Hsu, F.-C., Mojsilovic-Petrovic, J., Jablonski, A. M., Zhai, J., Coulter, D. A., & Kalb, R. G. (2015). Structure–function analysis of SAP97, a modular scaffolding protein that drives dendrite growth. *Molecular and Cellular Neuroscience*, **65**, 31-44.

Zhang, X., Davis, J. Q., Carpenter, S., & Bennett, V. (1998). Structural requirements for association of neurofascin with ankyrin. *Journal of Biological Chemistry*, **273**, 30785-30794.

Zhao, X., Ito, A., Kane, C. D., Liao, T. S., Bolger, T. A., Lemrow, S. M., Means, A. R., & Yao, T. P. (2001). The modular nature of histone deacetylase HDAC4 confers phosphorylation-dependent intracellular trafficking. *Journal of Biological Chemistry*, **276**, 35042-35048.

Zhao, X., Sternsdorf, T., Bolger, T. A., Evans, R. M., & Yao, T. P. (2005). Regulation of MEF2 by histone deacetylase 4- and SIRT1 deacetylase-mediated lysine modifications. *Molecular and Cellular Biology*, **25**, 8456-8464.

Zhou, D., Lambert, S., Malen, P. L., Carpenter, S., Boland, L. M., & Bennett, V. (1998). AnkyrinG is required for clustering of voltage-gated Na channels at axon initial segments and for normal action potential firing. *The Journal of Cell Biology*, **143**, 1295-1304.

Zhu, S., Ann-Shyn Chiang, A. –S., & Lee, T. (2003). Development of the Drosophila mushroom bodies: elaboration, remodelling and spatial organization of dendrites in the calyx. Development, 130, 2603-2610.

Ziemka-Nalecz, M., & Zalewska, T. (2014). Neuroprotective effects of histone deacetylase inhibitors in brain ischemia. *Acta Neurobioliae Experimentalis*, **74**, 383–395.

Zovkic, I. B., Guzman-Karlsson, M. C., & Sweatt, J. D. (2013). Epigenetic regulation of memory formation and maintenance. *Learning & Memory*, **20**, 61-74.

Zweier, M., Gregor, A., Zweier, C., Engels, H., Sticht, H., Wohlleber, E., Bijlsma, E. K., Holder, S. E., Zenker, M., Rossier, E., Grasshoff, U., Johnson, D. S., Robertson, L., Firth, H. V., Cornelia Kraus, Ekici, A. B., Reis, A. and Rauch, A. (2010), Mutations in MEF2C from the 5q14.3q15 microdeletion syndrome region are a frequent cause of severe mental retardation and diminish MECP2 and CDKL5 expression. *Human Mutation*, **31**, 722–733.

7 APPENDICES

7.1 Supplemental tables

Fly strain name	Source	Genotype
w^{1118}	BDSC	*w[1118]*
w^{CS10}	R. Davis	*w[CS10]*
w^{CS10};*TM3, Sb*	R. Davis	*w[CS10];TM3, Sb*
w^{CS10};*CyO/Sco*	R. Davis	*w[CS10];CyO, Sco*
Canton special (CS)	R. Davis	*Wild type CS strain*
attP-86F	Konrad Basler	*y w, P{hs-flp}; P{3xP3-RFP=attP-86F}; P{3xP3-RFP=phic-31{3xP3-GFP=vas-phic31}102F*
GMR-GAL4	BDSC 1104	*w[*];P{w[+mC]=GAL4ninaE.GMR}12*
UAS-HDAC4OE	H. Fitzsimons	*w[CS10];P{3XP3-RFP=attP-86F},UAS-HDAC4*
GMR-GAL4;UAS-HDAC4OE	H. Fitzsimons	*w[CS10];P{w[+mC]=GAL4-ninaEGMR}12}; P{3xP3-RFP=attP-86F},UAS-HDAC4*
ELAV - GAL4	BDSC 458	*P{w[+mW.hs]=GawB}elav[C155]*
ELAV-GAL4; UAS-HDAC4::YFP	H. Fitzsimons	*w[CS10];P{w[+mW.hs]=GawB}elav[C155],CPT I-000077*
ELAV-GAL4;UAS-CD8::GFP	BDSC 5146	*w[*]P{w[+mW.hs]=GawB}elav[C155],P{w[+mC]= UAS-mCD8::GFP.L}Ptp4E[LL4], P{ry[+t7.2]=hsFLP}1*
Tubulin-GAL4	BDSC 5138	*y[1] w[*]; P{w+mC=tubP-GAL4} LL7/TM3, Sb1 r*
Tubulin-GAL80^{ts}	BDSC 7108	*w[*]; P{w+mC=tubP-GAL80^{ts}}10; TM2/TM6B, Tb1; Gal80^{ts}*
Tubulin-GAL80^{ts}; tubulin-GAL4	H. Fitzsimons	*y, P{w+mC=tubP-GAL80ts}10; P{w+mC=tubP-GAL4} LL7/TM3, Sb1*
ELAV-GAL4; tubulin-GAL80^{ts}	H. Fitzsimons	*w[CS10]; P{w[+mW.hs]+GawB}elav[C155], P{w+mC=tubP-GAL80^{ts}}10*
MB247-GAL4; tubulin-GAL80^{ts}	H. Fitzsimons	*w[CS10]; P{w+mC=tubP-GAL80ts]10; MB247*
c305a-GAL4; tubulin-GAL80^{ts}	H. Fitzsimons	*w[CS10]; P{w+mC=tubP-GAL80^{ts}}10, P{w+mW.hs=GawB}c305a*
c739-GAL4; tubulin-GAL80^{ts}	H. Fitzsimons	*w[CS10]; P{w[+mW.hs]=GawB}c739, P{w+mC=tubP-GAL80^{ts}]10*
OK107-GAL4; tubulin-GAL80^{ts}	H. Fitzsimons	*w[CS10]; P{w+mC=tubP-GAL80ts}10; P{w+mW.hs=GawB}OK107*
1471-GAL4; tubulin-GAL80^{ts}	H. Fitzsimons	*w[CS10]; P{w+mC=tubP-GAL80ts]10, P{w+mW.hs=GawB}1471*
NP1131-GAL4; tubulin-GAL80^{ts}	H. Fitzsimons	*w[CS10]; P{w + mW.hs=GawB}NP1131, p{w[-]=UAS-lacZ. UW14} UW14, P{w+mC=tubP-GAL80^{ts}}10*
UAS-CD8::GFP	BDSC 5137	*y [1] w[*]; P{UAS-mCD8::GFP.L}LL5*
UAS-LacZ	BDSC 1776	*w[1118];P{w[+mC]=UAS-lacZ.B}melt[Bg4-1-2]*
Ankyrin1-MYC	S. Schwartz	*w[CS10]; P{3xP3-RFP=attP-86F} Ank1-MYC*
Ankyrin2-EGFP	DGRC 109758	*w[1118]; PBac{EGFP-IV}Ank2[KM0104]*

Table 7.1 *Drosophila melanogaster* GAL4-driver lines and control strains used in this study. Abbreviations: BDSC = Bloomington Drosophila Stock Centre. DGRC = Drosophila Genomic Research Centre. R. Davis: Prof Ron Davis. The Scripps Institute, Jupiter, Florida.

Gene name/symbol	Stock Centre ID	Symbol	Genotype
14-3-3 ε	VDRC 108129	CG31196	*y,w[1118];P{attP,y[+],w[3`] P{KK102462}VIE-260B*
14-3-3 ζ /Leo	VDRC 104496	CG17870	*y,w[1118];P{attP,y[+],w[3`] P{KK109378}VIE-260B*
A kinase anchor protein 200/ Akap200	VDRC 109996	CG13388	*y,w[1118];P{attP,y[+],w[3`] P{KK111598}VIE-260B*
Actin binding protein 1/Abp1	VDRC 38331	CG10083	*w[1118]; P{GD6858}v38331*
Activator of SUMO 1/Aos1	VDRC 47256	CG12276	*w[1118]; P{GD16818}v47256*
Activity-regulated cytoskeleton associated protein 1/Arc1	VDRC 31122 VDRC 109141	CG12505	*w[1118]; P{GD6751}v31122* *y,w[1118];P{attP,y[+],w[3`] P{KK115868}VIE-260B*
Adh transcription factor 1 /Adf1	VDRC 102176	CG15845	*y,w[1118];P{attP,y[+],w[3`] P{KK111012}VIE-260B*
Amnesiac/Amn	VDRC 5606	CG11937	*w[1118]; P{GD1178}v5606*
Ankyrin1/Ank1	VDRC 25945	CG1651	*w[1118]; P{GD10431}v25945*
Ank1 (cantonised)	S. Schwartz	N.A.	*w[CS10]; P{GD10431}v25945*
Ankyrin2/Ank2	VDRC 107369 VDRC 40638 VDRC 46224 VDRC107238	CG42734	*y,w[1118];P{attP,y[+],w[3`] P{KK106729}VIE-260B* *w[1118] P{GD12247}v40638* *w[1118]; P{GD16285}v46224* *y,w[1118];P{attP,y[+],w[3`]P{K K104937}VIE-260B*
Ank2 (cantonised)	S. Schwartz	N.A.	*y,w[CS10];P{attP,y[+],w[3`] P{KK106729}VIE-260B*
Annexin B10/Anx B10	VDRC 36107	CG9579	*w[1118]; P{GD14255}v36107*
Bendless/Ben	VDRC 109638	CG18319	*y,w[1118];P{attP,y[+],w[3`] P{KK101929}VIE-260B*
Blistered/bs	VDRC 100609	CG3411	*y,w[1118];P{attP,y[+],w[3`] P{KK108659}VIE-260B*
Brahma associated protein 55kD/Bap55	VDRC 24703	CG6546	*w[1118]; P{GD11955}v24703/CyO*
Calcineurin A at 14F/CanA-14F	VDRC 109858	CG9819	*y,w[1118];P{attP,y[+],w[3`] P{KK110900}VIE-260B*
Calcineurin B/CanB	VDRC 21611	CG4209	*w[1118]; P{GD10703}v21611*
Calcineurin B2/CanB2	VDRC 104370	CG11217	*y,w[1118];P{attP,y[+],w[3`] P{KK107988}VIE-260B*
Calcium/calmodulin-dependent protein kinase II/CaMKII	VDRC 100265	CG18069	*y,w[1118];P{attP,y[+],w[3`] P{KK107335}VIE-260B*
Calmodulin-binding transcription activator/Camta	VDRC 106025	CG42332	*y,w[1118];P{attP,y[+],w[3`] P{KK112864}VIE-260B*
Carbonic anhydrase 2/CAH2	VDRC 8357	CG6906	*w[1118]; P{GD2438}v8357*
CG42684	VDRC 109589	CG42684	*y,w[1118];P{attP,y[+],w[3`] P{KK110101}VIE-260B*
CG5846 (Rfxank)	VDRC 107793	CG5846	*y,w[1118];P{attP,y[+],w[3`] P{KK105728}VIE-260B*
CG6409	VDRC 102430	CG6409	*y,w[1118];P{attP,y[+],w[3`] P{KK111644}VIE-260B*
CG6503	VDRC 110301	CG6503	*y,w[1118];P{attP,y[+],w[3`] P{KK110623}VIE-260B*
CG9377	VDRC 42835	CG9377	*w[1118]; P{GD1319}v42835*

Chameau/chm	VDRC 105542	CG5229	*y,w[1118];P{attP,y[+],w[3`] P{KK105542}*
Chd3/Chd3	VDRC 102689	CG9594	*y,w[1118];P{attP,y[+],w[3`] P{KK112178}VIE-260B*
Cheerio/cher	VDRC 107451	CG3937	*y,w[1118];P{attP,y[+],w[3`] P{KK107518}VIE-260B*
Chickadee/chic	VDRC 102759	CG9553	*y,w[1118];P{attP,y[+],w[3`] P{KK112358}VIE-260B*
Crammer/cer	VDRC 22752	CG10460	*w[1118]; P{GD12961}v22752*
Cryptocephal/crc	VDRC 109014	CG8669	*y,w[1118];P{attP,y[+],w[3`] P{KK111018}VIE-260B*
Cyclic-AMP response element binding protein A/CrebA	VDRC 110650	CG7450	*y,w[1118];P{attP,y[+],w[3`] P{KK110650}*
Cyclic-AMP response element binding protein B/CrebB	VDRC 101512 BDSC 29332	CG6103	*y,w[1118];P{attP,y[+],w[3`] P{KK108927}VIE-260B* *y[1] v[1]; P{y[+t7.7] v[+t1.8]=TRiP.JF02494}attP 2/TM3, Sb[1]*
Delta/DI	VDRC 109491	CG3619	*y,w[1118];P{attP,y[+],w[3`] P{KK107312}VIE-260B*
Derailed/drl	VDRC 27053	CG17348	*w[1118]; P{GD14371}v27053*
Disc Large 1/dlg1	VDRC 109274	CG1725	*y,w[1118];P{attP,y[+],w[3`] P{KK116285}VIE-260B*
Embargoed/emb	VDRC 103767	CG13387	*y,w[1118];P{attP,y[+],w[3`] P{KK102552}VIE-260B*
Enoki mushroom/Enok	VDRC 37527	CG11290	*w[CS10]; P{GD4037}v37527*
Estrogen-related receptor/ERR	VDRC 108349	CG7404	*y,w[1118];P{attP,y[+],w[3`] P{KK108422}VIE-260B*
Fasciclin 2/FasII	VDRC 103807	CG3665	*y,w[1118];P{attP,y[+],w[3`] P{KK100888}VIE-260B*
Fat-spondin/Fat-spondin	VDRC 105844	CG6953	*y,w[1118];P{attP,y[+],w[3`] P{KK110998}VIE-260B*
Fmr1/Fmr1	VDRC 110800	CG6203	*y,w[1118];P{attP,y[+],w[3`] P{KK107935}VIE-260B*
Forkhead box, sub-group O/Foxo	VDRC 106097	CG3143	*y,w[1118];P{attP,y[+],w[3`] P{KK108485}VIE-260B*
Frazzled/fra	BDSC 31664	CG8581	*y[1] v[1]; P{y[+t7.7] v[+t1.8]=TRiP.JF01457}attP 2*
G9a/G9a	VDRC 110662	CG2995	*y,w[1118];P{attP,y[+],w[3`]; P{KK100579}VIE-260B*
Gcn5 ortholog/Gcn5	VDRC 21786	CG4107	*w[CS10]; P{GD11218}v21786*
Glutamate receptor IA/GluRI	VDRC 108019	CG8442	*y,w[1118];P{attP,y[+],w[3`] P{KK101533}VIE-260B*
Gryzun/gry	VDRC 105660	CG17569	*y,w[1118];P{attP,y[+],w[3`] P{KK101813}VIE-260B*
Heterochromatin protein 1C/HP1 C	VDRC 104893	CG6990	*y,w[1118];P{attP,y[+],w[3`] P{KK112389}VIE-260B*
Hikaru genki/Hig	VDRC 13266	CG2040	*w[1118] P{GD5279}v13266*
Histone Deacetylase 1/HDAC1	VDRC 30600	CG7471	*w[CS10]; P{GD4513}v30600*
Histone deacetylase 11/HDAC11	BDSC 32480	CG31119	*y[1] sc[*] v[1]; P{y[+t7.7] v[+t1.8]=TRiP.HMS00483}attP2*

Histone deacetylase 3/HDAC3	VDRC 20814	CG2128	*w[CS10]; P{GD9732}v20814*
Histone deacetylase 4/HDAC4	VDRC 20522	CG1770	*w[CS10]; P{GD9446}v20522*
Histone deacetylase 6/HDAC6	VDRC 108831	CG6170	*y,w[1118];P{attP,y[+],w[3`] P{KK100215}VIE-260B*
Hiw/Highwire	VDRC 26998	CG32592	*w[1118]; P{GD14101}v26998*
Homer/homer	VDRC 100271	CG11324	*y,w[1118];P{attP,y[+],w[3`] P{KK107359}VIE-260B*
IGF-II mRNA-binding protein/Imp	VDRC 20321	CG1691	*w[1118]; P{GD9232}v20321*
Kekkon 2/kek2	VDRC 4745	CG4977	*w[1118]; P{GD2505}v4745*
Krasavietz/kra	VDRC 102609	CG2922	*y,w[1118];P{attP,y[+],w[3`] P{KK102900}VIE-260B*
Kruppel/Kr	VDRC 40871	CG3340	*w[1118]; P{GD1471}v40871*
Laminin A/LanA	VDRC 18873	CG10236	*w[1118]; P{GD6022}v18873*
Latheo/lat	VDRC 103716	CG4088	*y,w[1118];P{attP,y[+],w[3`] P{KK100894}VIE-260B*
Lesswright/lwr (Ubc9)	VDRC 33685 BDSC 9318	CG3018	*w[1118]; P{GD10017}v33685* *w[*]; P{w[+mC]=UAS-lwr.DN}3/TM3, P { w[+mC]= ActGFP}JMR2,Ser[1]*
Little imaginal discs/lid	VDRC 103830	CG9088	*w[CS10]; P{KK102745}*
Mars/mars	VDRC 32841	CG17064	*w[1118]; P{GD9277}v32841*
Martik/mrt	VDRC 106951	CG3361	*y,w[1118];P{attP,y[+],w[3`] P{KK112537}VIE-260B*
Microtubule star/Mts	VDRC 35171	CG7109	*w[1118]; P{GD12133}v35171*
Mob2/Mob2	VDRC 107327	CG11711	*y,w[1118];P{attP,y[+],w[3`] P{KK109159}VIE-260B*
Moesin/Moe	VDRC 110654	CG10701	*y,w[1118];P{attP,y[+],w[3`] P{KK108480}VIE-260B*
Myocyte enhancer factor 2/Mef2	VDRC 15550	CG1429	*w[1118]; P{GD5039}v15550; w(CS10); P{GD5039}v1555*
Nejire/nej (CBP/p300)	VDRC 105115	CG15319	*y,w[1118];P{attP,y[+],w[3`] P{KK105115}*
Nemo/nmo	VDRC 104885	CG7892	*y,w[1118];P{attP,y[+],w[3`] P{KK107867}VIE-260B*
NetrinB/NetB	VDRC 100840	CG10521	*y,w[1118];P{attP,y[+],w[3`]; P{KK103672}VIE-260B*
Neurofibromin 1/Nf1	VDRC 109637	CG8318	*y,w[1118];P{attP,y[+],w[3`] P{KK101909}VIE-260B*
Neuroglian/Nrg	BDSC 37496	CG1634	*y[1] sc[*] v[1]; P{y[+t7.7] v[+t1.8]=TRiP.HMS01638}at tP40*
Neurotrophin 1/NT1	VDRC 108894	CG42576	*y,w[1118];P{attP,y[+],w[3`] P{KK104294}VIE-260B*
Niemann-Pick type C-2g/Npc2g	VDRC 104942	CG11314	*y,w[1118];P{attP,y[+],w[3`] P{KK112401}VIE-260B*
NMDA receptor 1/Nmdar1	VDRC 104773	CG2902	*y,w[1118];P{attP,y[+],w[3`] P{KK107519}VIE-260B*
No extended memory/nemy	VDRC 40803	CG8776	*w[1118]; P{GD15732}v40803*
Nord/nord	VDRC 102254	CG30418	*y,w[1118];P{attP,y[+],w[3`] P{KK111263}VIE-260B*
Notch/N	VDRC 100002	CG3936	*y,w[1118];P{attP,y[+],w[3`] P{KK102890}VIE-260B*
Nucleoporin 358KD/Nup358	VDRC 38583	CG11856	*w[1118]; P{GD7405}v38583*

Odorant binding protein 56d/Obp56d	VDRC 100671	CG11218	*y,w[1118];P{attP,y[+],w[3`] P{KK106790}VIE-260B*
Orb2	VDRC 107153	CG43782	*y,w[1118];P{attP,y[+],w[3`] P{KK107153}*
Oskar/osk	VDRC 107546	CG10901	*y,w[1118];P{attP,y[+],w[3`] P{KK104114}VIE-260B*
P38a MAP kinase/p38a	BDSC 27316	CG5475	*y[1] v[1]; P{y[+t7.7] v[+t1.8]=TRiP.JF02625}attP 2*
P38b MAP kinase/p38b	BDSC 29405	CG7393	*y[1] v[1]; P{y[+t7.7] v[+t1.8]=TRiP.JF03341}attP 2*
Pastrel/pst	VDRC 107243	CG8588	*y,w[1118];P{attP,y[+],w[3`] P{KK105159}VIE-260B*
Poly-(ADP-ribose) polymerase/Parp1	VDRC 46745	CG40411	*y[1] sc[*] v[1]; P{y[+t7.7] v [+t1.8] = TRiP.GL00229} attP2/TM3, Sb[1]*
PP2A B'	VDRC 107057	CG7913	*y,w[1118];P{attP,y[+],w[3`] P{KK102310}VIE-260B*
Prosap/Prosap	VDRC 103592	CG30483	*y,w[1118];P{attP,y[+],w[3`] P{KK101537}VIE-260B*
Prospero/pros	VDRC 101477	CG17228	*y,w[1118];P{attP,y[+],w[3`] P{KK101477}*
Protein kinase D/PKD	VDRC 106255	CG7125	*y,w[1118];P{attP,y[+],w[3`] P{KK102329}VIE-260B*
Protein phosphatase 1 at 87 B/Pp1-87B	VDRC 35025	CG5650	*w[1118]; P{GD11720}v35025*
Protein phosphatase 2B at 14D/Pp2B-14D	VDRC 103144	CG9842	*y,w[1118];P{attP,y[+],w[3`] P{KK107714}VIE-260B*
Pumilio/pum	VDRC 101399	CG9755	*y,w[1118];P{attP,y[+],w[3`] P{KK101399}*
Rac1/Rac1	BDSC 28985	CG2248	*y[1] v[1]; P{y[+t7.7] v[+t1.8]=TRiP.JF02813}attP 2 e[*]*
Radish/rad	VDRC 101811	CG44424	*y,w[1118];P{attP,y[+],w[3`] P{KK109743}VIE-260B*
RanBP21/RanBp21	VDRC 31706	CG12234	*w[1118]; P{GD7541}v31706*
Ribosomal protein S6 kinase II/S6KII	VDRC101451	CG17596	*y,w[1118];P{attP,y[+],w[3`] P{KK109199}VIE-260B*
Rogdi	VDRC 107310	CG7725	*y,w[1118];P{attP,y[+],w[3`] P{KK108321}VIE-260B*
Rolled/rl	VDRC 109108	CG12559	*y,w[1118];P{attP,y[+],w[3`] P{KK115768}VIE-260B*
Rugose/rg	VDRC 107056	CG44835	*y,w[1118];P{attP,y[+],w[3`] P{KK102295}VIE-260B*
Rutabaga/rut	VDRC 101759	CG9533	*y,w[1118];P{attP,y[+],w[3`] P{KK109441}VIE-260B*
Ryanodine receptor/RyR	VDRC 109631	CG10844	*y,w[1118];P{attP,y[+],w[3`]; P{KK101716}VIE-260B*
Sarah/sra	VDRC 107573	CG6072	*y,w[1118];P{attP,y[+],w[3`] P{KK107660}VIE-260B*
Scab/scab	VDRC 100949	CG8095	*y,w[1118];P{attP,y[+],w[3`] P{KK106326}VIE-260B*
Scamp/Scamp	VDRC 9130	CG9195	*w[1118]; P{GD3371}v9130/CyO*
Schnurri/shn	VDRC 105643	CG7734	*y,w[1118];P{attP,y[+],w[3`] P{KK101278}VIE-260B*
Short Spindle 7/ssp7	VDRC 110126	CG32667	*y,w[1118];P{attP,y[+],w[3`] P{KK115572}VIE-260B*

Similar/sima	VDRC 106187	CG45051	*y,w[1118];P{attP,y[+],w[3`] P{KK102226}VIE-260B*
Sin3A/Sin3A	VDRC 105852	CG8815	*y,w[1118];P{attP,y[+],w[3`] P{KK100700}VIE-260B*
Sirtuin 2/Sirt2	VDRC 23201	CG5216	*w[1118]; P{GD11580}v23201*
Smrter/Smr	VDRC 106701	CG4013	*y,w[1118];P{attP,y[+],w[3`] P{KK102611}VIE-260B*
Smt3/smt3	VDRC 105890	CG4494	*w[1118]; P{GD10521}v34113/CyO*
Specifically Rac1-associated protein 1/Sra1	VDRC 108876	CG4931	*y,w[1118];P{attP,y[+],w[3`] P{KK101432}VIE-260B*
Spoonbill/spoon	VDRC 105107	CG3249	*y,w[1118];P{attP,y[+],w[3`] P{KK101210}VIE-260B*
Staufen/stau	VDRC 106645	CG5753	*y,w[1118];P{attP,y[+],w[3`] P{KK106645}*
Stoned A/stnA	VDRC 105203	CG12500	*y,w[1118];P{attP,y[+],w[3`] P{KK113740}VIE-260B*
Stoned B/stnB	VDRC 24548	CG12473	*y[1] v[1]; P{y[+t7.7] v[+t1.8]=TRiP.JF03130}attP 2/TM3, Sb[1]*
Suppressor of variegation 2-10/Su(var)2-10 (PIAS)	VDRC 30709	CG8068	*w[1118]; P{GD5048}v30709/TM3*
Tat interactive protein60kDa /Tip60	VDRC 22233	CG6121	*w[CS10]; P{GD11826}v22233*
Tonalli/tna	VDRC 28071	CG7958	*w[1118]; P{GD12331}v28071/CyO*
Trio/trio	VDRC 40138	CG18214	*w[1118]; P{GD9531}v40138*
Twins/tws	VDRC 104167	CG6235	*y,w[1118];P{attP,y[+],w[3`] P{KK100308}VIE-260B*
Twinstar/tsr	VDRC 110599	CG4254	*y,w[1118];P{attP,y[+],w[3`] P{KK108706}VIE-260B*
Ubiquitin activating enzyme 2/Uba2	VDRC 110173	CG7528	*y,w[1118];P{attP,y[+],w[3`] P{KK102220}VIE-260B*
UDP-glycosyltransferase 35b/Ugt35b	VDRC 108160	CG6649	*y,w[1118];P{attP,y[+],w[3`] P{KK101899}VIE-260B*
Ulp1/ulp1	VDRC 31744	CG12359	*w[1118]; P{GD7581}v31744*
Will decrease acetylation/wda	VDRC 34847	CG4448	*w[CS10]; P{GD11319}v34847*
Z band alternatively spliced PDZ-motif protein 52/ Zasp52	VDRC 106177	CG30084	*y,w[1118];P{attP,y[+],w[3`] P{KK101276}VIE-260B*
α-actinin/Actn	VDRC 100719	CG4376	*y,w[1118];P{attP,y[+],w[3`] P{KK102286}VIE-260B*
β amyloid protein precursor-like/Appl	VDRC 42673	CG7727	*w[1118]; P{GD3170}v42673*
β-spectrin/β-Spec	VDRC 42053	CG5870	*w[1118]; P{GD11790}v42053*

Table 7.2 *Drosophila melanogaster* RNAi strains used in this study. The table includes *UAS*-RNAi strains used for the rough eye phenotype screen. Abbreviations: VDRC = Vienna Drosophila Resource Centre, BDSC = Bloomington Drosophila Stock Centre.

Gene name	Flybase ID	Molecular function/biological processes
14-3-3 ε	FBgn0020238	Protein heterodimerization activity, protein binding/ regulation of growth, neuron differentiation.
A kinase anchor protein 200	FBgn0027932	Protein kinase A binding/ negative regulation of Ras protein signal transduction; protein localization.
Actin binding protein 1	FBgn0036372	Phosphatidylinositol-4,5-bisphosphate binding, actin binding/positive regulation of synaptic growth at neuromuscular junction, terminal button organization.
Activator of SUMO 1	FBgn0029512	Small protein activating enzyme activity/protein sumoylation, SMT3-dependent protein catabolic process, neurogenesis.
Adh transcription factor-1	FBgn0000054	Transcriptional activator activity/ memory, regulation of neuron differentiation.
Annexin B10	FBgn0000084	Actin and calcium ion binding/Ca^{2+}-dependent, phospholipid-binding proteins with multiple roles in membrane traffic.
Bendless	FBgn0000173	Ubiquitin E2 conjugating enzyme/synapse assembly and regulation.
Blistered	FBgn0004101	DNA binding/short-term memory, larval development.
Brahma associated protein 55kD	FBgn0025716	Transcription co-activator activity/chromatin remodelling, histone acetylation, cell division.
Calcineurin A at 14F	FBgn0267912	Protein serine/threonine phosphatase activity/protein dephosphorylation.
Calcineurin B	FBgn0010014	Calmodulin binding/phosphatase activity, neurotransmitter secretion.
Calcineurin B2	FBgn0015614	Calmodulin binding/protein dephosphorylation, neurotransmitter release.
Calcium/calmodulin-dependent protein kinase II	FBgn0264607	Calmodulin-dependent protein kinase activity/behavior;cellular protein modification process.
Calmodulin-binding transcription activator	FBgn0259234	Transcriptional factor activity/positive regulation of transcription.
CG42684	FBgn0261570	GTPase activator activity/Ras protein signal transduction.
Chameau	FBgn0028387	Histone acetyltransferase/dendrite morphogenesis, protein acetylation.
Chd3	FBgn0023395	DNA binding/chromatin assembly or disassembly.
Cheerio	FBgn0014141	Actin binding protein/neurological system process, olfactory behaviour.
Chickadee	FBgn0000308	Phosphatidylinositol-4,5-bisphosphate binding/brain development, axon regeneration.
Cryptocephal	FBgn0000370	RNA polymerase II activating transcription factor binding/regulation of transcription.
Cyclic-AMP response element binding protein A	FBgn0004396	cAMP response element binding protein/positive regulation of transcription.
Delta	FBgn0000463	Calcium ion binding, Notch binding/biological adhesion, stem cell differentiation; cell division, peripheral nervous system development.
Disc Large 1	FBgn0001624	Structural molecule activity/synaptic transmission.

Embargoed	FBgn0020497	Nuclear export signal receptor activity/ protein transport; nuclear export.
Enoki mushroom	FBgn0034975	Histone acetyltransferase activity/regulation of transcription, mushroom body development.
Estrogen-related receptor	FBgn0035849	RNA polymerase II transcription factor activity/steroid hormone mediated signalling pathway.
Fasciclin II	FBgn0000635	Protein binding/synapse organisation, cell-cell adhesion via plasma-membrane adhesion molecules, olfactory behaviour.
Fat-spondin	FBgn0026721	Serine-type endopeptidase inhibitor activity/unknown.
Fmr 1	FBgn0028734	mRNA binding/brain development, neurotransmitter transport, long-term memory.
Forkhead box, sub-group O	FBgn0038197	Transcription factor activity/ regulation of behaviour, response to stress.
Frazzled	FBgn0011592	Netrin receptor activity/ dendrite morphogenesis, glial cell migration, axon guidance.
G9a	FBgn0040372	Histone-lysine N-methyltransferase activity/tube development, dendrite development.
Glutamate receptor IA	FBgn0004619	Extracellular-glutamate-gated ion channel activity/cation transport.
Gryzun	FBgn0035416	Unknown/ intracellular transport, learning or memory, long-term memory, olfactory learning.
Heterochromatin protein 1C	FBgn0039019	Methylated histone binding/positive regulation of chromatin silencing at telomere.
Hikaru genki	FBgn0010114	Immunoglobulin subtype/synaptic target recognition, cell adhesion.
Histone deacetylase 1 (Rpd3)	FBgn0015805	Histone deacetylase activity/ regulation of neuron projection development.
Histone deacetylase 11	FBgn0051119	Histone deacetylation/histone deacetylation.
Histone deacetylase 3	FBgn0025825	Histone deacetylase activity/chromatin silencing.
Histone deacetylase 6	FBgn0026428	Histone deacetylase activity/neurotransmitter secretion.
Homer	FBgn0025777	Protein binding/circadian sleep-wake cycle, adult behaviour.
Kruppel	FBgn0001325	Transcription factor activity/regulation of developmental process.
Latheo	FBgn0005654	DNA binding/learning and memory, centrosome organisation.
Little imaginal discs	FBgn0031759	Histone demethylase activity (H3-trimethyl-K4 specific)/chromatin organisation.
Mars	FBgn0033845	Protein phosphatase 1 binding; microtubule binding/mitotic spindle organization; chromosome segregation.
Martik	FBgn0039507	Unknown/learning and memory.
Microtubule star	FBgn0004177	Protein serine/threonine phosphatase activity/regulation of cell communication and morphology.
Mob2	FBgn0259481	Protein kinase binding/cell morphogenesis, long-term memory, negative regulation of synaptic growth at the neuromuscular junction.
Nemo	FBgn0011817	MAP kinase activity/ positive regulation of synapse assembly and nervous system development.
Neurofibromin 1	FBgn0015269	Ras GTPase activator activity/circadian rhythm, response to stress.
Neuroglian	FBgn0264975	Calcium ion binding/synapse organisation, cellular component assembly.

Neurotrophin 1	FBgn0261526	Growth factor activity/ regulation of neuron apoptotic process and synaptic plasticity, axon guidance
Nmda receptor 1	FBgn0010399	NMDA glutamate receptor activity/ion transport, associative learning, medium-term memory.
No extended memory	FBgn0261673	Carbon-monoxide oxigenase activity/memory, locomotor activity.
Nord	FBgn0050418	Fibronectin type III/learning and memory.
Orb2	FBgn0264307	mRNA binding/male courtship behaviour, long-term memory.
Oskar	FBgn0003015	Hydrolase activity/learning, regulation of RNA stability.
P38a MAP kinase	FBgn0015765	Protein serine/threonine kinase activity/signalling, response to hydrogen peroxide.
P38b MAP kinase	FBgn0024846	Protein serine/threonine kinase activity/ positive regulation of developmental growth, regulation of cell communication.
Pastrel	FBgn0035770	Protein secretion/learning, long-term memory.
Poly-(ADP-ribose) polymerase	FBgn0010247	NAD+ ADP-ribosyltransferase activity/regulation of transcription, nervous system development.
PP2A B'	FBgn0042693	Protein phosphatase type 2A regulator activity/ neuromuscular junction development, synaptic vesicle localization.
Prospero	FBgn0004595	Transcriptional repression activity/brain development, protein localisation.
Protein kinase D	FBgn0038603	Protein kinase C activity/protein phosphorylation.
Protein phosphatase 1 at 87B	FBgn0004103	Myosin phosphatase activity/ positive regulation of MAPK cascade, axon guidance.
Protein phosphatase 2B at 14D	FBgn0011826	Calcium-dependent protein serine/threonine phosphatase activity/meiotic nuclear division, protein dephosphorylation.
Pumilio	FBgn0003165	RNA binding protein/ modulation of synaptic transmission, neurogenesis
Rac1	FBgn0010333	GTPase activating protein binding/regulation of synapse organisation, cell proliferation.
Radish	FBgn0265597	GTPase activator activity/olfactory learning.
Ribosomal protein S6 kinase II	FBgn0262866	Serine/threonine kinase activity/associative learning, regulation of cell development.
Rolled (MapK)	FBgn0003256	Protein serine/threonine kinase activity, MAP kinase activity/ positive regulation of MAPK cascade, adherens junction organization.
Rugose	FBgn0266098	Protein kinase A binding/ short-term memory; neuromuscular junction development, olfactory learning; protein localization; mushroom body development.
Rutabaga	FBgn0003301	Adenylate-cyclase activity/neuromuscular junction development.
Ryanodine receptor	FBgn0011286	Ryanodine-sensitive calcium-release channel activity/ calcium ion transmembrane transport.
Sarah	FBgn0086370	Protein binding/regulation of cellular process, meiosis.
Scab	FBgn0003328	Laminin receptor activity/cell matrix adhesion, localisation.
Similar	FBgn0266411	Protein dimerization activity/response to stress, regulation of locomotion.

Sirtuin 2	FBgn0024291	NAD+ binding/ regulation of histone acetylation, chromatin silencing.
Spoonbill	FBgn0263987	Protein kinase A binding/learning or memory, RNA localisation.
Staufen	FBgn0003520	Double-stranded RNA binding/neural precursor cell proliferation, long-term memory.
StonedA	FBgn0016976	Protein binding/synaptic vesicle endocytosis/exocytosis and transport, neurotransmitter secretion.
StonedB	FBgn0016975	Protein binding/synaptic vesicle transport.
Tat interactive protein 60kDa	FBgn0026080	Histone acetyltransferase activity/regulation of synaptic plasticity.
Tonalli	FBgn0026160	Zinc ion binding/chromatin-mediated maintenance of transcription.
Twins	FBgn0004889	Protein phosphatase type 2A regulator activity/cytoskeleton organisation, signalling.
Will decrease acetylation	FBgn0039067	Histone acetyltransferase activity/histone H3 acetylation.
Z band alternatively spliced PDZ-motif protein 52	FBgn0265991	Protein binding/muscle structure development.
α-actinin	FBgn0000667	Actin filament binding/ cytoskeletal anchoring at plasma membrane.
β amyloid protein precursor-like	FBgn0000108	Protein binding/β amyloid precursor like protein, regulates nervous system development, synapse organisation, long-term memory.
β-spectrin	FBgn0250788	Structural constituent of cytoskeleton/ negative regulation of protein depolymerisation.

Table 7.3 Genes that resulted in additive effects in the *HDAC4*-induced rough eye phenotype screen. Genes that did not result in either suppression or enhancement of the *HDAC4*-induced rough eye phenotype suggesting they are not part of *HDAC4* genetic pathway.

7.2 Supplemental figures

7.2.1 Subcloning of DNA (Ankyrin1-MYC)

In view of the fact that an antibody for *Drosophila* Ank1 was not available, in order to enable examination the subcellular localisation of Ank1 within neurons, a MYC epitope tag was fused to the C-terminus of the Ank1 open reading frame. Following generation of transgenic flies, this would allow detection with an anti-MYC antibody. The Ank1-MYC construct was subcloned into a pUASTattB vector that allows one to land any UAS-gene-of-interest construct into a chosen attP site in the fly genome (described in more details in section 2.11). The pUASTattB vector, represented in Figure 7.1, contains a 285 bp attB donor site, the dominant white (w^+) marker, which allows transgenic lines to be selected by the change in eye colour from white (*w*-, attP injected stock) to red after the first cross to a *w*- line (Fish et al., 2007). A UAS-Multiple cloning site (MCS)-SV40 cassette is present that allows GAL4 driven expression of the transgene (due to the UAS sequence) and SV40 sequence serves to terminate transcription. Moreover, a single loxP site in included in the vector that can be used to excise the white marker and other unnecessary sequences after the integration (Bishof et al., 2007; Fish et al., 2007).

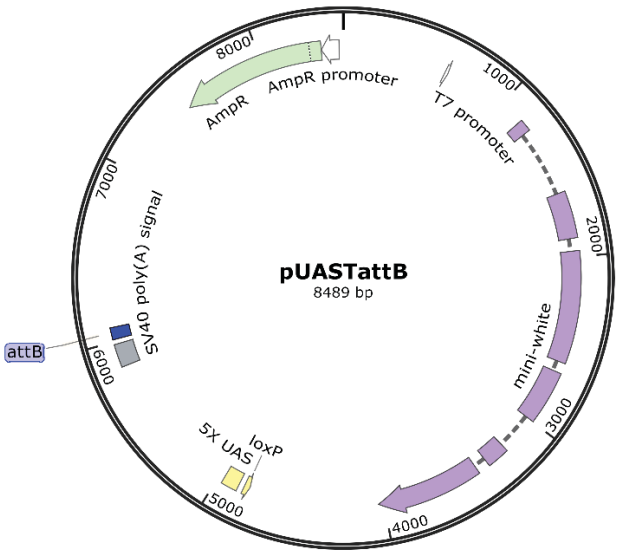

Figure 7.1 schematic physical map of the pUASTattB plasmid. Standard map of the pUASTattB vector comprising: i) the *white* gene for selection of transgeneic flies; ii) a loxP site which can be used to excise the *white* marker and other sequences after integration through the Cre-loxP system; iii) an UAS-MCS-SV40 region which allows for GAL4 mediated expression

through the UAS element and termination of transcription via SV40; iv) the attB donor site necessary for site-specific insertion of the transgene in the elected attP fly line.

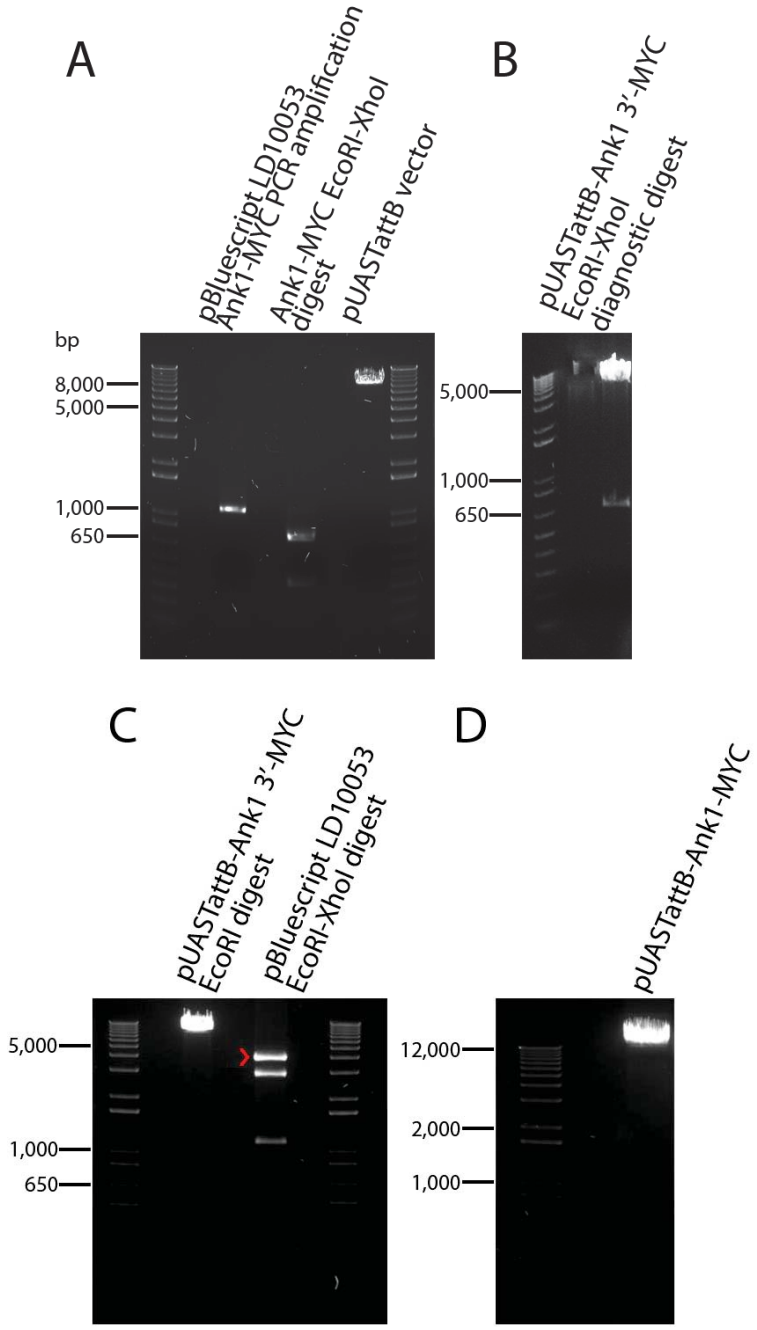

Figure 7.2 Ank1-MYC DNA gels. Image (A) shows the bands of the Ank1-MYC amplified product (~1,100 bp), Ank1-MYC EcoRI and XhoI digestion (~679 bp) and the pUASTattB vector (~8,489 bp). Image (B) shows the diagnostic restriction digest of the intermediate pUASTattB-Ank1 3' MYC vector (~9,168 bp). Image (C) shows the bands resulting from digest of the pBluescript vector containing the full length Ank1 LD10053 clone, from which the 5' end was digested. Expected band sizes: ~4,000 bp for the Ank1-5' end insert (red arrowhead), ~3,000 for

the pBluescript backbone and ~1,100 bp for the EcoRI-XhoI cut. (D) Final full length pUASTattB-Ank1-MYC vector (~13,168 bp). For details refer to section 2.10.5.

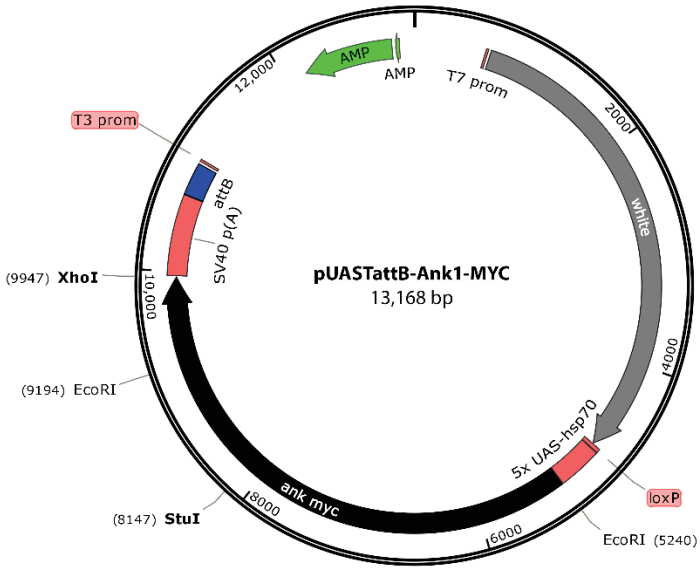

Figure 7.3 Physical map of pUASTattB-Ank1-MYC vector.

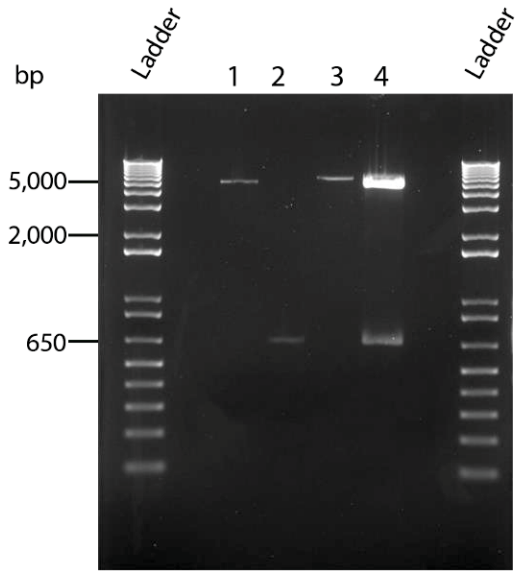

Figure 7.4 pGEX-2TK-HDAC4-GST DNA gel. Lane 1 shows the band of the pGEX-2TK vector (~4,981 bp). Lane 2 shows the amplified ankyrin repeat region of HDAC4 fused to GST (HDAC4-GST, ~ 660 bp). Lane 3 shows the product resulting from ligation between pGEX-2TK vector and HDAC4-GST insert (~ 5,641 bp). Lane 4 shows the EcoRI-BamHI digestion of pGEX-2TK-HDAC4-GST (~ 4,981 bp + ~ 660 bp).

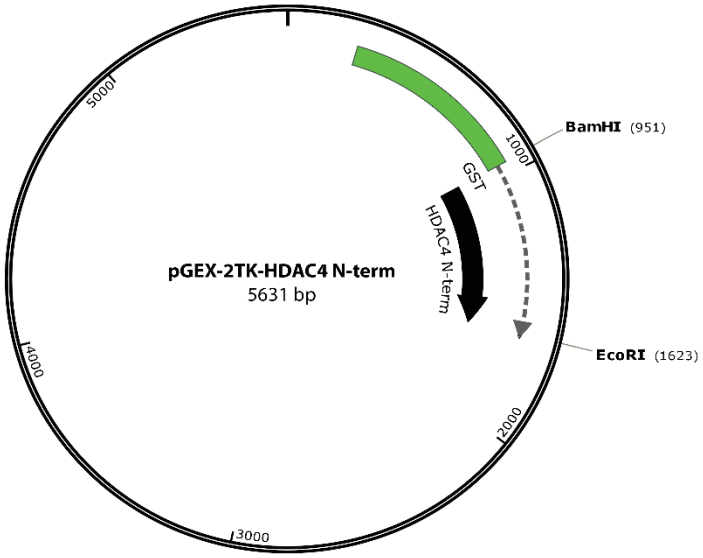

Figure 7.5 Physical map of pGEX-2TK-HDAC4-GST vector.

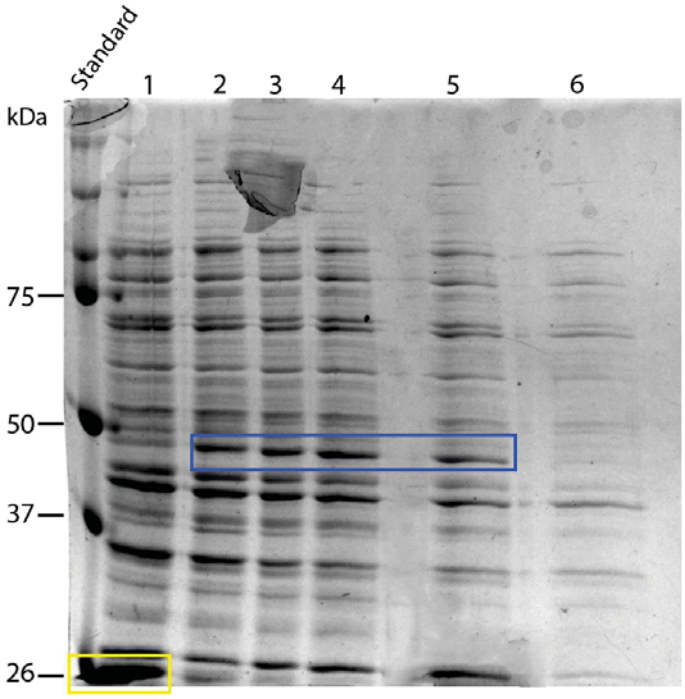

Figure 7.6 Protein gel showing IPTG induction of pGEX-2TK-HDAC4-GST. Blue rectangle shows HDAC4-GST protein (~50 kDa). Yellow rectangle shows GST (~26 kDa). Different concentrations of IPTG were adopted. (1) pGEX-2TK vector, (2-5) pGEX-2TK-HDAC4-GST vector induced at different IPTG concentrations (mM). 2 = IPTG 0.01 mM, 3 = 0.05 mM, 4 = 0.075 mM, 5 = 0.1 mM. (6) pGEX-2TK-HDAC4-GST not induced.

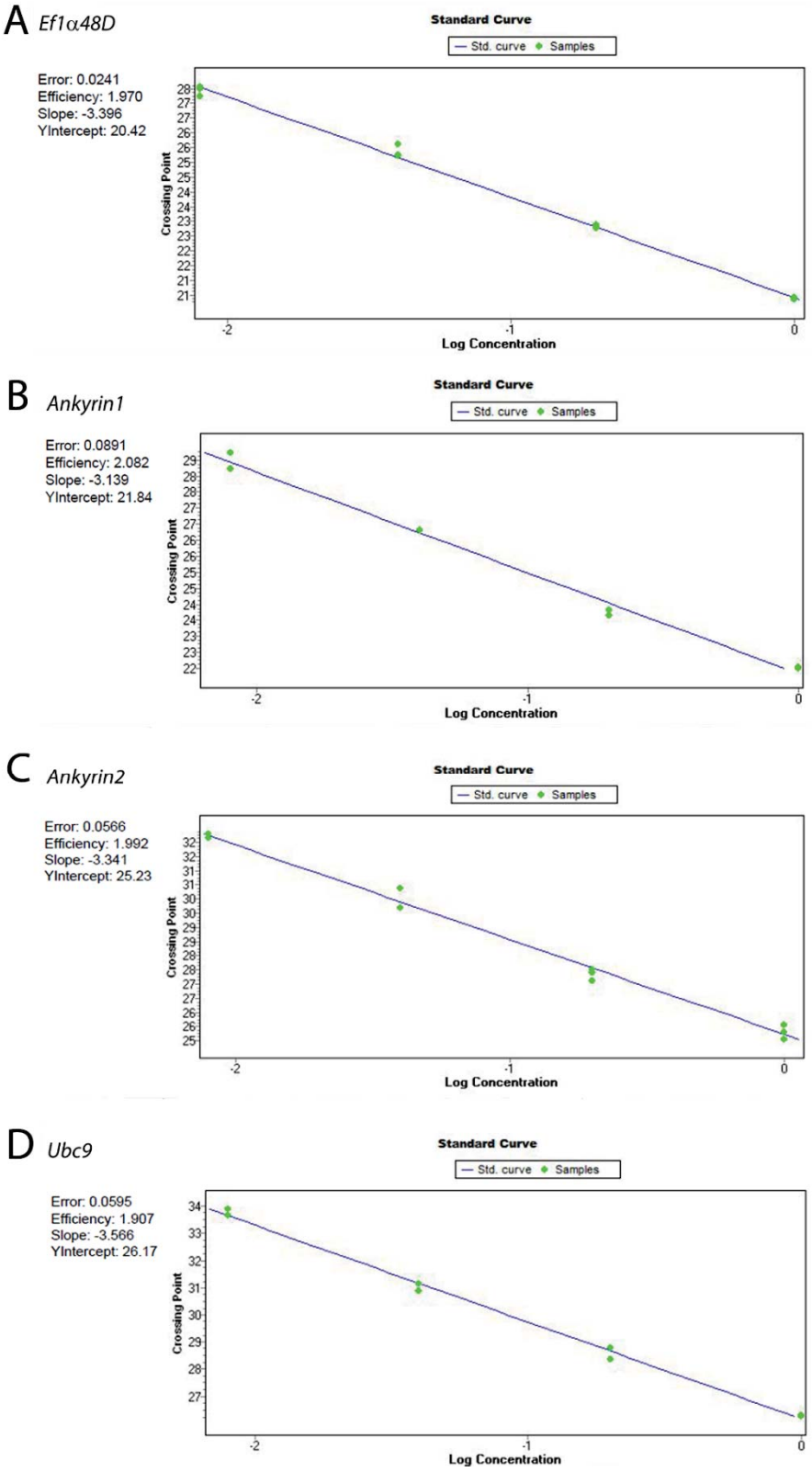

Figure 7.7 Standard curves from qPCR experiments. (A) Standard curves from housekeeping gene *Ef1α48D*. (B) *Ank1*RNAi, (C) *Ank2*RNAi, (D) *Ubc9*RNAi.

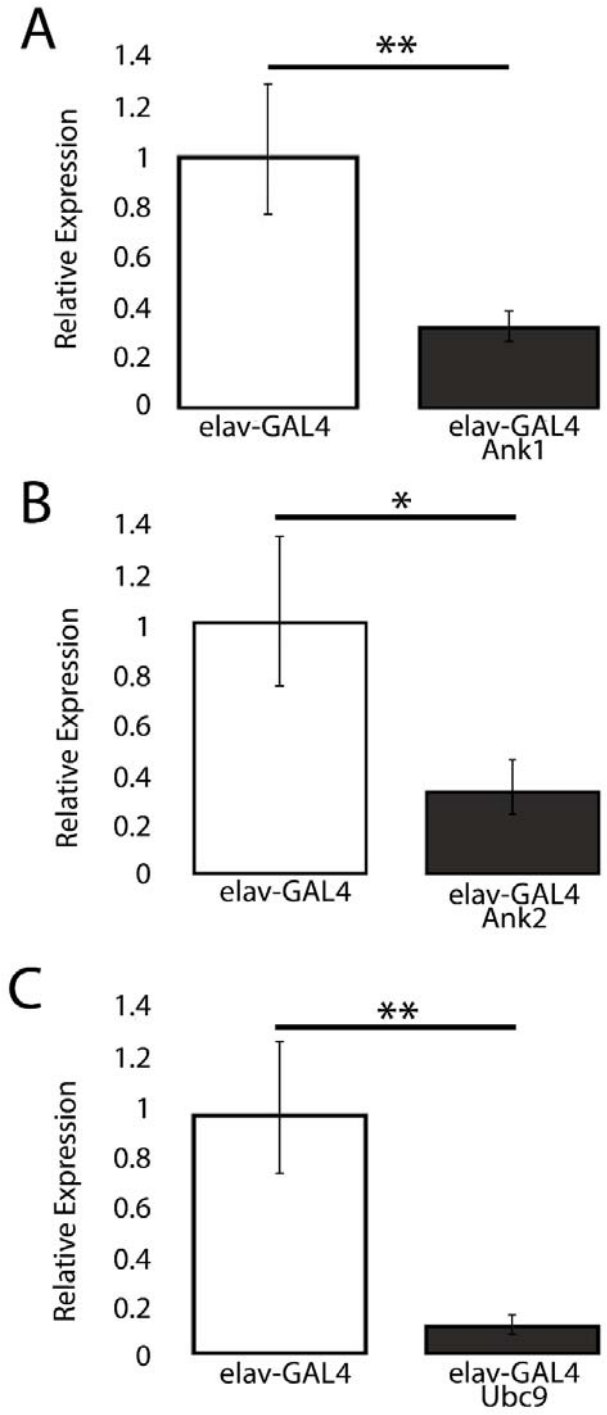

Figure 7.8 Assessment of RNAi knockdown via qPCR. RNAi of genes of interest was expressed pan-neuronally with *elav-GAL4*, followed by isolation of total RNA for qPCR analysis of RNA transcript levels. Gene expression was significantly reduced in presence of RNAi. (A) *Ank1*, (B) *Ank2*, (C) *Ubc9*. Significance of gene knockdown versus control was calculated using the Mann-Whitney test (*P < 0.05; **P < 0.01). Genotypes: elav-GAL4 = elav-GAL4/+; elav-GAL4 Ank1 = *elav-GAL4/+; Ank1RNAi/+*; elav-GAL4 Ank2 = *elav-GAL4/+; Ank2RNAi/+;* elav-GAL4 Ubc9 = *elav-GAL4/+; Ubc9RNAi/+*.